Oxidative Medicine and Cellular Longevity

Biological Efficacy of Medicinal Plant Extracts in Preventing Oxidative Damage

Lead Guest Editor: Jaideep Banerjee
Guest Editors: Amitava Das, Mithun Sinha, and Sudipta Saha

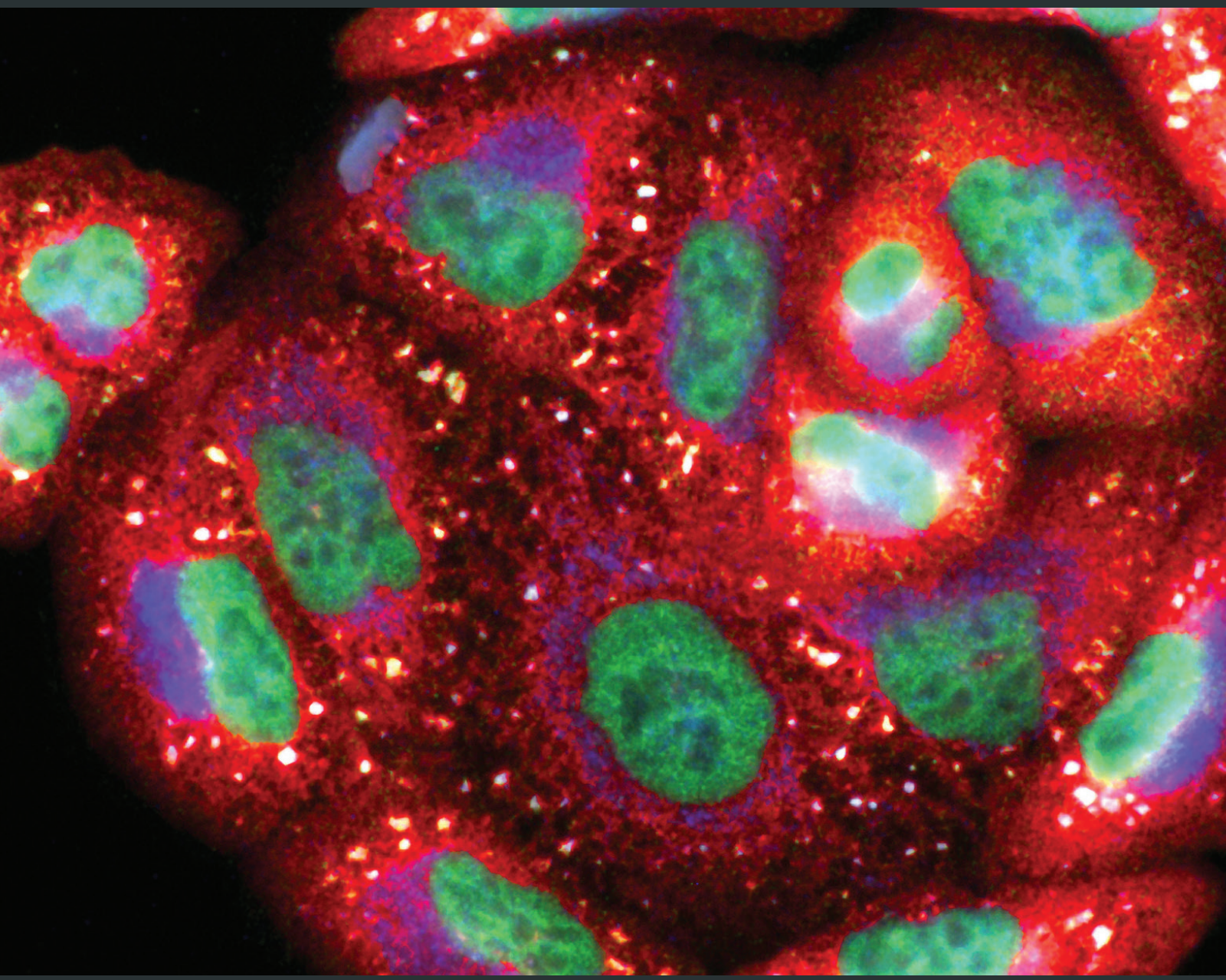

Biological Efficacy of Medicinal Plant Extracts in Preventing Oxidative Damage

Oxidative Medicine and Cellular Longevity

Biological Efficacy of Medicinal Plant Extracts in Preventing Oxidative Damage

Lead Guest Editor: Jaideep Banerjee
Guest Editors: Amitava Das, Mithun Sinha, and Sudipta Saha

Editorial Board

Contents

Hindawi
Oxidative Medicine and Cellular Longevity
Volume 2018, Article ID 7904349, 2 pages
https://doi.org/10.1155/2018/7904349

Editorial

Biological Efficacy of Medicinal Plant Extracts in Preventing Oxidative Damage

Jaideep Banerjee,[1] **Amitava Das**,[2] **Mithun Sinha**,[2] **and Sudipta Saha**[3]

[1]*George Washington University, Washington, USA*
[2]*The Ohio State University, Columbus, USA*
[3]*Babasaheb Ambedkar University, Lucknow, India*

Correspondence should be addressed to Jaideep Banerjee; banerjee.42@osu.edu

Received 12 August 2018; Accepted 13 August 2018; Published 13 September 2018

Reactive oxygen species (ROS) and reactive nitrogen species (RNS) are important signaling molecules that maintain cellular homeostasis. Redox imbalance or production of excess amounts of ROS and RNS, however, is either a cause or an important mediator in the pathogenesis and pathophysiology of many diseases. It results in oxidative damage to various biological macromolecules including DNA, lipids, and proteins, thereby altering several signaling pathways that ultimately promote cellular damage and death.

Natural product-based medicines have been used in medical practices for centuries. Naturally derived compounds have fewer reported side effects than allopathic medicine and may be safer to use over a longer period of time. F. Zhu et al. had reported in 2012 in *Plos One* that the active ingredients in combinations of natural products can achieve the same level of potency as synthetic drugs, although they may have to be taken in larger quantities or for a longer period. About 8% of hospital admissions in the United States of America are due to adverse or side effects of synthetic drugs, and approximately 100,000 people each year die due to these toxicities, as reported in *J Appl Pharmaceut Sci* in 2011 by G Philomena. However, toxicity of herbal medicines needs to be seen in context, and although generally considered safe, it can still have side effects.

Many natural compounds and natural product mimics are potential antioxidants that protect against oxidative damage in chronic diseases. Understanding and validating the bioactivities of the natural compounds and the molecular mechanisms are essential for a solid scientific foundation for their clinical use, improvement in their efficacy, and to meet the regulatory challenges. This special issue on the "Biological Efficacy of Medicinal Plant Extracts in Preventing Oxidative Damage" presents a collection of original reports and review articles on the scientific mechanism of action of some novel as well as traditionally used medicinal extracts in preventing oxidative damage-related diseases.

G.-H. Li et al. describe the bioactive constituents and the mechanism of action of Salviae Miltiorrhizae Radix et Rhizoma (SMRR), which is a traditional Chinese medicine and is commonly used for the therapy of cardiac cerebral diseases. The authors discuss the effect of the SMRR extract as well as the purified constituents tanshinone I, tanshinone IIA, and salvianolic acids A and B on the Nrf2 pathway and the resulting antioxidant therapeutic effects on cardiovascular diseases, neurodegenerative diseases, diabetes, nephropathy, inflammation, liver diseases, and lung diseases.

K. C. dos Santos et al. evaluated the effect of the leaves of Yacon (*Smallanthus sonchifolius*) on dysmetabolism and cardiomyopathy in type 1 diabetic rats. Yacon is a native Andean plant that is rich in phenolic compounds, and the treatment increased the activity of the antioxidant enzymes (catalase, superoxide dismutase, and glutathione peroxidase). This was also associated with reduced glycemia, increased insulin concentration, decreased serum triacylglycerol and fatty acid content, and decreased fibrosis and

cellular disorganization in the pancreas and cardiac tissue of diabetic animals.

Carapa guianensis (Aublet) is a neotropical tree found in the north of South America, Central America, Caribbean, and Sub-Saharan Africa. The seed oil is widely used in Brazilian traditional medicine because of its multiple curative properties against fever and rheumatism and as an anti-inflammatory agent, antibacterial agent, and insect repellant. Authors C. F. Araujo-Lima et al. have evaluated the chemical composition, free-radical scavenging activity, and mutagenic and genotoxicity properties of three *C. guianensis* oils obtained by different extraction methods and have identified the best procedure to extract the oil which makes it safe for use.

Authors D. Guo et al. report that natural *Gracilaria lemaneiformis* sulfated polysaccharide increased the cell viability and restored the cell morphology of human kidney proximal tubular epithelial cells (HK-2) damaged by oxalate. A decrease in released lactate dehydrogenase and an increase in mitochondrial membrane potential were observed. The authors also found that the repair ability of the GLP fractions are closely correlated with the molecular weight of the fractions, with GLP2 exhibiting the strongest repair effect. These results can therefore provide references for inhibiting the formation of kidney stones and developing original antistone polysaccharide drugs.

In the review article by M. A. Mendez-Encinas et al., the authors describe the functional properties and potential application as an antioxidant and anticancer agent of ferulated arabinoxylans, which are polysaccharides obtained from the cell walls of cereal grains. They also discuss the gel-forming characteristic of these polysaccharides, which has characteristics such as high water absorption capacity, stability to pH, temperature, and ionic charges, thus making them an excellent drug delivery system.

J. Meng et al. report a potential use of a traditional Tibetan medicine, *Rheum tanguticum* (*Rt*), for treatment in Alzheimer's disease. *Rt* has anti-inflammatory and antioxidative properties and inhibits the expression and production of inflammatory and oxidative molecules such as IL-1β, TNF-α, and nitric oxide by microglia. They further found that aloe-emodin and (+)-catechin are responsible for these properties through the secretion of IL-10 from microglia.

The effect of olive leaf extract (OLE) on testicular damage was tested in rats by R. S. Almeer et al. Cisplatin is widely used as an antineoplastic drug for treating various cancers. However, its use is mainly limited by severe toxicity to normal tissues, especially nephrotoxicity, neurotoxicity, and testicular damage. Cisplatin causes disorganization of germinal epithelium and apoptosis. And testicular weights, catalase, serum testosterone, and testicular enzymes are significantly reduced. The authors report that OLE treatment can markedly attenuate both biochemical and histopathological changes and is mediated, at least partly, by inducing the nuclear factor erythroid 2-related factor 2 (Nrf2)/heme oxygenase 1 (HO-1) pathway.

H. A. Ogaly et al., in their manuscript, have investigated the efficacy of *Mentha piperita L.* essential oil (MPEO) against liver fibrosis in rats and have explored this use of MPEO as an antifibrotic treatment for treating chronic liver diseases. Hepatoprotective effects of MPEO were observed as documented by the reduction of liver injury markers and lipid peroxidation (LPO) with ameliorated pathological and fibrotic liver injuries. Furthermore, reduced expression of desmin, α-SMA, TGF-β1, and SMAD3 proteins indicated that reduced hepatic stellate cell (HSC) activation. MPEO also resulted in downregulation of CCl4-stimulated p53 expression.

Lycopene, which is a potent antioxidant carotenoid, has been evaluated by N. Stojiljkovic et al. in methotrexate-induced kidney damage in rats. Lycopene was administered in two different forms: dissolved in corn oil or encapsulated in nanoliposomes. Application of both forms of lycopene concomitantly with methotrexate was found to be effective against changes in serum urea and creatinine and oxidative damage markers and markedly reversed structural changes of kidney tissue, with the nanoliposome-encapsulated form being more effective for recovery.

Resveratrol (RSV), a natural polyphenol, is known for its potent antioxidant and anticancer effects. Authors B. Yan et al. studied the effect of RSV on the biological properties of activated pancreatic stellate cells that initiate pancreatic fibrosis in chronic pancreatitis. The authors report that RSV downregulates miR-21 expression and induces PTEN expression, resulting in impeded reactive oxygen species induction in PSCs. Collectively, the authors conclude that RSV inhibits invasion and migration of pancreatic cancer cells through suppression of ROS/miR-21-mediated activation and glycolysis in PSCs and thus may serve as a new strategy for clinical prevention or treatment of pancreatic ductal adenocarcinoma.

Taken together, the articles in this special issue contributed by the experts in the fields of oxidative stress biology highlight the increasing importance of investigating the effect of natural products on ameliorating oxidative damage and thus identify safe therapeutic treatments for the plethora of oxidative stress-related diseases.

Conflicts of Interest

The authors declare that there is no conflict of interest regarding the publication of this article.

Jaideep Banerjee
Amitava Das
Mithun Sinha
Sudipta Saha

Hindawi
Oxidative Medicine and Cellular Longevity
Volume 2018, Article ID 2314759, 22 pages
https://doi.org/10.1155/2018/2314759

Review Article

Ferulated Arabinoxylans and Their Gels: Functional Properties and Potential Application as Antioxidant and Anticancer Agent

Mayra Alejandra Mendez-Encinas,[1] Elizabeth Carvajal-Millan,[1] Agustín Rascon-Chu,[2] Humberto Francisco Astiazaran-Garcia,[3] and Dora Edith Valencia-Rivera[4]

[1]*Biopolymers, Research Center for Food and Development, CIAD, A.C. Carretera a La Victoria Km. 0.6, 83304 Hermosillo, SON, Mexico*
[2]*Biotechnology, Research Center for Food and Development, CIAD, A.C. Carretera a La Victoria Km. 0.6, 83304 Hermosillo, SON, Mexico*
[3]*Nutrition, Research Center for Food and Development, CIAD, A.C. Carretera a La Victoria Km. 0.6, 83304 Hermosillo, SON, Mexico*
[4]*Department of Chemical Biological and Agropecuary Sciences, University of Sonora, Avenida Universidad e Irigoyen, 83621 Caborca, SON, Mexico*

Correspondence should be addressed to Elizabeth Carvajal-Millan; ecarvajal@ciad.mx

Received 12 December 2017; Revised 19 May 2018; Accepted 2 July 2018; Published 16 August 2018

Academic Editor: Jaideep Banerjee

In the last years, biomedical research has focused its efforts in the development of new oral delivery systems for the treatment of different diseases. Ferulated arabinoxylans are polysaccharides from cereals that have been gaining attention in the pharmaceutical field due to their prebiotic, antioxidant, and anticancer properties. The antioxidant and anticancer properties of these polysaccharides make them attractive compounds for the treatment of cancer, particularly colon cancer. In addition, ferulated arabinoxylans can form covalent gels through the cross-linking of their ferulic acids. Due to their particular characteristics, ferulated arabinoxylan gels represent an excellent alternative as colon-targeted drug delivery systems. The aim of the present work is to review the physicochemical and functional properties of ferulated arabinoxylans and their gels and to present the future perspectives for potential application as antioxidant and anticancer agents.

1. Introduction

Consumption of whole grains is associated with the prevention of cardiovascular diseases, diabetes, obesity, and cancer [1]. The dietary fiber and the antioxidant compounds of grains play an important role providing such benefits.

An inverse relationship between the dietary fiber of whole grain consumption and total cancer death has been established [2]. Particularly, a case study suggested that higher intake of dietary fiber reduces the risk of incident colorectal adenoma and distal colon cancer [3]. In addition, dietary fiber has shown to reduce type 2 diabetes mellitus risk through glycemic control or decrease energy intake, reduce blood glucose excursions, and lower insulin responses [4]. Moreover, insoluble antioxidants of whole grains which are bounded to arabinoxylan side chains can be released by microbial enzymatic hydrolysis in the colon and adsorbed, exhibiting an antioxidant protection [1]. On the other hand, certain components of dietary fiber such as arabinoxylans (AX) have prebiotic properties. In fact, phenolic acids of AX, such as ferulic acid (FA), exert antioxidant activity [5]. In this way, AX have gained attention in the pharmaceutical field due to their interesting functional and biological properties.

AX are nonstarch polysaccharides in the cell wall of cereal grains. A unique property of AX is their ability to form covalent gels by the oxidative coupling of the FA [6]. Due to their covalent nature, these gels have interesting characteristics such as high water absorption capacity and stability to pH, temperature, and ionic charges [7]. In addition, AX gels exhibit antioxidant activity [8] and can be fermented by the

colonic microbiota [9–11]. Furthermore, several studies have demonstrated the biological properties of AX, particularly their prebiotic, antioxidant, and more recently anticancer properties [12–16]. The anticancer activity of AX has been largely related to their prebiotic and antioxidant properties [17–19]. Thus, the particular characteristics and functional properties of AX make them promising polysaccharides for biopharmaceutical purposes.

The prebiotic and antioxidant properties of AX depend on its structural characteristics. It has been established that the presence and appearance of FA in AX impacts directly in its antioxidant and prebiotic properties [20]. A previous study showed that highly feruloylated AX oligosaccharides (AXOS), hydrolytic degradation products of AX, were less fermented than AXOS depleted in FA [20]. This appears to be a great advantage due to the selective inhibition of the growth of certain nonbeneficial bacteria, but the growth of probiotic bacteria, such as *Lactobacillus* and *Bifidobacterium*, which are able to produce FA esterases to release FA from AXOS and AX [21, 22]. In addition, the presence and amount of FA result to be the principal factor in providing the antioxidant capacity to AX and AXOS as has been well documented previously [10, 20]. Then, it could be interesting to investigate how the cross-linking of AX could impact on the prebiotic and antioxidant properties of AX gels.

Recently, researchers have focused their attention on the development of novel bioactive materials as colon-targeted oral delivery systems for the treatment of diseases such as colon cancer [23, 24]. AX gels with anticancer activity could be potential candidates for use as matrices for drug delivery in the treatment of colon cancer. AX with a high content of FA lead to the formation of high cross-linked density gels [25]. Since AX exhibit anticancer activity, the effect of the oxidative gelation and the cross-linking density of the gels on such property need to be investigated. In this context, the objective of the present review focuses on the functional and biological properties of AX and their gels and their potential application as antioxidant and anticancer agents.

2. Arabinoxylans

2.1. Chemical Structure. AX are polysaccharides from cereal grains constituted by a linear β-(1-4)-xylopyranosyl chain. Some α-L-arabinofuranosyl residues are linked to the main xylose chain at O-3 and/or O-2 positions, resulting in four different structures (monosubstituted at O-3 or O-2, disubstituted at O-2,3, and unsubstituted) (Figure 1(b)). The amount and distribution of these branches can vary depending on the source of the polysaccharide [26]. In addition to arabinose, some galactose, xylose, and glucuronic acid residues can exist as side branches in the main chain of AX [27].

A particular structural characteristic of AX is the presence of phenolic acids. Some FA and cumaric acid residues can be esterified to arabinose at the O-5 position [28] (Figure 1(a)). FA is the most abundant phenolic acid in AX, and its content depends on the origin of the tissue (Table 1). AX from endosperm contains very small amounts of FA, while AX from pericarp and aleurone layer are highly esterified to FA [20]. The FA contents in AX vary from 0.001 to 7.00 μg/mg AX [29, 30]. High contents of FA (6–7.00 μg/mg AX) have been detected in maize bran AX [25, 30], while AX extracted from finger millet bran and ispaghula seed contain very low or even undetectable amounts of FA (0.001 μg/mg AX) [29, 31]. These differences could be related to the source of the polysaccharide as well as the method used for its extraction.

Usually, the structure of AX in different cereal tissues is similar, although some differences in the fine structure can drastically modify its functional properties. These differences are reflected in the degree of polymerization (DP), arabinoxylan to xylose ratio (A/X), amount and sequence of glycosidic bonds, and the presence of other substituents [7]. AX can be classified according to their solubility in aqueous solvents as water-extractable (WE-AX) and water-unextractable (WU-AX) AX. In cereals, the cross-linking between AX and other components from the cell wall form structures that are insoluble in water. Alkali treatments are used to hydrolyze such cross-links, allowing the release of AX chains from the cell wall and making them soluble in the aqueous environment [27].

The substitution degree in the AX structure can be determined by the A/X. The A/X may vary from 0.3 to 1.1 in AX from different cereals depending on the origin of the polysaccharide; AX from pericarp present higher A/X values than those for endosperm or aleurone layer [46, 47]. However, this parameter does not describe detailed and exhaustive structural characteristics of AX, and therefore, it cannot be used to characterize its fine structure.

The molecular weight (Mw) of AX can vary depending on the polysaccharide origin and the method used for its determination. The average Mw estimated for AX ranges from 10 to 10,000 kDa [7]. The Mw and the Mw distribution (polydispersity index (PI)) of AX can be affected by the extraction conditions (time, pH, and temperature) [48].

2.2. Physicochemical Characteristics. AX show physicochemical characteristics, such as solubility and viscosity, which provide them different functional properties. Similar to other polysaccharides, the water solubility of AX depends on certain parameters such as the chain-chain and chain-solvent interactions. In addition, some structural factors including the chain length and the presence and distribution of side groups can also modify the solubility of the polymers. The substitution pattern of the polysaccharide chain is the main parameter controlling the solubility of AX. Since the mechanism of aggregation in the AX is due to the intermolecular interactions of the unsubstituted regions of the polysaccharide chain, the presence of arabinose residues in the xylose chain is determinant for the solubility of AX [48].

AX form very high viscous solutions in aqueous environments. The apparent viscosity of the AX solutions is concentration- and shear rate-dependent. The viscosity values increase as the polymer concentration increases, and decrease as the shear rate increases [27]. The Mw is another important factor that determines the viscosity of the AX solutions. Izydorczyk and Biliaderis [49] demonstrated that wheat AX solutions with high Mw fractions showed weak

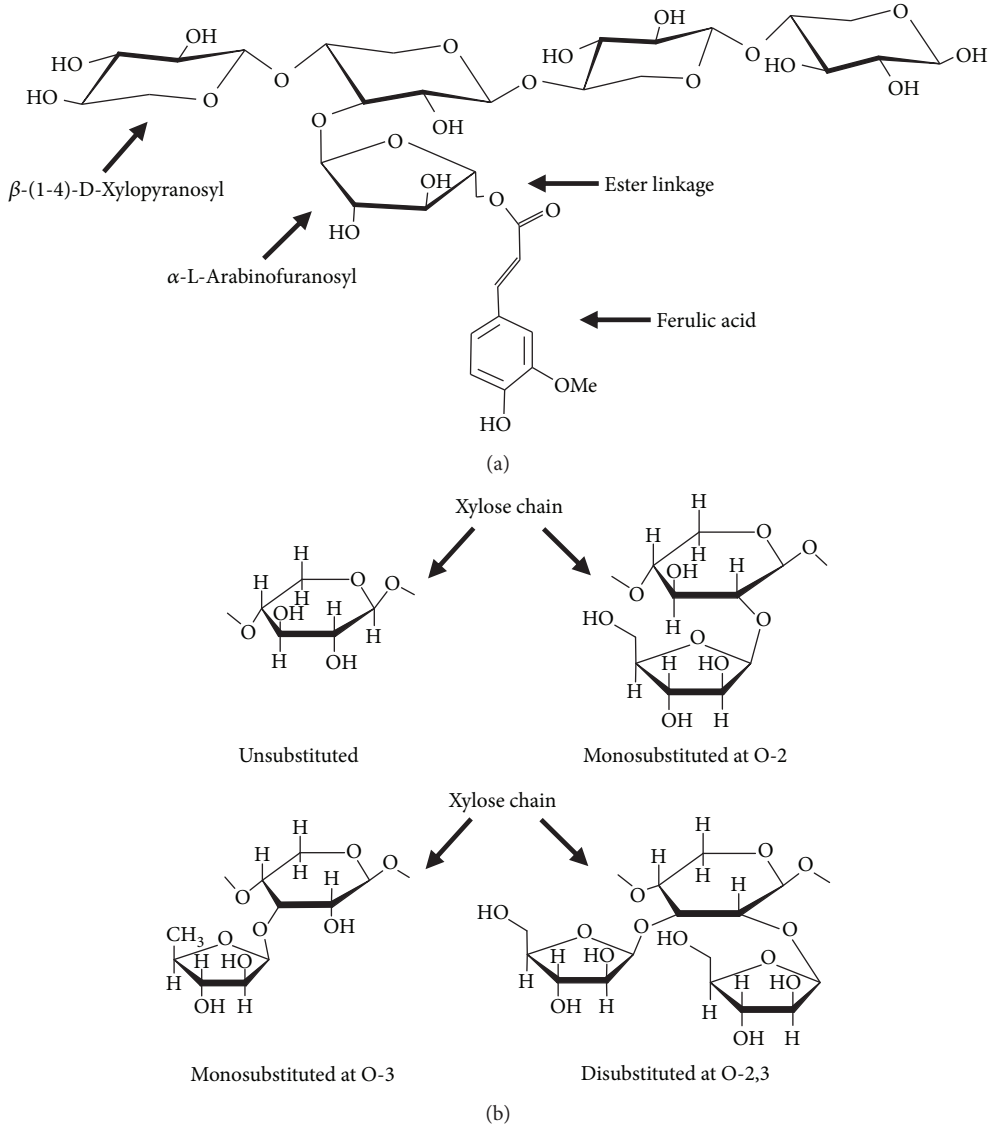

Figure 1: (a) Chemical structure of AX and (b) arabinose substitution in AX chain.

elastic properties. The viscous behavior of AX solutions is the most important characteristic responsible for the functional properties that AX exhibit in the human gastrointestinal tract [27].

2.3. Functional Properties. Functional properties of AX such as prebiotic, antioxidant, and anticancer as well as its gelling capacity result to be of great interest for biomedical and pharmaceutical applications. Therefore, research has focused its efforts on exploiting different sources of AX in order to explore and take advantage of such properties for several applications (Table 1). Maize, wheat, and rice are the main sources of AX which have been investigated for biomedical and pharmaceutical applications. Maize and wheat AX gels have shown promising results for their potential application as controlled-release matrices [11, 32–35, 37]. On the other hand, the use of AX from rice bran has been widely investigated as an adjuvant in cancer immunotherapy [41, 42].

2.3.1. Prebiotic. The products of AX degradation have been of great interest due to their prebiotic properties. Prebiotics are defined as "a non digestible compound that, through its metabolization by microorganisms in the gut, modulates the composition and/or activity of the gut microbiota, thus conferring a beneficial physiological effect on the host" [50]. AX are resistant to gastric acid, proteolytic enzymes, and absorption in the stomach or small intestine. In addition, AX are fermented by the gut microbiota and selectively stimulate the growth and/or activity of beneficial bacteria in the colon, so they may be considered as prebiotics.

AX stimulate the growth of beneficial bacteria for the gastrointestinal tract. *In vivo* assays have demonstrated that AX

Table 1: Origin, FA content, and current/potential application of AX in biomedical and pharmaceutical fields.

AX origin	FA content (μg/mg AX)	Currently/potential application in biomedical/pharmaceutical field	Reference
Nejayote/maize bran	0.012/0.025	Entrapment of probiotic	[32]
Nejayote/maize bran	0.012/0.025	Entrapment and controlled release of insulin and probiotics targeted to colon	[11]
Maize bran	0.34	Controlled release of insulin and β-lactoglobulin	[33]
Maize bran	0.25	Controlled release of insulin targeted to colon	[34]
Maize bran	4.0	Entrapment and controlled release of methyl xanthine	[35]
Wheat endosperm	2.3	Controlled release of proteins	[36]
Wheat endosperm	0.53	Entrapment of probiotics	[37]
Wheat bran	0.435	Antitumor and immunomodulatory activity	[16, 38]
Wheat bran	—	Prebiotic	[39]
Rice bran	—	Antitumor and immunomodulatory activity	[40]
Rice bran (MGN-3/Biobran)	—	Cancer immunotherapy Prevention and inhibition of cancer Synergistic effect with chemotherapeutic agents	[15, 41, 42]
Finger millet bran	0.001	Immunomodulatory activity	[29]
Ispaghula (*Plantago ovata*) seed	nd	Drug carrier	[31, 43]
Ispaghula (*Plantago ovata*) seed	—	Controlled release of mucoadhesive oral films	[44, 45]

nd: no detectable; –: no reported.

promote the growth of *Bifidobacterium* and *Lactobacillus*, both considered as beneficial species for the gut [51]. These modifications in the gut microbiota are associated with health benefits, reduction in gastrointestinal infections, and improvement in the mineral absorption and the suppression of colon cancer [52, 53].

It has been established that some phenolic acids modulate the composition of microbiota through the selective inhibition of some pathogenic bacteria, while the growth of commensal anaerobes and probiotic bacteria is less affected or even increased [22, 54]. In this regard, the growth of probiotic such as *Bifidobacterium* and *Lactobacillus* during AX fermentation can be explained by the fact that these bacteria produce the FA esterases to release the FA residues from AX [21, 55, 56].

Another benefit of AX as a prebiotic is the production of beneficial bacterial metabolites, such as short-chain fatty acids (SCFA). The fermentation of AX increases the production of acetic, propionic, and butyric acids. Particularly, AX are characterized by increasing the butyric acid levels, which play an important role in the maintenance of health and gastrointestinal function [57]. The fermentation of AX is associated with the growth of butyric acid-producing bacteria, such as *Eubacterium* and *Roseburia* [58]. Nielsen et al. [59] evaluated the effect of AX-rich and high-fat diets on the production of SCFA in pigs. The supplementation of the AX-rich diet increased the SCFA levels, particularly the butyric acid level which was 5-fold higher compared with that obtained for the high-fat diet.

Butyric acid is considered an essential metabolite for the human colon as it is the main source of energy for its epithelial cells (colonocytes), contributes to the maintenance of the gut barrier functions, and has immunomodulatory and anti-inflammatory properties [58]. In addition, the proliferation of butyrate-producing bacteria protects the colon from pathogenic microbiota [60]. For those reasons, AX have been considered as polysaccharides with excellent prebiotic properties. The consumption of this polysaccharide provides many health benefits, especially those related with the prevention of colon cancer.

Recently, long-chain AX (LC-AX) have demonstrated to modulate the luminal and mucosal microbiota. Experiments using a dynamic *in vitro* model of the human digestive tract (M-SHIME) showed that supplementation of LC-AX to the proximal colon compartments of the M-SHIME increased *Bifidobacterium* population in both lumen and mucus compared with the control. The levels of propionate as well as the activity of enzymes β-xylanase, β-xylosidase, and α-arabinofuranosidase were also increased in the lumen region. These findings suggest that LC-AX could exert a potential prebiotic effect on the host, as the mucosa-associated microbiota impacts directly in health by protecting against pathogen colonization and host immunity [61].

2.3.2. Antioxidant. The antioxidant activity of AX has been mainly associated with their content of phenolic acids, particularly FA. Phenolic acids have beneficial effects against chronic and cardiovascular diseases, cancer, diabetes, inflammatory diseases, and aging [62]. Phenolic acids exhibit their antioxidant activity through diverse mechanisms such as free radical scavenging, metal chelation, and reducing potential, blocking the free radical chain, modulation of enzymatic activity, and alteration of signal transduction pathways [63–65].

The main function of antioxidants is delaying or prevention of the oxidation produced by free radicals [66]. The free

radicals are generated by diverse factors such as normal metabolic activity, diet, and environment. In a natural manner, the body uses antioxidant endogenous enzymes as a defense mechanism against the free radicals. An increase in the production of free radicals and other reactive oxygen species exceeding normal levels in the body results in oxidative stress. This imbalance causes damage to biomolecules such as membrane lipids, lipoproteins, and DNA, increasing the risk of developing chronic diseases [67]. Therefore, the use of antioxidants results to be adequate to decrease the effects of free radicals and the risk of chronic diseases, such as cancer.

Although the antioxidant activity of AX is associated with the presence of phenolic acids, some studies suggest that this activity is mainly attributed to FA. The antioxidant activity of FA is attributed to its structural characteristics. The presence of electron-donating groups on its benzene ring gives it the property of terminating the free radical chain reactions. In addition, its COOH– group can bind to the lipid bilayer, providing protection against the free radicals attack and the lipid peroxidation [62]. Since FA is the most abundant phenolic acid in AX, it may be the main responsible for the antioxidant activity of the polysaccharide, as has been observed in different studies.

Recently, Kamboj and Rana [68] compared the antioxidant activity of maize bran gum with the antioxidant activity from other natural gums as xanthan and guar gums. They found that the maize fiber gum exhibited a higher antioxidant activity compared to the other gums, regardless of the method used for the determination. They suggested that maize fiber gum could be a promising excipient with antioxidant activity in the food and pharmaceutical industry.

Feruloyl oligosaccharides (FOS), hydrolytic products of AX, exhibit a protective effect on the cells against the damage produced by the free radicals. Wang et al. [14] evaluated the protective effect of FOS against the oxidative stress in rat plasma. The levels of oxidized glutathione and malondialdehyde and the activity of antioxidant enzymes in plasma from rats fed with the FOS diet decreased with respect to the control group. In a previous study, the protective activity of FOS against the oxidative DNA damage in normal human lymphocytes induced by hydrogen peroxide was investigated. The DNA damage was inhibited by FOS, observing a 91% inhibition of lymphocyte DNA damage at 500 μmol/L as compared with control [69].

The content and appearance of FA determine the antioxidant capacity of AX. Higher contents of trimers of FA (tri-FA) in AX result in higher antioxidant activity [5]. This behavior is attributed to three units of FA, which provide higher amounts of OH– groups, increasing the hydrogen donor capacity and, therefore, protecting from radical scavenging [70]. This highlights the close relationship existing between the structural characteristics of the polysaccharide and its functional properties. Therefore, when discussing about the antioxidant capacity of AX, not only the FA content should be considered but also how it is found in the molecule. The knowledge of such structural characteristics would help to predict the antioxidant activity of AX in order to consider it for specific applications.

2.3.3. Anticancer. Cancer is among the leading causes of death worldwide, and the second most common in the United States [71]. Usually, conventional cancer treatments including surgery, chemotherapy, and radiotherapy which focus on eliminating cancer cells are short-term effective, but not enough for a complete eradication of all cancer cells, resulting in recurrence of disease [72]. The repeated sessions of treatments lead to the suppression of the immune system and promote multidrug resistance and toxicity [41, 73]. Therefore, the search for natural products with chemopreventive properties and without side effects has been increasing.

AXOS exhibit protective effects against colon cancer, which have been related to their prebiotic effect. Femia et al. [17] observed that the administration of AXOS reduced the preneoplastic lesions in the colon of rats. The authors suggest that AXOS exhibited a chemopreventive effect on colon carcinogenesis due to their prebiotic activity. On the other hand, Glei et al. [74] showed that the fermentation products of wheat AX (SCFA) inhibited the growth of colon cancer cells (HT29) and induced the antioxidant activity of the endogenous enzyme glutathione transferase.

A close relationship between the proliferation of cancer cells and the antioxidant systems has been suggested. Cancer cells produce large amounts of hydrogen peroxide, which may favor mutations, damage, and invasion of other tissues. Then, cancer cell proliferation impacts directly in the antioxidant machinery, and according to this, some anticancer agents can act as antioxidants [19]. Thus, the antitumor potential of AX has been related to its antioxidant effect. Noaman et al. [19] supplied AX from rice to rats, which were previously inoculated with Erlich cancer cells. The results showed the inhibition of the development and growth of tumors, as well as a decrease in lipid peroxidation and increase in the activity of endogenous antioxidant enzymes (catalase, superoxide dismutase, and glutathione transferase). The authors suggested that AX exerted an antioxidant effect through its ability to increase the gene expression and activity of endogenous antioxidant enzymes in the cells and normalize the lipid peroxidation in blood, liver, and tumor tissue in animals bearing tumors.

In a previous study, the antitumor activity of MGN-3/Biobran on mice bearing a solid Erlich carcinoma (SEC) tumor was attributed to mechanisms involving induction of apoptosis and immune modulation. The administration of MGN-3 significantly decreased tumor volume (63.27%) and tumor weight (45.2%) in comparison to the control group. Flow cytometry and histopathological analyses showed an increase in the number of apoptotic SEC cells. In addition, an improvement of cytokine production was observed as shown by increasing levels of tumor necrosis factor-α and interferon-γ, while the levels of immune suppressing IL-10 were downregulated. In addition, the activity of natural killer (NK) cells was also increased [75].

The synergistic anticancer effect of MGN-3/Biobran with natural anticancer agents as well as chemotherapeutic drugs has been widely explored using *in vitro* studies. The synergistic apoptotic potential of MGN-3 and curcumin on human multiple myeloma cell line U266 was determined. Treatment

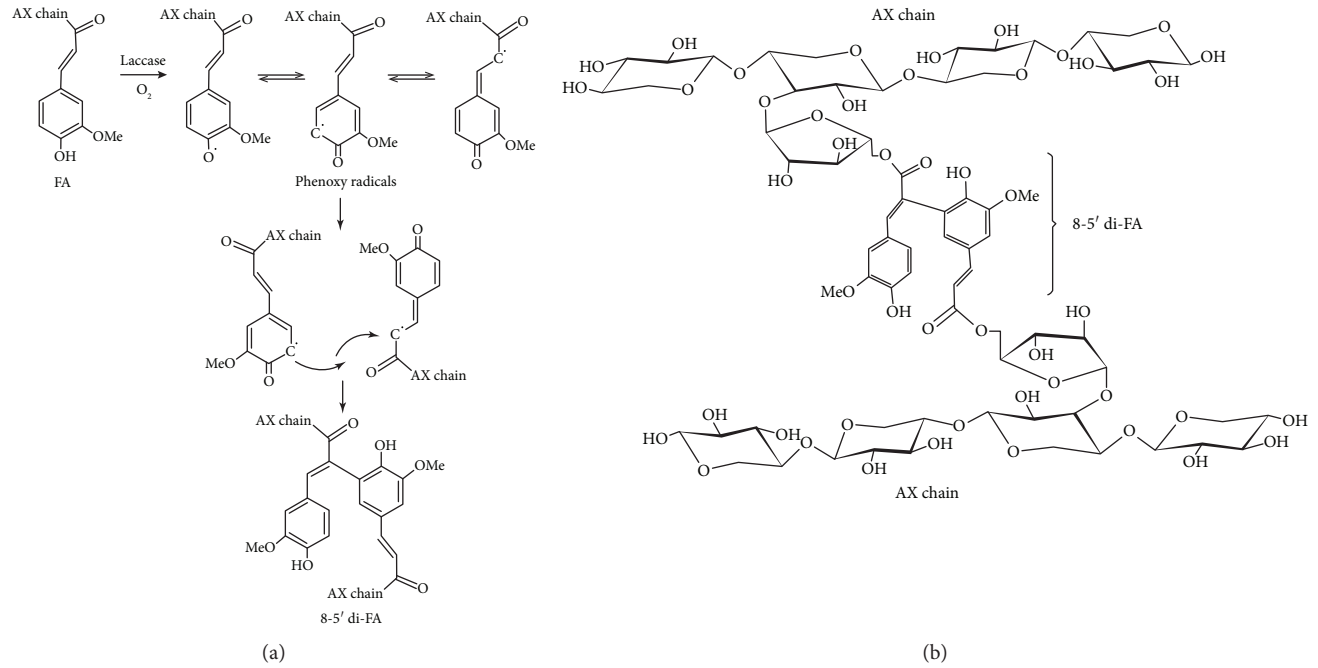

Figure 2: (a) Schematic representation of FA dimerization. (b) Covalent cross-linking of ferulated AX. Formation of 8-5′ di-FA is presented as an example. AX: arabinoxylan; FA: ferulic acid; di-FA: ferulic acid dimer.

of MGN-3 or curcumin alone showed an inhibition of cell proliferation in a dose-dependent manner. The combination of MGN-3 and curcumin caused a synergistic effect characterized by a decrease in cell number and an increase in apoptotic cells. The expression of the proapoptotic protein (Bax) increased, while antiapoptotic protein (Bcl-2) decreased, which favored apoptosis. These findings indicated that Biobran and curcumin synergize in the induction of apoptosis [76]. A similar behavior was observed when Biobran was combined with paclitaxel in order to sensitize human and murine breast cancer cells (MCF-7 and 4T1) to paclitaxel. A synergistic effect between Biobran and paclitaxel resulted in damage of DNA, enhancement of apoptosis, and inhibition of 4T1 cell proliferation [77].

In sum, researches have demonstrated the anticancer potential of the AX. Such property is attributed to both the antioxidant and prebiotic capacity of the polysaccharide. In addition, it is suggested that AX exerts its anticancer effect by a mechanism which involves its immune-modulation ability. *In vitro* as well as *in vivo* studies have evidenced the anticancer effect of AX on different types of cancer. Nevertheless, most studies highlight its beneficial effects in the prevention of colon cancer, due to the benefits of its prebiotic activity and immunostimulatory activity.

2.3.4. Gelling. A particular property of AX is their capacity to form covalent hydrogels. AX can gel through the covalent cross-linking of FA [6], under the action of different chemical (ferric chloride, ammonium persulphate) or enzymatic (laccase/O_2, peroxidase/H_2O_2, linoleic acid/lipoxygenase) oxidizing agents [78–83] (Figure 2(b)). The ability of AX to gel depends on the concentration of the polysaccharide, Mw, and particularly the FA content [27].

The oxidative gelation of AX results from the dimerization of FA residues of adjacent polysaccharide chains leading to the formation of the three-dimensional network where the aqueous phase is retained. The FA dimerization mechanism occurs as follows: first, an oxidizing agent attacks the H atom of the OH group at the ring position of FA resulting in a phenoxy radical. Then, this radical is stabilized by resonance and located at three different positions onto the whole molecule, two on the aromatic ring (C-4 and C-5) and one at the double bound (C-8) of its side chain. In the next step, the cross-linking between two phenoxy radicals is carried out; the coupling of unpaired electrons of two different radicals forms a covalent linkage which connects the two polysaccharide chains. Thus, the structure of the dimers formed during gelation will depend on the radical position [48] (Figure 2(a)).

During gelling, the coupling of FA results in different structures. In AX gels, five di-FA, 8-5′, 8-O-4′, 5-5′, 8-5′ benzo, and 8-8′, have been detected, with 8-5′ and 8-O-4′ being the most abundant [48], and one tri-FA (4-O-8′/5′-5′) [84]. In addition, the presence of noncovalent weak interactions (hydrogen bonds) may contribute to the stability of the gel [85, 86].

During the formation of the AX gel, the FA is oxidized and disappears as a result of the formation of cross-links (di-FA and tri-FA). Nevertheless, the concentrations of di-FA and tri-FA formed at the end of gelation do not compensate for the decrease in the FA monomers. Therefore, the formation of superior FA oligomers (FA tetramers, FA pentamers) have been proposed by several authors [84, 86]. In the cell wall of cereals, five tri-FA, 5-5′/8-O-4′, 8-O-4/8-O-4′, 8-8′ (cyclic)/8-O-4′, 8-O-4′/8-5′ (noncyclic), 5-5/8-O-4′(H_2O), and two FA tetramers, 4-O-8′/5–5′/8-O-4′ and 4-O-8′/5–5′/8–5′, have been identified and characterized

Table 2: *In vivo* studies on the evaluation of the prebiotic effect of AX.

Animal model	Diet/experimental time	Findings	Reference
Male chickens	Control diet (CT), diet supplemented with XOS, wheat bran-derived AXOS, wheat endosperm alkali-solubilized AX. 2 w	All treatments increased bifidobacteria. AX decreased body weight gain after 2 weeks of feeding compared with CT.	[89]
Male C57bl6/J mice	Control diet, high-fat (HF) diet, HF diet supplemented with AX. 4 w	HF diet supplemented with AX restored microbiota with a major effect on *Roseburia* spp., *Bacteroides-Prevotella* spp., and bifidobacteria. Improvement of gut barrier function, decrease in adipocyte size, fatty acid uptake, fatty acid oxidation and inflammation, and decrease in key lipogenic enzyme activity in the subcutaneous adipose tissue.	[39]
Male germ-free Fisher 344 albino rats inoculated with human faecal microbiota	Control diet, diet supplemented with long-chain AX (LC-AX) and diet supplemented with inulin (IN). 6 w	LC-AX and IN increased SCFA levels (propionate and butyrate, resp.). Stimulation of butyrate-producing bacteria and bifidobacteria, respectively. Reduction of mucin-degrading *Akkermansia muciniphila* and more mucin production by the host. Less weight gain.	[90]
Male Wistar rats	Diets supplemented with WU-AX, WE-AX, and AXOS. 14 days	WU-AX supplementation increased butyrate production and butyrate-producing bacteria. WE-AX and/or AXOS reduced pH, suppressed relevant markers of proteolytic breakdown, and induced selective bifidogenic response. Combination of WU-AX, WE-AX, and AXOS showed a synergic effect.	[91]
Male C57bl6/J mice	Control diet, high-fat (HF) diet, HF diet supplemented with AXOS. 8 w	AXOS supplementation exerted a bifidogenic effect. Improvement of the HF-induced body weight gain, fat mass development, hyperinsulinemia, insulin resistance, endotoxemia, and inflammatory disorders in a model of HF diet-induced obesity.	[13]
Pigs	Low dietary fiber and high-fat diet (WSD), AX-rich diet (AXD), and resistant starch diet (RS). 3 w	AXD feeding shifted the microbial composition towards butyrogenic species in the faeces and increased the large-intestinal butyrate pool size.	[59]

w: week.

[87]. The latest evidence suggests the possibility that the missing FA at the end of the gelling process could be related with the formation of superior structures that are not yet identified.

The AX gels present interesting features with a wide range of applications. These gels have neutral flavor, odor, and color as well as high water absorption and exhibit pH, temperature, and ionic stability [7]. They usually form quickly, and they are strong and thermostable [88]. In addition, they acquire a meso- and macroporous structure and have a dietary fiber nature. Due to their interesting characteristics, AX gels could be good candidates for their use as controlled release matrices for bioactive agents in the pharmaceutical, cosmetic, and food industries [7].

As previously mentioned, the antioxidant and prebiotic properties depend on the structure of AX. The presence of phenolic acids in AX, particularly FA, has been related to its prebiotic as well as antioxidant capacities. In addition, the resulting products of the enzymatic hydrolysis of AX exert important prebiotic properties. Then, it can be possible that the cross-linking process and formation of superior ferulate structures may contribute to some extent to the antioxidant and prebiotic properties of AX gels.

2.4. Preclinical Studies. Several *in vivo* studies have been performed in order to explore the potential of AX to exert its prebiotic, antioxidant, and anticancer effects. Following, the characteristics and findings of some of the most recent studies evaluating the effects of AX administration on animal models (mainly rats and mice) are presented.

2.4.1. Prebiotic Effect. The prebiotic effect of AX and their derivatives, xylooligosaccharides (XOS) and AXOS, has been tested *in vivo*. Several studies using animal models (mainly rats) demonstrate the potential prebiotic effect of AX through different observations: showing a bifidogenic effect, modulation of mucosa and gut microbiota, and increasing SCFA levels (mainly propionic and butyric acid), among others. Table 2 shows the characteristics and observations of some studies performed during the last 10 years related to the evaluation of the prebiotic properties of AX.

The supplementation of wheat AX to high-fat (HF) diet in mice led to an increase in bifidobacteria, particularly *B. animalis lactis*. In addition, AX modulated the microbiota by restoring the levels of bacteria (*Bacteroides-Prevotella* spp., *Roseburia* spp.) that were decreased with the HF. The bifidogenic effect of AX was correlated with lower levels of inflammatory markers in the serum which resulted in the improvement of the gut barrier functions. The consumption of AX also decreased body weight gain and fat mass development in the HF diet-induced obesity group. Moreover, the hypercholesteremia and the content of free cholesterol in the liver decreased in HF diet feeding. The presence of smaller adipocytes in the group treated with HF diet and AX was also observed which was attributed to the ability of AX to decrease the expression of genes involved in adipocyte differentiation, fatty acid uptake and oxidation, lipolysis, and fatty acid synthesis. The authors proposed a positive correlation between the modulation of microbiota and the antiobesity action as well as the cholesterol-lowering effect observed in the experiment [39]. Similar effects were observed when diet-induced obese mice were fed with a HF diet supplemented with wheat-derived AXOS. A positive correlation between the increase of bifidobacteria and improvement of metabolic endotoxemia and inflammatory markers was also observed with administration of AXOS. A higher expression of the tight junction proteins Z01 and claudin 3 led to a better function of the gut barrier. Moreover, the peptides GLP-1 and PYY, which are involved in the regulation of food intake and glucose homeostasis, respectively, increased after AXOS supplementation. This increase could be related with lower food intake and the improvement of insulin sensitivity in mice [13].

The supplementation of long-chain AX (LC-AX) in rats inoculated with human faecal microbiota has been associated with the production of propionic acid and stimulation of *B. longum*. LC-AX administration also increased the production of mucin, while it shifted mucin degradation from the caecum to the colon. The degradation of mucin in the distal regions of colon could be beneficial as most chronic colonic diseases, such as ulcerative colitis and colorectal cancer, originate in this region [90].

2.4.2. Antioxidant Effect. The antioxidant property of AX has been related with several beneficial effects. *In vivo* studies, using rats, show that AX exerts its antioxidant effect by modulating lipid peroxidation, improving the activity of antioxidant enzymes, and protecting against oxidative stress. These positive effects have been related to the mechanisms of AX to exert its anticancer effect as well as improve lipid metabolic disorder and suppress lipid peroxidation.

Recently, male Sprague-Dawley fed with a HF diet supplemented with AX (HF-AX) showed lower triglyceride concentration in serum in comparison with the HF diet group. Higher lipoprotein lipase (LPL), hepatic lipase (HL), total lipase, and acyl-CoA oxidase (ACO) activities and lower triglyceride and cholesterol levels in the liver of the HF-AX group were observed. The authors suggest that intake of AX helped to alleviate lipid metabolic disorder by reducing triglycerides and low-density lipoprotein in serum of rats. The administration of HF-AX changed the lipid metabolism by improving the activity of fatty acid oxidation enzymes (LPL, HL, and ACO) which helped to reduce the triglyceride levels in liver. AX could help to maintain normal fat levels by activating lipid catabolism and oxidation rather than inhibiting lipid synthesis. Moreover, the activity of antioxidant enzymes glutathione peroxidase and total superoxide dismutase was also improved by the ingestion of AX resulting in a reduction of the oxidative stress in serum and tissues. The results also indicated that AX may alleviate the damage of hepatic morphology by regulation of liver cell apoptosis (Bax). These findings showed that supplementation of AX improved lipid metabolic disorder and alleviated liver damage by activation of liver lipid catabolism and suppression of lipid peroxidation in rats [92].

2.4.3. Anticancer Effect. AX and AXOS have been investigated in order to explore their anticancer effects. The anticancer property of these polysaccharides on different types of cancer such as colon cancer, glandular stomach cancer, neuroblastoma, and liver cancer, among others, has been tested *in vivo*. According to the observations of the research done in the last 10 years, it is proposed that AX and AXOS may exert its anticancer effect through different mechanisms involving antioxidant, prebiotic, and immunomodulatory properties (Table 3).

The inhibition of growth of tumors in S180 tumor-bearing mice was significant when animals were administered with wheat bran AX. According to the results obtained in this study, it is suggested that AX exerts its antitumor activity via the improvement in immune response. The administration of AX enhanced the macrophage phagocytosis of chicken red blood cells (CRBCs) in tumor-bearing mice. The killing activity of NK cells from splenocytes in mice was increased, suggesting that AX could enhance the cytotoxic activity against spontaneously derived tumor cells. Moreover, AX treatment improved the production of IL-2 in blood serum of mice and subsequent proliferation of T cells, B cells, NK cells, and monocytes, increasing the cytotoxicity of T and NK cells. It is also proposed that the immunostimulating activity of AX may be related to the metabolism *in vivo* [16].

More recently, the chemopreventive activity of MGN-3/Biobran on glandular chemical induction of stomach carcinogenesis in rats was evaluated. The Biobran administration (40 mg/kg weight, 8 months) showed a significant reduction in the incidence of animals bearing dysplasia and adenocarcinoma. In addition, Biobran induced cancer cell apoptosis via cell cycle arrest of gastric cancer cells in the sub-G1 phase and also via the mitochondria-dependent pathway as indicated by upregulation of p53, Bax expression, downregulation of Blc-2, and an increase in Bax/Bcl-2 ratio. The authors suggest that the immunomodulatory effects of Biobran may represent another mechanism by which this agent suppresses the growth of adenocarcinoma [15].

2.5. Mechanisms Underlying the Anticancer and Antioxidant Effects of AX

2.5.1. Immune-Modulation. In the last years, research efforts have focused on elucidating the mechanisms by which AX

Table 3: Description of studies evaluating the anticancer potential of AX and AXOS, *in vivo*.

Type of cancer/animal model	Carcinogenic agent/ cancer cells	Dosage/experimental time	Findings	Reference
Solid Erlich carcinoma Female albino mice	Erlich ascites, carcinoma cells, and intramuscular inoculation	MGN-3/Biobran (25 mg/kg bw) ip Six times/week for 25 days at either day 4 or day 11 post-cancer cell inoculation.	MGN-3 suppressed the growth of tumors, normalized lipid peroxidation, and increased glutathione contents. Increased activity of endogenous antioxidant scavenging enzymes (superoxide dismutase, glutathione peroxidase, catalase, and glutathione-S-transferase) in blood, liver, and tumor tissue.	[19]
Colon carcinogenesis Male F344 rats	1,2,-Dimethylhydrazine (DMH), subcutaneous injection.	High-fat diet plus AXOS (48 g/kg). 10 days before receiving carcinogen and continued for 13 weeks.	Lower counts of preneoplastic lesions (mucin depleted foci (MDF)) in comparison to the control group. Fewer preneoplastic lesions (aberrant crypt foci (ACF)) in the distal part of the colon.	[17]
S180 tumor-bearing mice ICR male mice	Mouse sarcoma S180 cells, intramuscular inoculation.	AX orally administered (100, 200, and 400 mg/kg bw).	Administration of AX significantly inhibited the growth of mouse transplantable tumors and promoted thymus and spleen indexes, splenocyte proliferation, NK cell and macrophage phagocytosis activity, and IL-2 production. Increased peripheral leukocyte count and bone marrow cellularity.	[16]
Neuroblastoma NOD-scid IL-2Rgnull mice	Injection of NB1691luc cells.	NK cells activated with 100 μg/mL MGN-3/ Biobran injected intravenously. 7 days after injection of tumor cells and performed twice a week for 4 weeks.	Significant inhibition of neuroblastoma growth and improvement in survival in the group treated with Biobran. Increase in the activation-associated receptors CD69 and CD25 on NK cells.	[93]
Glandular stomach carcinogenesis. Male Wistar rats	Methylnitrosoguanidine (MNNG), via oral gavage.	MNNG plus Biobran (40 mg/kg bw) every other day via oral gavage. 8 months	Biobran reduced incidence of animals bearing gastric dysplasia and adenocarcinoma. Decrease in expression of tumor marker Ki-67 and increase in the level of apoptotic gastric cancer cells via cell cycle arrest (sub-G1) and mitochondria-dependent pathway. Protection against lymphocytopenia.	[15]
Hepatocarcinogenesis. Male albino rats	N-nitrosodiethylamine (NDEA) and carbon tetrachloride (CCl_4).	MGN-3/Biobran (25 mg/kg bw), 5 times/week ip 2 weeks prior to receiving carcinogen and continued for 20 weeks.	Reduction in liver tumor incidence, decrease of preneoplastic foci in hepatic parenchyma, and inhibition of development of hepatocellular carcinoma. Regulation of AST, ALT, ALP, and gamma GT levels. Increase in cell cycle sub-G0/G1 population. Downregulation of expression of NF-κBp65 and Bcl2, upregulated p53, Bax, and caspase-3 and increased the Bax/Bcl-2 ratio.	[94]

bw: body weight; ip: intraperitoneal; AST: serum aspartate aminotransferase; ALT: alanine aminotransferase; ALP: alkaline phosphatase; gamma GT: gamma glutamyl transpeptidase.

exerts its anticancer effects. In this regard, several studies have demonstrated that one of such mechanisms could involve the immune-modulation properties of AX.

It has been proposed that MGN-3/Biobran (AX from rice) exhibits its anticancer effects due to its ability to act as a biological response modifier (BRM). BRM are designed to activate the host immune response to destroy cancer cells [41]. Thus, Biobran has demonstrated to improve the activities of different arms of the immune system to attack cancer cells (Figure 3). Biobran improves the reactivity of cells with anticancer activity such as NK cells and CD8+ T cells and modulates the production of certain cytokines such as interferon-gamma (IFN-γ), -lambda (IFN-λ), IL-2, and IL-12 [41]. The basis of the mechanism behind the immune

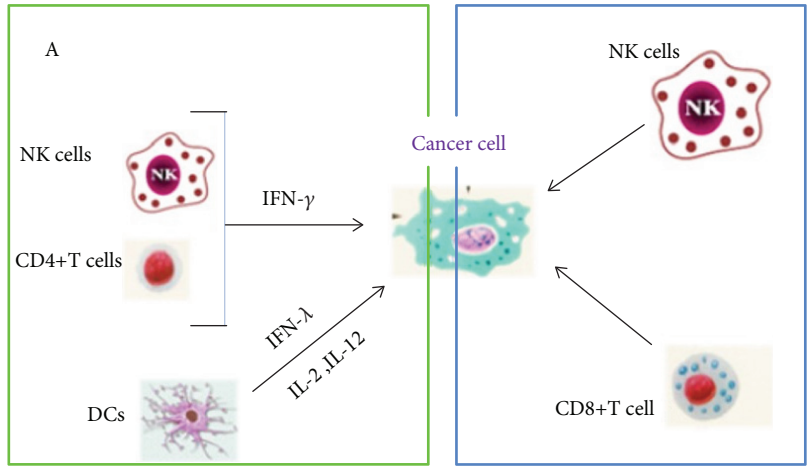

Figure 3: MGN-3/Biobran enhances the cytotoxicity reactivity of immune cells with anticancer effect and the production of certain cytokines (adapted from [41]).

modulatory effects of Biobran is not completely elucidated. However, it is proposed that these AX are hydrolyzed in order to reduce its MW so they can diffuse through intestinal walls or directly into the blood stream and then be transported to the lymph nodes where immune cells reside [95, 96].

NK cells play an important role in the natural defense of the immune system against cancer and viral infections [93]. These cells work by attaching to cancer cells and releasing their granules which form holes causing cell death [41]. AX has the ability to increase the cytotoxicity activity of NK cells as confirmed by several *in vitro* and *in vivo* studies [16, 93]. Dendritic cells (DCs) are important antigen-presenting cells (APCs) involved in generating antitumor immune response. Biobran upregulates CD80 and CD86 which are molecules expressed on mature DCs. This stimulation promotes the production of proinflammatory and immune-regulatory cytokines. It is proposed that Biobran could bind to the cell surface receptors (TLRs and/or C type lectins) or to intracellular receptors (NLRP3 inflammasome) and trigger signaling pathways involved in cell activation and cytokine production [41].

A recent study evaluated the potential capacity of Biobran to activate and improve the cytotoxicity of NK cell activity against neuroblastoma *in vitro*, using several pediatric cell lines (acute leukaemia, neuroblastoma, Ewig sarcoma, embryonic rhabdomyosarcoma, and alveolar rhabdomyosarcoma) and *in vivo* (NOD/scid/IL-2Rγnull neuroblastoma model) [93]. The stimulation of NK cells with Biobran resulted in a higher expression of the activation-associated receptors CD25 and CD69 than in unstimulated cells. In addition, the stimulation increased NK cell cytotoxicity against cancer cell lines and reduced the neuroblastoma growth *in vivo*. Several mechanisms are proposed in order to explain how Biobran could stimulate NK cell activity. One of those theories establishes an apoptotic effect mediated by the activation of NK cells releasing TNF-α and IFN-γ [75]. Other mechanisms could be related with the increasing of activating receptors on Biobran-stimulated NK cells. The authors observed an increase in the activation-associated receptor CD69 and CD25 on stimulated NK cells. The increase of CD69 is associated with a higher cytotoxicity of NK cells, while CD25 expression on NK cells is indicative of proliferation potential [97, 98]. NK cells attack cancer and viral cells through the release of their granules that cause cell death. In this regard, Biobran treatment increases the granular content (perforin and granzyme) of NK cells favoring its activity against malignant cells [99]. In addition, the treatment with Biobran helps NK cells to attach cancer cells [41].

AX can stimulate the production of interleukins such as cytokines IL-2 and IL-12 which are the main anticancer cytokines in humans [41]. In S180 tumor-bearing mice, the treatment with AX led to an increase in the secretion of IL-2 in the blood of mice. It is postulated that increase of IL-2 may be a mechanism for AX to exert antitumor effects, as IL-2 can improve the proliferation of T cells, B cells, NK cells, and monocytes and increase the cytotoxicity of T cells and NK cells [16, 100]. In addition, the ingestion of Biobran increased the production of IL-12 in multiple myeloma patients at one and two months post-ingestion [101].

AX can induce the production of TNFs (IFN-λ and IFN-γ) which have been found to exhibit antitumor activity [75, 101, 102]. In a previous study, the oral administration of partially hydrolyzed AX from corn husk to mice increased the production of IL-2 and IFN-γ and slightly increased IL-4 in mitogen-induced proliferation spleen cells. In addition, an increase in the activity of NK cells in spleen cells from transplanted-tumor mice was observed [102]. T helper 1 (Th1) promotes antitumor immunity through the production of IL-2 and IFN-γ, which activates NK cells to attack cancer and virus-infected cells [103]. In this study, the administration of AX also decreased ear inflammation of a model mouse of atopic dermatitis. According to the results obtained, it is suggested that the anti-inflammatory effect of AX is attributed to the activation of an IFN-γ-dependent Th1-like immune response in mice. In another study, multiple myeloma patients presented an increase of IFN-γ at two months post-treatment with MGN-3 [101].

T regulatory lymphocytes (T reg) or CD4+CD25+ lymphocytes act by suppressing the antitumor cytotoxic immune response [104]. In this regard, it is proposed that the counteracting of T reg cell activity could interfere in a positive way

with the progression of neoplastic diseases by improving the efficacy of the anticancer immune response [41]. AX from rice was given orally to 22 patients with solid tumor for two months. The results showed an increase in TH cells, while T reg cells decreased, but the differences were not statistically significant. On the contrary, the TH/T reg ratio significantly enhanced after AX therapy [40].

2.5.2. Induction of Apoptosis. Induction of apoptosis appears to be another mechanism by which MGN-3/Biobran may exert its anticancer effects. *In vivo* studies evaluated the effect of Biobran on mice bearing a SEC tumor as well as in chemically induced glandular stomach adenocarcinoma rats. According to the results observed in those experiments, the anticancer activity exhibited by Biobran was explained through a mechanism via induction of apoptosis.

The administration of Biobran in mice bearing a SEC tumor caused a significant delay in the volume and weight of the tumor in comparison to the control. The authors proposed that the antitumor activity of Biobran was related to its ability to induce apoptosis and immune modulation. The intraperitoneal treatment of Biobran on mice increased the number of apoptotic SEC cells. Moreover, cytokine production was influenced by increasing the levels of tumor necrosis factor-α and IFN-γ, while a downregulation of the immune suppressing cytokine IL-10 was observed. In addition, a considerable increase in NK cell activity was observed in mice treated with Biobran [75]. Biobran can cause tumor regression by the induction of cancer cell apoptosis via its immunumodulatory effects on NK cells and cytokine production. It is known that NK cells kill cancer cells by different pathways, and one of those involves the ligation of FasL to its Fas receptor to induce apoptosis [105]. It is also possible that Biobran could exert its apoptotic effect via the increase of TNF-α and IFN-γ. In this regard, both TNF-α and IFN-γ have been shown to act synergistically to induce cancer cell death through apoptotic and necrotic effects [106, 107].

Recently, the chemopreventive activity of Biobran against chemical induction of glandular stomach carcinogenesis in rats was associated with the ability of Biobran to induce apoptosis via the mitochondrial-dependent pathway in gastric cancer cells [15]. Biobran treatment caused a significant reduction in the incidence of animals bearing gastric dysplasia and adenocarcinoma in comparison to the untreated group. The upregulation in p53 expression, Bax expression, downregulation in Bcl-2 expression, the increase in Bax/Blc-2 ratio, and the activation of caspase-3 as well as the induction of cell-cycle arrest in the sub-G1 phase may explain the mitochondria-dependent pathway as the mechanism involved in the anticancer effect observed in the present study. Changes in p53, Bax, and Bcl-2 can alter the outer mitochondrial membrane and subsequent release of cytochrome C, which finally activates caspase-3. In this regard, Biobran has shown to induce apoptosis via activation of caspase-8, -9, and -3 [108]. Although the mechanism by which Biobran exerts its apoptotic effect is not completely elucidated, it could be related to the capacity of Biobran to sensitize the surface CD95 receptor that is involved in the triggering of apoptosis [109]. On the other hand, another possible mechanism by which Biobran suppresses the growth of tumor could be related to its immunomodulatory properties. It was observed that treatment with Biobran protected against chemical-induced lymphocytopenia in rats. Lymphocytes are white blood cells which are part of the immune system [15].

2.5.3. Antioxidant. AX has been found to exert antioxidant effects through the modulation of lipid peroxidation, promoting the antioxidant defense system and protecting against oxidative stress [19]. Although the mechanisms behind the antioxidant property of AX are not fully understood, some studies suggest that its capacity to increase the activity of endogenous antioxidant enzymes, suppress lipid peroxidation, and induce apoptosis could be involved in such mechanisms [19, 92]. The antioxidant activity of AX has been related to its capacity to exert anticancer effect, improve lipid metabolic disorder, and alleviate liver damage in rats.

Noaman et al. [19] evaluated the antioxidant activity as a possible mechanism of Biobran to exert its antitumor potential on mice inoculated with Erlich ascites carcinoma (EAC) cells. Biobran administration suppressed tumor growth by normalizing the lipid peroxidation level and augmentation of glutathione (GSH) contents. In addition, the expression and activity of endogenous antioxidant scavenging enzymes (superoxide dismutase, glutathione peroxidase, catalase, and glutathione-S-transferase) in the cells of normal and tumor-bearing animals were increased in blood, liver, and tumor tissue. The ability of Biobran to induce apoptosis was proposed as the mechanism by which it could exert those antioxidant effects. Reactive oxygen species (ROS) act as signaling molecules for the initiation and execution of apoptosis. GSH and thioredoxin not only regulate ROS levels but could act as reversible redox modifiers of enzyme function [110]. In this regard, higher levels of GSH content in tissues of mice treated with Biobran were observed in comparison to the untreated mice. Among other functions, glutathione-S-transferase enzymes detoxify carcinogens [111]. This also could be a possible mechanism for Biobran to prevent cancer as elevated levels of such enzymes were observed in mice treated with Biobran.

The antioxidant capacity of AX has been also related to the improvement of metabolic disorder and alleviate liver damage in rats induced by high-fat diet [92]. Lipid peroxidation is one of the most common free radical chain reactions that causes oxidative damage [112]. In this study, mice fed with a high-fat diet presented an increase in serum and tissue oxidative stress and subsequent reduction of the antioxidant enzymes glutathione peroxidase and total superoxide dismutase as well as an increase in malondialdehyde level. On the contrary, supplementation of AX in high-fat diet catalyzed the dismutation of the superoxide (O_{-2}) radical into either molecular oxygen (O_2) or hydrogen peroxide (H_2O_2) by the promotion of total superoxide dismutase. In addition, the increase in glutathione peroxidase activity reduced lipid hydroperoxides [92]. On the other hand, AX supplementation could alleviate damage liver morphology by regulating the liver cell apoptosis through the modulation of the expression of proapoptotic and antiapoptotic proteins, Bax and Bcl-

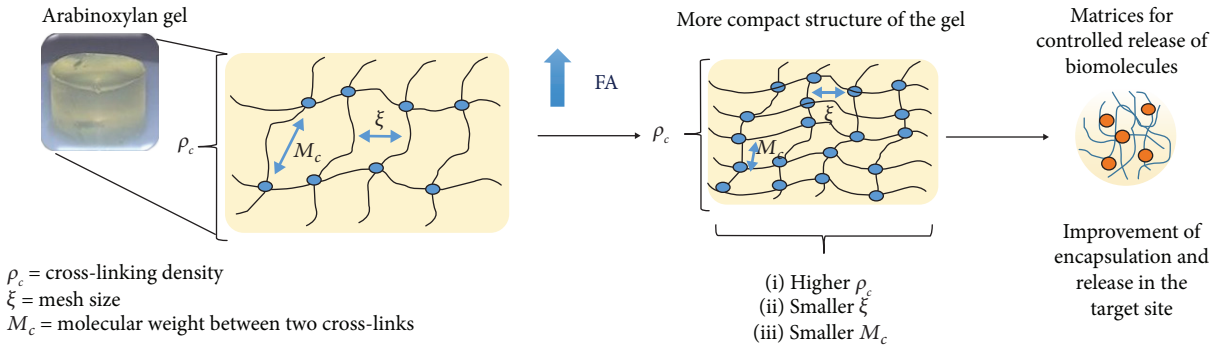

Figure 4: Structural parameters of ferulated AX gels.

2. Moreover, Biobran has the ability to change the lipid metabolism by regulating the expression of UCP2, a mitochondrial membrane protein that works by accelerating the fatty acid β-oxidation and minimizing the production of reactive oxygen species [113]. These results may suggest that Biobran improved lipid catabolism and protected liver damage via an antioxidant mechanism.

3. Arabinoxylan Gels

3.1. Structural Parameters. The structural characteristics of the AX gels can be measured as a function of the determination of different parameters. The cross-linking density (ρ_c), the mesh size (ξ), and the molecular weight between cross-links (M_c) can be calculated by the determination of the swelling ratio of the gels [84] (Figure 4). These parameters allow to elucidate how the cross-linking between the AX chains could occur during the gel formation. Therefore, the knowledge of such structural characteristics is determinant to understand the gel properties and thus their possible applications.

The content of FA in AX is an important factor affecting the gel structure. Table 4 shows the structural parameters and the FA content of maize and wheat AX gels at 2% (*w*/*v*). Usually, the increase in the FA content results in a decrease in mesh size and the molecular weight between cross-links, as well as an increase in the cross-linking density. This behavior results in the formation of gels with a more compact structure [9, 25, 84] (Figure 4). Gels with a compact structure are suitable for potential applications in the controlled release of biomolecules because they provide a better encapsulation and ensure the release of biomolecules in the site of interest.

The swelling ratio (q) indicates the amount of water that can be absorbed by the gel inside its tridimensional network. Martínez-López et al. [9] observed that when the AX concentration increased from 4 to 6% (*w*/*v*) in the gel, the q value decreased from 18 to 9 g water/g AX. Similar results have been reported by other authors [33, 84]. The results are explained in terms of a higher concentration of AX in the gel, which involves a high amount of FA, and it is related with a more compact polymeric structure that limits the water absorption capacity. In contrast, gels with lower polymer concentrations present higher q values due to a decrease in the covalent cross-links (di-FA and tri-FA). This decrease is attributed to longer uncross-linked chain sections in the gel, which facilitate its expansion, leading to high water absorption [114, 115].

Table 4: Structural parameters of AX gels at 2% (*w*/*v*).

Origin of AX	$M_c \times 10^3$ (g/mol)	ξ (nm)	$\rho_c \times 10^{-6}$ (mol/cm^3)
Wheat (2 μg AF/mg AX)[a]	119	201	14
Maize (6 μg AF/mg AX)[b]	34	96	67

[a][85]. [b][25].

The knowledge of the structural characteristics of the gel allows proposing different applications according to its functional properties. In this sense, we can take advantage about the quite relationship between the polysaccharide characteristics and the structural parameters of the gel (ξ, M_c, and ρ_c). This information can help to predict the gel structure and thus consider it for specific applications.

3.2. Microstructure. The microstructure of the AX gels has been studied by different microscopy techniques, with scanning electron microscopy (SEM) being the most used. The SEM micrographs have permitted a thorough understanding about the network of the AX gels. Several reports agree that lyophilized AX gels exhibit an imperfect honeycomb-like structure (Figure 5) [25, 35, 116]. This structure is mainly attributed to the polysaccharide characteristics. Although such structure could be established as a pattern for the gel networks, certain factors such as the molecule characteristics, structural parameters of the gel, or even the methods used prior to the analyses could affect the microstructure of these gels.

AX gels are characterized for presenting a porous and heterogeneous structure. However, depending on the polysaccharide characteristics, gels with different morphologies can be obtained. In SEM images, Martínez-López et al. [117] observed that maize bran AX gels showed an irregular honeycomb structure, while the nejayote AX gels appeared as a mix of sheets and rigid plates. The method used for freezing prior to the freeze drying process is another important factor affecting the gel microstructure. A rapid freezing (nitrogen immersion) of the gel results in the formation of smaller pores, compared to those obtained when using a slow freezing method [116, 118]. The freezing rate affects the quality of the frozen material, particularly those containing high

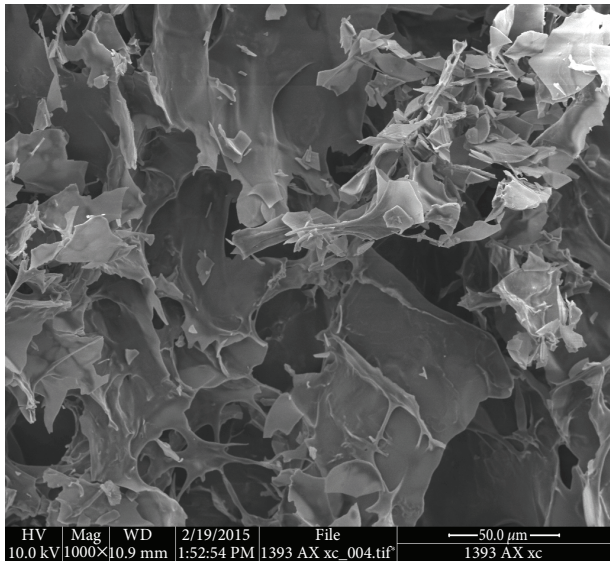

Figure 5: SEM image of the microstructure of lyophilized AX gel from maize at 1000x.

amounts of water such as gels [118]. Therefore, a fast freezing results in a better-preserved structure of the gels.

Martínez-López et al. [119] evaluated the microstructure of AX microspheres by SEM. The microsphere's morphology presented a heterogeneous network, with irregular pore sizes and geometries, similar to those reported for other micro gels. In addition, the authors reported the presence of clusters of interconnected nodular structures. These clusters resulted in the formation of small pores (10–70 nm), while the binding between clusters led to a macroporous structure. The authors explain that the pore size of the gels formed via phenolic acid cross-linking is determined by the presence of nodular conglomerates.

The microstructural analysis of the gel provides a thorough understanding about the morphological characteristics of this material. Among other aspects, this analysis permits to study the conformation of the gel obtained as a result of the interactions between the polysaccharide chains. In this regard, the knowledge of the microstructural characteristics of the gel allows establishing a relationship between the morphology of the gel and its functional properties.

3.3. Viscoelastic Characteristics. The viscoelastic characteristics of AX can be studied by small-amplitude shear oscillatory rheology. The rheological analysis allows identifying the nature of a viscoelastic material, as well as the rheological behavior of the gel formed. The gelation ability of AX depends on the concentration of the polysaccharide, the Mw, the substitution degree, and particularly, the content of FA [26, 48].

The AX gels present a typical kinetic of a solid-like material. The kinetic of gelation of AX exhibits a rapid increase in the elastic modulus (G'), followed by a stability region, known as *plateau* [26] (Figure 6(a)). This behavior is due to the formation of covalent cross-links between the FA residues of the AX chains. The formation of cross-links in sufficient quantity limits the movement of the polysaccharide chains and leads to the formation of new cross-links. On the other hand, the mechanical spectrum for AX shows a behavior of a typical solid-like material with a linear G'-independent of time and a G'' much smaller than G' and dependent of time [25, 84, 117] (Figure 6(b)).

Higher contents of FA result in the formation of stronger gels. Méndez-Encinas et al. [25] obtained stronger AX gels ($G' = 687$ Pa) than Carvajal-Millan et al. [85] ($G' = 44$ Pa), with a FA content of 6.05 and 2.3 μg/mg AX, respectively, and using similar polysaccharide concentrations. The latter shows the impact of the FA content on the rheological properties of the gels.

3.4. Functional Properties

3.4.1. Encapsulating. One of the most interesting properties of AX gels is their ability to encapsulate different agents. Several knowledge areas, such as the pharmaceutical, food, and medical, have special interest in investigating the encapsulating capacity of these gels. The research done on this respect ranges from the encapsulation of biomolecules and pharmaceuticals to cells (yeast and bacteria) [33, 37, 85, 86, 120]. The results have been quite promising, which has led to further research in this area.

In previous studies, Vansteenkiste et al. [86] evaluated the entrapment of a model protein (bovine serum albumin (BSA)) in AX gels and their protective effect against pepsin proteolysis and heating. The results indicated that the AX gel protected the embedded protein against enzymatic hydrolysis and also protected against heat.

Carvajal-Millan et al. [85] studied the capacity of AX gels with different FA contents to load model proteins. The results showed that the total protein loaded in the AX gels decreased as the concentration of AX in the gel increased. The authors proposed this decrease was due to the presence of a more compact network resulting from higher ferulate cross-linking structures, which turn down the protein movement within the gel. These results indicate that the structural characteristics of the gel affect its loading capacity, which in turn could also be true to proteins, other biomolecules, and even cells.

Regarding the medicine field, the search for, and the development of, novel encapsulating agents for the entrapment of probiotics has been of growing interest. Morales-Ortega et al. [37] evaluated the entrapment of bacteria (*B. longum* and *B. adolescentis*) in AX gels. The study showed the bacterial cells entrapped inside the network of the AX gel, suggesting that AX gels can be potential candidates for use in the entrapment of probiotics and even other cells of interest.

The encapsulation of small molecules such as methyl xanthine (caffeine) has also been investigated, with excellent results. Iravani et al. [35] encapsulated caffeine in AX gels. In addition, these gels were subjected to acidic conditions (HCl 0.1 M) in order to simulate the gastrointestinal fluid. AX gels are stable to acidic conditions due to its dietary fiber nature. Therefore, they have been a focus of study for their application as colon-targeted controlled-release systems.

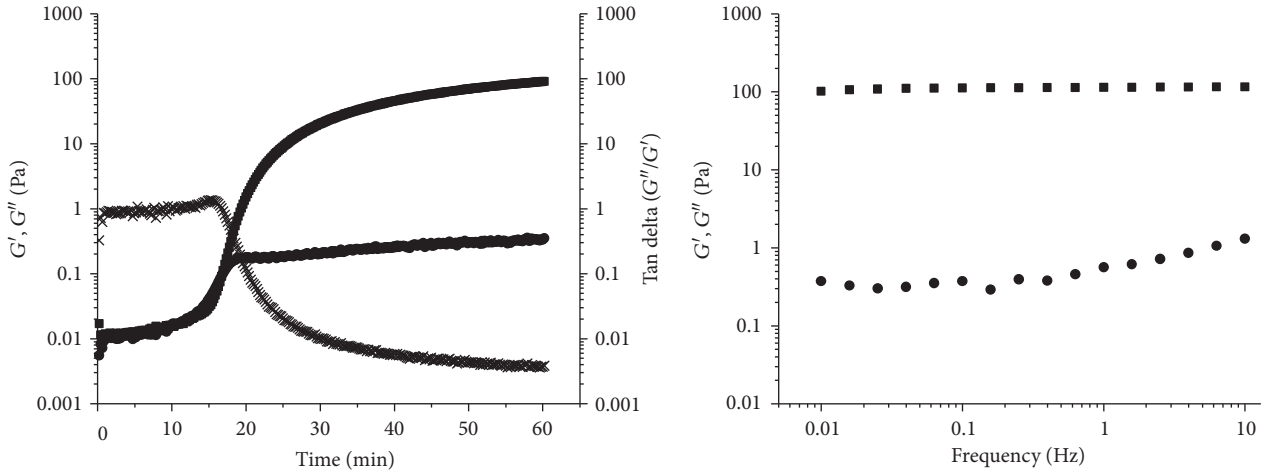

Figure 6: (a) Kinetic of gelation of AX solution (2% *w*/*v*) at 0.25 Hz and 5% strain (G'■, G''●, tan δ X) and (b) mechanical spectrum of the AX gel formed, registered at 5% strain (G'■, G''●).

3.4.2. Colon-Targeted Drug Delivery Systems. Polysaccharide-based matrices have been widely studied for their use as colon-targeted drug delivery systems. Most of the time, the use of a single polysaccharide does not permit a targeted release, so it is common to use the combining and modifying of polysaccharides. The variations in the pH and transit time in the gastrointestinal tract result in a premature or even absent drug release [24]. AX can form covalent gels, which are stable to temperature [88], pH, and ionic strength changes [7]. Thus, AX gels have been considered as excellent candidates for their potential application in colon-targeted drug delivery systems.

AX gels have shown ability for use in controlled release of biomolecules, as well as cells (Table 5) [33, 35, 36, 85]. Previous studies evaluated the controlled-release properties of AX gels using model proteins such as ovalbumin, β-lactoglobulin, and insulin [33, 36]. The study of Berlanga-Reyes et al. [33] showed that only 11–18% of the proteins (insulin and β-lactoglobulin, resp.) was released by the end of a 15 h *in vitro* test. The authors suggest that AX gels could be used as a carrier to protect the proteins from the gastric environment and assure their release at the colonic region where AX gels can be fermented by the microbiota.

Polysaccharide hydrogels are a good alternative for the protection and controlled release of proteins and peptides in the colon. These systems protect biomolecules from protease degradation in the gastrointestinal tract and assure its release in the target site. Chitosan and alginate are the most studied polysaccharides for the controlled release of molecules. Although chitosan has been widely used in drug delivery, its solubility in acidic conditions (<pH 6.0) limits its application in the intestinal tract (>pH 6.5) due to the early degradation and release of the molecule [122]. Covalent AX gels resist changes in pH [27], allowing their stability in the acidic conditions of the stomach and subsequent degradation in the colonic region by the microbiota [32].

Paz-Samaniego et al. [32] designed core-shell AX particles for the entrapment of insulin and probiotics (*Bifidobacterium*). The authors evaluated the degradation and release using a simulator of the gastrointestinal tract (Simgi). The encapsulation efficiency was 72 and 90% for insulin and probiotic, respectively. The results showed that only 24% of the insulin was lost before the particles reach the colon, while 76% of the protein was released in the colon region, mainly in the transverse section. In addition, an increase in the *Bifidobacterium* population was observed due to the fermentation of the particles by these bacteria in the colonic region. This study suggests that AX particles could be excellent candidates for the controlled release of insulin and probiotics in the colonic region as an alternative for the treatment of diabetes. A low percentage of insulin release (33%) has been reported for insulin-loaded chitosan gel nanoparticles in pH 6.8 phosphate buffer solution (intestinal conditions). Moreover, *in vivo* studies showed a low hypoglycemic effect in diabetes-induced rats administered with the nanoparticles indicating the poor drug release in the colon. These results were attributed to the insolubility of chitosan in neutral and alkaline media, affecting the degradation and subsequent release of insulin in the colonic region. Concerning the encapsulation efficiency, the authors reported an efficiency of 84% which was a higher value in comparison to that observed in the AX microspheres [32, 122]. These differences could be related to the electrostatic charges between insulin and chitosan which favored its association.

Calcium alginate gels are also widely used for the controlled release of biomolecules. Insulin-loaded alginate microspheres present good encapsulation efficiency from 65 to 79% [123] which is similar to that reported in AX particles (72%) [32]. However, high percentage of insulin release (above 75%) has been observed under acidic conditions (pH 1.2) [123], resulting in a poor release in the intestinal region. This behavior is a consequence of dissociation of ionic linkages which leads to a weaker gel and release of the molecule by diffusion [123]. Lower release percentages of

Table 5: Potential application of AX gels in controlled release of biomolecules and cells.

AX source	Biomolecule/cell	Potential controlled-release system	Reference
Wheat	Ovalbumin (Ov)	Ov-AX gels for entrapment and controlled release of proteins. 70–88% protein release as Ov/AX ratio increased (24 h *in vitro* test).	[36]
Maize bran	Insulin and β-lactoglobulin	AX gels for controlled release of proteins. 11–18% of protein release at the end of a 15 h *in vitro* test.	[33]
Maize bran	Lycopene	Lycopene/AX gels for controlled delivery of biomolecules. 3–4% lycopene release at the end of a 4 h *in vitro* test.	[121]
Maize bran	Methyl xanthine (caffeine)	AX microparticles. 10% of caffeine release at a 3 h *in vitro test* (0.1 M HCl).	[35]
Ispaghula (*Plantago ovata*) seed husk	Metronidazole hydrochloride (MH)	MH-loaded calcium gelled AX microspheres for extended drug delivery. 90% MH release at a 70–80 min *in vitro* test.	[43]
Maize bran	Insulin	AX microspheres as insulin carriers for colon-specific drug delivery. Insulin release in the colonic region of diabetic rats.	[34]
Maize waste water (nejayote) and maize bran	Insulin, *Bifidobacterium*	Core-shell AX particle (AX-insulin/AX-*Bifidobacterium*) for entrapment and delivery of insulin and probiotics targeted to colon for diabetes treatment. 76% insulin release in colonic region using a simulator of the gastrointestinal tract (Simgi).	[32]

molecules (10–24%) have been observed using AX gels [32, 35] which could assure the release of a higher content of the molecule in the target site.

Swelling behavior is an important characteristic of hydrogels for its application as controlled-release systems. Hydrophilic groups of the polymer network lead to water uptake, resulting in a swelled gel that favors the release of the entrapped molecule by diffusion [124]. However, this also could be a disadvantage when gels exhibit high degrees of swelling because of the complete release of the molecule before reaching its target site. Swelling of alginate gels depends on the pH medium as they are sensible to ionic strength changes. In acidic conditions (pH 1.2), alginate gels have shown low swelling degrees, while in alkaline medium (pH 6.8–7.4) the swelling degree increases and then decreases abruptly because of the complete disintegration of the gel. In alkaline conditions, an ion exchange occurs between monovalent and divalent ions, resulting in the breakup of the gel network favoring swelling and subsequent degradation [124]. On the other hand, covalent AX gels resist pH changes so its swelling behavior is not affected by ionic charges. Among other factors, the swelling degree of AX depends on the content of FA as higher values of FA form higher content of cross-links leading to a more compact structure. The more compact the structure of the gel network, the less the capability of the gel to absorb water [25]. Thus, the swelling behavior of gels affects directly in drug release. In this regard, the percentage of drug (celecoxib) released from alginate gels in acidic medium was near 25%, while in alkaline conditions a complete release was observed at 8 h [124]. Similar values were reported for AX gels where 24% of insulin was released in stomach conditions, while 75% was released in the colon [32].

Iravani et al. [35] encapsulated methyl xanthine in AX gels and evaluated its release under acidic pH (HCl 0.1 M) in order to predict the behavior of the gels in the gastrointestinal tract. The results indicated that only 10% of caffeine is released at the beginning of a 3 h test. This suggests that a minimum of active molecules would be released in the stomach, while the rest of the drug could be dissolved later in the colon.

Recently, studies performed *in vivo* confirmed that insulin encapsulated in AX gels can be released into the colon [34]. In this study, insulin encapsulated in AX gels was administered to diabetic rats. The results showed a decrease in blood glucose levels, which suggest that insulin was released and absorbed in the colon of rats and maintains its functionality. The above results confirm that AX gels can transport the hormone through the gastrointestinal tract to the colon and to release it at this point, so they could be used as carriers for colon-specific drug delivery.

3.4.3. Prebiotics. AX can be degraded by the colonic microbiota; however, the gelling process involves the cross-linking of the polysaccharide. Therefore, when discussing about the use of AX gels as colon-specific drug delivery systems, it is important to understand the impact of the gelling process on its degradation by the colonic microbiota. In this regard, an efficient release of the administered drug in the target site will depend on the capacity of the intestinal microbiota to ferment the gels.

A combination of several specific enzymes is necessary for the complete degradation of AX (Figure 7). Among the main enzymes participating in its degradation are endo-1-4-β-xylanases (commonly called xylanases) which cleave the xylose backbone randomly to shorter fragments and β-xylosidases that attack the nonreducing ends of the xylose

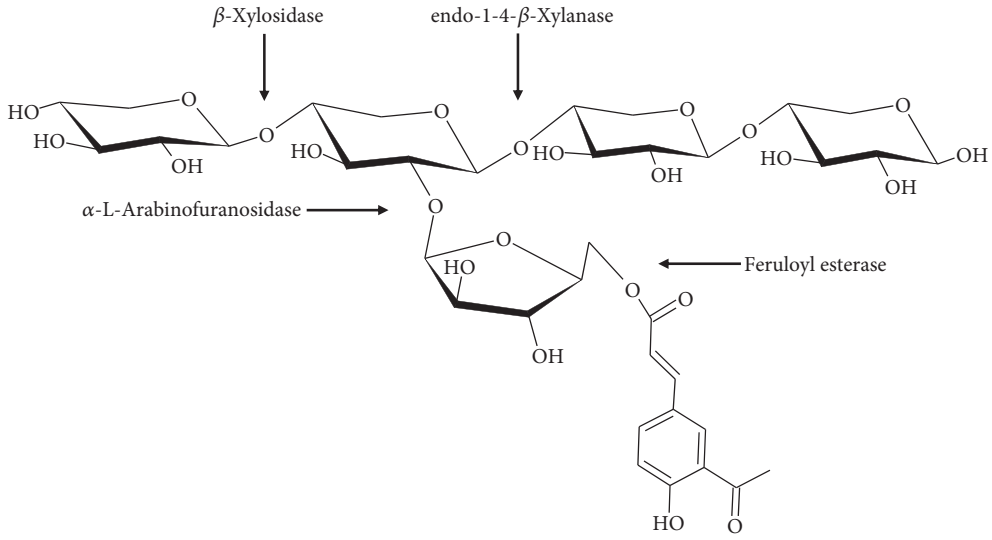

Figure 7: Sites of action of enzymes involved in AX degradation.

chain [125]. Other enzymes as α-L-arabinofuranosidades detach the arabinose residues from the xylan backbone, while FA esterases are needed to release the FA residues from AX [12]. The combination of these enzymes results in the transformation of AX to shorter fragments known as AXOS [12]. AX and AXOS degradation exhibits a bifidogenic effect by the increase of the *Bifidobacterium* population [12, 39].

The cross-linking of AX reduces the fermentation rate in comparison with the non-cross-linked molecule. The cross-links limit the access of bacterial enzymes for degrading the xylose chain. In addition, the cross-linking promotes a selective degradation, limiting the growth of *Bacteroides*. This bacterial genus does not produce the endoxylanases necessary to degrade the xylan chain, resulting in the incomplete degradation of the polysaccharide and therefore in a limited growth of these bacteria. In this regard, the selective degradation limits the growth of bacteria that are not considered beneficial at all, but it may favor the growth of bacteria that are so [10].

In a recent study, the ability of AX gels to modulate the gut microbiota and lipid metabolism in high-fat diet-induced obese rats was evaluated. The results showed that administration of a high-fat diet with AX gels increased the levels of *Bifidobacteria* and decreased those of *Bacteroides* in comparison with the high-fat diet and control groups. Moreover, the addition of AX to high-fat diet resulted in smaller adipocytes in comparison with the control and high-fat diet groups as was observed by histological analyses of the subcutaneous adipose tissue. These findings suggest the potential prebiotic properties of AX gels by the modulation of microbiota and antiobesity effect in high-fat diet-induced obese rats [126].

Recently, the degradation of AX gels at different concentrations (4 and 6% *w*/*v*) was compared. In this study, a slower degradation in the gels of higher concentration was observed. The authors explained this behavior was attributed to the higher cross-linking density of the gels, which results in a more compact structure and limits the access for the enzymes [9]. In this regard, it can be suggested that although a high cross-linking density decreases the fermentation rate of the AX gels, this can favor the growth of probiotic bacteria. Since the AX gels present potential prebiotic activity, they also could exhibit beneficial effects (possibly anticancer) due to the positive effects of their fermentation products (SCFA) and the increase of probiotic bacteria. Thus, the AX gel application as a colon-targeted drug delivery system would be highly possible, which would also exert effects with anticancer properties.

3.4.4. Antioxidant. The antioxidant activity of the AX has been extensively related with their FA content. Nevertheless, only few studies have explored the effect of the oxidative gelation of AX regarding this property. Although the gelling of AX involves the oxidative coupling of FA, the cross-links could be affecting in some way the antioxidant activity of the AX.

It is known that the structural features of AX affect the fermentability of AX, and therefore, it will also impact its antioxidant capacity. The fermentation patterns of AX and cross-linked AX differs in how the bacterial enzymes can degrade the molecule. In AX, α-arabinofuranosidades begin with the detaching of the arabinosyl moieties and subsequent fermentation of the available xylose chain. On the contrary, in AX gels the arabinose moieties are firstly utilized and even when the side branches are removed, the arabinose residues are preferred over the xylan chain. This behavior is because the gel-like structure restricts the access of xylanolytic enzymes to their target sites and the xylan backbone becomes more resistant to fermentation [10]. In AXOS, the presence of FA esterified to arabinose results in a steric effect that limits the access of arabinofuranosidases to their target sites and also slows down the activity of FA esterases, leading to a decrease of the degradation and subsequent fermentation of the molecule [20].

It has been demonstrated that the presence of FA and di-FA in cereal brans can be released by FA esterases present in the gastrointestinal tract (intestinal mucosa and microbiota)

of humans and rats [127]. In this way, probiotics present in the colonic microbiota, such as *Lactobacillus* and *Bifidobacterium*, are able to produce FA esterases, enzymes required for the release of the FA moieties from AX and AXOS [21, 55, 56]. A previous study showed that the presence of two *Bifidobacterium* strains (*B. longum and B. adolescentis*) is required for the fermentation of maize bran AX gels [9]. Therefore, even if some bacteria produce the specific enzymes to release the FA moieties in AX gels, the cross-feeding between different bacteria producing different enzymes is highly needed for the complete degradation of AX and AX gels.

The antioxidant capacity of phenolic acids depends on uptake and further metabolism [127]. Once the FA is released, it is then metabolized by the intestinal microbiota. The FA can be transformed into phenylpropionic acids and/or vinyl phenol derivatives, which still exert certain antioxidant capacity but in a lower extent than FA. According to this, it could be stated that the metabolism of FA by bacteria will lead to a decrease in its antioxidant capacity as has been demonstrated by Snelders et al. [20]. In this study, AXOS with FA esterified to arabinose exhibited good antioxidant capacity; however, the release and subsequent metabolization of FA decreased its antioxidant capacity. The authors suggested that AXOS-bound FA will reach the colon, where FA can be released and then metabolized by FA esterases located in this region [20]. In the colonic region, FA (bound or free) as well as its metabolites can exert its antioxidant activity through a direct interaction with the colon epithelium cells and thus reduce colorectal cancer [128]. On the other hand, the absorption of di-FA from cereal bran in the gut and its subsequent reach to the vascular system was demonstrated in rats [127]. These compounds also exhibit good antioxidant capacity and may exert its beneficial effects in the colonic region as they can interact directly with the intestinal barrier.

Previous studies have shown that not only the level of FA but also the condition under which it appears (free, bond, or dimerized) impacts the antioxidant capacity of AX [129]. The presence of dimers and trimers (di-FA, tri-FA) or more complex ferulated structures decreases the antioxidant capacity of AX in comparison to the FA molecule esterified to AX. The availability of hydroxyl groups and resonance systems of FA vary according to the cross-linking position and are important factors to exert the antioxidant function of FA [87]. Thus, it is confirmed that the gelling process impacts on the antioxidant capacity of the gels.

Several studies agree that the antioxidant activity of AX decreases after the gelation process due to the formation of di-FA and tri-FA [8, 119]. It is well documented that the formation of the AX gel involves the cross-linking of FA and consequently its oxidation. Nevertheless, the di-FA and tri-FA amounts produced during gelation do not compensate the FA oxidized. The remnant FA can continue to react and form higher ferulated structures [84]. Trimers and tetramers of FA have been identified in the cell wall of cereal grains, and even more complex ferulated structures are suggested [87]. Since the remaining FA could react and continue to form more complex structures, then it would be possible that such FA could keep stabilizing the free radicals and therefore exhibit antioxidant activity.

According to the above mentioned, the antioxidant activity of AX gels could be mainly related to the FA remaining after the gelation process. Thus, a higher FA content in AX gels may result in better antioxidant activity. AX with higher FA content (6 μg/mg AX) can form gels with high cross-linking density and still exhibit antioxidant activity [8]. In addition, these gels preserve high amounts of FA after their gelation [130], which would allow them to exert a greater antioxidant activity.

The antioxidant activity of AX gels depends on the polysaccharide structure. The content and appearance of FA in the gel are the main factors affecting such property. AX gels with high cross-linking density can exhibit antioxidant activity. In this logical order, since the anticancer activity of AX is related to its antioxidant activity, the AX gels could also exhibit this property. However, the evaluation of the anticancer activity of AX gels and its antioxidant property relationship is necessary. These findings could allow obtaining AX gels for colon-targeted drug delivery systems with protective effect against colon cancer.

Ferulated AX exhibit prebiotic and antioxidant properties, which confer anticancer potential to the polysaccharide. Since AX gels preserve their prebiotic and antioxidant properties, they would also exert antiproliferative activity. Furthermore, the high cross-linking density of the gels would increase such properties. In recent years, the investigation of the properties of AX gels has been the focus of numerous studies due to its potential application as colon-targeted drug delivery systems. In this regard, it is necessary to evaluate the effect of gelation on the antiproliferative activity of AX. Moreover, the relationship between the structural characteristics and the functional properties of the AX gels should be investigated, particularly the effect of the high cross-linking density of the gels on their antiproliferative activity. High cross-linking density AX gels could be a good alternative for the colon-targeted drug delivery in the treatment of colon cancer.

4. Conclusion

This review describes the functional properties of AX and AX gels and their potential application as antioxidant and anticancer agents. Ferulated AX have prebiotic, antioxidant, and anticancer properties which can be exploited by the pharmaceutical field. Recently, the research has focused in the development of novel colon-targeted delivery systems for the treatment of colon associated diseases, such as inflammatory bowel disease, irritable bowel disease, and particularly colon cancer. Due to their gelling ability, AX have gained interest as promising polysaccharides for the designing of drug delivery systems with bioactive properties such as prebiotic, antioxidant, and anticancer.

The antioxidant and prebiotic activity of AX has been previously demonstrated. The fermentation products of AX exhibit a prebiotic effect, providing benefits for the gut health. Moreover, its antioxidant activity exerts a protective effect against the free radicals and oxidative stress. Regarding the gelling ability of AX, specific studies are needed to elucidate such beneficial effects in the AX gels. The anticancer

activity of AX appears to be strongly related to its antioxidant and prebiotic properties. Future studies will be needed to evaluate the effect of gelation on the anticancer activity of AX gels. Furthermore, this information will allow establishing a relationship between the anticancer activity of AX with its antioxidant and prebiotic properties.

The AX gels are promising candidates for application as colon-targeted drug delivery systems for the treatment of colon cancer. However, only few studies regarding the evaluation of the antioxidant and prebiotic effect of AX gels have been conducted *in vitro*, and no evidence of *in vivo* data is available. Therefore, it is important to conduct research on the performance of *in vitro* and *in vivo* studies focusing on the effect of gelation on the biological properties (prebiotic, antioxidant, and anticancer) of AX and to elucidate the relationship between the properties of the gel by itself, not only as a mere carrier.

Conflicts of Interest

The authors declare that there is no conflict of interest regarding the publication of this article.

Acknowledgments

This research was supported by "Fondo Institucional CONACyT-Investigación en Fronteras de la Ciencia", México (Grant FON.INST./31/2016 to Elizabeth Carvajal-Millan). The authors are pleased to acknowledge Alma C. Campa-Mada, Karla G. Martínez-Robinson, and Alma R. Toledo-Guillén (CIAD, México).

References

[1] J. Slavin, "Why whole grains are protective: biological mechanisms," *Proceedings of the Nutrition Society*, vol. 62, no. 1, pp. 129–134, 2003.

[2] Y. Park, A. F. Subar, A. Hollenbeck, and A. Schatzkin, "Dietary fiber intake and mortality in the NIH-AARP diet and health study," *Archives of Internal Medicine*, vol. 171, no. 12, pp. 1061–1068, 2011.

[3] A. T. Kunzmann, H. G. Coleman, W. Y. Huang, C. M. Kitahara, M. M. Cantwell, and S. I. Berndt, "Dietary fiber intake and risk of colorectal cancer and incident and recurrent adenoma in the prostate, lung, colorectal, and ovarian cancer screening trial," *The American Journal of Clinical Nutrition*, vol. 102, no. 4, pp. 881–890, 2015.

[4] J. M. Lattimer and M. D. Haub, "Effects of dietary fiber and its components on metabolic health," *Nutrients*, vol. 2, no. 12, pp. 1266–1289, 2010.

[5] F. E. Ayala-Soto, S. O. Serna-Saldívar, S. García-Lara, and E. Pérez-Carrillo, "Hydroxycinnamic acids, sugar composition and antioxidant capacity of arabinoxylans extracted from different maize fiber sources," *Food Hydrocolloids*, vol. 35, pp. 471–475, 2014.

[6] R. K. Durham, "Effect of hydrogen peroxide on relative viscosity measurements of wheat and flour suspensions," *Cereal Chemistry*, vol. 2, no. 2, pp. 297–305, 1925.

[7] M. S. Izydorczyk and C. G. Biliaderis, "Cereal arabinoxylans: advances in structure and physicochemical properties," *Carbohydrate Polymers*, vol. 28, no. 1, pp. 33–48, 1995.

[8] R. Paz-Samaniego, M. Méndez-Encinas, J. M. Fierro-Islas et al., "Ferulated arabinoxylans recovered from low-value maize by-products: gelation and antioxidant capacity," in *Ferulic Acid: Antioxidant Properties, Uses and Potential Health Benefits*, W. Bryce, Ed., pp. 151–164, Nova Science Publishers, Hauppauge, Inc, 2015.

[9] A. L. Martínez-López, E. Carvajal-Millan, V. Micard et al., "*In vitro* degradation of covalently cross-linked arabinoxylan hydrogels by bifidobacteria," *Carbohydrate Polymers*, vol. 144, no. 1, pp. 76–82, 2016.

[10] M. J. Hopkins, H. N. Englyst, S. Macfarlane, E. Furrie, G. T. Macfarlane, and A. J. McBain, "Degradation of cross-linked and non-cross-linked arabinoxylans by the intestinal microbiota in children," *Applied and Environmental Microbiology*, vol. 69, no. 11, pp. 6354–6360, 2003.

[11] R. Paz-Samaniego, A. Rascón-Chu, F. Brown-Bojorquez et al., "Electrospray-assisted fabrication of core-shell arabinoxylan gel particles for insulin and probiotics entrapment," *Journal of Applied Polymer Science*, vol. 135, no. 26, article 46411, 2018.

[12] C. Grootaert, J. A. Delcour, C. M. Courtin, W. F. Broekaert, W. Verstraete, and T. van de Wiele, "Microbial metabolism and prebiotic potency of arabinoxylan oligosaccharides in the human intestine," *Trends in Food Science & Technology*, vol. 18, no. 2, pp. 64–71, 2007.

[13] A. M. Neyrinck, V. F. van Hée, N. Piront et al., "Wheat-derived arabinoxylan oligosaccharides with prebiotic effect increase satietogenic gut peptides and reduce metabolic endotoxemia in diet-induced obese mice," *Nutrition & Diabetes*, vol. 2, no. 1, pp. 1–9, 2012.

[14] J. Wang, B. Sun, Y. Cao, and C. Wang, "Wheat bran feruloyl oligosaccharides enhance the antioxidant activity of rat plasma," *Food Chemistry*, vol. 123, no. 2, pp. 472–476, 2010.

[15] N. K. Badr El-Din, S. M. Abdel Fattah, D. Pan, L. Tolentino, and M. Ghoneum, "Chemopreventive activity of MGN-3/Biobran against chemical induction of glandular stomach carcinogenesis in rats and its apoptotic effect in gastric cancer cells," *Integrative Cancer Therapies*, vol. 15, no. 4, pp. NP26–NP34, 2016.

[16] L. Cao, X. Liu, T. Qian et al., "Antitumor and immunomodulatory activity of arabinoxylans: a major constituent of wheat bran," *International Journal of Biological Macromolecules*, vol. 48, no. 1, pp. 160–164, 2011.

[17] A. P. Femia, M. Salvadori, W. F. Broekaert et al., "Arabinoxylan-oligosaccharides (AXOS) reduce preneoplastic lesions in the colon of rats treated with 1,2-dimethylhydrazine (DMH)," *European Journal of Nutrition*, vol. 49, no. 2, pp. 127–132, 2010.

[18] W. F. Broekaert, C. M. Courtin, K. Verbeke, T. van de Wiele, W. Verstraete, and J. A. Delcour, "Prebiotic and other health-related effects of cereal-derived arabinoxylans, arabinoxylan-oligosaccharides, and xylooligosaccharides," *Critical Reviews in Food Science and Nutrition*, vol. 51, no. 2, pp. 178–194, 2011.

[19] E. Noaman, N. K. Badr el-Din, M. A. Bibars, A. A. Abou Mossallam, and M. Ghoneum, "Antioxidant potential by arabinoxylan rice bran, MGN-3/biobran, represents a mechanism for its oncostatic effect against murine solid

Ehrlich carcinoma," *Cancer Letters*, vol. 268, no. 2, pp. 348–359, 2008.

[20] J. Snelders, H. Olaerts, E. Dornez et al., "Structural features and feruloylation modulate the fermentability and evolution of antioxidant properties of arabinoxylanoligosaccharides during in vitro fermentation by human gut derived microbiota," *Journal of Functional Foods*, vol. 10, pp. 1–12, 2014.

[21] D. Szwajgier and A. Jakubczyk, "Biotransformation of ferulic acid by Lactobacillus acidophilus K1 and selected Bifidobacterium strains," *ACTA Scientiarum Polonorum Technologia Alimentaria*, vol. 9, pp. 45–59, 2010.

[22] R. S. Govardhan Singh, P. S. Negi, and C. Radha, "Phenolic composition, antioxidant and antimicrobial activities of free and bound phenolic extracts of Moringa oleifera seed flour," *Journal of Functional Foods*, vol. 5, no. 4, pp. 1883–1891, 2013.

[23] A. Gulbake, A. Jain, A. Jain, A. Jain, and S. K. Jain, "Insight to drug delivery aspects for colorectal cancer," *World Journal of Gastroenterology*, vol. 22, no. 2, pp. 582–599, 2016.

[24] L. Zhang, Y. Sang, J. Feng, Z. Li, and A. Zhao, "Polysaccharide-based micro/nanocarriers for oral colon-targeted drug delivery," *Journal of Drug Targeting*, vol. 24, no. 7, pp. 579–589, 2016.

[25] M. Méndez-Encinas, E. Carvajal-Millan, M. Yadav et al., "Gels of ferulated arabinoxylans: rheology, structural parameters and microstructure," in *Advances in Physicochemical Properties of Biopolymers*, M. A. Masuelli and D. Renard, Eds., pp. 215–228, Bentham Science Publishers, Beijing, 2017.

[26] M. S. Izydorczyk and J. E. Dexter, "Barley β-glucans and arabinoxylans: molecular structure, physicochemical properties, and uses in food products–a review," *Food Research International*, vol. 41, no. 9, pp. 850–868, 2008.

[27] M. S. Izydorczyk and C. G. Biliaderis, "Arabinoxylans: technologically and nutrionally functional plant polysaccharides," in *Functional Food Carbohydrates*, C. G. Biliaderis and M. S. Izydorczyk, Eds., pp. 249–283, CRC Press, Boca Raton, FL, USA, 2007.

[28] M. M. Smith and R. D. Hartley, "Occurrence and nature of ferulic acid substitution of cell-wall polysaccharides in graminaceous plants," *Carbohydrate Research*, vol. 118, no. 1, pp. 65–80, 1983.

[29] M. R. Savitha Prashanth, R. R. Shruthi, and G. Muralikrishna, "Immunomodulatory activity of purified arabinoxylans from finger millet (Eleusine coracana, v. Indaf 15) bran," *Journal of Food Science and Technology*, vol. 52, no. 9, pp. 6049–6054, 2015.

[30] A. Morales-Burgos, E. Carvajal-Millan, Y. López-Franco et al., "Syneresis in gels of highly ferulated arabinoxylans: characterization of covalent cross-linking, rheology, and microstructure," *Polymers*, vol. 9, no. 12, 2017.

[31] M. S. Iqbal, J. Akbar, M. A. Hussain, S. Saghir, and M. Sher, "Evaluation of hot-water extracted arabinoxylans from ispaghula seeds as drug carriers," *Carbohydrate Polymers*, vol. 83, no. 3, pp. 1218–1225, 2011.

[32] R. Paz-Samaniego, E. Carvajal-Millan, N. Sotelo-Cruz et al., "Maize processing waste water upcycling in Mexico: recovery of arabinoxylans for probiotic encapsulation," *Sustainability*, vol. 8, no. 11, p. 1104, 2016.

[33] C. M. Berlanga-Reyes, E. Carvajal-Millán, J. Lizardi-Mendoza, A. Rascón-Chu, J. Marquez-Escalante, and A. L. Martínez-López, "Maize arabinoxylan gels as protein delivery matrices," *Molecules*, vol. 14, no. 4, pp. 1475–1482, 2009.

[34] A. L. Martínez-López, E. Carvajal-Millan, J. Lizardi-Mendoza et al., "Matrices covalentes biodegradables para el suministro de insulina por vía oral dirigida al colon activado por la microbiota y proceso para su obtención," México, Patente mexicana No. MX/a/2015/017857, 2016.

[35] S. Iravani, C. S. Fitchett, and D. M. R. Georget, "Physical characterization of arabinoxylan powder and its hydrogel containing a methyl xanthine," *Carbohydrate Polymers*, vol. 85, no. 1, pp. 201–207, 2011.

[36] E. Carvajal-Millan, S. Guilbert, J. L. Doublier, and V. Micard, "Arabinoxylan/protein gels: structural, rheological and controlled release properties," *Food Hydrocolloids*, vol. 20, no. 1, pp. 53–61, 2006.

[37] A. Morales-Ortega, E. Carvajal-Millan, F. Brown-Bojorquez et al., "Entrapment of probiotics in water extractable arabinoxylan gels: rheological and microstructural characterization," *Molecules*, vol. 19, no. 3, pp. 3628–3637, 2014.

[38] S. Zhou, X. Liu, Y. Guo, Q. Wang, D. Peng, and L. Cao, "Comparison of the immunological activities of arabinoxylans from wheat bran with alkali and xylanase-aided extraction," *Carbohydrate Polymers*, vol. 81, no. 4, pp. 784–789, 2010.

[39] A. M. Neyrinck, S. Possemiers, C. Druart et al., "Prebiotic effects of wheat arabinoxylan related to the increase in bifidobacteria, roseburia and bacteroides/prevotella in diet-induced obese mice," *PLoS One*, vol. 6, no. 6, p. e20944, 2011.

[40] P. Lissoni, G. Messina, F. Brivio et al., "Modulation of the anticancer immunity by natural agents: inhibition of T regulatory lymphocyte generation by arabinoxylan in patients with locally limited or metastatic solid tumors," *Cancer Therapy*, vol. 6, pp. 1011–1016, 2008.

[41] M. Ghoneum, "From bench to bedside: the growing use of arabinoxylan rice bran (MGN-3/Biobran) in cancer immunotherapy," *Austin Immunology*, vol. 1, no. 2, p. 1006, 2016.

[42] S. L. Ooi, D. McMullen, T. Golombick, D. Nut, and S. C. Pak, "Evidence-based review of BioBran/MGN-3 arabinoxylan compound as a complementary therapy for conventional cancer treatment," *Integrative Cancer Therapies*, vol. 17, pp. 1–14, 2017.

[43] C. J. Lee, C. S. Nah, C. S. Teng, W. W. Jun, and M. Saravanan, "Spray dried calcium gelled arabinoxylan microspheres: A novel carrier for extended drug delivery," *Chemical Papers*, vol. 69, no. 10, 2015.

[44] M. Hanif and M. Zaman, "Thiolation of arabinoxylan and its application in the fabrication of controlled release mucoadhesive oral films," *Daru Journal of Pharmaceutical Sciences*, vol. 25, no. 1, p. 6, 2017.

[45] M. Zaman, M. Hanif, and M. A. Khan, "Arabinoxylan-based mucoadhesive oral films of tizanidine HCL designed and optimized using central composite rotatable design," *Polymer-Plastics Technology and Engineering*, vol. 57, no. 5, pp. 471–483, 2018.

[46] C. Antoine, S. Peyron, F. Mabille et al., "Individual contribution of grain outer layers and their cell wall structure to the mechanical properties of wheat bran," *Journal of Agricultural and Food Chemistry*, vol. 51, no. 7, pp. 2026–2033, 2003.

[47] C. Barron, A. Surget, and X. Rouau, "Relative amounts of tissues in mature wheat (Triticum aestivum L.) grain and their

carbohydrate and phenolic acid composition," *Journal of Cereal Science*, vol. 45, no. 1, pp. 88–96, 2007.

[48] L. Saulnier, F. Guillon, P.-E. Sado, A.-L. Chateigner-Boutin, and X. Rouau, "Plant cell wall polysaccharides in storage organs : xylans (Food applications)," in *Elsevier Reference Module in Chemistry, Molecular Sciences and Chemical Engineering*, J. Reedijk, Ed., pp. 1–32, Elsevier Inc, Waltham, 2013.

[49] M. S. Izydorczyk and C. G. Biliaderis, "Effect of molecular size on physical properties of wheat arabinoxylan," *Journal of Agricultural and Food Chemistry*, vol. 40, no. 4, pp. 561–568, 1992.

[50] L. B. Bindels, N. M. Delzenne, P. D. Cani, and J. Walter, "Towards a more comprehensive concept for prebiotics," *Nature Reviews Gastroenterology & Hepatology*, vol. 12, no. 5, pp. 303–310, 2015.

[51] M. Vardakou, C. N. Palop, P. Christakopoulos, C. B. Faulds, M. A. Gasson, and A. Narbad, "Evaluation of the prebiotic properties of wheat arabinoxylan fractions and induction of hydrolase activity in gut microflora," *International Journal of Food Microbiology*, vol. 123, no. 1-2, pp. 166–170, 2008.

[52] S. Macfarlane, G. T. Macfarlane, and J. H. Cummings, "Review article: prebiotics in the gastrointestinal tract," *Alimentary Pharmacology & Therapeutics*, vol. 24, no. 5, pp. 701–714, 2006.

[53] J. M. W. Wong, R. de Souza, C. W. C. Kendall, A. Emam, and D. J. A. Jenkins, "Colonic health: fermentation and short chain fatty acids," *Journal of Clinical Gastroenterology*, vol. 40, no. 3, pp. 235–243, 2006.

[54] H. C. Lee, A. M. Jenner, C. S. Low, and Y. K. Lee, "Effect of tea phenolics and their aromatic fecal bacterial metabolites on intestinal microbiota," *Research in Microbiology*, vol. 157, no. 9, pp. 876–884, 2006.

[55] C. Nishizawa, T. Ohta, Y. Egashira, and H. Sanada, "Ferulic acid esterase activities of typical intestinal bacteria," *Food Science and Technology International*, vol. 4, no. 1, pp. 94–97, 1998.

[56] J. Ou and Z. Sun, "Feruloylated oligosaccharides: structure, metabolism and function," *Journal of Functional Foods*, vol. 7, pp. 90–100, 2014.

[57] K. E. Bach Knudsen, "Microbial degradation of whole-grain complex carbohydrates and impact on short-chain fatty acids and health," *Advances in Nutrition*, vol. 6, no. 2, pp. 206–213, 2015.

[58] A. Rivière, M. Selak, D. Lantin, F. Leroy, and L. de Vuyst, "Bifidobacteria and butyrate-producing colon bacteria: importance and strategies for their stimulation in the human gut," *Frontiers in Microbiology*, vol. 7, 2016.

[59] T. S. Nielsen, H. N. Lærke, P. K. Theil et al., "Diets high in resistant starch and arabinoxylan modulate digestion processes and SCFA pool size in the large intestine and faecal microbial composition in pigs," *British Journal of Nutrition*, vol. 112, no. 11, pp. 1837–1849, 2014.

[60] N. Yacoubi, F. van Immerseel, R. Ducatelle, L. Rhayat, E. Bonnin, and L. Saulnier, "Water-soluble fractions obtained by enzymatic treatment of wheat grains promote short chain fatty acids production by broiler cecal microbiota," *Animal Feed Science and Technology*, vol. 218, no. 1, pp. 110–119, 2016.

[61] P. Truchado, E. Hernandez-Sanabria, B. N. Salden et al., "Long chain arabinoxylans shift the mucosa-associated microbiota in the proximal colon of the simulator of the human intestinal microbial ecosystem (M-SHIME)," *Journal of Functional Foods*, vol. 32, pp. 226–237, 2017.

[62] M. Srinivasan, A. R. Sudheer, and V. P. Menon, "Ferulic acid: therapeutic potential through its antioxidant property," *Journal of Clinical Biochemistry and Nutrition*, vol. 40, no. 2, pp. 92–100, 2007.

[63] J.-C. Cheng, F. Dai, B. Zhou, L. Yang, and Z.-L. Liu, "Antioxidant activity of hydroxycinnamic acid derivatives in human low density lipoprotein: mechanism and structure-activity relationship," *Food Chemistry*, vol. 104, no. 1, pp. 132–139, 2007.

[64] J. J. Reiners Jr, R. Clift, and P. Mathieu, "Suppression of cell cycle progression by flavonoids; dependence on the aryl hydrocarbon receptor," *Carcinogenesis*, vol. 20, no. 8, pp. 1561–1566, 1999.

[65] C. A. Rice-Evans, N. J. Miller, and G. Paganga, "Structure-antioxidant activity relationships of flavonoids and phenolic acids," *Free Radical Biology & Medicine*, vol. 20, no. 7, pp. 933–956, 1996.

[66] A. Kolakowska and G. Bartosz, "Oxidation of food components: an introduction," in *Food Oxidants and Antioxidants. Chemical, Biological and Functional Properties*, G. Bartosz, Ed., pp. 1–17, CRC Press, Boca Raton, FL, USA, 2014.

[67] F. Shahidi and A. Chandrasekara, "Hydroxycinnamates and their in vitro and in vivo antioxidant activities," *Phytochemistry Reviews*, vol. 9, no. 1, pp. 147–170, 2010.

[68] S. Kamboj and V. Rana, "Physicochemical, rheological and antioxidant potential of corn fiber gum," *Food Hydrocolloids*, vol. 39, no. 1, pp. 1–9, 2014.

[69] J. Wang, B. Sun, Y. Cao, H. Song, and Y. Tian, "Inhibitory effect of wheat bran feruloyl oligosaccharides on oxidative DNA damage in human lymphocytes," *Food Chemistry*, vol. 109, no. 1, pp. 129–136, 2008.

[70] R. L. Prior, X. Wu, and K. Schaich, "Standardized methods for the determination of antioxidant capacity and phenolics in foods and dietary supplements," *Journal of Agricultural and Food Chemistry*, vol. 53, no. 10, pp. 4290–4302, 2005.

[71] P. Anand, A. B. Kunnumakara, C. Sundaram et al., "Cancer is a preventable disease that requires major lifestyle changes," *Pharmaceutical Research*, vol. 25, no. 9, pp. 2097–2116, 2008.

[72] A. Sudhakar, "History of cancer, ancient and modern treatment methods," *Journal of Cancer Science & Therapy*, vol. 1, no. 2, pp. i–iv, 2009.

[73] J. Qiao, Z. Liu, and Y. X. Fu, "Adapting conventional cancer treatment for immunotherapy," *Journal of Molecular Medicine*, vol. 94, no. 5, pp. 489–495, 2016.

[74] M. Glei, T. Hofmann, K. Küster, J. Hollmann, M. G. Lindhauer, and B. L. Pool-Zobel, "Both wheat (*Triticum aestivum*) bran arabinoxylans and gut flora-mediated fermentation products protect human colon cells from genotoxic activities of 4-hydroxynonenal and hydrogen peroxide," *Journal of Agricultural and Food Chemistry*, vol. 54, no. 6, pp. 2088–2095, 2006.

[75] N. K. Badr el-Din, E. Noaman, and M. Ghoneum, "In vivo tumor inhibitory effects of nutritional rice bran supplement MGN-3/biobran on Ehrlich carcinoma-bearing mice," *Nutrition and Cancer*, vol. 60, no. 2, pp. 235–244, 2008.

[76] M. Ghoneum and S. Gollapudi, "Synergistic apoptotic effect of arabinoxylan rice bran (MGN-3/biobran) and curcumin (turmeric) on human multiple myeloma cell line U266 in vitro," *Neoplasma*, vol. 58, no. 2, pp. 118–123, 2011.

[77] M. Ghoneum, N. K. Badr el-Din, D. A. Ali, and M. A. el-Dein, "Modified arabinoxylan from rice bran, MGN-3/biobran, sensitizes metastatic breast cancer cells to paclitaxel in vitro," *Anticancer Research*, vol. 34, no. 1, pp. 81–87, 2014.

[78] M. C. Figueroa-Espinoza and X. Rouau, "Oxidative cross-linking of pentosans by a fungal laccase and horseradish peroxidase: mechanism of linkage between feruloylated arabinoxylans," *Cereal Chemistry*, vol. 75, no. 2, pp. 259–265, 1998.

[79] T. Geissman and H. Neukom, "On the composition of the water-soluble wheat flour pentosans and their oxidative gelation," *Lebensmittel-Wissenschaft & Technologie*, vol. 6, no. 1, pp. 59–62, 1973.

[80] D. M. R. Georget, A. Ng, A. C. Smith, and K. W. Waldron, "Thermal characterisation of oxidatively cross-linked American corn bran hemicellulose," *Journal of the Science of Food and Agriculture*, vol. 79, no. 3, pp. 481–483, 1999.

[81] R. C. Hoseney and J. M. Faubion, "A mechanism of the oxidative gelation of wheat flour," *Cereal Chemistry*, vol. 58, no. 5, pp. 421–424, 1981.

[82] M. S. Izydorczyk, C. G. Biliaderis, and W. Bushuk, "Oxidative gelation studies of water-soluble pentosans from wheat," *Journal of Cereal Science*, vol. 11, no. 2, pp. 153–169, 1990.

[83] A. Ng, R. N. Greenshields, and K. W. Waldron, "Oxidative cross-linking of corn bran hemicellulose: formation of ferulic acid dehydrodimers," *Carbohydrate Research*, vol. 303, no. 4, pp. 459–462, 1997.

[84] E. Carvajal-Millan, V. Landillon, M. H. Morel, X. Rouau, J. L. Doublier, and V. Micard, "Arabinoxylan gels: impact of the feruloylation degree on their structure and properties," *Biomacromolecules*, vol. 6, no. 1, pp. 309–317, 2005.

[85] E. Carvajal-Millan, S. Guilbert, M. Morel, and V. Micard, "Impact of the structure of arabinoxylan gels on their rheological and protein transport properties," *Carbohydrate Polymers*, vol. 60, no. 4, pp. 431–438, 2005.

[86] E. Vansteenkiste, C. Babot, X. Rouau, and V. Micard, "Oxidative gelation of feruloylated arabinoxylan as affected by protein. Influence on protein enzymatic hydrolysis," *Food Hydrocolloids*, vol. 18, no. 4, pp. 557–564, 2004.

[87] M. Bunzel, "Chemistry and occurrence of hydroxycinnamate oligomers," *Phytochemistry Reviews*, vol. 9, no. 1, pp. 47–64, 2010.

[88] E. Carvajal-Millan, B. Guigliarelli, V. Belle, X. Rouau, and V. Micard, "Storage stability of laccase induced arabinoxylan gels," *Carbohydrate Polymers*, vol. 59, no. 2, pp. 181–188, 2005.

[89] C. M. Courtin, K. Swennen, W. F. Broekaert et al., "Effects of dietary inclusion of xylooligo-saccharides, arabinoxylooligosaccharides and soluble arabinoxylan on the microbial composition of caecal contents of chickens," *Journal of the Science of Food and Agriculture*, vol. 88, no. 14, pp. 2517–2522, 2008.

[90] P. van den Abbeele, P. Gérard, S. Rabot et al., "Arabinoxylans and inulin differentially modulate the mucosal and luminal gut microbiota and mucin-degradation in humanized rats," *Environmental Microbiology*, vol. 13, no. 10, pp. 2667–2680, 2011.

[91] B. Damen, J. Verspreet, A. Pollet, W. F. Broekaert, J. A. Delcour, and C. M. Courtin, "Prebiotic effects and intestinal fermentation of cereal arabinoxylans and arabinoxylan oligosaccharides in rats depend strongly on their structural properties and joint presence," *Molecular Nutrition & Food Research*, vol. 55, no. 12, pp. 1862–1874, 2011.

[92] H. Chen, Y. Fu, X. Jiang et al., "Arabinoxylan activates lipid catabolism and alleviates liver damage in rats induced by high-fat diet," *Journal of the Science of Food and Agriculture*, vol. 98, no. 1, pp. 253–260, 2018.

[93] A. Pérez-Martínez, J. Valentín, L. Fernández et al., "Arabinoxylan rice bran (MGN-3/Biobran) enhances natural killer cell–mediated cytotoxicity against neuroblastoma in vitro and in vivo," *Cytotherapy*, vol. 17, no. 5, pp. 601–612, 2015.

[94] N. K. Badr El-Din, D. A. Ali, R. Othman, and M. Ghoneum, "Prevention of hepatocarcinogenesis in rats by arabinoxylan rice bran, MGN-3/Biobran," in *Proceedings: AACR 107th Annual Meeting*, New Orleans, LA, USA, April 2016.

[95] M. Ghoneum, "Anti-HIV activity in Vitroof MGN-3, an activated Arabinoxylane from rice bran," *Biochemical and Biophysical Research Communications*, vol. 243, no. 1, pp. 25–29, 1998.

[96] M. Ghoneum and A. Jewett, "Production of tumor necrosis factor-alpha and interferon-gamma from human peripheral blood lymphocytes by MGN-3, a modified arabinoxylan from rice bran, and its synergy with interleukin-2 in vitro," *Cancer Detection and Prevention*, vol. 24, no. 4, pp. 314–324, 2000.

[97] B. V. Dons'koi, V. P. Chernyshov, and D. V. Osypchuk, "Measurement of NK activity in whole blood by the CD69 up-regulation after co-incubation with K562, comparison with NK cytotoxicity assays and CD107a degranulation assay," *Journal of Immunological Methods*, vol. 372, no. 1-2, pp. 187–195, 2011.

[98] J. Clausen, B. Vergeiner, M. Enk, A. L. Petzer, G. Gastl, and E. Gunsilius, "Functional significance of the activation-associated receptors CD25 and CD69 on human NK-cells and NK-like T-cells," *Immunobiology*, vol. 207, no. 2, pp. 85–93, 2003.

[99] M. Ghoneum and S. Abedi, "Enhancement of natural killer cell activity of aged mice by modified arabinoxylan rice bran (MGN-3/Biobran)," *Journal of Pharmacy and Pharmacology*, vol. 56, no. 12, pp. 1581–1588, 2004.

[100] Y. Asano, K. Kaneda, J. Hiragushi, T. Tsuchida, and K. Higashino, "The tumor-bearing state induces augmented responses of organ-associated lymphocytes to high-dose interleukin-2 therapy in mice," *Cancer Immunology, Immunotherapy*, vol. 45, no. 2, pp. 63–70, 1997.

[101] D. Cholujova, J. Jakubikova, B. Czako et al., "MGN-3 arabinoxylan rice bran modulates innate immunity in multiple myeloma patients," *Cancer Immunology, Immunotherapy*, vol. 62, no. 3, pp. 437–445, 2013.

[102] K. Ogawa, M. Takeuchi, and N. Nakamura, "Immunological effects of partially hydrolyzed arabinoxylan from corn husk in mice," *Bioscience, Biotechnology, and Biochemistry*, vol. 69, no. 1, pp. 19–25, 2005.

[103] H. Arase, N. Arase, and T. Saito, "Interferon gamma production by natural killer (NK) cells and NK1.1+ T cells upon NKR-P1 cross-linking," *Journal of Experimental Medicine*, vol. 183, no. 5, pp. 2391–2396, 1996.

[104] D. Dieckmann, H. Plottner, S. Berchtold, T. Berger, and G. Schuler, "Ex vivo isolation and characterization of $CD4^+CD25^+$ T cells with regulatory properties from human blood," *Journal of Experimental Medicine*, vol. 193, no. 11, pp. 1303–1310, 2001.

[105] H. Arase, N. Arase, and T. Saito, "Fas-mediated cytotoxicity by freshly isolated natural killer cells," *Journal of Experimental Medicine*, vol. 181, no. 3, pp. 1235–1238, 1995.

[106] K. Suk, Y. H. Kim, I. Chang et al., "IFNα sensitizes ME-180 human cervical cancer cells to TNFα-induced apoptosis by inhibiting cytoprotective NF-κB activation," *FEBS Letters*, vol. 495, no. 1-2, pp. 66–70, 2001.

[107] T. Sasagawa, M. Hlaing, and T. Akaike, "Synergistic induction of apoptosis in murine hepatoma Hepa1-6 cells by IFN-γ and TNF-α," *Biochemical and Biophysical Research Communications*, vol. 272, no. 3, pp. 674–680, 2000.

[108] M. Ghoneum and S. Gollapudi, "Modified arabinoxylan rice bran (MGN-3/Biobran) enhances yeast-induced apoptosis in human breast cancer cells *in vitro*," *Anticancer Research*, vol. 25, no. 2A, pp. 859–870, 2005.

[109] M. Ghoneum and S. Gollapudi, "Modified arabinoxylan rice bran (MGN-3/Biobran) sensitizes human T cell leukemia cells to death receptor (CD95)-induced apoptosis," *Cancer Letters*, vol. 201, no. 1, pp. 41–49, 2003.

[110] R. J. Carmody and T. G. Cotter, "Signalling apoptosis: a radical approach," *Redox Report*, vol. 6, no. 2, pp. 77–90, 2001.

[111] E. M. van Lieshout, M. M. Bedaf, M. Pieter, C. Ekkel, W. A. Nijhoff, and W. H. Peters, "Effects of dietary anticarcinogens on rat gastrointestinal glutathione S-transferase theta 1-1 levels," *Carcinogenesis*, vol. 19, no. 11, pp. 2055–2057, 1998.

[112] B. Halliwell and S. Chirico, "Lipid peroxidation: its mechanism, measurement, and significance," *The American Journal of Clinical Nutrition*, vol. 57, no. 5, pp. 715S–725S, 1993.

[113] C. Pheiffer, C. Jacobs, O. Patel, S. Ghoor, C. Muller, and J. Louw, "Expression of UCP2 in Wistar rats varies according to age and the severity of obesity," *Journal of Physiology and Biochemistry*, vol. 72, no. 1, pp. 25–32, 2016.

[114] T. K. L. Meyvis, S. C. de Smedt, J. Demeester, and W. E. Hennink, "Influence of the degradation mechanism of hydrogels on their elastic and swelling properties during degradation," *Macromolecules*, vol. 33, no. 13, pp. 4717–4725, 2000.

[115] S. B. Ross-Murphy and K. P. Shatwell, "Polysaccharide strong and weak gels," *Biorheology*, vol. 30, no. 3-4, pp. 217–227, 1993.

[116] R. Paz-Samaniego, E. Carvajal-Millan, F. Brown-Bojorquez et al., "Gelation of arabinoxylans from maize wastewater — effect of alkaline hydrolysis conditions on the gel rheology and microstructure," in *Waste Water Treatment Engineering*, A. P. M. Samer, Ed., pp. 101–114, InTech, Houston, TX, USA, 2015.

[117] A. L. Martínez-López, E. Carvajal-Millan, A. Rascón-Chu, J. Márquez-Escalante, and K. Martínez-Robinson, "Gels of ferulated arabinoxylans extracted from nixtamalized and non-nixtamalized maize bran: rheological and structural characteristics," *CyTA - Journal of Food*, vol. 11, Supplement 1, pp. 22–28, 2013.

[118] J. A. Marquez-Escalante, E. Carvajal-Millan, Y. L. López-Franco et al., "Gels of water extractable arabinoxylans from a bread wheat variety: swelling and microstructure," in *Breeding and Genetic Engineering: The Biology and Biotechnology Research*, pp. 1–12, IConcept Press Ltd, USA, 2016.

[119] A. Martínez-López, E. Carvajal-Millan, M. Miki-Yoshida et al., "Arabinoxylan microspheres: structural and textural characteristics," *Molecules*, vol. 18, no. 4, pp. 4640–4650, 2013.

[120] R. González-Estrada, M. Calderón-Santoyo, E. Carvajal-Millan et al., "Covalently cross-linked arabinoxylans films for Debaryomyces hansenii entrapment," *Molecules*, vol. 20, no. 6, pp. 11373–11386, 2015.

[121] A. B. Hernández-Espinoza, M. I. Piñón-Muñiz, A. Rascón-Chu, V. M. Santana-Rodríguez, and E. Carvajal-Millan, "Lycopene/arabinoxylan gels: rheological and controlled release characteristics," *Molecules*, vol. 17, no. 3, pp. 2428–2436, 2012.

[122] A. Bayat, F. A. Dorkoosh, A. R. Dehpour et al., "Nanoparticles of quaternized chitosan derivatives as a carrier for colon delivery of insulin: ex vivo and in vivo studies," *International Journal of Pharmaceutics*, vol. 356, no. 1-2, pp. 259–266, 2008.

[123] C. M. Silva, A. J. Ribeiro, I. V. Figueiredo, A. R. Gonçalves, and F. Veiga, "Alginate microspheres prepared by internal gelation: development and effect on insulin stability," *International Journal of Pharmaceutics*, vol. 311, no. 1-2, pp. 1–10, 2006.

[124] L. Segale, L. Giovannelli, P. Mannina, and F. Pattarino, "Calcium alginate and calcium alginate-chitosan beads containing celecoxib solubilized in a self-emulsifying phase," *Scientifica*, vol. 2016, Article ID 5062706, 8 pages, 2016.

[125] C. M. Courtin and J. A. Delcour, "Arabinoxylans and endoxylanases in wheat flour bread-making," *Journal of Cereal Science*, vol. 35, no. 3, pp. 225–243, 2002.

[126] J. M. Fierro-Islas, *Anti-Obesogenic and Prebiotic Effect of Arabinoxilan Gels in Rats Fed with a High-Fat Diet, [M.S. Thesis]*, Centro de Investigación en Alimentación y Desarrollo, A.C., 2017.

[127] M. F. Andreasen, P. A. Kroon, G. Williamson, and M. T. Garcia-Conesa, "Intestinal release and uptake of phenolic antioxidant diferulic acids," *Free Radical Biology & Medicine*, vol. 31, no. 3, pp. 304–314, 2001.

[128] B. Halliwell, K. Zhao, and M. Whiteman, "The gastrointestinal tract: a major site of antioxidant action?," *Free Radical Research*, vol. 33, no. 6, pp. 819–830, 2000.

[129] J. Snelders, E. Dornez, J. A. Delcour, and C. M. Courtin, "Ferulic acid content and appearance determine the antioxidant capacity of arabinoxylanoligosaccharides," *Journal of Agricultural and Food Chemistry*, vol. 61, no. 42, pp. 10173–10182, 2013.

[130] M. Méndez-Encinas, *Asociación arabinoxilano-proteína y efecto de la fraccción proteica en la capacidad gelificacante del polisacárido, [M.S. thesis]*, Centro de Investigación en Alimentación y Desarrollo, A.C., 2015.

Hindawi
Oxidative Medicine and Cellular Longevity
Volume 2018, Article ID 7410389, 15 pages
https://doi.org/10.1155/2018/7410389

Research Article

Structural Characterization and Repair Mechanism of *Gracilaria lemaneiformis* Sulfated Polysaccharides of Different Molecular Weights on Damaged Renal Epithelial Cells

Da Guo, Kai Yu, Xin-Yuan Sun, and Jian-Ming Ouyang

Institute of Biomineralization and Lithiasis Research, Jinan University, Guangzhou 510632, China

Correspondence should be addressed to Jian-Ming Ouyang; toyjm@jnu.edu.cn

Received 1 December 2017; Revised 30 April 2018; Accepted 12 July 2018; Published 5 August 2018

Academic Editor: Amitava Das

Natural *Gracilaria lemaneiformis* sulfated polysaccharide (GLP0, molecular weight = 622 kDa) was degraded by H_2O_2 to obtain seven degraded fragments, namely, GLP1, GLP2, GLP3, GLP4, GLP5, GLP6, and GLP7, with molecular weights of 106, 49.6, 10.5, 6.14, 5.06, 3.71, and 2.42 kDa, respectively. FT-IR and NMR results indicated that H_2O_2 degradation does not change the structure of GLP polysaccharides, whereas the content of the characteristic $-OSO_3H$ group (13.46% ± 0.10%) slightly increased than that of the natural polysaccharide (13.07%) after degradation. The repair effects of the polysaccharide fractions on oxalate-induced damaged human kidney proximal tubular epithelial cells (HK-2) were compared. When 60 μg/mL of each polysaccharide was used to repair the damaged HK-2 cells, cell viability increased and the cell morphology was restored, as determined by HE staining. The amount of lactate dehydrogenase released decreased from 16.64% in the injured group to 7.55%–13.87% in the repair groups. The SOD activity increased, and the amount of MDA released decreased. Moreover, the mitochondrial membrane potential evidently increased. All polysaccharide fractions inhibited S phase arrest through the decreased percentage of cells in the S phase and the increased percentage of cells in the G2/M phase. These results reveal that all GLP fractions exhibited repair effect on oxalate-induced damaged HK-2 cells. The repair ability is closely correlated with the molecular weight of the fractions. GLP2 with molecular weight of about 49.6 kDa exhibited the strongest repair effect, and GLP with higher or lower molecular weight than 49.6 kDa showed decreased repair ability. Our results can provide references for inhibiting the formation of kidney stones and developing original anti-stone polysaccharide drugs.

1. Introduction

Seaweed polysaccharides possess an extensive range of biological activities [1]. However, native seaweed polysaccharides cannot easily penetrate the cell membrane to exert their biological activity because of their large molecular size and poor solubility [2, 3]; as such, these polysaccharides have limited applications. The biological activity of polysaccharides with high molecular weight may be improved by degradation. Jo and Choi [4] performed degradation of *Sargassum fulvellum* polysaccharide to obtain three polysaccharide fractions with low molecular weights of 2, 23, and 36 kDa; the antioxidant and anticoagulant activities increased with decreasing molecular weight of the polysaccharides. Zhu et al. [5] revealed that sulfated fucoidan with low molecular weight (5–7 kDa) showed higher anticoagulant effect than that of sulfated fucoidan with molecular weight of 120–82 kDa.

Gracilaria lemaneiformis, which belongs to Rhodophyta, Florideae, Gigarfinales, Gracilariaceae, and Gracilaria, is widely distributed in the south coastal areas of China and coastal areas near Japan and Korea [6] *G. lemaneiformis* is consumed as food in many Asian countries and mainly used in food industries as gelling agent [7]. *G. lemaneiformis* polysaccharide (GLP) mainly consists of alternating 3-linked β-D-galactopyranosyl agarose with $-OSO_3H$ and 4-linked α-L-galactopyranosyl carrageenan units [6]. The 3-linked unit belongs to the D-series, and the 4-linked unit may have the D or L configuration, often occurring as a 3,6-anhydrogalactopyranosyl moiety [6–8]. Many reports are available with

regard to the chemical structure and biological activity of GLPs. GLP exerts many beneficial bioactivities, such as antitumor, antiviral, and antioxidant activities and hypoglycemic properties [6, 9, 10]. Fan et al. [9] isolated an acidic polysaccharide (GLSP) with carbohydrate content of 72.06% and sulfate content of 6.13% from *G. lemaneiformis*; the GLSP significantly inhibited the growth of tumor, promoted splenocyte proliferation and macrophage phagocytosis, and increased the levels of IL-2 and $CD8^+$ T cells in blood of tumor-bearing mice. The results suggest that the isolated GLSP displayed remarkable antitumor and immunomodulatory activities. Liao et al. [6] studied the hypoglycemic and antioxidant effects of a polysaccharide extracted from *G. lemaneiformis* (GLP; Mw, 121.89 kDa). The intragastric administration of GLP for 21 d induced an obvious decrease in the blood glucose level. Furthermore, GLP evidently increased the activities of superoxide dismutase and glutathione peroxidase and total antioxidant capacity and significantly decreased the level of malondialdehyde in the liver, pancreas, and kidney of diabetic mice. Di et al. [10] extracted a crude polysaccharide of *G. lemaneiformis* (GRPS) by hot water extraction and obtained three purified polysaccharides, namely, GRPS-1-1, GRPS-2-1, and GRPS-3-2, with average molecular weights of 1310, 691, and 923 kD, respectively. All the polysaccharides exhibited antioxidant effects, including clearance of ABTS and superoxide radicals and inhibition of lipid peroxidation.

The incidence of kidney stone has gradually increased in recent years [11, 12]. Currently, the main prescription drugs for treatment of urinary calculi are citrate, magnesium preparations, orthophosphate, allopurinol, and thiazide diuretics. However, the action mechanism of these drugs remains unclear, and their curative effects can be marginal [13]. Thus, scholars must develop new highly efficient, nontoxic, and inexpensive anti-stone drugs for scientific and practical applications [14].

Oxalic acid is a metabolism product of the human body and a main component for the formation of kidney stones. When oxalic acid in urine reaches a certain concentration, human kidney proximal tubular epithelial cells (HK-2 cells) will be oxidatively damaged [15], which is correlated with the formation of kidney stones [16, 17]. The damaged cells can be repaired by plant polysaccharides [18, 19].

In our previous study [18], we have studied the effect of sulfate group ($-OSO_3H$) content of six kinds of seaweed polysaccharides (SPSs) on repair ability to damaged HK-2 cells. The six SPSs were extracted from *Laminaria japonica*, *Porphyra yezoensis*, *Gracilaria lemaneiformis* (GLP), *Sargassum fusiforme*, *Eucheuma gelatinae*, and *Undaria pinnatifida*, respectively. The six SPSs have a narrow difference of molecular weight (from 3343 to 4020 Da), and their sulfate group ($-OSO_3H$) content was 21.7%, 17.9%, 13.3%, 8.2%, 7.0%, and 5.5%, respectively. The results showed that the repair ability of polysaccharide was positively correlated with $-OSO_3H$ content. Polysaccharide with higher $-OSO_3H$ content exhibited a better repair ability on damaged cells. In addition, the molecular weight is also an important factor affecting the viability of polysaccharides. However, the antioxidant activity and repair effect of GLP with different molecular weights on HK-2 cells have not been investigated yet. In the present study, natural GLP was degraded by H_2O_2 to obtain eight GLP fractions with different molecular weights ranging from 2.42 kDa to 622 kDa. The repair effect of the fractions on oxalate-induced damaged HK-2 cells was also studied to elucidate the mechanism of kidney stone formation and provide experimental evidence for development of new anti-stone drugs.

2. Experiments

2.1. Reagents and Instruments. *Gracilaria lemaneiformis* sulfated polysaccharide (GLP0) was produced by Beijing New Probe Bioscience & Technology Co., Ltd (Beijing, China). Samples of *G. lemaneiformis* were collected from the Qingdao province of China from September to December 2016. The material was sorted, washed, and dried immediately by forced air circulation at 50–60°C.

The cell proliferation assay kit Cell Counting Kit-8 (CCK-8) and lactate dehydrogenase (LDH) assay kit were purchased from Dojindo Laboratories (Kumamoto, Japan). Hematoxylin and eosin (HE) staining kit, 5,5′,6,6′-tetrachloro-1,1′,3,3′-tetraethylbenzimidazolylcarbocyanine iodide (JC-1) kit, and propidium iodide (PI) were purchased from Shanghai Beyotime Bioscience & Technology Co., Ltd. (Shanghai, China). Hydrogen peroxide, KBr (SP), and other chemical reagents were of analytical grade and purchased from Guangzhou Chemical Reagent Company (Guangzhou, China) and D_2O from Sigma (99.9%). Experimental water is secondary distilled water.

The apparatus used include an enzyme mark instrument (SafireZ, Tecan, Switzerland), upright fluorescence microscope (22DI-E-D282, Leica, Germany), flow cytometer (FACSAria, BD company, USA), FT-IR spectrometer (Equinox 55, Bruker, Germany), ultraviolet-visible spectrophotometer (Cary 500, Varian company, USA), conductivity meter (DDS-11A, Leici, Shanghai, China), and NMR spectrometer (Varian Bruker 300 MHz, Germany).

2.2. Preparation of G. lemaneiformis Polysaccharides. Algal powder of *G. lemaneiformis* (diameter, 200 μm) was subjected to hot water extraction with 90-fold volumes of distilled water for 5 h at 90°C according to the method described by Liao et al. [6] to obtain polysaccharide. After centrifugation to remove residues (7000 rpm, 10 min), the supernatant was concentrated to one-third of its volume in a vacuum rotary evaporator. The concentrated solution was precipitated with three volumes of absolute ethanol overnight at 4°C. The precipitates were collected by centrifugation (3500g, 10 min) and resolved in warm water. Proteins were removed using the Sevag method. The supernatant containing the polysaccharide was dialyzed in distilled water for 72 h and vacuum freeze-dried.

2.3. Degradation of Polysaccharides. Natural GLP0 was degraded using previously reported methods [20]. Briefly, 1.2 g of crude polysaccharide (GLP0) was weighed accurately and dissolved in distilled water at 70°C. After heating to 90°C, the reaction system was quickly added with 0.1%, 0.4%, 1%,

3%, 6%, 10%, and 15% H_2O_2 solution. The degradation reaction was allowed to proceed for 2 h, at which point the solution pH was adjusted to 7.0 by adding 2 mol/L NaOH solution. The degraded solution was concentrated to one-third of its original volume at 60°C. The product was precipitated by adding anhydrous ethanol three times. The solution was stored overnight and filtered. The filtrate was dried in vacuum to obtain the degraded polysaccharide. Productivity can be calculated after weighing the polysaccharide.

2.4. Measurement of Average Molecular Weights (M_r) of Polysaccharide. According to the reference [21], the viscosity of a sample in an aqueous solution was measured using an Ubbelohde viscosity method at 30 ± 0.2°C. After measuring the fall time of polysaccharide before and after degradation in the viscometer, specific (η_{sp}) and relative (η_r) viscosity was calculated according to the formulas $\eta_r = T_i/T_0$ and $\eta_{sp} = \eta_r - 1$, where T_0 and T_i are the falling time of deionized water and GLP solutions, respectively. $\eta = (2(\eta_{sp} - \ln \eta_r))^{1/2}/c$, where c is the sample concentration. The M_r of GLP was calculated through its η value. $\eta = \kappa M_r{}^{\alpha}$, where κ and α are constants. For GLP, $\kappa = 0.07$ and $\alpha = 0.72$ [21].

2.5. Analysis of Sulfate Group Content. The sulfate group ($-OSO_3H$) content of GLP was measured by the $BaCl_2$-gelatin turbidity method [18, 22]. The polysaccharide sample of 70 mg was placed in 10.0 mL of 1.0 mol/L HCl solution, then hydrolysated for 6 h at 100°C. After cooling, the HCl solution was added to the calibration line. A 0.3% gelatin solution is prepared in hot water (60 ~ 70°C) and stored at 4°C overnight. 2 g of $BaCl_2$ was dissolved in a gelatin solution and left at room temperature for 2–3 hours. 0.2 mL of GLP solution with the concentration of 1.4 mg/mL was added to 1 mL of $BaCl_2$-gelatin reagent and 3.8 mL of 0.5 mol/L HCl. After that, the mixture was allowed to stand at 25°C for 10–20 minutes. The blank was prepared by substituting 0.2 mL of water for the GLP solution. The released $BaSO_4$ suspension was measured at $\lambda = 360$ nm by a UV-VIS spectrophotometer using K_2SO_4 as standard, and the regression equation is $Y = 0.01042 + 1.27905X$, $n = 11$, and $R = 0.99324$, from which the percentage of sulfate content of polysaccharide can be calculated.

2.6. Analysis of Carboxyl Content. The carboxyl (–COOH) content of GLP is determined by conductometric titration [18, 23]. The conductivity titration curve was plotted using the conductivity value as the y-axis and the corresponding volume of consumed NaOH as the x-axis. The conductivity titration curve can be divided into three parts, namely, the conductivity decrease phase (A), the balance phase (B), and the conductivity increase phase (C). Three tangents were constructed from the three-stage curves, and the intersections were stoichiometric points. The intersection of the A line and the B line gives the volume of NaOH (V_1) such that excess HCl and $-OSO_3H$ are consumed, and the intersection of line B and line C gives the volume of NaOH (V_2), excess HCl, and co-consumed GLP's $-OSO_3H$ and –COOH; therefore, $V_2 - V_1$ (platform portion) is the volume of consumed NaOH by –COOH alone of GLP. The –COOH content can be obtained according to the following formula:

$$-\mathrm{COOH}(\%) = \frac{C_{\mathrm{NaOH}} \times (V_2 - V_1) \times 45/1000}{C_{\mathrm{sample}} \times 40/1000} \times 100. \quad (1)$$

C_{NaOH} (mol/L) represents the molar concentration of NaOH, C_{sample} (g/L) represents the mass concentration of GLP polysaccharide, 45 g/mol is the molar mass of –COOH, and 40 mL is the volumetric solution of polysaccharide. The final value is the average of three parallel experiments.

2.7. Fourier-Transform Infrared Spectroscopy (FT-IR) Analysis of GLP [24]. FT-IR spectra of polysaccharides were determined using films prepared by the dried polysaccharides and KBr pellets on a Fourier-transform infrared spectrophotometer in the wave number range of 4000–400 cm^{-1} with a resolution of 4 cm^{-1}.

2.8. ^1H and ^{13}C NMR Spectrum Detection [24]. Approximately 20 mg of purified GLP was dissolved in 0.5 mL of deuterium oxide in an NMR tube (5 mm diameter), and analysis was performed using a Varian Bruker 300 MHz spectrophotometer. The chemical shifts recorded were given in parts per million (ppm).

2.9. Cell Viability Assay of Polysaccharide on HK-2 Cells. The HK-2 cells were cultured in DMEM medium containing 10% fetal bovine serum at 37°C and 5% CO_2 humidified environment. When 80% to 90% confluent monolayers were reached, cells were lightly blown after trypsinization to form cell suspensions for the following cell experiments.

One hundred microliters of cell suspension with a cell concentration of 1×10^5 cells/mL was inoculated per well in 96-well plates and incubated in a 5% CO_2-humidified atmosphere at 37°C for 24 h. The culture medium was removed by suction, and cells were divided into four groups as follows: (A) cell-free culture medium group (control group of background); (B) control cells without polysaccharide treatment (sample control group); (C) damaged group of oxalic acid: the serum-free medium containing 2.8 mmol/L oxalic acid was added and incubated for 3 h; and (D) repair group: serum-free medium containing 60 μg/mL GLP with different molecular weight was added to damaged cells and repaired for 10 h. Each experiment was repeated in three parallel wells. Then, the medium was changed to fresh serum-free DMEM culture medium and 10 μL CCK-8 was added to each well and incubated for 1.5 h at 37°C. Absorbance (A) was measured by using the enzyme mark instrument at 450 nm. Cell viability was calculated based on the following equation.

$$\text{Cell viability}(\%) = \frac{A(\text{treatment group})}{A(\text{control group})} \times 100\%. \quad (2)$$

2.10. Lactate Dehydrogenase (LDH) Release Assay. One hundred microliters of cell suspension with a cell concentration of 1×10^5 cells/mL was inoculated per well in 96-well plates and incubated for 24 h. Then, the cells were divided into five groups in which the first 4 groups were divided as

Table 1: Degradation conditions and physico-chemical properties of crude *G. lemaneiformis* polysaccharide and seven degraded polysaccharide fractions.

GLP fraction	Concentration of H_2O_2/%	Intrinsic viscosity η (mL/g)	Mean molecular weight M_r (kDa)	Yield (%)	$-OSO_3H$ content (%)	–COOH content (%)
GLP0	0	1039 ± 42	622 ± 35		13.07	1.26
GLP1	0.1	298.8 ± 37.8	106 ± 15	63.5	13.37	1.27
GLP2	0.4	168.3 ± 12.0	49.6 ± 4.8	58.4	13.41	1.28
GLP3	1	54.9 ± 1.4	10.5 ± 3.9	56.0	13.46	1.28
GLP4	3	37.4 ± 1.5	6.14 ± 0.35	52.1	13.55	1.36
GLP5	6	33.7 ± 0.9	5.06 ± 0.2	61.3	13.55	1.54
GLP6	10	26.0 ± 0.9	3.71 ± 0.18	53.0	13.56	1.76
GLP7	15	19.7 ± 0.9	2.42 ± 0.16	60.0	13.46	1.77

in Section 2.9, and the E group (E) was added: (E) cells without GLP treatment for the subsequent cleavage of the wells (sample maximum enzyme activity control wells). After repair for 12 h, the absorbances were analyzed at 490 nm according to the LDH kit instruction. LDH release (%) was calculated using the formula as follows:

$$\text{LDH\%} = \frac{A(\text{group D}) - A(\text{group A})}{A(\text{group C}) - A(\text{group A})} \times 100\%. \quad (3)$$

2.11. Hematoxylin and Eosin (He) Staining. One milliliter of cell suspension with a cell concentration of 1.5×10^5 cells/mL was inoculated per well in 12-well plates and incubated for 24 h. The cells were divided into three groups according to Section 2.9: (A) control group, (B) damaged group of oxalic acid, and (C) repair group of GLP. After the repair effect was completed, the supernatant was removed by suction and the cells were washed twice with PBS. The cells on the plate were fixed with 4% paraformaldehyde for 15 min and stained by hematoxylin and eosin according to the manufacturer's instruction. The cellular morphological changes were observed under microscope, and the nuclei were stained in violet and cytoplasm in pink or red.

2.12. Superoxide Dismutase (SOD) Activity and Malondialdehyde (MDA) Content Detection. The cell suspension with a density of 1×10^5 cells/mL was plated per well in 96-well plates and incubated in DMEM containing 10% fetal bovine for 24 h. The cells were divided into three groups: (A) control group, (B) damaged group of oxalic acid, and (C) repair group of GLPs. Cellular SOD activity and MDA content were determined by using the SOD and MDA kits, respectively, according to the instructions provided with kits.

2.13. Measurement of Mitochondrial Membrane Potential ($\Delta\psi$m). One milliliter of cell suspension with a concentration of 4.0×10^5 cells/mL was inoculated per well in 6-well plates for 24 h. After the cells were synchronized, the cells were grouped as in Section 2.9. Incubated for 12 h, the supernatant was aspirated and the cells were washed twice with PBS and digested with 0.25% trypsin. The cells were suspended by pipetting, followed by centrifugation (1000 rpm, 5 min). The supernatant was aspirated, and the cells were washed with PBS and centrifuged again to obtain a cell pellet. The cells were resuspended by adding and thoroughly mixing 500 μL of PBS in a microcentrifuge tube. Finally, the samples were stained with JC-1 and then analyzed.

2.14. Cell Cycle Progression Assay. Cell concentration and group were the same as in Section 2.9. The medium was changed to serum-free DMEM culture media and then incubated for another 12 h to achieve synchronization. The cells were blown and suspended, followed by centrifugation (1000 rpm, 15 min). The supernatant was aspirated, and the cells were washed with PBS and centrifuged again to obtain a cell pellet. Afterwards, 300 μL PBS containing 10% serum was added to resuspend cells and precooling 700 μL absolute alcohol was added with constant shaking, sealed with sealing film, and stored at 4°C overnight. Then, cells were centrifuged at 2000 rpm for 5 min, and supernatant was aspirated. 500 μL PBS was added to wash cells, followed by centrifugation again, and supernatant was removed. Finally, 200 μL PI was added and mixed at 37°C for 15 min. The cell cycle was analyzed by a flow cytometer.

2.15. Statistical Analysis. Experimental data were expressed as mean ± SD. The experimental results were analyzed statistically using SPSS 13.0 software. The differences of means between the experimental groups and the control group were analyzed by Tukey's test. $p < 0.05$ indicates significant difference; $p < 0.01$ indicates extremely significant.

3. Results

3.1. Degradation of G. lemaneiformis Polysaccharide. Seven degraded polysaccharide fractions were obtained from crude *G. lemaneiformis* polysaccharide (GLP0) by using different concentrations of H_2O_2 (Table 1). When the concentration of H_2O_2 ($c(H_2O_2)$) was 0.1%, the molecular weight of the degraded products decreased from 622 kDa (GLP0) to 106 kDa, indicating that GLP0 was easily degraded. The molecular weight of the polysaccharide quickly decreased to 49.6 and 10.5 kDa when the H_2O_2 concentration added was increased to 0.4% and 1%, respectively (Figure 1). The molecular weight slowly decreased to 6.14 and 2.42 kDa when the H_2O_2 concentration was increased to 3% and 15%, respectively.

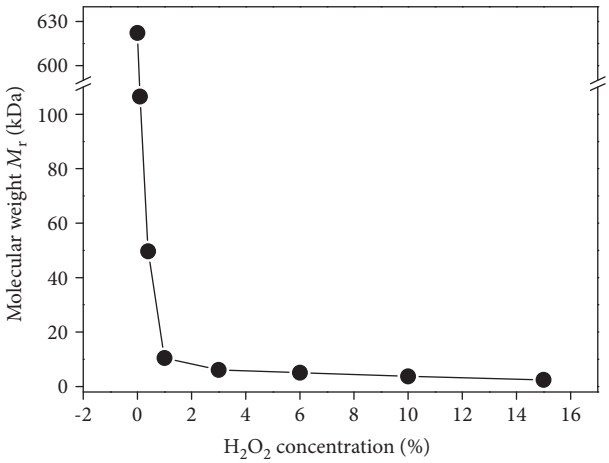

FIGURE 1: Relationship between H_2O_2 concentration and molecular weight of degraded GLPs.

3.2. Change in the Contents of $-OSO_3H$ and $-COOH$ Groups of the Polysaccharides before and after Degradation. The $-OSO_3H$ content of each degraded polysaccharide fraction was about 13.46% (Figure 2(a)), which is slightly higher than 13.07% of natural GLP (Figure 2(a)). Similarly, the $-COOH$ content of the degraded fractions was 1.27%–1.77%, which is higher than 1.26% of the crude GLP. Moreover, the $-COOH$ content increased with decreasing molecular weight of the polysaccharides (Figure 2(b)), but the increase was not obvious.

3.3. Structural Characterization of GLP by FT-IR Spectra. The FT-IR spectra of polysaccharide from *G. lemaneiformis* before and after degradation were similar (Figure 3, Table 2), the peak intensity of GLP after degradation was increased, and no new peaks appeared, which indicated that the degradation of H_2O_2 did not cause a significant effect on the overall structure of polysaccharides.

The peak of 3409–3432 cm^{-1} was caused by the stretching vibration of O-H, and 2920–2928 cm^{-1} was caused by the stretching vibration of C-H; the peak near 1380 cm^{-1} was caused by the deforming vibration of C-H bond. The peak at about 1625 cm^{-1} was attributed to the asymmetric and symmetrical stretching vibration of $-COOH$ [24, 25]. The peak at 1370 cm^{-1} was the signal area of ester sulfate [26], and the peak near 1260 cm^{-1} corresponds to S=O vibration of the sulfate groups [27]. The absorption near 1053 cm^{-1} and 1043 cm^{-1} was due to the stretching vibration of C-O, while the absorbance at 930 cm^{-1} is weak, indicating that galactose is substantially free of internal ether type [26].

3.4. ^1H and ^{13}C NMR Spectrum Analysis. Figure 4 shows the NMR spectra of four GLP. The NMR spectra of polysaccharides before and after degradation were similar, which indicated that the degradation of H_2O_2 did not cause a significant effect on the overall structure of GLP. The signal from the anomeric proton at δ 4.43 was assigned to H-1 of β-D-galactose, and the signal at δ 5.34 was attributed to anomeric proton of 3,6-α-L-galactose. The peaks at 930 cm^{-1} of FT-IR spectra are weak, indicating that the GLP contains little endogenous ether galactose [26]. It indicated that GLP consists of β-D-galactose and 6-O-sulfate-3,6-α-L-galactose, which is different with earlier reported literatures [6–8]. According to the number and the chemical shift value of ^{13}C NMR in the 95–110 interval, the number of sugars and the conformation of the glycosidic bond in the oligosaccharide and its glycoside can be deduced [26]. As shown in Figure 4(d), there are two main peaks in the heterogeneous carbon region δ (95–110 ppm): the terminal carbon C-1 of β-D-galactose is at δ 102.35 ppm, and the terminal carbon C-1 of 3,6-α-L-galactose is at δ 99.48 ppm (Table 3).

3.5. Changes in Viability of HK-2 Cells after Repair by GLP with Different Molecular Weights. Six GLP fractions with molecular weights of 622, 106, 49.6, 10.5, 3.71, and 2.42 kDa were used to repair oxalate-induced damaged HK-2 cells. In our preliminary study [18], we found that when damaged cells were repaired by different concentrations (20, 40, 60, 80, and 100 μg/mL) of polysaccharides, the cell viability of damaged cells was initially increased, reaching the maximum at 60 μg/mL and then decreasing at higher concentrations (100 μg/mL), indicating that 60 μg/mL was adequate for the polysaccharides to play a role. Thus, 60 μg/mL of GLP was used to repair damaged HK-2 cells. The changes in cell viability after repair are shown in Figure 5. The cell viability of the damaged cells was only 61.9%, which increased to 79.2%–89.5% after treatment with various polysaccharides. The repair ability of nondegraded polysaccharide (GLP0) with molecular weight of 622 kDa was the weakest, and cell viability after repair was 79.2%. The repair ability of the degraded fraction GLP2 with molecular weight of 49.6 kDa was the strongest, and the cell viability after GLP2 repair was 89.5%. When the molecular weight of GLP was higher or lower than 49.6 kDa, the repair ability was reduced. The larger the deviation of the molecular weight from 49.6 kDa, the weaker the repair capacity of the polysaccharide will be.

3.6. Changes in Lactate Dehydrogenase (LDH) Release after Repair by GLP with Different Molecular Weights. LDH release is an important indicator of the integrity of the cell membrane. LDH is located in the cytoplasm under normal conditions [28]. When cells are attacked by foreign materials, the structure of the cell membrane will be destructed and cytoplasmic enzymes, such as LDH, will be released into the cell culture media. Thus, cytotoxicity can be quantitatively analyzed by detecting the amount of LDH released into culture media to evaluate the integrity of the cell membrane [28].

Figure 6 shows the changes in the amount of LDH released from the damaged HK-2 cells after treatment with six GLP fractions with different molecular weights. Compared with the damaged group (16.64%), the amount of LDH released decreased at different degrees (7.55–13.87%) after being repaired with various polysaccharide fractions. This finding indicates that GLP with different molecular weights exhibited a repair effect on the membrane of damaged HK-2 cells. Moreover, the amount of LDH released was the lowest (7.55%) after the cells were repaired by

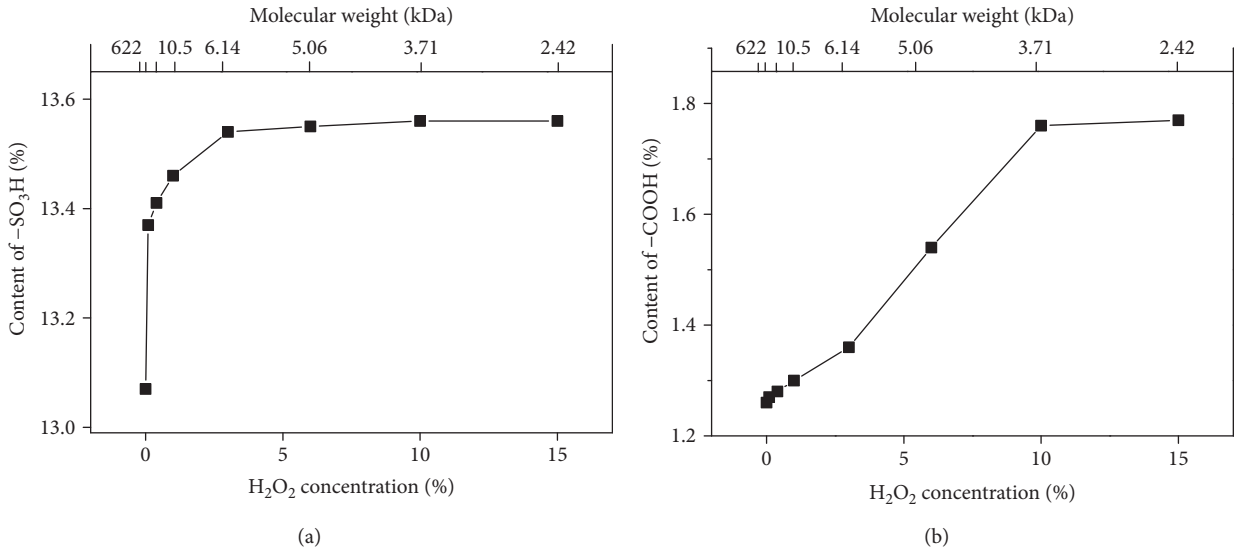

Figure 2: Relationship between the contents of $-OSO_3H$ and $-COOH$ groups and the molecular weight of GLPs. (a) $-OSO_3H$ group and (b) $-COOH$ group.

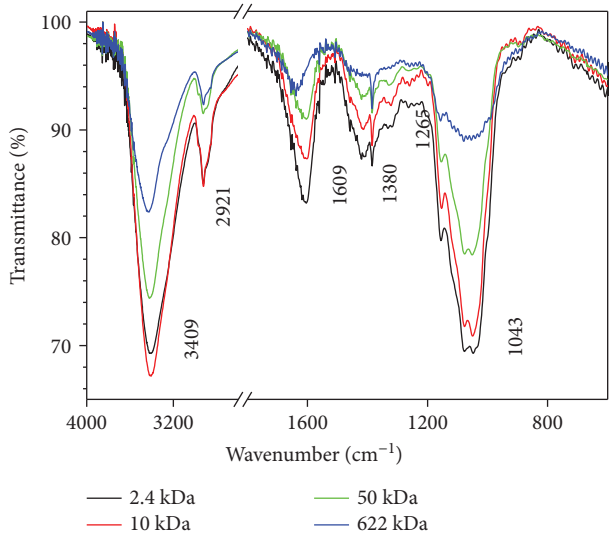

Figure 3: FT-IR spectra of different molecular weights of GLP.

GLP2. Hence, GLP2 exhibited the strongest repair effect. When the molecular weight of various polysaccharide fractions was higher or lower than 49.6 kDa, the repair effect of the polysaccharides decreased. These results are in accordance with the findings on cell viability detected by the CCK-8 kit (Figure 5).

3.7. Cell Morphology Observation by Hematoxylin-Eosin Staining. Hematoxylin, an alkaline dye with a positive charge, stains the chromatin of the nucleus and the ribosome of the cytoplasm in violet. Eosin, an acidic dye with a negative charge, stains positively charged proteins in the cytoplasm and extracellular matrix in pink or red.

As shown in Figure 7, junctions between normal HK-2 cells were tight and the cells were plump. When HK-2 cells were exposed to oxalate (2.8 mmol/L) for 3 h, the cells lost their natural shape, the cell number evidently decreased, and the cells become concentrated. After being repaired by GLP with different molecular weights, the number of cells with intact shape increased, and the number of damaged condensed cells decreased (Figures 7(a)–7(e)). After the damaged cells were repaired by GLP2, the cell number reached the maximum and the morphology of the repaired cells became closest to the normal cells (Figure 7(c)). The repair effect of polysaccharides with molecular weights higher or lower than 49.6 kDa was weaker than that of GLP2.

3.8. Effect of GLP Repair on Superoxide Dismutase (SOD) Activity. SOD activity can reflect the function of the antioxidant system. After HK-2 cells were injured by oxalate, the SOD activity decreased to 3.59 ± 0.25 U/mL, suggesting that the antioxidant capacity of the cells decreased (Figure 8(a)). The extracellular SOD of the repair group was all higher than that of the injury group, indicating that GLPs can repair cells by resisting oxidative damage. GLP2 with a molecular weight of about 49.6 kDa showed the strongest antioxidant capacity on injured cells.

3.9. Effect of GLP Repair on Malondialdehyde (MDA) Generation Amount. Changes in MDA content can reflect the degree of lipid peroxidation in the biomembrane. Figure 8(b) shows the generation amount of MDA in the control, injured, and repaired group cells. The released MDA of injured cells increased, indicating that oxalic acid produces cell oxidative damage. The MDA amount in the repair groups was lower than that of the injury group, indicating that the oxidative damage level of cells decreased. In particular, GLP2 with a molecular weight of about 49.6 kDa showed the strongest repair effect; the amount of MDA was significantly ($p < 0.01$) reduced to 2.43 ± 0.10 nmol/L compared with that of the injury group (7.31 ± 0.19 nmol/L).

Table 2: FT-IR characteristic absorption peaks of GLP.

Sample	Molecular weight M_r (kDa)	Content of $-OSO_3H$ (%)	Content of −COOH (%)	Characteristic absorption peak (cm^{-1})			
				−OH	−COOH	$-OSO_3$	Sugar ring
GLP0	622 ± 35	13.07	1.26	3432	1643	1380, 1257	2928, 1048
GLP2	49.6 ± 4.8	13.41	1.28	3421	1604	1380, 1263	2928, 1053
GLP3	10.5 ± 3.9	13.46	1.30	3408	1604	1380, 1258	2920, 1043
GLP7	2.42 ± 0.16	13.56	1.77	3409	1609	1380, 1268	2920, 1043

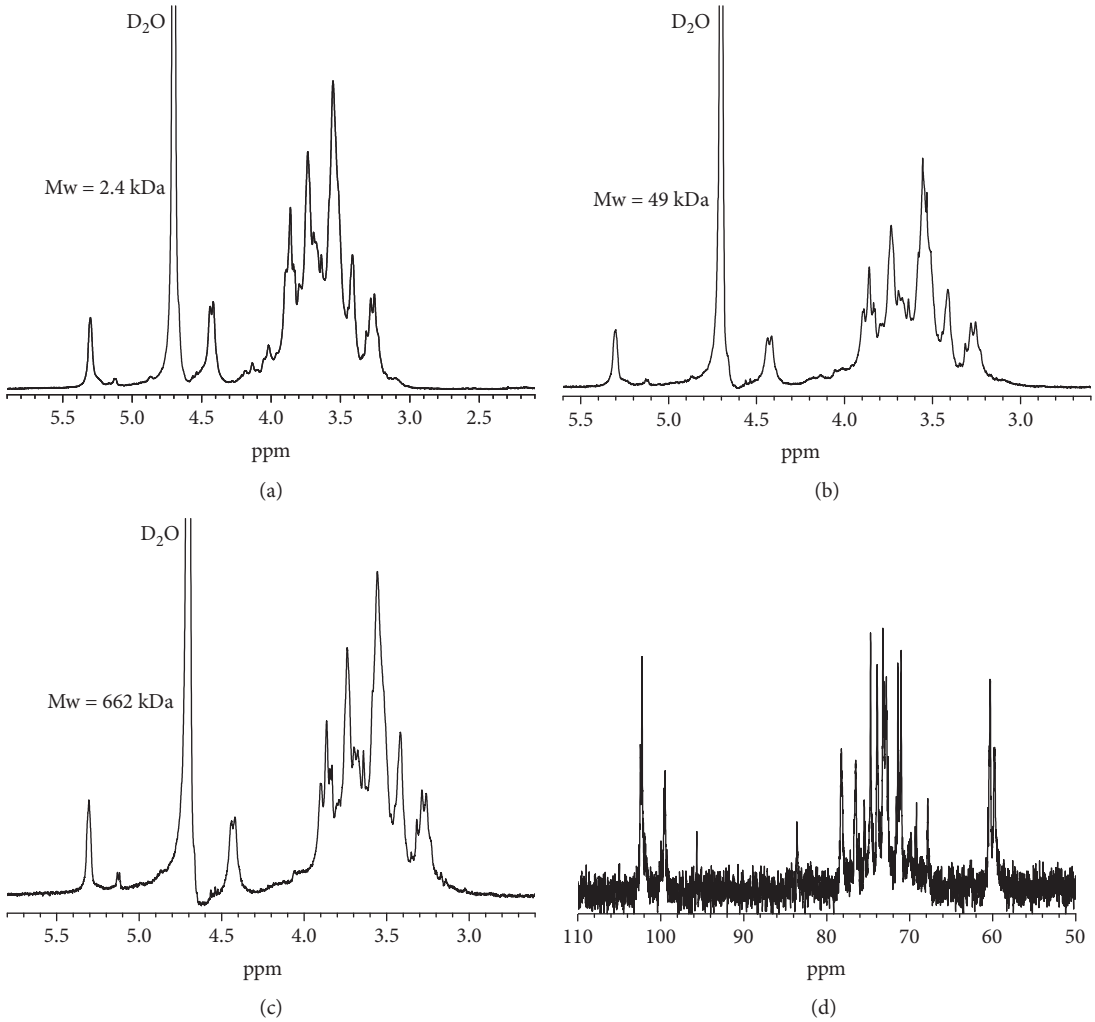

Figure 4: NMR spectra of GLP. (a–c) ^1H NMR spectra and (d) ^{13}C NMR spectrum.

Table 3: ^{13}C NMR chemical shift data of GLP.

Monosaccharide types	^{13}C chemical shift (ppm)					
	C-1	C-2	C-3	C-4	C-5	C-6
β-D-Galactose	102.28	71.14	78.28	71.46	73.96	59.73
6-O-Sulfate-L-α-galactopyranose	99.50	72.82	74.74	72.76	73.26	60.35

3.10. Changes in Mitochondrial Membrane Potential ($\Delta\Psi$m). Fluorescent probe JC-1 is a cationic lipophilic dye that can freely pass through the cell membrane and maintains a dynamic balance at both sides of the membrane by changing the cell membrane potential. JC-1 differentially labels mitochondria with high and low $\Delta\psi$m by forming J-aggregates or monomers that emit orange-red or green light, respectively. Thus, the fluorescent intensity ratio (A/M) of J-aggregates/

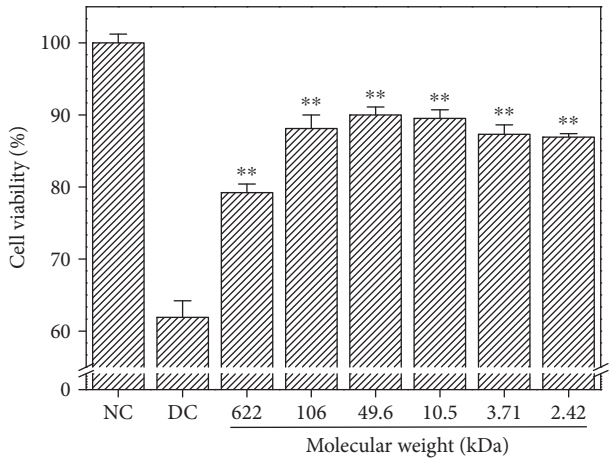

Figure 5: Cell viability of damaged HK-2 cells after being exposed to six GLP fractions with molecular weights of 622, 106, 49.6, 10.5, 3.71, and 2.42 kDa. NC: normal control; DC: damaged control by 2.8 mmol/L oxalate. GLP concentration: 60 μg/mL. Compared to DC group: $^{**}p < 0.01$.

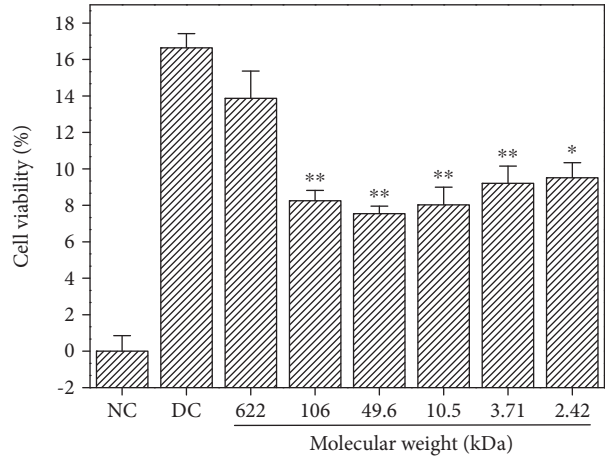

Figure 6: Changes in the amount of LDH released from the damaged HK-2 cells after treatment with six GLP fractions with different molecular weights. NC: normal control; DC: damaged control by 2.8 mmol/L oxalate. GLP concentration: 60 μg/mL. Repaired time: 12 h. Compared to DC group: $^{*}p < 0.05$ and $^{**}p < 0.01$.

J-monomers in mitochondria can be detected to determine early apoptosis.

Figure 9(a) shows the changes in $\Delta\psi$m of the damaged HK-2 cells after being repaired by GLP with different molecular weights. The $\Delta\psi$m of living cells was high, so the red fluorescence was very strong. Figure 9(b) shows the changes in the fluorescent intensity ratio of A/M in the mitochondria of each repair group. The A/M ratio in the mitochondria of normal HK-2 cells was higher (34.71), but the A/M ratio decreased to 2.7 in the oxalate-induced damaged group. This finding suggests that $\Delta\psi$m evidently decreased in the damaged cells. When the damaged cells were repaired by GLP with different molecular weights, the A/M ratio increased at different degrees (9.1–13.08). The increased $\Delta\psi$m caused by GLP2 with a molecular weight of 49.6 kDa was the most obvious, and the A/M ratio increased to 13.08, which is higher than that in the other GLP repair groups.

3.11. Changes in Cell Cycle before and after Repair. Propidium iodide (PI) is a DNA double-strand fluorescent dye. The fluorescent intensity produced by the combination of PI and double-strand DNA was positively correlated with DNA content. After intracellular DNA was stained by PI, DNA content can be measured by flow cytometry. Cell cycle can be analyzed according to DNA distribution [29, 30].

Figure 10(a) shows the changes in the cycle of the damaged HK-2 cells after being repaired by GLP fractions with different molecular weights. Compared with the damaged group, the percentage of cells in the S phase evidently decreased (Figure 10(b)), whereas the percentage of cells in the G2/M phase increased (Figure 10(c)). After being repaired by GLP2, the percentage of cells in the S phase was the lowest (41.1%) and those in the G2/M phase increased (17.6%). Hence, GLP2 with molecular weight of 49.6 kDa promoted cells from the S phase to the G2/M phase most efficiently and exhibited the strongest repair effect on the damaged cells.

4. Discussion

4.1. GLP Degradation and Structure Characterization. Several methods are used for degradation of polysaccharides; such methods include acid hydrolysis, oxidative degradation, and enzymatic methods. The widely used method is H_2O_2 degradation, where the dissociation reaction of H_2O_2 forms hydroxyl radicals. Hydroxyl radicals are powerful oxidizing substances and can attack the glycosidic bonds of polysaccharides [31]. The degradation reaction of H_2O_2 is moderate, and its extent can be controlled without changing the structure of the main chain of polysaccharides. In recent years, H_2O_2 degradation has been widely accepted. For example, Hou et al. [32] performed degradation of *Laminaria japonica* fucoidan by changing H_2O_2 concentration, reaction temperature, and pH and obtained seven degraded fractions of Mw: 1.0, 3.8, 8.3, 13.2, 35.5, 64.3, and 144.5 kDa. All of these polysaccharide fractions exhibited no significant changes in the major backbone structure and sulfate group content.

The structure of polysaccharides is the basis for their biological activity [4, 5, 10, 33]. Galactans from red seaweeds possess structures based on a linear chain of alternating 3-linked β-D-galactopyranose residues (A units) and 4-linked α-D- or α-L-galactopyranose residues or its 3,6-anhydro derivative (B units). These galactans are mainly classified as carrageenans, in which the B unit belongs to the D series, and agarans, in which the B unit is in the L configuration [34]. "Agaran" refers to polysaccharides with a backbone of [→3) β-D-Gal-(1→4)-(3,6-An)-α-L-Gal]. In the present study, the monosaccharide composition and type of sugar residues of GLP were analyzed by ^{1}H NMR, ^{13}C NMR, and FT-IR spectroscopy methods. The signals at δ 4.43 and 5.34 ppm in the ^{1}H NMR spectra correspond to the H1 of β-D-galactose and 3,6-α-L-galactoptoside, respectively. The signals at δ 102.35 and 99.48 ppm in the ^{13}C NMR spectra correspond to the anomeric protons of β-D-galactose and

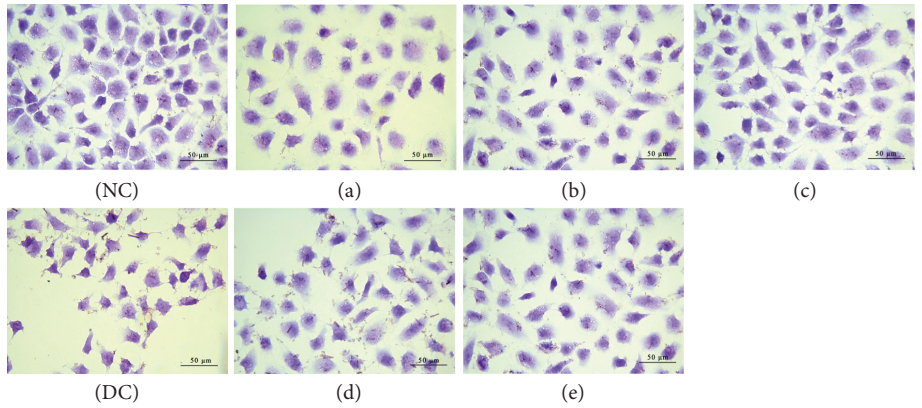

Figure 7: Cell morphology observation of damaged HK-2 cells by hematoxylin-eosin staining after treatment with six GLP fractions with different molecular weights. NC: normal control; DC: damaged control by 2.8 mmol/L oxalate; (a) GLP0, (b) GLP1, (c) GLP2, (d) GLP3, and (e) GLP6. GLP concentration: 60 μg/mL. Repaired time: 12 h.

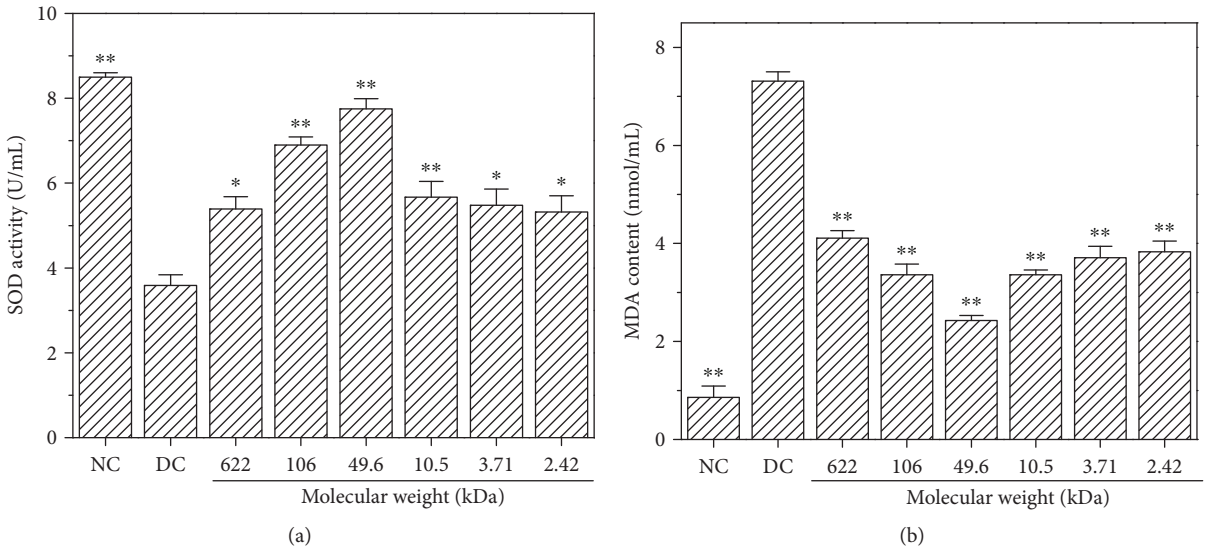

Figure 8: SOD activity (a) and MDA content (b) of the damaged HK-2 cells after treatment with six GLP fractions with different molecular weights. NC: normal control; DC: damaged control by 2.8 mmol/L oxalate. GLP concentration: 60 μg/mL. Repaired time: 12 h. Compared to DC group: $^{*}p < 0.05$ and $^{**}p < 0.01$.

3,6-α-L-galactoptoside, respectively. The peak at 1370 cm^{-1} in the FT-IR spectra is assigned to ester sulfate, and the peak at 1260 cm^{-1} corresponds to the stretching vibration of S=O [26, 27]. These findings indicate that GLP is a sulfated polysaccharide. Based on the spectroscopy analysis results, GLP mainly consists of β-D-galactose and 6-O-sulfate-3,6-L-galactose (Scheme 1). The presence of L-galactose indicates that GLP contains agaran structures. Duarte et al. [35] showed that B units in the L configuration are not of primary importance because of its biological activity, but the substitution of the sulfate group on the agaran backbone affects its biological activity. Thus, the substitution content and position of the sulfate group on the agaran backbone may affect the repair ability of GLP to damaged HK-2 cells.

Polysaccharides contain galactose residue, which is prone to be attacked by free radicals, resulting in fracture of the chain backbone [36]. Thus, GLP can be easily degraded by H_2O_2. Depolymerization with H_2O_2, a widely used method, changes the side groups of the polysaccharide but does not induce distinct changes in the structures of the main chain (Figure 4) [37]. The FT-IR and ^{1}H NMR spectra of GLP before and after degradation were similar (Figure 3, Table 2), and no new peaks appeared. This finding indicated that the degradation of H_2O_2 did not significantly affect the overall structure of the polysaccharides. Therefore, the main structure of polysaccharide before and after degradation slightly changed. The molecular weight of the degraded polysaccharides and the H_2O_2 concentration showed a negative correlation (Figure 1); this finding provides references for obtaining target polysaccharides with different molecular weights.

As shown in Figures 2 and 3, the contents of the $-OSO_3H$ and $-COOH$ groups of the polysaccharide fractions slightly increased after degradation because of the following: (1) free radicals produced by H_2O_2 during degradation will break the

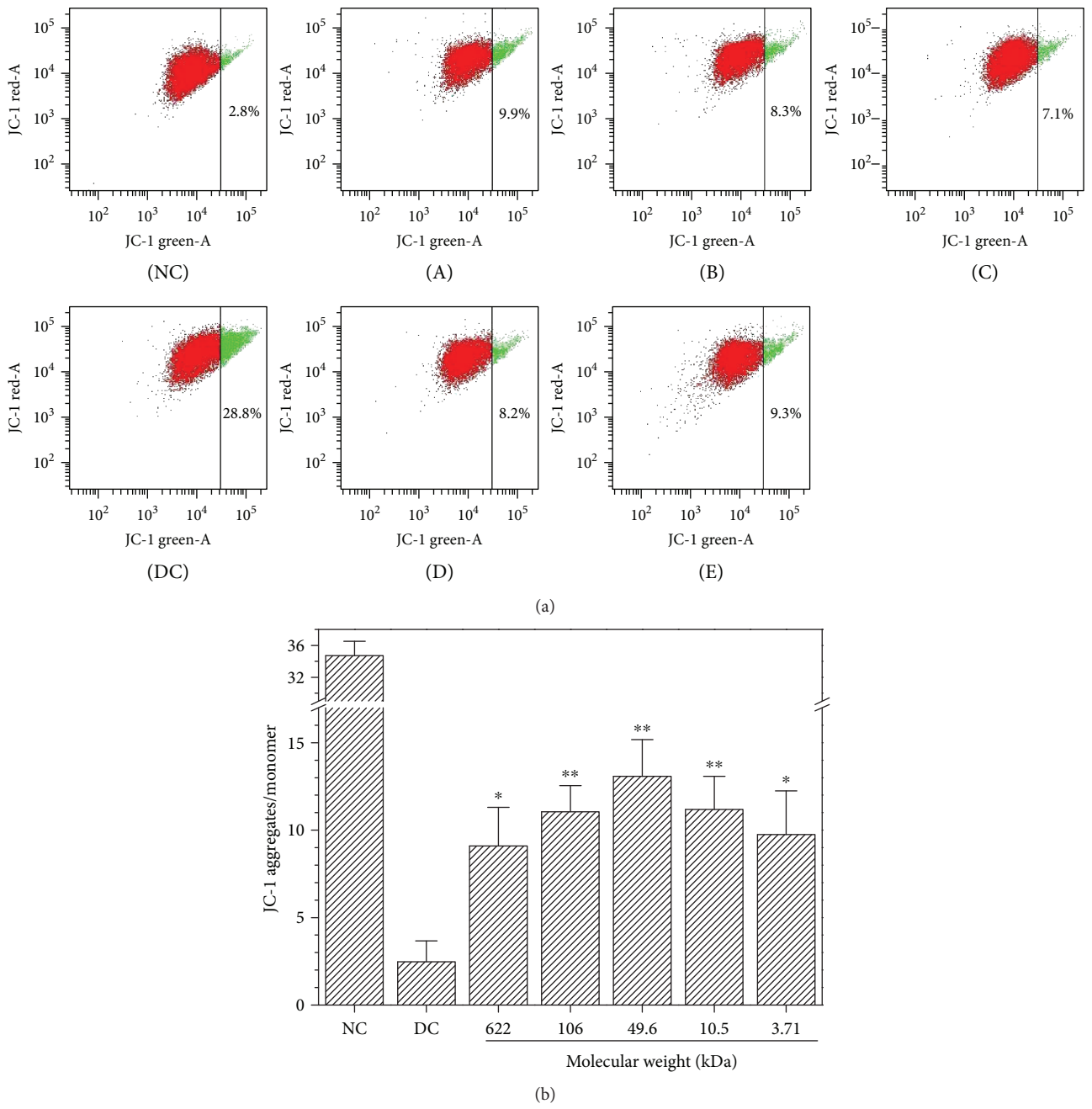

Figure 9: Changes in mitochondrial membrane potential ($\Delta\Psi m$) of the damaged HK-2 cells after being repaired by GLP with different molecular weights. (a) Dot plot of $\Delta\Psi m$; (b) changes in the fluorescent intensity ratio (A/M) of J-aggregates/J-monomers in the mitochondria of each repair group. NC: normal control; DC: damaged control by 2.8 mmol/L oxalate; (A) GLP0, (B) GLP1, (C) GLP2, (D) GLP3, and (E) GLP6. GLP concentration: 60 μg/mL. Repaired time: 12 h. Compared to the DC group: $^{*}p < 0.05$ and $^{**}p < 0.01$.

highly compact sugar chain structure of natural polysaccharide, thereby exposing the $-OSO_3H$ and $-COOH$ groups of the polysaccharide, and (2) the water solubility of the degraded polysaccharide slightly increased and was higher than that of nondegraded GLP0 because of the large molecular weight of the latter, resulting in the concealment of small parts of the acidic groups of polysaccharides [38, 39].

Similar results were reported by previous studies [38, 39]. Zhang et al. [39] obtained polysaccharide fractions with different molecular weights (725, 216, 124, 61.9, and 26.0 kDa) through H_2O_2 degradation of the crude *Monostroma latissimum* polysaccharide; the $-OSO_3H$ group content (21.20%, 22.71%, 24.73%, 25.48%, and 27.28%, resp.) increased with decreasing molecular weight of the polysaccharide. Sun et al. [38] used H_2O_2 and Vc to degrade *Pavlova viridis* and *Sarcinochrysis marina* Geitler. When the molecular weight of *P. viridis* decreased from 3645 kDa to 55.0 kDa, the $-COOH$ content increased from 3.41% to 8.78%. The $-COOH$ content increased from 5.82% to 9.99% when the molecular weight of *S. marina* Geitler decreased from 2595 kDa to 169 kDa.

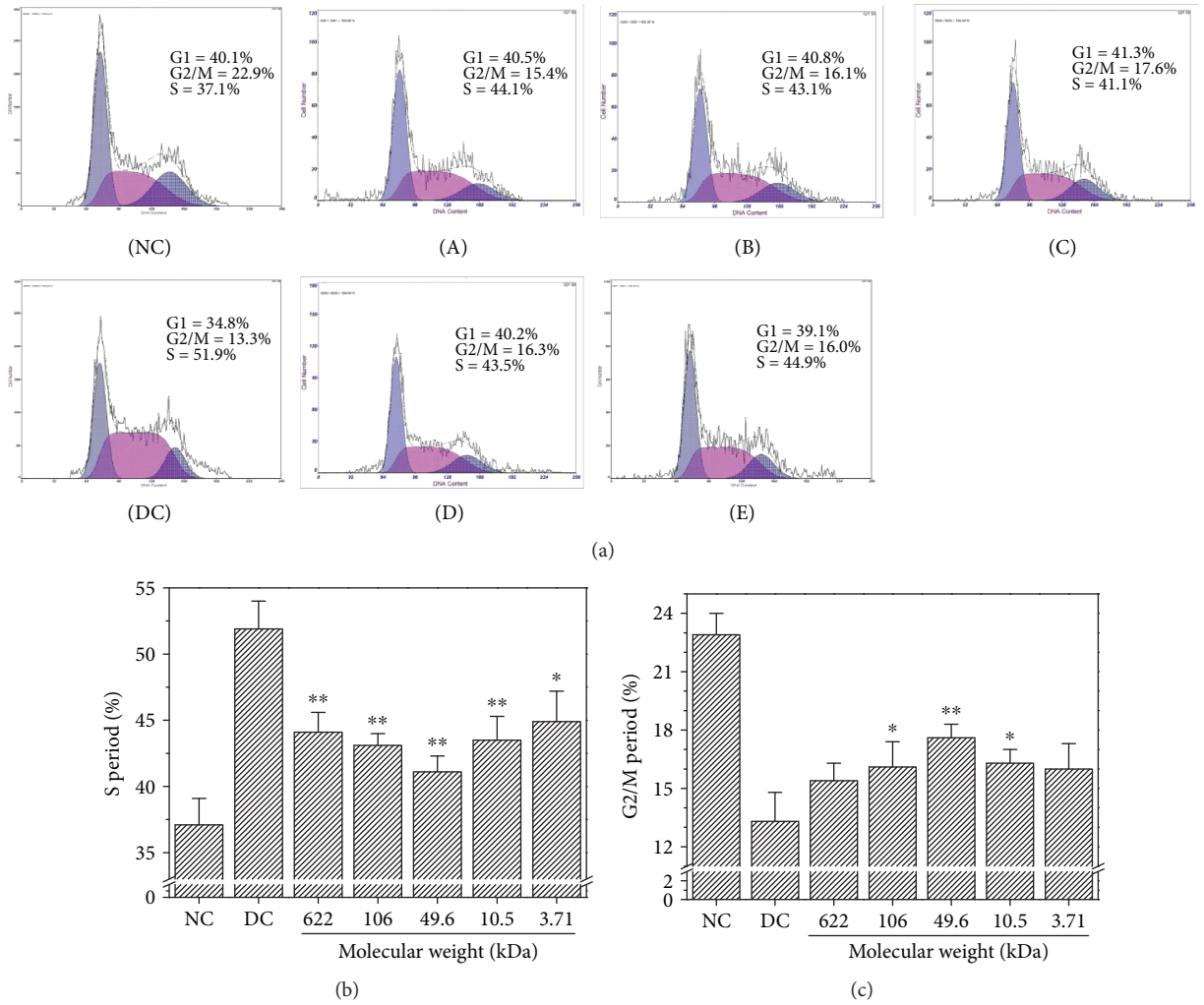

Figure 10: Changes in the cycle of the damaged HK-2 cells after being repaired by GLP fractions with different molecular weights. (a) Cell cycle histogram; (b) the percentage of cells in the S phase; (c) the percentage of cells in the G2/M phase. NC: normal control; DC: damaged control by 2.8 mmol/L oxalate; (A) GLP0, (B) GLP1, (C) GLP2, (D) GLP3, and (E) GLP6. GLP concentration: 60 μg/mL. Repaired time: 12 h. Compared to the DC group: $^{*}p < 0.05$ and $^{**}p < 0.01$.

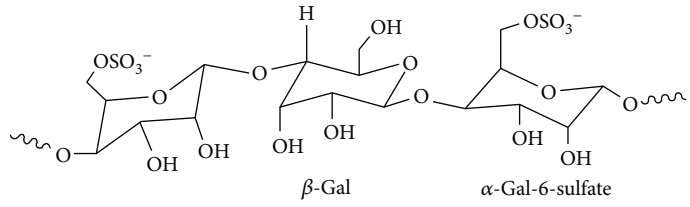

Scheme 1: Basic structure unit of GLP.

4.2. Repair Effect of GLP on Damaged HK-2 Cells. High concentrations of oxalate in urine will cause lipid peroxidation; this phenomenon leads to excessive production of reactive oxygen species (ROS) and MDA (Figure 8(b)) and damage to renal epithelial cells, resulting in enhanced adhesion of urinary crystallites and promoted formation of early microcalculus [40, 41]. Excessive ROS generation resulted in depletion of SOD enzyme activity of cells (Figure 8(a)), indicating that oxalate reduced the antioxidant capacity of cells. GLPs showed significant antioxidant activity and effectively repaired cells against oxidative stress caused by oxalate. The SOD activity was obviously increased when the damaged cells were repaired with 60 μg/mL GLPs, and the MDA content was obviously reduced compared with the injured cells. In addition, the present results indicate that cell viability decreased (Figure 5) and the amount of LDH released into

the extracellular matrix increased (Figure 6) when HK-2 cells were damaged by oxalate. After the damaged HK-2 cells were repaired through treatment with various fractions of GLP, the cell viability increased, the amount of LDH released decreased, the cell morphology was improved, and the number of living cells increased (Figure 7). Subha and Varalakshmi [42] reported that sodium pentosan polysulfate can reduce LDH secretion in calculogenic rat urine. Meanwhile, glycosaminoglycan can prevent the changes of cytosolic Ca^{2+} levels in renal tubular epithelial cells induced by oxalic acid and recover the cell morphology [43].

Mitochondrial membrane potential ($\Delta\Psi m$) is higher in normal cells than that in damaged cells [44]. When the cells were oxidatively damaged by oxalate, the permeability of the mitochondrial membrane increased, which induced Ca^{2+} influx and depolarization of the mitochondria [45], resulting in decreased $\Delta\psi m$ (Figure 9(b)). GLP fractions with different molecular weights can be used to repair the membrane potential of cells. The increase in $\Delta\psi m$ is related to the molecular weight of GLP (Figures 8(a)–8(e)); that is, the $\Delta\psi m$ of the cell was closest to the normal group after being repaired by GLP with molecular weight of 49.6 kDa. Li et al. [46] reported that *Ganoderma atrum* polysaccharide (PSG-1) increased Bcl-2 protein expression in the mitochondria; the polysaccharide inhibited Bax translocation, cytochrome c release, and caspase activation, resulting in an increase in $\Delta\psi m$ of the cell. *Sparassis crispa* polysaccharide fraction with a molecular weight of 75 kDa reduced the accumulation of reactive oxygen species, blocked Ca^{2+} influx, and prevented depolarization of the mitochondrial membrane potential to protect PC12 cells against L-Glu-induced injury [45]. GLP can repair the mitochondria in damaged cells because $-OSO_3H$ and $-COOH$ functional groups are rich in GLP, which can scavenge reactive oxygen species [24].

In damaged cells, the percentage of cells in the S phase (51.9%) increased but that in the G2/M phase decreased (Figure 10). The cell cycle was arrested in the S phase. This result could be due to the cell initiated DNA repair when the DNA in the cell was damaged. When DNA cannot repair by itself, the cells cannot enter the G2/M phase and block the S phase [30]. After treatment with GLP with different molecular weights, the percentage of cells in the S phase decreased and that in the G2/M phase increased. Hence, GLP promoted cell cycle progression from the S phase to the G2/M phase and repaired DNA replication. The repair ability on cell cycle progression was associated with the molecular weight of GLP (Figures 9(A)–9(E)), and GLP2 with a molecular weight of 49.6 kDa exhibited the strongest repair ability.

4.3. Differences in Repair Effect of Polysaccharides with Different Molecular Weights. The repair effect of GLP on damaged HK-2 cells could be due to polysaccharide molecules, which are dispersed to the damaged cell membrane gap to repair the cell or adhered to the cell membrane to block further oxidative damage by oxalate; the dispersion and adhesion of the polysaccharide are closely correlated with its molecular weight [47].

(1) The high molecular weight of polysaccharides limited their physical properties, such as highly compact molecular structure, large molecular size, and low water solubility, resulting in decreased possibility of migrating to the cell membrane [32]; the polysaccharides cannot easily widen the cell membranes to exert their biological effects.

(2) For example, the biological availability of low-molecular-weight heparin is higher than that of the ordinary heparin, the former thereby inhibiting atherosclerosis [48]. A previous study on three degraded porphyran fractions (with molecular weights of 29,695, 6893, and 5876 Da) reported that fractions with low molecular weight exhibited strong DPPH radical scavenging ability and antioxidant activity [49]. Sun et al. [50] degraded the crude *Porphyridium cruentum* and obtained six degraded polysaccharide fractions, with molecular weights of 6.53, 256, 606, 802.6, 903.3, and 1002 kDa; the polysaccharide fraction with molecular weight of 6.53 kDa exhibited the optimal effect on enhancing immunomodulatory ability.

(3) If the polysaccharide molecular weight is too low, it cannot form an active polymer structure for the biological activity. Liao et al. [6] studied the hypoglycemic effect of GLP with different molecular weights in diabetic mice and discovered that GLP with high molecular weight (such as 121.89 kDa) did not easily pass through the cell membrane to play its biological role; moreover, GLP with low molecular weight (such as 5 kDa) cannot form an active polymer structure for the biological activity, leading to decreased bioactivity. Cai et al. [51] also reported that the anticoagulant activity of GSP-2, with molecular weight of 28 kDa and which was extracted from *G. scabrabunge*, is lower than that of GSP-3, with a high molecular weight of 58 kDa.

(4) Polysaccharides with appropriate molecular weight have high freedom degree and small steric hindrance; they require less energy to diffuse into cell membrane breach [47]; therefore, these polysaccharides exhibit great potential to be absorbed by the cell membrane through electrostatic interactions and repair the cell. Thus, degradation of high-molecular-weight polysaccharides into their counterparts with appropriate molecular weight can improve their biological activity [32]. The appropriate molecular weight to obtain optimal bioactivity varies among different plant polysaccharides. For example, Meng et al. [52] reported that polysaccharides with molecular weight of 10–20 kDa exhibited higher hydroxyl radical scavenging activity than did polysaccharide fractions with molecular weight of 43 and 4.7 kDa.

Renal tubular cell injury plays a key role in the pathophysiological processes of renal stone diseases. Abnormally elevated urinary oxalate induces tubular dysfunction or

damage, thereby promoting the retention of CaOx crystals. This phenomenon is believed to be a prerequisite for the eventual formation of kidney stones [53]. Our results demonstrated that the GLP fractions can repair oxalate-induced oxidatively damaged HK-2 cells, and their repair ability is correlated with the molecular weight of the fractions. These results may help design structure-based drugs with specific actions on urolithiasis.

5. Conclusions

Seven fractions with molecular weights of 106, 49.6, 10.5, 6.14, 5.06, 3.71, and 2.42 kDa were obtained by controlling H_2O_2 concentration during degradation of crude GLP. GLP consists of β-D-galactose and 6-O-sulfate-3,6-α-L-galactose. H_2O_2 degradation does not change the structure of GLP polysaccharides, whereas the contents of the $-OSO_3H$ and $-COOH$ groups of the polysaccharides slightly increased after degradation. Various polysaccharide fractions can repair oxalate-induced oxidatively damaged HK-2 cells. After being repaired by polysaccharides, the cell viability and SOD activity increased, the amount of LDH and MDA released decreased, the cell morphology was gradually restored to normal cells, the mitochondrial membrane potential increased, the percentage of cells in the S phase decreased, and the percentage of cells in the G2/M phase increased. The repair ability of each polysaccharide fraction of GLP is associated with its molecular weight. GLP2 with a molecular weight of 49.6 kDa exhibited a superior repair effect than did other degraded polysaccharide segments and crude polysaccharide. Moreover, polysaccharides with a molecular weight largely deviating from 49.6 kDa elicited weak repair capacity. Our results suggested that degraded GLP fractions, especially GLP2, could be developed into novel anti-stone polysaccharide drugs.

Conflicts of Interest

The authors declare that they have no competing interests.

Acknowledgments

This research work was granted by the National Natural Science Foundation of China (no. 81670644 and 21701050).

References

[1] C. Faggio, M. Pagano, A. Dottore, G. Genovese, and M. Morabito, "Evaluation of anticoagulant activity of two algal polysaccharides," *Natural Product Research*, vol. 30, no. 17, pp. 1934–1937, 2016.

[2] L. Sun, J. Chu, Z. Sun, and L. Chen, "Physicochemical properties, immunomodulation and antitumor activities of polysaccharide from Pavlova viridis," *Life Sciences*, vol. 144, pp. 156–161, 2016.

[3] G.-J. Wu, S.-M. Shiu, M.-C. Hsieh, and G.-J. Tsai, "Anti-inflammatory activity of a sulfated polysaccharide from the brown alga *Sargassum cristaefolium*," *Food Hydrocolloids*, vol. 53, pp. 16–23, 2016.

[4] B. W. Jo and S.-K. Choi, "Degradation of fucoidans from Sargassum fulvellum and their biological activities," *Carbohydrate Polymers*, vol. 111, pp. 822–829, 2014.

[5] Z. Zhu, Q. Zhang, L. Chen et al., "Higher specificity of the activity of low molecular weight fucoidan for thrombin-induced platelet aggregation," *Thrombosis Research*, vol. 125, no. 5, pp. 419–426, 2010.

[6] X. Liao, L. Yang, M. Chen, J. Yu, S. Zhang, and Y. Ju, "The hypoglycemic effect of a polysaccharide (GLP) from Gracilaria lemaneiformis and its degradation products in diabetic mice," *Food & Function*, vol. 6, no. 8, pp. 2542–2549, 2015.

[7] Q.-M. Liu, Y. Yang, S. J. Maleki et al., "Anti-food allergic activity of sulfated polysaccharide from *gracilaria lemaneiformis* is dependent on immunosuppression and inhibition of p38 MAPK," *Journal of Agricultural and Food Chemistry*, vol. 64, no. 22, pp. 4536–4544, 2016.

[8] R. O. Silva, A. P. M. Santana, N. S. Carvalho et al., "A sulfated-polysaccharide fraction from seaweed *gracilaria birdiae* prevents naproxen-induced gastrointestinal damage in rats," *Marine Drugs*, vol. 10, no. 12, pp. 2618–2633, 2012.

[9] Y. Fan, W. Wang, W. Song, H. Chen, A. Teng, and A. Liu, "Partial characterization and anti-tumor activity of an acidic polysaccharide from Gracilaria lemaneiformis," *Carbohydrate Polymers*, vol. 88, no. 4, pp. 1313–1318, 2012.

[10] T. Di, G. Chen, Y. Sun, S. Ou, X. Zeng, and H. Ye, "Antioxidant and immunostimulating activities in vitro of sulfated polysaccharides isolated from Gracilaria rubra," *Journal of Functional Foods*, vol. 28, pp. 64–75, 2017.

[11] I. Sorokin, C. Mamoulakis, K. Miyazawa, A. Rodgers, J. Talati, and Y. Lotan, "Epidemiology of stone disease across the world," *World Journal of Urology*, vol. 35, no. 9, pp. 1301–1320, 2017.

[12] L. H. R. Xu, B. Adams-Huet, J. R. Poindexter, N. M. Maalouf, O. W. Moe, and K. Sakhaee, "Temporal changes in kidney stone composition and in risk factors predisposing to stone formation," *The Journal of Urology*, vol. 197, no. 6, pp. 1465–1471, 2017.

[13] J.-M. Ouyang, M. Wang, P. Lu, and J. Tan, "Degradation of sulfated polysaccharide extracted from algal *Laminaria japonica* and its modulation on calcium oxalate crystallization," *Materials Science and Engineering: C*, vol. 30, no. 7, pp. 1022–1029, 2010.

[14] T. Alelign and B. Petros, "Kidney stone disease: an update on current concepts," *Advances in Urology*, vol. 2018, Article ID 3068365, 12 pages, 2018.

[15] S. Unlu and E. Saglar, "Evaluation of cytogenetic and genotoxic effects of oxalic acid by the alkaline comet assay and QRT PCR in human buccal epithelial cells," *Analytical and quantitative cytopathology and histopathology*, vol. 37, no. 6, pp. 347–352, 2015.

[16] X. Y. Sun, J. M. Ouyang, and K. Yu, "Shape-dependent cellular toxicity on renal epithelial cells and stone risk of calcium oxalate dihydrate crystals," *Scientific Reports*, vol. 7, no. 1, article 7250, 2017.

[17] X. Y. Sun, K. Yu, and J. M. Ouyang, "Time-dependent subcellular structure injuries induced by nano-/micron-sized calcium oxalate monohydrate and dihydrate crystals," *Materials Science and Engineering: C*, vol. 79, pp. 445–456, 2017.

[18] P. Bhadja, C.-Y. Tan, J.-M. Ouyang, and K. Yu, "Repair effect of seaweed polysaccharides with different contents of sulfate

group and molecular weights on damaged HK-2 cells," *Polymer*, vol. 8, no. 5, p. 188, 2016.

[19] X.-T. Ma, X.-Y. Sun, K. Yu, B.-S. Gui, Q. Gui, and J.-M. Ouyang, "Effect of content of sulfate groups in seaweed polysaccharides on antioxidant activity and repair effect of subcellular organelles in injured HK-2 cells," *Oxidative Medicine and Cellular Longevity*, vol. 2017, Article ID 2542950, 13 pages, 2017.

[20] A. M. Faure, J. Werder, and L. Nystroem, "Reactive oxygen species responsible for beta-glucan degradation," *Food Chemistry*, vol. 141, no. 1, pp. 589–596, 2013.

[21] S. Mazumder, P. K. Ghosal, C. A. Pujol, M. J. Carlucci, E. B. Damonte, and B. Ray, "Isolation, chemical investigation and antiviral activity of polysaccharides from *Gracilaria corticata* (Gracilariaceae, Rhodophyta)," *International Journal of Biological Macromolecules*, vol. 31, no. 1–3, pp. 87–95, 2002.

[22] R. Sakthivel and K. P. Devi, "Evaluation of physicochemical properties, proximate and nutritional composition of *Gracilaria edulis* collected from Palk Bay," *Food Chemistry*, vol. 174, pp. 68–74, 2015.

[23] L. Luo, M. Wu, L. Xu et al., "Comparison of physicochemical characteristics and anticoagulant activities of polysaccharides from three sea cucumbers," *Marine Drugs*, vol. 11, no. 12, pp. 399–417, 2013.

[24] S. Sudharsan, N. Subhapradha, P. Seedevi et al., "Antioxidant and anticoagulant activity of sulfated polysaccharide from Gracilaria debilis (Forsskal)," *International Journal of Biological Macromolecules*, vol. 81, pp. 1031–1038, 2015.

[25] J. He, Y. Xu, H. Chen, and P. Sun, "Extraction, structural characterization, and potential antioxidant activity of the polysaccharides from four seaweeds," *International Journal of Molecular Sciences*, vol. 17, no. 12, p. 1988, 2016.

[26] P. Salehi, Y. Dashti, F. M. Tajabadi, F. Safidkon, and R. Rabei, "Structural and compositional characteristics of a sulfated galactan from the red alga Gracilariopsis persica," *Carbohydrate Polymers*, vol. 83, no. 4, pp. 1570–1574, 2011.

[27] M. E. R. Duarte, M. D. Noseda, M. A. Cardoso, S. Tulio, and A. S. Cerezo, "The structure of a galactan sulfate from the red seaweed Bostrychia montagnei," *Carbohydrate Research*, vol. 337, no. 12, pp. 1137–1144, 2002.

[28] F. Laffleur, J. Psenner, and W. Suchaoin, "Permeation enhancement via thiolation: in vitro and ex vivo evaluation of hyaluronic acid-cysteine ethyl ester," *Journal of Pharmaceutical Sciences*, vol. 104, no. 7, pp. 2153–2160, 2015.

[29] F. Yu, X. Li, L. Cai et al., "Achyranthes bidentata polysaccharides induce chondrocyte proliferation via the promotion of the G1/S cell cycle transition," *Molecular Medicine Reports*, vol. 7, no. 3, pp. 935–940, 2013.

[30] J. A. Seiler, C. Conti, A. Syed, M. I. Aladjem, and Y. Pommier, "The intra-S-phase checkpoint affects both DNA replication initiation and elongation: single-cell and -DNA fiber analyses," *Molecular and Cellular Biology*, vol. 27, no. 16, pp. 5806–5818, 2007.

[31] S. Wu and H. Pan, "Characteristics of maltose degradation by hydrogen peroxide," *Journal of Food Processing and Preservation*, vol. 40, no. 1, pp. 14–19, 2016.

[32] Y. Hou, J. Wang, W. Jin, H. Zhang, and Q. Zhang, "Degradation of Laminaria japonica fucoidan by hydrogen peroxide and antioxidant activities of the degradation products of different molecular weights," *Carbohydrate Polymers*, vol. 87, no. 1, pp. 153–159, 2012.

[33] X. Ji, Q. Peng, Y. Yuan, J. Shen, X. Xie, and M. Wang, "Isolation, structures and bioactivities of the polysaccharides from jujube fruit (Ziziphus jujuba Mill.): a review," *Food Chemistry*, vol. 227, pp. 349–357, 2017.

[34] M. Perez Recalde, D. J. Canelon, R. S. Compagnone, M. C. Matulewicz, A. S. Cerezo, and M. Ciancia, "Carrageenan and agaran structures from the red seaweed Gymnogongrus tenuis," *Carbohydrate Polymers*, vol. 136, pp. 1370–1378, 2016.

[35] M. E. Duarte, J. P. Cauduro, D. G. Noseda et al., "The structure of the agaran sulfate from *Acanthophora spicifera* (Rhodomelaceae, Ceramiales) and its antiviral activity. Relation between structure and antiviral activity in agarans," *Carbohydrate Research*, vol. 339, no. 2, pp. 335–347, 2004.

[36] A. P. Narrainen and P. A. Lovell, "Mechanism and kinetics of free-radical degradation of xyloglucan in aqueous solution," *Polymer*, vol. 51, no. 26, pp. 6115–6122, 2010.

[37] F. Tian, Y. Liu, K. Hu, and B. Y. Zhao, "The depolymerization mechanism of chitosan by hydrogen peroxide," *Journal of Materials Science*, vol. 38, no. 23, pp. 4709–4712, 2003.

[38] L. Sun, L. Wang, J. Li, and H. Liu, "Characterization and antioxidant activities of degraded polysaccharides from two marine Chrysophyta," *Food Chemistry*, vol. 160, pp. 1–7, 2014.

[39] H.-J. Zhang, W.-J. Mao, F. Fang et al., "Chemical characteristics and anticoagulant activities of a sulfated polysaccharide and its fragments from *Monostroma latissimum*," *Carbohydrate Polymers*, vol. 71, no. 3, pp. 428–434, 2008.

[40] C. Zhao, H. Yang, X. Zhu et al., "Oxalate-degrading enzyme recombined lactic acid bacteria strains reduce hyperoxaluria," *Urology*, vol. 113, pp. 253.e1–253.e7, 2018.

[41] Y. Jin, K. Liu, J. Peng et al., "*Rhizoma Dioscoreae* Nipponicae polysaccharides protect HUVECs from H_2O_2-induced injury by regulating PPARγ factor and the NADPH oxidase/ROS–NF-κB signal pathway," *Toxicology Letters*, vol. 232, no. 1, pp. 149–158, 2015.

[42] K. Subha and P. Varalakshmi, "Alterations in some risk factors and urinary enzymes in urolithiatic rats treated with sodium pentosan polysulphate," *Biochemistry and Molecular Biology International*, vol. 29, no. 2, pp. 271–280, 1993.

[43] S. Iida, M. Ishimatsu, S. Chikama et al., "Protective role of heparin/heparan sulfate on oxalate-induced changes in cell morphology and intracellular Ca^{2+}," *Urological Research*, vol. 31, no. 3, pp. 198–206, 2003.

[44] J. Zhang, Q. Wang, C. Xu et al., "MitoTEMPO prevents oxalate induced injury in NRK-52E cells via inhibiting mitochondrial dysfunction and modulating oxidative stress," *Oxidative Medicine and Cellular Longevity*, vol. 2017, Article ID 7528090, 9 pages, 2017.

[45] S. Hu, D. Wang, J. Zhang et al., "Mitochondria related pathway is essential for polysaccharides purified from sparassis crispa mediated neuro-protection against glutamate-induced toxicity in differentiated PC12 cells," *International Journal of Molecular Sciences*, vol. 17, no. 2, p. 133, 2016.

[46] W.-J. Li, S.-P. Nie, Y.-F. Yao et al., "*Ganoderma atrum* polysaccharide ameliorates hyperglycemia-induced endothelial cell death via a mitochondria-ROS pathway," *Journal of Agricultural and Food Chemistry*, vol. 63, no. 37, pp. 8182–8191, 2015.

[47] B. Chen, D. Bohnert, R. Ben Borgens, and Y. Cho, "Pushing the science forward: chitosan nanoparticles and functional repair of CNS tissue after spinal cord injury," *Journal of Biological Engineering*, vol. 7, no. 1, p. 15, 2013.

[48] E. Holmer, K. Kurachi, and G. Soderstrom, "The molecular-weight dependence of the rate-enhancing effect of heparin on the inhibition of thrombin, factor Xa, factor IXa, factor XIa, factor XIIa and kallikrein by antithrombin," *The Biochemical Journal*, vol. 193, no. 2, pp. 395–400, 1981.

[49] T. T. Zhao, Q. B. Zhang, H. M. Qi et al., "Degradation of porphyran from *Porphyra haitanensis* and the antioxidant activities of the degraded porphyrans with different molecular weight," *International Journal of Biological Macromolecules*, vol. 38, no. 1, pp. 45–50, 2006.

[50] L. Sun, L. Wang, and Y. Zhou, "Immunomodulation and antitumor activities of different-molecular-weight polysaccharides from Porphyridium cruentum," *Carbohydrate Polymers*, vol. 87, no. 2, pp. 1206–1210, 2012.

[51] W. Cai, H. Xu, L. Xie et al., "Purification, characterization and in vitro anticoagulant activity of polysaccharides from Gentiana scabra Bunge roots," *Carbohydrate Polymers*, vol. 140, pp. 308–313, 2016.

[52] L. Meng, S. Sun, R. Li, Z. Shen, P. Wang, and X. Jiang, "Antioxidant activity of polysaccharides produced by Hirsutella sp. and relation with their chemical characteristics," *Carbohydrate Polymers*, vol. 117, pp. 452–457, 2015.

[53] S. R. Khan, "Hyperoxaluria-induced oxidative stress and antioxidants for renal protection," *Urological Research*, vol. 33, no. 5, pp. 349–357, 2005.

Hindawi
Oxidative Medicine and Cellular Longevity
Volume 2018, Article ID 7309073, 13 pages
https://doi.org/10.1155/2018/7309073

Review Article

Therapeutic Potential of Salviae Miltiorrhizae Radix et Rhizoma against Human Diseases Based on Activation of Nrf2-Mediated Antioxidant Defense System: Bioactive Constituents and Mechanism of Action

Guo-Hui Li,[1] Yan-Ru Li,[2] Ping Jiao,[1] Yu Zhao,[2] Hui-Xin Hu,[2] Hong-Xiang Lou,[2] and Tao Shen[2]

[1]*Department of Pharmacy, Jinan Maternity and Child Care Hospital, Jinan, China*
[2]*Key Laboratory of Chemical Biology (MOE), School of Pharmaceutical Sciences, Shandong University, Jinan, China*

Correspondence should be addressed to Tao Shen; shentao@sdu.edu.cn

Received 10 January 2018; Revised 17 March 2018; Accepted 29 April 2018; Published 27 June 2018

Academic Editor: Jaideep Banerjee

Oxidative stress plays a central role in the pathogenesis of many human diseases. The nuclear factor erythroid 2-related factor 2 (Nrf2) is a key transcription factor regulating the intracellular antioxidant response and is an emerging target for the prevention and therapy of oxidative stress-related diseases. Salviae Miltiorrhizae Radix et Rhizoma (SMRR) is a traditional Chinese medicine (TCM) and is commonly used for the therapy of cardiac cerebral diseases. Cumulative evidences indicated that the extract of SMRR and its constituents, represented by lipophilic diterpenoid quinones and hydrophilic phenolic acids, were capable of activating Nrf2 and inhibiting oxidative stress. These bioactive constituents demonstrated a therapeutic potential against human diseases, exemplified by cardiovascular diseases, neurodegenerative diseases, diabetes, nephropathy, and inflammation, based on the induction of Nrf2-mediated antioxidant response and the inhibition of oxidative stress. In the present review, we introduced the SMRR and Nrf2 signaling pathway, summarized the constituents with an Nrf2-inducing effect isolated from SMRR, and discussed the molecular mechanism and pharmacological functions of the SMRR extract and its constituents.

1. Introduction

Oxidative stress is defined as an imbalance of the oxidants/antioxidants tilting toward an oxidative status and characterized by the overproductions of reactive oxygen species (ROS) and reactive nitrogen species (RNS) compared with the basal state [1]. Cumulative evidences have verified that oxidative stress impairs cellular components (e.g., lipids, proteins, and nucleic acids) and plays a central role in the pathogenesis of many human diseases, such as cardiovascular diseases, neurodegenerative diseases, chronic obstructive pulmonary disease (COPD), atherosclerosis, chronic kidney diseases, diabetes, and cancer [2–8]. To eliminate excess oxidants and maintain intracellular redox homeostasis, cells have developed an adaptive and dynamic antioxidant defense system, including antioxidant molecules, antioxidant enzymes, and phase II detoxifying enzymes, to protect cells and tissues against oxidative insults.

The nuclear factor erythroid 2-related factor 2 (Nrf2) is a key transcription factor regulating the intracellular antioxidant response and plays a vital role in maintaining intracellular redox homeostasis [9]. The predominant biological function of Nrf2 is to activate the transcriptions of a wide array of cytoprotective genes that are capable of counteracting the harmful effects caused by oxidative stress and toxicants. Activation of the Nrf2-mediated cellular defense system definitely intervenes the pathogenesis of oxidative stress-induced diseases, such as cancer [10], diabetes [11], respiratory diseases [12], chronic inflammation [13], cardiovascular diseases [14], and neurodegenerative diseases

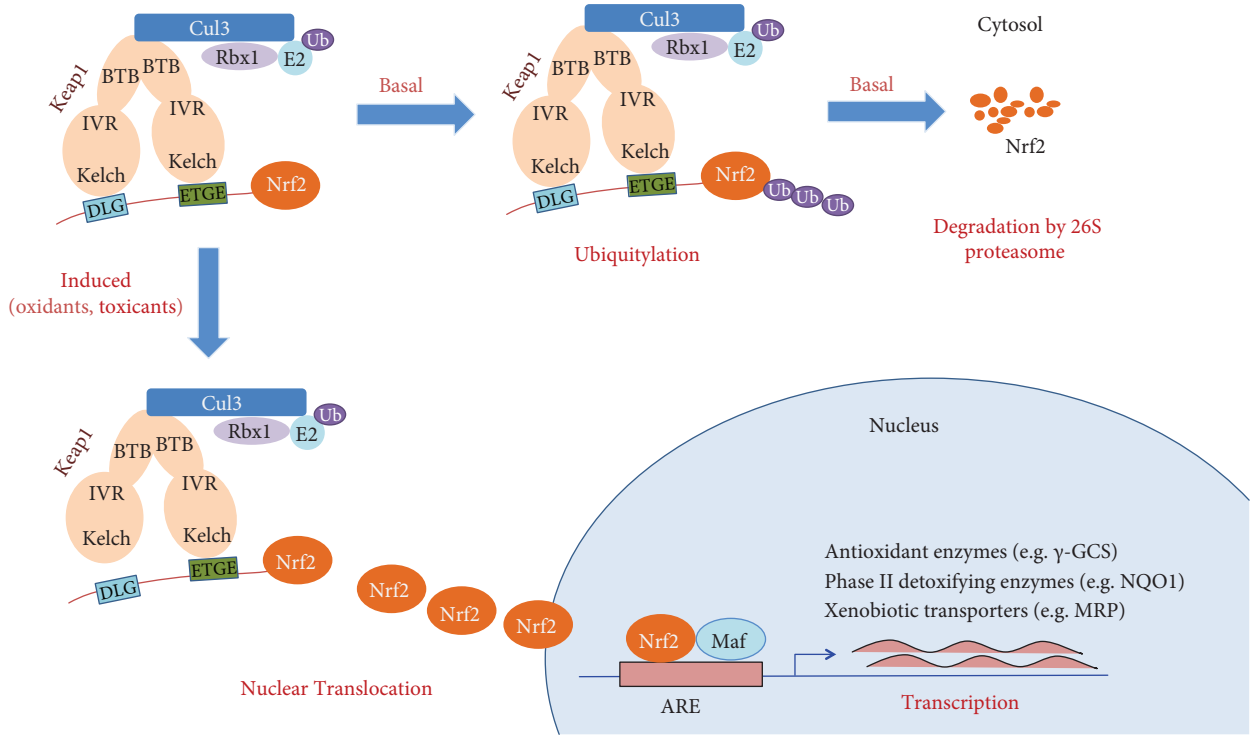

Figure 1: Schematic model of the regulation of the Nrf2 signaling pathway. Under basal conditions, Nrf2 undergoes Keap1-mediated ubiquitylation and 26S proteasome-mediated degradation. In response to oxidants, toxicants, or Nrf2 inducers, Nrf2 is released from Keap1, translocates into the nucleus, and activates the transcription of ARE-mediated protective genes.

[15]. The protective roles of Nrf2 against oxidative insults and xenobiotic have also been verified by bioassays using Nrf2-null mice. For example, Nrf2-null mice are more susceptible to cigarette smoke-induced emphysema [16], acetaminophen-induced hepatotoxicity [17], and benzo[a]-pyrene-induced carcinogenesis [18]. Therefore, the activation of the Nrf2-mediated antioxidant defense system is an efficient strategy for the prevention and therapy of these diseases.

Natural product without a doubt is an invaluable source for discovering Nrf2 activators, and nowadays, plenty of natural molecules demonstrate therapeutic potentials against oxidative stress-related disease due to their functions on the activation of Nrf2 [19]. In our systematic investigation of Nrf2 activators from traditional Chinese medicines (TCM) [1, 20–22], we found that the extract of Salviae Miltiorrhizae Radix et Rhizoma (SMRR) promoted the activity of Nrf2-mediated phase II detoxifying enzyme, NAD(P)H: quinone reductase, and thus displayed potency on the activation of the Nrf2 signaling pathway [21]. Consistent with our observations, some literatures indicated that lipophilic diterpenoid quinones and hydrophilic phenolic acids, two types of predominant bioactive ingredients of SMRR, possessed evident Nrf2-inducing properties and inhibited the pathogenesis of diseases, exemplified by Alzheimer's disease [23], cardiovascular diseases [24, 25], and hepatic injury [26].

Although some reviews concerning the chemistry and pharmacology of SMRR have been published [27, 28], chemical constituents with Nrf2-inducing effects and their pharmacological functions based on the activation of Nrf2 have not been summarized. In this review, we introduced the SMRR and Nrf2 pathway, summarized the Nrf2 activators from SMRR, and discussed their molecular mechanisms and pharmacological functions against human diseases.

2. Nrf2 Signaling Pathway

Nrf2 is a basic leucine zipper (bZIP) transcription factor bearing a Cap'n'collar (CNC) structure [29]. It possesses seven functional domains, named as Neh1–Neh7. The Neh2 domain is the key regulatory domain with two binding sites (termed as ETGE and DLG motifs) that interact with its negative regulator, Kelch-like ECH-associated protein 1 (Keap1), a substrate adaptor protein for the cullin 3-(Cul3-) containing E3 ubiquitin ligase (Figure 1) [30, 31]. Keap1 contains three functional domains that are the broad complex/tramtrack/bric-a-brac (BTB) domain, intervening region (IVR), and Kelch domain. The N-terminal BTB domain is involved in the dimerization of Keap1 via binding with Cul3. The Kelch domain interacts with the Neh2 domain of Nrf2 and regulates its physiological functions.

Under a normal state, Nrf2 is primarily localized in a complex with its repressor Keap1 via direct protein-protein interactions and is maintained at a low level in cytosol through Keap1-mediated ubiquitylation and 26S proteasome-mediated degradation. Upon exposure of cells to oxidative stress, Nrf2 is released from Keap1, translocates into the nucleus, binds to the antioxidant response element (ARE) located in the promoter region of

(a) (b) (c)

Figure 2: Pictures of *Salvia miltiorrhiza* and Salviae Miltiorrhizae Radix et Rhizoma: (a) the whole plant of *S. miltiorrhiza*; (b) the roots of *S. miltiorrhiza*; and (c) medicinal materials of SMRR used in TCM.

cytoprotective genes, and activates their transcription. These ARE-containing genes are mainly divided into three groups: (i) intracellular redox-balancing proteins, including γ-glutamyl cysteine synthetase (γ-GCS), thioredoxin reductase (TrxR), and heme oxygenase-1 (HO-1) that maintain the cellular redox capacity and eliminate ROS; (ii) phase II detoxifying enzymes, exemplified by NAD(P)H: quinone oxidoreductase 1 (NQO1) and glutathione S-transferase (GST), which promote excretion of toxicants; and (iii) xenobiotic transporters: multidrug resistance-associated protein (MRP) [9, 32]. The schematic model of the Nrf2 pathway is shown in Figure 1. Based on the biological functions of these genes, the activation of Nrf2-mediated defensive response efficiently counteracts oxidative insults.

3. Salviae Miltiorrhizae Radix et Rhizoma (SMRR)

Salviae Miltiorrhizae Radix et Rhizoma, named as "Danshen" in Chinese, is the roots and rhizomes of *Salvia miltiorrhiza* Bunge (Labiatae) (Figure 2) and has a long history for the therapy of human diseases in China. Its medical applications have been recorded in many Chinese medical documents, including "Shennong's Classic of Materia Medica" (Shennong Ben Cao Jing) and "Compendium of Materia Medica" (Ben Cao Gang Mu). According to the theory of TCM, it possesses the capabilities of promoting blood flow in menstruation, removing blood stasis, relieving pain, resolving mental uneasiness and restlessness, nourishing the blood, and tranquilizing the mind (Chinese Pharmacopoeia, 2015). Presently, it is predominantly used in multicomponent preparations (e.g., Fufang Danshen Tablets, Fufang Danshen Dripping Pills, and Guanxin Danshen Capsules) to treat cardiac cerebral diseases (e.g., ischemic heart disease, ischemic stroke, coronary heart disease, angina, and thrombosis) owing to SMRR's biological functions of inhibiting platelet aggregation, modulating endothelial cell permeability, and protecting cells from ischemia-reperfusion (I/R) injury. Besides these pharmacological effects, a growing body of data indicated that SMRR potently activated intracellular antioxidant enzymes, upregulated endogenous antioxidants, and scavenged intracellular ROS. Therefore, SMRR demonstrated potential therapeutic effects against oxidative stress-induced diseases, such as cardiovascular diseases, inflammation, and renal disease [33–35].

4. Chemical Ingredients from SMRR and Their Potential Nrf2-Inducing Effects

Since the long history of traditional applications and significant therapeutic effects against human diseases, a large

number of phytochemical investigations of SMRR have been performed to give the isolation of diverse chemical ingredients. The structural information of the purified ingredients has been summarized by some reviews [27, 36, 37]. Based on their structural characteristics and molecular polarity, SMRR-derived chemical ingredients are classified into two groups: (i) lipophilic diterpenoid quinones, which are commonly abietane-type diterpenoid skeleton with quinone moiety, including tanshinone I (**12**), tanshinone IIA (**16**), and miltirone (**17**), and (ii) hydrophilic phenolic acids that are condensed caffeic acid derivatives with different linkage and degree of polymerization, such as danshensu (**22**) and salvianolic acids A-B (**24**-**25**). Up to now, more than fifty diterpenoid quinones and forty phenolic acids have been reported from SMRR [27]. Among them, tanshinone IIA (**16**) and salvianolic acid B (**25**) are considered to be biologically active substances of SMRR and thus are selected as the markers for the quality control of SMRR (Chinese Pharmacopoeia, 2015). In this section, we have only summarized the chemical ingredients with Nrf2-inducing activity. As depicted in Table 1 and Figure 3, diterpenoid quinones are the predominant Nrf2 inducers of SMRR. For instance, Zhang et al. identified twenty diterpenoid quinones, including constituents 1–17, using a strategy combining a HPLC-based high-resolution peak fractionation approach and an ARE luciferase assay in HEK 293 T cells [38]. Furthermore, diterpenoid quinones 1, 5, 9, 11, and 15–21 were verified to be potential Nrf2 inducers by a HPLC/MS/MS method combined with QR-inducing assay in Hepa 1c1c7 cells [39]. Of which, 15,16-dihydrotanshinone I (**9**), tanshinone I (**12**), tanshinone IIA (**16**), and miltirone (**17**) have been extensively investigated. The phenolic acids, including danshensu (**22**), rosmarinic acid (**23**), and salvianolic acids A-B (**24**-**25**), are capable of activating Nrf2-mediated cytoprotective responses.

5. Nrf2-Based Therapeutic Potential of SMRR and Its Constituents against Human Diseases

Plenty of reviews have summarized the pharmacological functions and therapeutic effects of SMRR and its constituents on cardiovascular diseases [25, 55–57], neurodegenerative disease [23], cancer [58], osteoporosis [59], diabetes, and liver fibrosis [28]. In this section, we focused on their therapeutic effects related to the activation of Nrf2-mediated antioxidant response and inhibition of oxidative stress.

5.1. Cardiovascular Diseases. Oxidative stress plays an important role in the pathogenesis of cardiovascular diseases, including hypertension, I/R injury, atherosclerosis, and heart failure [7, 60–62]. Inductions of the Nrf2-regulated enzymes [e.g., superoxide dismutase (SOD), HO-1, catalase (CAT), and glutathione peroxidase (GPx)] are beneficial for the therapy of these cardiovascular diseases. The aqueous extract of SMRR prevented myocardium oxidative injury in an I/R rat model [34]. It enhanced capacities of antioxidant enzymes (e.g., SOD, CAT, and GPx) and prevented myocardium cell apoptosis. Similarly, the ethanol extract of SMRR, together with tanshinone IIA (**16**) and salvianolic acid B (**25**), dose-dependently reduced the levels of myocardium malondialdehyde (MDA) and ROS and enhanced myocardium glutathione (GSH) levels in the I/R rat model [63].

Tanshinone IIA (**16**) induced the Nrf2 signaling pathway via activating ERK and PKB, as well as downregulating the levels of tumor necrosis factor (TNF-α) and angiotensin II, and inhibited H_2O_2-induced ROS production in human aortic smooth muscle cells [45]. It reversed TNF-α-induced downregulations of intracellular GSH, NADPH, and glucose 6-phosphate dehydrogenase (G6PDH). Tanshinone IIA (**16**) also increased the expressions of Nrf2-mediated proteins, HO-1, ATP-binding cassette transporter A1 (ABCA1), and ATP-binding cassette transporter G1 (ABCG1) in lipid-laden macrophages, and thus suppressed accumulation of cholesterol in human macrophages [64]. Tanshinone IIA (**16**) increased Nrf2 and HO-1 expressions through the activation of phosphoinositide 3-kinase (PI3K)/Akt in human umbilical vein endothelial cells (HUVECs) and protected cells against H_2O_2-induced HUVEC oxidative injury [65–67]. It also upregulated the GPx activity and protected J774 macrophages against H_2O_2-induced cell death [68]. Tanshinone IIA (**16**) attenuated cardiac dysfunction and fibrosis and prevented cardiac remodeling via downregulating NAD(P)H oxidase-derived ROS production in 2K2C hypertensive rats [69]. In addition, tanshinone IIA (**16**) inhibited the productions of oxidized low-density lipoprotein (ox-LDL) and superoxide anion and reduced MDA level in the excessive vitamin D2 and high-cholesterol diet-induced rat atherosclerotic calcification model [70].

Ox-LDL induces endothelial dysfunction and changes of intercellular adhesion molecule-1 (ICAM-1), vascular cell adhesion molecule-1 (VCAM-1), and E-selectin, which are involved in the pathogenesis of atherosclerosis. Cryptotanshinone (**11**) inhibited ox-LDL-induced membrane expressions of ICAM-1, VCAM-1, and E-selectin, which was associated with its capability of inhibiting ROS production and nuclear factor-κB (NF-κB) activation [71]. Miltirone (**17**) enhanced the expressions of Nrf2, HO-1, and NQO1 in human EA.hy926 endothelial cells [47]. It protected EA.hy926 cells against ox-LDL-induced endothelial insults via inhibiting ROS synthesis and upregulating SOD and glutathione S-transferase (GST) in an Nrf2/HO-1 dependent manner.

Danshensu (**22**) was investigated for its cardioprotective activity using isolated rat hearts of the I/R model [48]. It attenuated I/R injury through scavenging ROS and inhibiting the oxidative stress. A further study indicated that danshensu (**22**) upregulated endogenous antioxidant enzymes (e.g., SOD, CAT, MDA, GPx, and HO-1), which was associated with the activation of the Nrf2/Akt/ERK1/2 signaling pathway. Salvianolic acid A (**24**) inhibited the productions of intracellular ROS and MDA and alleviated the change of mitochondrial membrane potential (MMP), in the *tert*-butyl hydroperoxide- (*t*-BHP-) induced HUVEC oxidative injury model [72].

5.2. Neurodegenerative Diseases. Oxidative stress and its impairment to the mitochondria play a dominant role in the onset and progression of multiple neurodegenerative disorders, including Alzheimer's disease, Parkinson's disease,

Table 1: Chemical constituents with Nrf2-inducing activity.

Structural type	No	Name of compounds	Nrf2-inducing activity	Cell or animal models	Ref
Diterpenoid quinones	**1**	Tanshindiol B	6.80-fold induction of ARE luciferase activity	HEK 293 T cells	[38]
			4.85 μM for 2-fold induction of QR activity	Hepa 1c1c7 cells	[39]
	2	17-Hydroxycryptotanshinone	3.97-fold induction of ARE luciferase activity	HEK 293 T cells	[38]
	3	Isotanshinone IIA	6.45-fold induction of ARE luciferase activity	HEK 293 T cells	[38]
	4	Trijuganone A	4.31-fold induction of ARE luciferase activity	HEK 293 T cells	[38]
	5	Tanshinone IIB	5.34-fold induction of ARE luciferase activity	HEK 293 T cells	[38]
			4.85 μM for 2-fold induction of QR activity	Hepa 1c1c7 cells	[39]
	6	Przewaquinone A	6.01-fold induction of ARE luciferase activity	HEK 293 T cells	[38]
	7	Przewaquinone B	7.27-fold induction of ARE luciferase activity	HEK 293 T cells	[38]
	8	1-Ketoisocryptotanshinone	5.65-fold induction of ARE luciferase activity	HEK 293 T cells	[38]
			3.38-fold induction of ARE luciferase activity	HEK 293 T cells	[38]
			4.80 μM for 2-fold induction of QR activity	Hepa 1c1c7 cells	[39]
	9	15,16-Dihydrotanshinone I	Induction of ARE luciferase and upregulation of Nrf2 protein level	MDA-MB-231 cells	[40]
			Induction of Nrf2, NQO1, and γ-GCS protein levels	Human dermal fibroblasts.	[41]
	10	1,2,15,16-Tetrahydrotanshinone I	4.37-fold induction of ARE luciferase activity	HEK 293 T cells	[38]
	11	Cryptotanshinone	3.61-fold induction of ARE luciferase activity	HEK 293 T cells	[38]
			5.07 μM for 2-fold induction of QR activity	Hepa 1c1c7 cells	[39]
			Induction of ARE luciferase and upregulation of Nrf2 protein level	MDA-MB-231 cells	[40]
			Induction of ARE-luciferase activity	Hep G2 cells	[26]
	12	Tanshinone I	2.60-fold induction of ARE luciferase activity	HEK 293 T cells	[38]
			5.90 μM for 2-fold induction of QR activity	Hepa 1c1c7 cells	[39]
			Induction of ARE luciferase and upregulation of Nrf2 protein level	MDA-MB-231 cells	[40]
			Upregulation of Nrf2, HO-1, GCLC, and GCLM	SH-SY5Y cells	[42, 43]
			Induction of ARE-luciferase activity	Hep G2 cells	[26]
			Induction of Nrf2, NQO1, and γ-GCS protein levels	Human dermal fibroblasts	[41]
	13	RO-090680	3.06-fold induction of ARE luciferase activity	HEK 293 T cells	[38]
	14	Methylenetanshinquinone	2.77-fold induction of ARE luciferase activity	HEK 293 T cells	[38]
	15	1,2-Didehydromilitirone	3.79-fold induction of ARE luciferase activity	HEK 293 T cells	[38]
			1.04 μM for 2-fold induction of QR activity	Hepa 1c1c7 cells	[39]
	16	Tanshinone IIA	2.58-fold induction of ARE luciferase activity	HEK 293 T cells	[38]
			5.10 μM for 2-fold induction of QR activity	Hepa 1c1c7 cells	[39]
			Upregulation of Nrf2, HO-1, and NQO-1 protein levels	JB6 cells	[44]
			Induction of ARE luciferase and upregulation of Nrf2 protein level	MDA-MB-231 cells	[40]
			Upregulation of Nrf2, NOQ-1, HO-1, GCLC, and GCLM protein levels	Human aortic smooth muscle cells.	[45]
			Induction of ARE-luciferase activity and upregulation of mRNA levels of GCLC, NQO1, and HO-1	Hepa G2 cells	[26]
			Induction of Nrf2 and upregulation of mRNA and protein levels of HO-1, NQO1, and GCLC	SH-SY5Y cells	[46]

Table 1: Continued.

Structural type	No	Name of compounds	Nrf2-inducing activity	Cell or animal models	Ref
			3.32-fold induction of ARE luciferase activity	HEK 293 T cells	[38]
			0.92 μM for 2-fold induction of QR activity	Hepa 1c1c7 cells	[39]
	17	Miltirone	Enhancement of Nrf2 translocation and upregulation mRNA and protein levels of Nrf2, HO-1, and NQO1	EA.hy926 cells	[47]
	18	17-Hydroxycryptotanshinone	4.85 μM for 2-fold induction of QR activity	Hepa 1c1c7 cells	[39]
	19	1-Oxomiltirone	0.40 μM for 2-fold induction of QR activity	Hepa 1c1c7 cells	[39]
	20	4-Methylenemiltirone	0.46 μM for 2-fold induction of QR activity	Hepa 1c1c7 cells	[39]
	21	1,2-Dihydrotanshinone I	5.40 μM for 2-fold induction of QR activity	Hepa 1c1c7 cells	[39]
Phenolic acids	**22**	Danshensu	Upregulation of mRNA and protein levels of Nrf2	Rat heart	[48]
	23	Rosmarinic acid	Upregulation of Nrf2 and HO-1 protein level	Rat cochlea	[49]
	24	Salvianolic acid A	Induction of mRNA and protein levels of Nrf2 and HO-1	RPE cells	[50, 51]
			Induction of Nrf2 and HO-1	Rat lung tissue	[52]
	25	Salvianolic acid B	Induction of Nrf2 protein level	Rat primary neurons	[53]
			Induction of Nrf2, HO-1, and GCLC protein levels	Hepa G2 cells	[54]

and Huntington's disease [73]. Based on its function on inhibiting oxidative stress, Nrf2 is considered to be an emerging target for the treatment of neurodegenerative disorders [73, 74]. Tanshinone I (**12**) activated the expressions of Nrf2, HO-1, glutamate-cysteine ligase catalytic subunit (GCLC), and glutathione cysteine ligase modulatory subunit (GLCM) in SH-SY5Y cells [42]. Tanshinone I (**12**) inhibited 6-hydroxydopamine- (6-OHDA-) induced cell death and ROS production in SH-SY5Y neuroblastoma cells [42]. In an *in vivo* assay, tanshinone I (**12**) attenuated 6-OHDA-induced striatal oxidative stress and blocked dopaminergic neurotoxicity in 6-OHDA-lesion mice. It also protected the mitochondria against paraquat-induced redox impairment via upregulating Nrf2-regulated antioxidant enzymes, such as Mn-superoxide dismutase (Mn-SOD), GPx, and γ-glutamate-cysteine ligase (γ-GCL) [43]. Similarly, tanshinone IIA (**16**) induced the expressions of Nrf2, HO-1, GCLC, and GCLM in SH-SY5Y cells and protected cells against 6-OHDA-induced ROS production and cell death in an Nrf2-dependent manner *in vitro* [46]. It ameliorated neurodegeneration in a 6-OHDA-induced rat model of Parkinson's disease.

Salvianolic acid A (**24**) enhanced neuronal survival and stabilized MMP in SH-SY5Y cells and protected SH-SY5Y cells against H_2O_2-induced oxidative injury [75]. This protective effect was caused by the inhibition of the AMP-activated protein kinase (AMPK) and the Akt signaling pathway. Salvianolic acid B (**25**) was evaluated for the protection against cognitive decline using a high-fat diet-fed mouse model [76]. It upregulated antioxidant enzymes (e.g. SOD and GPx), attenuated hippocampal redox status, and thus counteracted cognitive decline [76]. Salvianolic acid B (**25**) was also investigated for its neuroprotection using lipopolysaccharide- (LPS-) and 1-methyl-4-phenylpyridinium- (MPP^+-) induced neuronal injury model *in vitro* [53]. Salvianolic acid B (**25**) upregulated Nrf2 expression and decreased LPS- and MPP^+-induced toxicities of dopamine neurons in the primary neuroglia of a mouse. Salvianolic acid B (**25**) attenuated dopaminergic neuronal loss, inhibited neuroinflammation, and improved the neurological function of neurotoxin 1-methyl-4-phenyl-1,2,3,6-tetrahydropyridine- (MPTP-) treated mice [53].

5.3. Diabetes. Oxidative stress triggers the mitochondrial damage which is the predominant contributing factor of excessive β-cell death [77]. Furthermore, high glucose-induced redox imbalance provokes oxidative insults of human tissues and organs (e.g., cardiovascular system, kidney, and eyes) [78]. The activation of Nrf2-regulated antioxidant response relieved the pathogenesis and progression of diabetes [79, 80]. Salvianolic acid B (**25**) inhibited the development of diabetes-related nephropathy and vascular complications in a type 2 diabetic animal model [81]. It also protected pancreatic β-cells against cytokines, interferon-γ (INF-γ), and interleukin- (IL-) 1β and induced INS-1 cell death through activating the expressions of Nrf2, HO-1, and Sirt1 [82]. Salvianolic acid A (**24**) reduced the levels of advanced glycation end products (AGEs) and MDA and improved intestinal motility in diabetic rats [83].

5.4. Nephropathy. Oxidative stress has been implicated in the onset and promotion of nephropathy, and the modulation of Nrf2 is an efficient strategy for the therapy of renal diseases [84]. Ethyl acetate extract of SMRR enhanced the expression of Nrf2 and inhibited ROS production in high-glucose-induced mouse mesangial cells (MMCs) [33]. It reduced albuminuria and alleviated renal damage in streptozocin-induced mice. SMRR injection inhibited N(G)-nitro-d-arginine-induced oxidative injury in a rat kidney [85]. It upregulated the activities of endogenous antioxidant enzymes

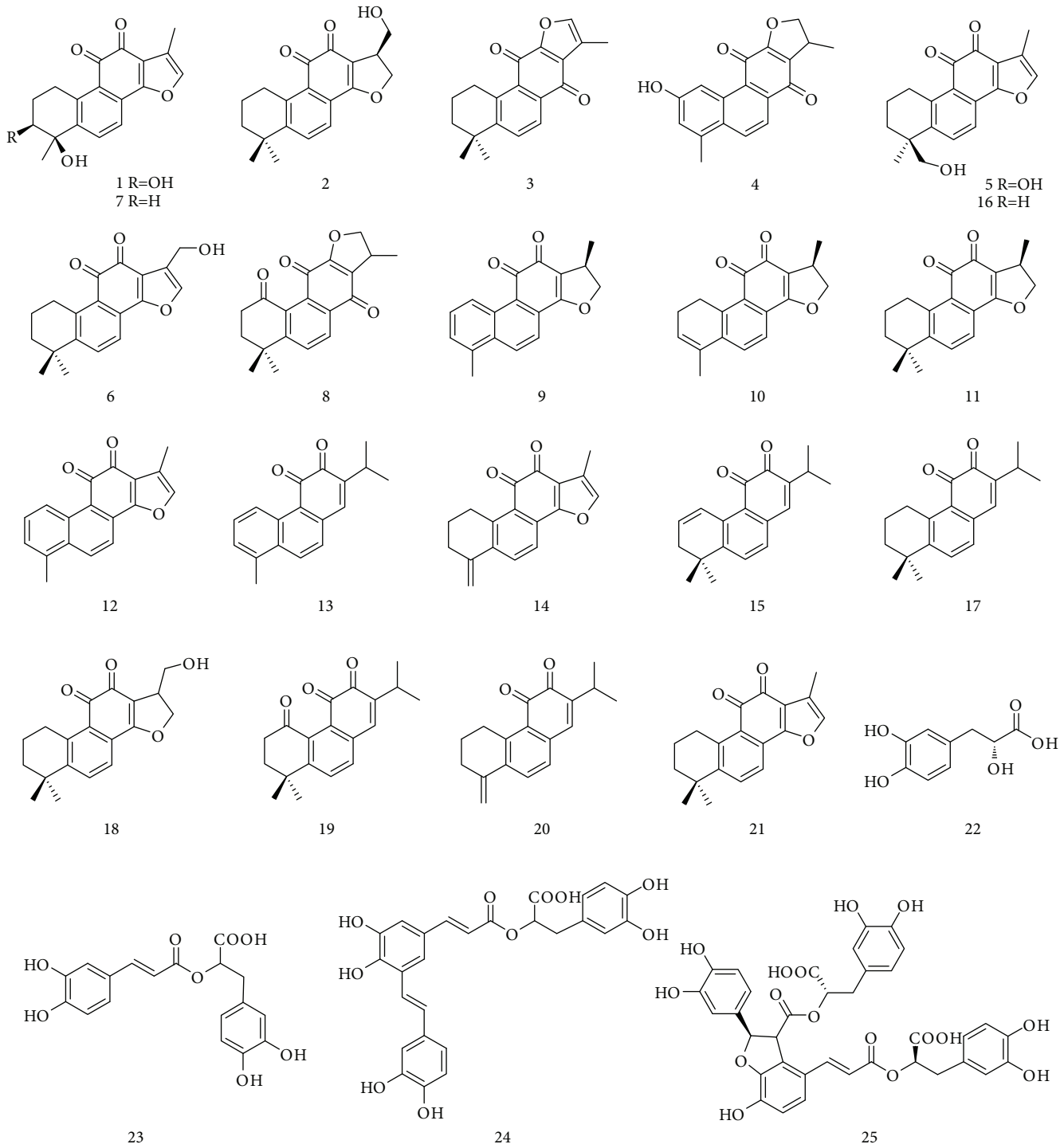

Figure 3: Chemical constituents with potential Nrf2-inducing effects isolated from SMRR.

(e.g., SOD and GPx) and decreased the level of MDA. Salvianolic acid B (**25**) activated Nrf2, reduced cellular ROS level in HK-2 cells, and protected cells against H_2O_2-induced cell death [86]. Furthermore, an *in vivo* study indicated that it activated Nrf2 expression, inhibited renal oxidative stress, and attenuated renal tubular injury in iodinated contrast media-induced acute renal injury in rats. This protection against renal damage was associated with the activation of the PI3K/Akt/Nrf2 pathway.

5.5. Inflammation. Oxidative stress activates redox-sensitive NF-κB and subsequently triggers the overproductions of proinflammatory cytokines and enzymes, such as tumor necrosis factor-α (TNF-α), ILs, cyclooxygenase-2 (COX-2), and inducible NO synthesis (iNOS) [87]. Nrf2 negatively regulated these proinflammatory cytokines and enzymes and thus inhibited inflammatory response. SMRR upregulated the GSH level and inhibited MDA level in the synovium and articular cartilage of the rabbits and prevented articular

cartilage degeneration in rabbits with osteoarthritis [35]. Extract of SMRR induced the expressions of HO-1 and Nrf2 and inhibited H_2O_2-stimulated production of ROS in RAW 264.7 macrophages [88]. The activation of Nrf2 was attributed to the PI3K/Akt and MEK1 signaling pathway. Tanshinone IIA (**16**) induced HO-1 expression in RAW 264.7 macrophages and inhibited LPS-stimulated upregulation of COX-2 and iNOS [89]. A high-fat diet gave rise to the decrease of Nrf2 expression, accumulation of oxidative stress, and inflammation in C57BL/6 mouse. Salvianolic acid B (**25**) upregulated the expressions of Nrf2, HO-1, and NQO1 and thus inhibited the expressions of NF-κB, COX-2, and iNOS in mice fed a high-fat diet [90].

5.6. Liver Diseases. As the major metabolism organ of xenobiotics, the liver is apt to be kept in a sustained oxidative state, which causes a variety of liver diseases, covering fibrosis, cirrhosis, and carcinoma [91, 92]. The extract of SMRR inhibited aflatoxin B1- (AFB_1-) induced cytotoxicity in cultured primary rat hepatocytes since its capability of inhibiting oxidative stress [93]. AFB_1-induced ROS formation and GSH depletion could be reverted by SMRR extract treatment. Tanshinone IIA (**16**) upregulated the protein level of Nrf2 and enhanced the mRNA levels of GCLC, NQO1, and HO-1 in HepG2 cells and in a C57BL/6J mouse liver [26]. Tanshinone IIA (**16**) alleviated acetaminophen- (APAP-) induced upregulations of serum alanine aminotransferase (ALT), aspartate aminotransferase (AST), and lactate dehydrogenase (LDH). It reverted the APAP-induced decreases of GSH, GST, GPx, SOD, and CAT in a mouse liver and thus prevented APAP-induced hepatotoxicity. Similarly, tanshinone IIA (**16**) upregulated the levels of Nrf2-mediated antioxidant enzymes (e.g., HO-1, SOD, CAT, and GPx) and inhibited fibrosis in a rat model of cirrhosis.

Salvianolic acid A (**24**) evidently reduced oxidative stress, evidenced by decreasing the levels of ROS and MDA and increasing the levels of hepatic superoxide dismutase and GSH, in rat liver tissue [94]. Furthermore, salvianolic acid A (**24**) significantly inhibited carbon tetrachloride- (CCl_4-) induced hepatotoxicity. Decreased levels of serum ALT and AST in response to CCl_4 exposure were recovered after treatment with **24**. Salvianolic acid A (**24**) demonstrated radioprotective effects against γ-radiation-induced damage in human embryo liver L-02 cells, which was associated with inhibitions of ROS generation and mitochondrial cytochrome C release [95]. Salvianolic acid B (**25**) demonstrated APAP-induced liver injury in mice [54]. It upregulated the expressions of Nrf2, GCLC, and HO-1 via the activation of the PI3K and protein kinase C (PKC) pathway in HepG2 cells.

5.7. Lung Diseases. The lung is directly and continuously exposed to the external oxidants and toxicants, and thus excessive ROS are produced in the lung tissue. These endogenous and exogenous oxidants contribute to the pathophysiology of lung diseases, exemplified by chronic obstructive pulmonary disease and pulmonary fibrosis [96, 97]. Tanshinone I (**12**) enhanced Nrf2-mediated expressions of NQO1 and γ-GCS through hindering Nrf2 ubiquitination and specifically reacting with cysteine residue at amino acid 151 in Keap1 protein [40]. It protected human bronchial epithelial HBE cells against As(III)-induced oxidative damage in an Nrf2-dependent manner. An *in vivo* study using $Nrf2^{+/+}$ and $Nrf2^{-/-}$ mice indicated that tanshinone I (**12**) attenuated As(III)-induced inflammatory lung damage in $Nrf2^{+/+}$ mice, and this protective effect vanished in $Nrf2^{-/-}$ mice.

Salvianolic acid B (**25**) upregulated the expressions of Nrf2 and HO-1, enhanced GSH production, and inhibited cigarette smoke-induced lung pathological changes and inflammatory responses [52]. Salvianolic acid B (**25**) reduced the expression of ROS-generating enzyme NADPH oxidase-4 (Nox4) in lung tissue of mice [98]. It inhibited paraquat-induced structure distortion, collagen overproduction, proinflammatory cytokine release, and oxidative insults. Salvianolic acid B (**25**) inhibited PQ-induced activation of the transforming growth factor-β (TGF-β1)/Smad3 pathway, which was a key regulator of pulmonary fibrosis [99]. The capability of **25** in activating Nrf2 and inhibiting pulmonary fibrosis was further confirmed by a MRC-5 human lung fibroblast cell model and a bleomycin-induced rat pulmonary fibrosis model [100].

5.8. Ocular Diseases. Oxidative stress is involved in the pathogenesis of age-related macular degeneration [101]. Salvianolic acid A (**24**) inhibited H_2O_2-induced ROS production and prevented H_2O_2-induced primary and transformed retinal pigment epithelial cell death and apoptosis [51]. Activations of Nrf2 and HO-1 by salvianolic acid A (**24**) are essential for this protective effect. The Nrf2-inducing effect of **24** is associated with the activations of PI3K and the mammalian target of rapamycin (mTOR) signaling pathway [50]. It attenuated ox-LDL-induced lipidosis and apoptosis in the retinal pigment epithelium layer and inhibited ox-LDL-induced elevated ROS level and RPE inflammation in a rat model. These data suggested that salvianolic acid A (**24**) was a potential therapeutic agent against age-related macular degeneration.

5.9. Others. Because of wide distribution in the human tissues and organs, the activation of Nrf2 is an effective method for the therapy of many human diseases [102, 103]. Noise-induced hearing loss is associated with oxidative stress and lipoperoxidative damage. Rosmarinic acid (**23**) enhanced Nrf2/HO-1-mediated endogenous antioxidant defense system, attenuated hearing loss, and promoted hair cell survival in a noise-induced rat model [49]. Tanshinone I (**12**) and 15,16-dihydrotanshinone (**9**) induced the expressions of Nrf2, GCLC, and NQO1 through inhibiting Nrf2 ubiquitination in human Hs27 dermal fibroblasts and HaCaT keratinocytes [41]. These two constituents significantly suppressed solar-simulated UV and riboflavin-sensitized ultraviolet-induced skin cell death. A solar-simulated UV-induced human skin reconstruct model was established for evaluating the photoprotective effect of 15,16-dihydrotanshinone (**9**). Treatment with 15,16-dihydrotanshinone (**9**) definitely attenuated epidermal solar insult.

6. Conclusion and Future Perspectives

Oxidative stress plays a vital role in the pathogenesis of many human diseases. The activation of the Nrf2-mediated antioxidant defense system inhibits oxidative stress and thus effectively blocks the onset and progression of oxidative stress-induced human diseases. SMRR is a traditional Chinese medicine that has been long used for the treatment of cardiac cerebral diseases. Lipophilic diterpenoid quinones and hydrophilic phenolic acids are predominant constituents and contribute to the pharmacological functions of SMRR. These two types of constituents demonstrate potent Nrf2-inducing effects and hence are potential agents for the treatment of oxidative stress-related diseases. The SMRR extract, as well as the purified constituents, tanshinone I (**12**), tanshinone IIA (**16**), salvianolic acids A (**24**), and B (**25**), has been extensively investigated, and their inductions on the Nrf2 pathway and therapeutic effects on cardiovascular diseases, neurodegenerative diseases, diabetes, nephropathy, inflammation, liver diseases, and lung diseases have been verified by multiple models *in vitro* and *in vivo*.

Although there has been great progress on SMRR and its constituents, important areas on their phytochemistry, pharmacology, and medical applications related to the activation of Nrf2 remain to be explored. (i) Plenty of diterpenoid quinones have been isolated from SMRR; however, extensive researches still focused on several active constituents, including 15,16-dihydrotanshinone I (**9**), tanshinone I (**12**), tanshinone IIA (**16**), and miltirone (**17**). Miscellaneous diterpenoid quinones should be extensively investigated, such as their structure-activity relationship and mechanisms of action on the activation of Nrf2. (ii) Besides these verified medical applications, SMRR and its constituents possess potential pharmacological functions (e.g., chemoprevention on cancer and therapeutic effect on diabetic nephropathy) because of their activation of Nrf2. Thus, these unconfirmed pharmacological activities should be noted. (iii) Based on the traditional uses, chemical constituents, and pharmacological functions of SMRR, future works on discovering new lead compounds and developing SMRR and its constituents into new drugs for the therapy of oxidative stress-related diseases are significant.

Abbreviations

ABCA1: ATP-binding cassette transporter A1
AFB_1: Aflatoxin B1
AGEs: Advanced glycation end products
ALT: Alanine aminotransferase
APAP: Acetaminophen
AST: Aspartate aminotransferase
ARE: Antioxidant response element
BTB: Broad complex/tramtrack/bric-a-brac
CAT: Catalase
COX-2: Cyclooxygenase-2
γ-GCL: γ-Glutamate cysteine ligase
GCLC: Glutamate cysteine ligase catalytic subunit
GCLM: Glutathione cysteine ligase modulatory subunit
γ-GCS: γ-Glutamyl cysteine synthetase
GPx: Glutathione peroxidase
GSH: Glutathione
GST: Glutathione S-transferase
HO-1: Heme oxygenase-1
ICAM-1: Intercellular adhesion molecule-1
HUVECs: Human umbilical vein endothelial cells
IL: Interleukin
INF-γ: Interferon-γ
iNOS: Inducible NO synthesis
I/R: Ischemia-reperfusion
IVR: Intervening region
Keap1: Kelch-like ECH-associated protein 1
LDH: Lactate dehydrogenase
LPS: Lipopolysaccharide
MDA: Malondialdehyde
MMP: Mitochondrial membrane potential
Mn-SOD: Mn-superoxide dismutase
MPP^+: 1-Methyl-4-phenylpyridinium
MPTP: 1-Methyl-4-phenyl-1,2,3,6-tetrahydropyridine
mTOR: Mammalian target of rapamycin
NF-κB: Nuclear factor-κB
NQO1: NAD(P)H: quinone oxidoreductase 1
Nrf2: Nuclear factor erythroid 2-related factor 2
6-OHDA: 6-Hydroxydopamine
ox-LDL: Oxidized low-density lipoprotein
PKC: Protein kinase C
PI3K: Phosphoinositide 3-kinase
RNS: Reactive nitrogen species
ROS: Reactive oxygen species
SMRR: Salviae Miltiorrhizae Radix et Rhizoma
SOD: Superoxide dismutase
t-BHP: *tert*-Butyl hydroperoxide
TCM: Traditional Chinese medicines
TGF-β1: Transforming growth factor-β
TNF-α: Tumor necrosis factor-α
TrxR: Thioredoxin reductase
VCAM-1: Vascular cell adhesion molecule-1.

Conflicts of Interest

The authors declare that there is no conflict of interest.

Acknowledgments

This work was financially supported by NSF of Shandong Province (ZR2014HM019), NNSFs of China (31470419 and 81673558), and Young Scholars Program of Shandong University (2015WLJH50).

References

[1] M.-X. Zhou, G.-H. Li, B. Sun et al., "Identification of novel Nrf2 activators from *Cinnamomum chartophyllum* H.W. Li and their potential application of preventing oxidative insults in human lung epithelial cells," *Redox Biology*, vol. 14, pp. 154–163, 2018.

[2] E. Bargagli, C. Olivieri, D. Bennett, A. Prasse, J. Muller-Quernheim, and P. Rottoli, "Oxidative stress in the pathogenesis of diffuse lung diseases: a review," *Respiratory Medicine*, vol. 103, no. 9, pp. 1245–1256, 2009.

[3] X. Chen, C. Guo, and J. Kong, "Oxidative stress in neurodegenerative diseases," *Neural Regeneration Research*, vol. 7, no. 5, pp. 376–385, 2012.

[4] D. Jay, H. Hitomi, and K. K. Griendling, "Oxidative stress and diabetic cardiovascular complications," *Free Radical Biology & Medicine*, vol. 40, no. 2, pp. 183–192, 2006.

[5] J. E. Klaunig, L. M. Kamendulis, and B. A. Hocevar, "Oxidative stress and oxidative damage in carcinogenesis," *Toxicologic Pathology*, vol. 38, no. 1, pp. 96–109, 2010.

[6] A. C. Maritim, R. A. Sanders, and J. B. Watkins, "Diabetes, oxidative stress, and antioxidants: a review," *Journal of Biochemical and Molecular Toxicology*, vol. 17, no. 1, pp. 24–38, 2003.

[7] D. Harrison, K. K. Griendling, U. Landmesser, B. Hornig, and H. Drexler, "Role of oxidative stress in atherosclerosis," *The American Journal of Cardiology*, vol. 91, no. 3, pp. 7–11, 2003.

[8] N. D. Vaziri, "Roles of oxidative stress and antioxidant therapy in chronic kidney disease and hypertension," *Current Opinion in Nephrology and Hypertension*, vol. 13, no. 1, pp. 93–99, 2004.

[9] M. C. Jaramillo and D. D. Zhang, "The emerging role of the Nrf2–Keap1 signaling pathway in cancer," *Genes & Development*, vol. 27, no. 20, pp. 2179–2191, 2013.

[10] T. O. Khor, M.-T. Huang, A. Prawan et al., "Increased susceptibility of Nrf2 knockout mice to colitis-associated colorectal cancer," *Cancer Prevention Research*, vol. 1, no. 3, pp. 187–191, 2008.

[11] B. Li, S. Liu, L. Miao, and L. Cai, "Prevention of diabetic complications by activation of Nrf2: diabetic cardiomyopathy and nephropathy," *Experimental Diabetes Research*, vol. 2012, Article ID 216512, 7 pages, 2012.

[12] T. E. Sussan, S. Biswal et al.N. Ganguly, S. Jindal, S. Biswal et al., "Oxidative stress and respiratory diseases: the critical role of Nrf2," in *Studies on Respiratory Disorders*, Oxidative Stress in Applied Basic Research and Clinical Practice, pp. 335–348, Humana Press, New York, NY, USA, 2014.

[13] T. O. Khor, M.-T. Huang, K. H. Kwon, J. Y. Chan, B. S. Reddy, and A.-N. Kong, "Nrf2-deficient mice have an increased susceptibility to dextran sulfate sodium–induced colitis," *Cancer Research*, vol. 66, no. 24, pp. 11580–11584, 2006.

[14] J. Li, T. Ichikawa, J. S. Janicki, and T. Cui, "Targeting the Nrf2 pathway against cardiovascular disease," *Expert Opinion on Therapeutic Targets*, vol. 13, no. 7, pp. 785–794, 2009.

[15] M. C. Barone, G. P. Sykiotis, and D. Bohmann, "Genetic activation of Nrf2 signaling is sufficient to ameliorate neurodegenerative phenotypes in a *Drosophila* model of Parkinson's disease," *Disease Models & Mechanisms*, vol. 4, no. 5, pp. 701–707, 2011.

[16] T. Rangasamy, C. Y. Cho, R. K. Thimmulappa et al., "Genetic ablation of Nrf2 enhances susceptibility to cigarette smoke–induced emphysema in mice," *The Journal of Clinical Investigation*, vol. 114, no. 9, pp. 1248–1259, 2004.

[17] A. Enomoto, K. Itoh, E. Nagayoshi et al., "High sensitivity of Nrf2 knockout mice to acetaminophen hepatotoxicity associated with decreased expression of ARE-regulated drug metabolizing enzymes and antioxidant genes," *Toxicological Sciences*, vol. 59, no. 1, pp. 169–177, 2001.

[18] M. Ramos-Gomez, P. M. Dolan, K. Itoh, M. Yamamoto, and T. W. Kensler, "Interactive effects of *nrf2* genotype and oltipraz on benzo[*a*]pyrene–DNA adducts and tumor yield in mice," *Carcinogenesis*, vol. 24, no. 3, pp. 461–467, 2003.

[19] H. Kumar, I. S. Kim, S. V. More, B. W. Kim, and D. K. Choi, "Natural product-derived pharmacological modulators of Nrf2/ARE pathway for chronic diseases," *Natural Product Reports*, vol. 31, no. 1, pp. 109–139, 2014.

[20] T. Shen, T. Jiang, M. Long et al., "A curcumin derivative that inhibits vinyl carbamate-induced lung carcinogenesis *via* activation of the Nrf2 protective response," *Antioxidants & Redox Signaling*, vol. 23, no. 8, pp. 651–664, 2015.

[21] M.-X. Zhou, X. Wei, A.-L. Li et al., "Screening of traditional Chinese medicines with therapeutic potential on chronic obstructive pulmonary disease through inhibiting oxidative stress and inflammatory response," *BMC Complementary and Alternative Medicine*, vol. 16, no. 1, p. 360, 2016.

[22] T. Shen, X.-M. Chen, B. Harder et al., "Plant extracts of the family Lauraceae: a potential resource for chemopreventive agents that activate the nuclear factor-erythroid 2-related factor 2/antioxidant response element pathway," *Planta Medica*, vol. 80, no. 5, pp. 426–434, 2014.

[23] X.-Z. Zhang, S.-S. Qian, Y.-J. Zhang, and R.-Q. Wang, "*Salvia miltiorrhiza*: a source for anti-Alzheimer's disease drugs," *Pharmaceutical Biology*, vol. 54, no. 1, pp. 18–24, 2016.

[24] G. Cui, L. Shan, M. Hung et al., "A novel danshensu derivative confers cardioprotection via PI3K/Akt and Nrf2 pathways," *International Journal of Cardiology*, vol. 168, no. 2, pp. 1349–1359, 2013.

[25] S. Gao, Z. Liu, H. Li, P. J. Little, P. Liu, and S. Xu, "Cardiovascular actions and therapeutic potential of tanshinone IIA," *Atherosclerosis*, vol. 220, no. 1, pp. 3–10, 2012.

[26] W. Wang, C. Guan, X. Sun et al., "Tanshinone IIA protects against acetaminophen-induced hepatotoxicity *via* activating the Nrf2 pathway," *Phytomedicine*, vol. 23, no. 6, pp. 589–596, 2016.

[27] C.-Y. Su, Q.-L. Ming, K. Rahman, T. HAN, and L.-P. Qin, "*Salvia miltiorrhiza*: traditional medicinal uses, chemistry, and pharmacology," *Chinese Journal of Natural Medicines*, vol. 13, no. 3, pp. 163–182, 2015.

[28] W.-y. Wu and Y.-p. Wang, "Pharmacological actions and therapeutic applications of *Salvia miltiorrhiza* depside salt and its active components," *Acta Pharmacologica Sinica*, vol. 33, no. 9, pp. 1119–1130, 2012.

[29] P. Moi, K. Chan, I. Asunis, A. Cao, and Y. W. Kan, "Isolation of NF-E2-related factor 2 (Nrf2), a NF-E2-like basic leucine zipper transcriptional activator that binds to the tandem NF-E2/AP1 repeat of the beta-globin locus control region," *Proceedings of the National Academy of Sciences of the United States of America*, vol. 91, no. 21, pp. 9926–9930, 1994.

[30] Y. Mitsuishi, H. Motohashi, and M. Yamamoto, "The Keap1–Nrf2 system in cancers: stress response and anabolic metabolism," *Frontiers in Oncology*, vol. 2, 2012.

[31] W. Li and A. N. Kong, "Molecular mechanisms of Nrf2-mediated antioxidant response," *Molecular Carcinogenesis*, vol. 48, no. 2, pp. 91–104, 2009.

[32] A. Lau, N. F. Villeneuve, Z. Sun, P. K. Wong, and D. D. Zhang, "Dual roles of Nrf2 in cancer," *Pharmacological Research*, vol. 58, no. 5-6, pp. 262–270, 2008.

[33] L. An, M. Zhou, F. M. M. T. Marikar et al., "*Salvia miltiorrhiza* lipophilic fraction attenuates oxidative stress in diabetic

nephropathy through activation of nuclear factor erythroid 2-related factor 2," *The American Journal of Chinese Medicine*, vol. 45, no. 7, pp. 1441–1457, 2017.

[34] G. Ge, Q. Zhang, J. Ma et al., "Protective effect of *Salvia miltiorrhiza* aqueous extract on myocardium oxidative injury in ischemic–reperfusion rats," *Gene*, vol. 546, no. 1, pp. 97–103, 2014.

[35] B. Bai and Y. Li, "Danshen prevents articular cartilage degeneration via antioxidation in rabbits with osteoarthritis," *Osteoarthritis and Cartilage*, vol. 24, no. 3, pp. 514–520, 2016.

[36] H.-Y. Liu, C.-T. Jiang, J. Feng, and X. Wang, "Research progress of Tanshinones," *Chinese Pharmacological Bulletin*, vol. 32, pp. 1643–1647, 2016.

[37] A. R. Jassbi, S. Zare, O. Firuzi, and J. Xiao, "Bioactive phytochemicals from shoots and roots of *Salvia* species," *Phytochemistry Reviews*, vol. 15, no. 5, pp. 829–867, 2016.

[38] H. Zhang, L.-P. Luo, H.-P. Song et al., "A high-resolution peak fractionation approach for streamlined screening of nuclear-factor-E2-related factor-2 activators in *Salvia miltiorrhiza*," *Journal of Chromatography A*, vol. 1326, pp. 47–55, 2014.

[39] Z. Ma, M. Zhang, and Z. Song, "Characterization of tanshinones with quinone reductase induction activity from Radix *Salvia miltiorrhiza* by liquid chromatography/tandem mass spectrometry," *Rapid Communications in Mass Spectrometry*, vol. 23, no. 18, pp. 2857–2866, 2009.

[40] S. Tao, Y. Zheng, A. Lau et al., "Tanshinone I activates the Nrf2-dependent antioxidant response and protects against As(III)-induced lung inflammation *in vitro* and *in vivo*," *Antioxidants & Redox Signaling*, vol. 19, no. 14, pp. 1647–1661, 2013.

[41] S. Tao, R. Justiniano, D. D. Zhang, and G. T. Wondrak, "The Nrf2-inducers tanshinone I and dihydrotanshinone protect human skin cells and reconstructed human skin against solar simulated UV," *Redox Biology*, vol. 1, no. 1, pp. 532–541, 2013.

[42] X. Jing, X. Wei, M. Ren, L. Wang, X. Zhang, and H. Lou, "Neuroprotective effects of tanshinone I against 6-OHDA-induced oxidative stress in cellular and mouse model of Parkinson's disease through upregulating Nrf2," *Neurochemical Research*, vol. 41, no. 4, pp. 779–786, 2016.

[43] M. R. de Oliveira, P. F. Schuck, and S. M. D. Bosco, "Tanshinone I induces mitochondrial protection through an Nrf2-dependent mechanism in paraquat-treatedhuman neuroblastoma SH-SY5Y cells," *Molecular Neurobiology*, vol. 54, no. 6, pp. 4597–4608, 2017.

[44] L. Wang, C. Zhang, Y. Guo et al., "Blocking of JB6 cell transformation by tanshinone IIA: epigenetic reactivation of Nrf2 antioxidative stress pathway," *The AAPS Journal*, vol. 16, no. 6, pp. 1214–1225, 2014.

[45] H.-S. Zhang and S.-Q. Wang, "Nrf2 is involved in the effect of tanshinone IIA on intracellular redox status in human aortic smooth muscle cells," *Biochemical Pharmacology*, vol. 73, no. 9, pp. 1358–1366, 2007.

[46] X. S. Zhang, S. Ha, X. L. Wang, Y. L. Shi, S. S. Duan, and Z. A. Li, "Tanshinone IIA protects dopaminergic neurons against 6-hydroxydopamine-induced neurotoxicity through miR-153/NF-E2-related factor 2/antioxidant response element signaling pathway," *Neuroscience*, vol. 303, pp. 489–502, 2015.

[47] L. Zhang, H. Zhang, X. Li et al., "Miltirone protects human EA.hy926 endothelial cells from oxidized low-density lipoprotein-derived oxidative stress via a heme oxygenase-1 and MAPK/Nrf2 dependent pathway," *Phytomedicine*, vol. 23, no. 14, pp. 1806–1813, 2016.

[48] J. Yu, L. Wang, M. Akinyi et al., "Danshensu protects isolated heart against ischemia reperfusion injury through activation of Akt/ERK1/2/Nrf2 signaling," *International Journal of Clinical and Experimental Medicine*, vol. 8, no. 9, pp. 14793–14804, 2015.

[49] A. R. Fetoni, F. Paciello, R. Rolesi et al., "Rosmarinic acid up-regulates the noise-activated Nrf2/HO-1 pathway and protects against noise-induced injury in rat cochlea," *Free Radical Biology & Medicine*, vol. 85, pp. 269–281, 2015.

[50] K. Mao, W. Shu, Q. Qiu, Q. Gu, and X. Wu, "Salvianolic acid a protects retinal pigment epithelium from OX-LDL-induced inflammation in an age-related macular degeneration model," *Discovery Medicine*, vol. 23, pp. 129–148, 2017.

[51] H. Zhang, Y. Y. Liu, Q. Jiang et al., "Salvianolic acid A protects RPE cells against oxidative stress through activation of Nrf2/HO-1 signaling," *Free Radical Biology & Medicine*, vol. 69, pp. 219–228, 2014.

[52] D.-F. Zhang, J. Zhang, and R. Li, "Salvianolic acid B attenuates lung inflammation induced by cigarette smoke in mice," *European Journal of Pharmacology*, vol. 761, pp. 174–179, 2015.

[53] J. Zhou, X. D. Qu, Z. Y. Li et al., "Salvianolic acid B attenuates toxin-induced neuronal damage via Nrf2-dependent glial cells-mediated protective activity in Parkinson's disease models," *PLoS One*, vol. 9, no. 7, article e101668, 2014.

[54] M. Lin, X. Zhai, G. Wang et al., "Salvianolic acid B protects against acetaminophen hepatotoxicity by inducing Nrf2 and phase II detoxification gene expression via activation of the PI3K and PKC signaling pathways," *Journal of Pharmacological Sciences*, vol. 127, no. 2, pp. 203–210, 2015.

[55] C.-C. Chang, Y.-C. Chang, W.-L. Hu, and Y.-C. Hung, "Oxidative stress and *salvia miltiorrhiza* in aging-associated cardiovascular diseases," *Oxidative Medicine and Cellular Longevity*, vol. 2016, Article ID 4797102, 11 pages, 2016.

[56] W. Chen and G. Chen, "Danshen (Salvia miltiorrhiza Bunge): a prospective healing sage for cardiovascular diseases," *Current Pharmaceutical Design*, vol. 23, no. 34, pp. 5125–5135, 2017.

[57] Z. An, G. Yang, G. Liu, H. Zheng, C. Li, and W. Zhang, "Novel insights on the vascular protective effects of tanshinone," *International Journal of Clinical and Experimental Medicine*, vol. 9, pp. 20711–20718, 2016.

[58] Y. Zhang, P. Jiang, M. Ye, S. H. Kim, C. Jiang, and J. Lü, "Tanshinones: sources, pharmacokinetics and anti-cancer activities," *International Journal of Molecular Sciences*, vol. 13, no. 12, pp. 13621–13666, 2012.

[59] Y. Guo, Y. Li, L. Xue et al., "*Salvia miltiorrhiza*: an ancient Chinese herbal medicine as a source for anti-osteoporotic drugs," *Journal of Ethnopharmacology*, vol. 155, no. 3, pp. 1401–1416, 2014.

[60] R. Howden, "*Nrf2* and cardiovascular defense," *Oxidative Medicine and Cellular Longevity*, vol. 2013, Article ID 104308, 10 pages, 2013.

[61] D. G. Harrison and M. C. Gongora, "Oxidative stress and hypertension," *Medical Clinics of North America*, vol. 93, no. 3, pp. 621–635, 2009.

[62] J. L. Zweier, "Measurement of superoxide-derived free radicals in the reperfused heart. Evidence for a free radical mechanism of reperfusion injury," *Journal of Biological Chemistry*, vol. 263, no. 3, pp. 1353–1357, 1988.

[63] Z. Qiao, J. Ma, and H. Liu, "Evaluation of the antioxidant potential of *Salvia miltiorrhiza* ethanol extract in a rat model of ischemia-reperfusion injury," *Molecules*, vol. 16, no. 12, pp. 10002–10012, 2011.

[64] Z. Liu, J. Wang, E. Huang et al., "Tanshinone IIA suppresses cholesterol accumulation in human macrophages: role of heme oxygenase-1," *Journal of Lipid Research*, vol. 55, no. 2, pp. 201–213, 2014.

[65] S. Zhuang, T.-H. Cheng, N.-L. Shih et al., "Tanshinone IIA induces heme oxygenase 1 expression and inhibits cyclic strain-induced interleukin 8 expression in vascular endothelial cells," *The American Journal of Chinese Medicine*, vol. 44, no. 2, pp. 377–388, 2016.

[66] P. Chan, Y.-C. Chen, L.-J. Lin et al., "Tanshinone IIA attenuates H_2O_2-induced injury in human umbilical vein endothelial cells," *The American Journal of Chinese Medicine*, vol. 40, no. 6, pp. 1307–1319, 2012.

[67] H. Zhu, Z. Chen, Z. Ma et al., "Tanshinone IIA protects endothelial cells from H_2O_2-induced injuries via PXR activation," *Biomolecules & Therapeutics*, vol. 25, no. 6, pp. 599–608, 2017.

[68] Y.-I. Li, G. Elmer, and R. C. LeBoeuf, "Tanshinone IIA reduces macrophage death induced by hydrogen peroxide by upregulating glutathione peroxidase," *Life Sciences*, vol. 83, no. 15-16, pp. 557–562, 2008.

[69] P. Wang, X. Wu, Y. Bao et al., "Tanshinone IIA prevents cardiac remodeling through attenuating NAD (P)H oxidase-derived reactive oxygen species production in hypertensive rats," *Pharmazie*, vol. 66, no. 7, pp. 517–524, 2011.

[70] F. Tang, X. Wu, T. Wang et al., "Tanshinone II A attenuates atherosclerotic calcification in rat model by inhibition of oxidative stress," *Vascular Pharmacology*, vol. 46, no. 6, pp. 427–438, 2007.

[71] W. Zhao, C. Wu, and X. Chen, "Cryptotanshinone inhibits oxidized LDL-induced adhesion molecule expression via ROS dependent NF-κB pathways," *Cell Adhesion & Migration*, vol. 10, no. 3, pp. 248–258, 2016.

[72] D. Jia, T. Li, X. Chen et al., "Salvianic acid A sodium protects HUVEC cells against *tert*-butyl hydroperoxide induced oxidative injury via mitochondria-dependent pathway," *Chemico-Biological Interactions*, vol. 279, pp. 234–242, 2018.

[73] D. A. Johnson and J. A. Johnson, "Nrf2—a therapeutic target for the treatment of neurodegenerative diseases," *Free Radical Biology & Medicine*, vol. 88, Part B, pp. 253–267, 2015.

[74] I. Buendia, P. Michalska, E. Navarro, I. Gameiro, J. Egea, and R. Leon, "Nrf2–ARE pathway: an emerging target against oxidative stress and neuroinflammation in neurodegenerative diseases," *Pharmacology & Therapeutics*, vol. 157, pp. 84–104, 2016.

[75] H.-a. Zhang, M. Gao, L. Zhang et al., "Salvianolic acid A protects human SH-SY5Y neuroblastoma cells against H_2O_2-induced injury by increasing stress tolerance ability," *Biochemical and Biophysical Research Communications*, vol. 421, no. 3, pp. 479–483, 2012.

[76] S.-F. Xia, Z.-X. Xie, Y. Qiao et al., "Salvianolic acid B counteracts cognitive decline triggered by oxidative stress in mice fed with high-fat diets," *Journal of Functional Foods*, vol. 11, pp. 278–292, 2014.

[77] E. Bhakkiyalakshmi, D. Sireesh, P. Rajaguru, R. Paulmurugan, and K. M. Ramkumar, "The emerging role of redox-sensitive Nrf2-Keap1 pathway in diabetes," *Pharmacological Research*, vol. 91, pp. 104–114, 2015.

[78] F. Giacco and M. Brownlee, "Oxidative stress and diabetic complications," *Circulation Research*, vol. 107, no. 9, pp. 1058–1070, 2010.

[79] A. Uruno, Y. Furusawa, Y. Yagishita et al., "The Keap1-Nrf2 system prevents onset of diabetes mellitus," *Molecular and Cellular Biology*, vol. 33, no. 15, pp. 2996–3010, 2013.

[80] A. Uruno, Y. Yagishita, and M. Yamamoto, "The Keap1–Nrf2 system and diabetes mellitus," *Archives of Biochemistry and Biophysics*, vol. 566, pp. 76–84, 2015.

[81] E. S. Kang, G. T. Lee, B. S. Kim et al., "Lithospermic acid B ameliorates the development of diabetic nephropathy in OLETF rats," *European Journal of Pharmacology*, vol. 579, no. 1-3, pp. 418–425, 2008.

[82] B.-W. Lee, S. W. Chun, S. H. Kim et al., "Lithospermic acid B protects beta-cells from cytokine-induced apoptosis by alleviating apoptotic pathways and activating anti-apoptotic pathways of Nrf2–HO-1 and Sirt1," *Toxicology and Applied Pharmacology*, vol. 252, no. 1, pp. 47–54, 2011.

[83] X. Y. Yu, L. Zhang, X. Y. Yang, X. T. Li, and G. H. Du, "Salvianolic acid A improves intestinal motility in diabetic rats through antioxidant capacity and upregulation of nNOS," *Journal of Digestive Diseases*, vol. 17, no. 7, pp. 441–447, 2016.

[84] C. Zoja, A. Benigni, and G. Remuzzi, "The Nrf2 pathway in the progression of renal disease," *Nephrology Dialysis Transplantation*, vol. 29, Supplement 1, pp. I19–I24, 2014.

[85] Z. You, Y. Xin, Y. Liu et al., "Protective effect of Salvia Miltiorrhizae injection on N(G)-nitro-D-arginine induced nitric oxide deficient and oxidative damage in rat kidney," *Experimental and Toxicologic Pathology*, vol. 64, no. 5, pp. 453–458, 2012.

[86] L. Tongqiang, L. Shaopeng, Y. Xiaofang et al., "Salvianolic acid B prevents iodinated contrast media-induced acute renal injury in rats via the PI3K/Akt/Nrf2 pathway," *Oxidative Medicine and Cellular Longevity*, vol. 2016, Article ID 7079487, 11 pages, 2016.

[87] J. Kim, Y.-N. Cha, and Y.-J. Surh, "A protective role of nuclear factor-erythroid 2-related factor-2 (Nrf2) in inflammatory disorders," *Mutation Research/Fundamental and Molecular Mechanisms of Mutagenesis*, vol. 690, no. 1-2, pp. 12–23, 2010.

[88] S. E. Lee, S. I. Jeong, H. Yang et al., "Extract of *Salvia miltiorrhiza* (Danshen) induces Nrf2-mediated heme oxygenase-1 expression as a cytoprotective action in RAW 264.7 macrophages," *Journal of Ethnopharmacology*, vol. 139, no. 2, pp. 541–548, 2012.

[89] T.-H. Chen, Y.-T. Hsu, C.-H. Chen, S.-H. Kao, and H.-M. Lee, "Tanshinone IIA from *Salvia miltiorrhiza* induces heme oxygenase-1 expression and inhibits lipopolysaccharide-induced nitric oxide expression in RAW 264.7 cells," *Mitochondrion*, vol. 7, no. 1-2, pp. 101–105, 2007.

[90] B. Wang, J. Sun, Y. Shi, and G. Le, "Salvianolic acid B inhibits high-fat diet-induced inflammation by activating the Nrf2 pathway," *Journal of Food Science*, vol. 82, no. 8, pp. 1953–1960, 2017.

[91] S. M. Shin, J. H. Yang, and S. H. Ki, "Role of the Nrf2-ARE pathway in liver diseases," *Oxidative Medicine and Cellular Longevity*, vol. 2013, Article ID 763257, 9 pages, 2013.

[92] L. M. Aleksunes and J. E. Manautou, "Emerging role of Nrf2 in protecting against hepatic and gastrointestinal disease," *Toxicologic Pathology*, vol. 35, no. 4, pp. 459–473, 2007.

[93] J. Liu, C. F. Yang, B. L. Lee, H. M. Shen, S. G. Ang, and C. N. Ong, "Effect of *Salvia miltiorrhiza* on aflatoxin B_1-induced oxidative stress in cultured rat hepatocytes," *Free Radical Research*, vol. 31, no. 6, pp. 559–568, 1999.

[94] Z.-m. Wu, T. Wen, Y.-f. Tan, Y. Liu, F. Ren, and H. Wu, "Effects of salvianolic acid A on oxidative stress and liver injury induced by carbon tetrachloride in rats," *Basic & Clinical Pharmacology & Toxicology*, vol. 100, no. 2, pp. 115–120, 2007.

[95] J. Guo, Y. Zhang, L. Zeng, J. Liu, J. Liang, and G. Guo, "Salvianic acid A protects L-02 cells against γ-irradiation-induced apoptosis via the scavenging of reactive oxygen species," *Environmental Toxicology and Pharmacology*, vol. 35, no. 1, pp. 117–130, 2013.

[96] J. Ciencewicki, S. Trivedi, and S. R. Kleeberger, "Oxidants and the pathogenesis of lung diseases," *The Journal of Allergy and Clinical Immunology*, vol. 122, no. 3, pp. 456–468, 2008.

[97] A. Boutten, D. Goven, E. Artaud-Macari, J. Boczkowski, and M. Bonay, "NRF2 targeting: a promising therapeutic strategy in chronic obstructive pulmonary disease," *Trends in Molecular Medicine*, vol. 17, no. 7, pp. 363–371, 2011.

[98] B. Liu, B. Cao, D. Zhang et al., "Salvianolic acid B protects against paraquat-induced pulmonary injury by mediating Nrf2/Nox4 redox balance and TGF-β1/Smad3 signaling," *Toxicology and Applied Pharmacology*, vol. 309, pp. 111–120, 2016.

[99] V. Della Latta, A. Cecchettini, S. Del Ry, and M. A. Morales, "Bleomycin in the setting of lung fibrosis induction: from biological mechanisms to counteractions," *Pharmacological Research*, vol. 97, pp. 122–130, 2015.

[100] M. Liu, H. Xu, L. Zhang et al., "Salvianolic acid B inhibits myofibroblast transdifferentiation in experimental pulmonary fibrosis via the up-regulation of Nrf2," *Biochemical and Biophysical Research Communications*, vol. 495, no. 1, pp. 325–331, 2018.

[101] Z. Zhao, Y. Chen, J. Wang et al., "Age-related retinopathy in NRF2-deficient mice," *PLoS One*, vol. 6, no. 4, article e19456, 2011.

[102] B. M. Hybertson, B. Gao, S. K. Bose, and J. M. McCord, "Oxidative stress in health and disease: the therapeutic potential of Nrf2 activation," *Molecular Aspects of Medicine*, vol. 32, no. 4-6, pp. 234–246, 2011.

[103] K. J. Trouba, H. K. Hamadeh, R. P. Amin, and D. R. Germolec, "Oxidative stress and its role in skin disease," *Antioxidants & Redox Signaling*, vol. 4, no. 4, pp. 665–673, 2002.

Hindawi
Oxidative Medicine and Cellular Longevity
Volume 2018, Article ID 3246719, 11 pages
https://doi.org/10.1155/2018/3246719

Research Article

Antioxidant Activity and Genotoxic Assessment of Crabwood (Andiroba, *Carapa guianensis* Aublet) Seed Oils

Carlos F. Araujo-Lima,[1,2] **Andreia S. Fernandes**,[1] **Erika M. Gomes**,[1] **Larisse L. Oliveira**,[2,3] **Andrea F. Macedo**,[3] **Rosemar Antoniassi**,[4] **Allan E. Wilhelm**,[4] **Claudia A. F. Aiub**,[2] **and Israel Felzenszwalb**[1]

[1]*Environmental Mutagenesis Laboratory, Department of Biophysics and Biometry, Rio de Janeiro State University (UERJ), Rio de Janeiro, RJ, Brazil*
[2]*Genotoxicity Laboratory, Department of Genetics and Molecular Biology, Federal University of the State of Rio de Janeiro (UNIRIO), Rio de Janeiro, RJ, Brazil*
[3]*Integrated Laboratory of Plant Biology, Department of Botany, Institute of Biosciences, Federal University of State of Rio de Janeiro, Rio de Janeiro, RJ, Brazil*
[4]*Embrapa Food Technology, Brasília, DF, Brazil*

Correspondence should be addressed to Israel Felzenszwalb; uerj.felzen@gmail.com

Received 13 December 2017; Revised 22 February 2018; Accepted 3 April 2018; Published 2 May 2018

Academic Editor: Jaideep Banerjee

The seed oil of *Carapa guianensis* (Aublet), a tree from the Meliaceae family commonly known as andiroba, is widely used in Brazilian traditional medicine because of its multiple curative properties against fever and rheumatism and as an anti-inflammatory agent, antibacterial agent, and insect repellant. Since there is no consensus on the best way to obtain the *C. guianensis* oil and due to its ethnomedicinal properties, the aim of the present research was to evaluate the chemical composition, free-radical scavenging activity, and mutagenic and genotoxicity properties of three *C. guianensis* oils obtained by different extraction methods. The phenolic contents were evaluated by spectrophotometry. Oil 1 was obtained by pressing the dried seeds at room temperature; oil 2 was obtained by autoclaving, drying, and pressing; oil 3 was obtained by Soxhlet extraction at 30–60°C using petroleum ether. The oil from each process presented differential yields, physicochemical properties, and phenolic contents. Oil 1 showed a higher scavenging activity against the DPPH radical when compared to oils 2 and 3, suggesting a significant antioxidant activity. All oils were shown to be cytotoxic to bacteria and to CHO-K1 and RAW264.7 cells. At noncytotoxic concentrations, oil 2 presented mutagenicity to *Salmonella enterica* serovar Typhimurium and induced micronuclei in both cell types. Under the same conditions, oil 3 also induced micronucleus formation. However, the present data demonstrated that oil 1, extracted without using high temperatures, was the safest for use as compared to the other two oils, not showing mutagenicity or micronucleus induction.

1. Introduction

Carapa guianensis (Aublet) is a large neotropical tree belonging to the Meliaceae family. It can be found in the north of South America, Central America, the Caribbean, and Sub-Saharan Africa. In Brazil, it is known as andiroba occurring mainly in lowlands and flooded areas throughout the Amazon region [1, 2].

Some studies have reported several activities produced by the seed oil from *C. guianensis* and used in folk medicine, such as treating fever and rheumatism, antiallergic, analgesic, chemotherapeutic, and anti-inflammatory effects [3–7], as well as acaricidal and insect repellent action [8–10]. It is also effective against rheumatism and arthritis [1]. Furthermore, the infusion prepared with the bark and flowers of *C. guianensis* is used both as an anthelmintic and wound-healing agent in humans [11].

There is no consensus on the best way to obtain *C. guianensis* seed oil. Traditional techniques are time-consuming and may include cooking, drying in the sun, and allowing

enzymatic action and fermentation [12, 13], and the mechanical extraction of chopped seeds, including drying and pressing at around 90°C, has also been used [14].

These processes generate a large quantity of residual seed material as a by-product, which contains many bioactive constituents including limonoids or tetranortriterpenoids [9]. The chemical components of *C. guianensis* seeds have been extensively studied over the years, mainly gedunin-type limonoids bearing the 4,4,8-trimethyl-17-furanylsteroid. Limonoids present several biological activities, including antifungal and bactericidal activities and a variety of medical effects in animals and humans [15].

Crude vegetable oils or fixed oils are composed mainly of triacylglycerols (around 95%) along with some free acids, monoacylglycerols, and diacylglycerols. They also contain variable amounts of other components such as phospholipids, free and esterified sterols, triterpene alcohols, tocopherols and tocotrienols, phenolic compounds, carotenes, chlorophylls, hydrocarbons, oxidation compounds, metals, and minor and trace compounds. The amounts of each of these compounds depend on the extraction and oil-refining processes [16].

The biological activity of fixed oils has been associated with the fatty acids or their glycerides, to different lipid classes (such as phospholipids and glycolipids) and to a plethora of minor compounds present in the oils [17].

According to the Organization for Economic Cooperation and Development [18], all products intended for human use must be evaluated regarding toxicological aspects. In general, the first toxicological evaluation of new chemicals is the *Salmonella*/microsome reverse mutation assay, which detects punctual mutations in the DNA sequence, followed by an evaluation of the clastogenicity potential using the micronucleus assay [19].

Thus, the aim of the present study was to evaluate the chemical composition, the free radical scavenging activity, and the mutagenic and genotoxicity properties of *C. guianensis* oils obtained via three different extraction methods. Phenolic contents were evaluated by spectrophotometry.

2. Methods

2.1. C. guianensis Oil Preparation. The *C. guianensis* Aublet C. seeds were harvested from December 2013 to February 2014 from under identified parent trees in the Rio de Janeiro Botanical Gardens, with prior authorization. The seeds were superficially cleaned and frozen at −18°C, and for oil extraction, the frozen seeds were first sliced and air-dried at 60°C.

After preparing the sliced and dried seeds, oil 1 was obtained by pressing using a model CA59G expeller-type laboratory press (Komet) with a maximum processing capacity of 5 kg/h of raw material. Screws with 12 mm between the grooves were used, with an oil outlet grid with 1 mm diameter holes and a 10 mm diameter outlet nozzle. The oil obtained was centrifuged at 10,000 rpm for 10 minutes at room temperature to remove particles and then frozen at −18°C.

To evaluate the effects of the thermal treatment, the frozen seeds were autoclaved at 121°C for 15 min and then submitted to slicing, drying, and pressing conditions as presented above to obtain oil 2.

Oil 3 was obtained using the Soxhlet extraction method (30–60°C for 16 h) with petroleum ether, extracting from the dried seeds with no further heat treatment. The solvent was evaporated off in a rotary evaporator under a stream of nitrogen, and the oil obtained was frozen at −18°C.

2.2. Fatty Acid Composition. In order to analyze the fatty acid profile, methyl esters were obtained according to Hartman and Lago [20]. Gas chromatography was carried out using an Agilent 7890 gas chromatograph with a fused silica capillary column (60 m; 0.32 mm internal diameter; and 0.25 μm stationary phase of 78% cyanopropyl methylpolysiloxane) with a temperature program from 150 to 200°C at a rate of 1.3°C/min.

The injector temperature was 250°C maintaining the injector in the split flow mode with a ratio of 50 : 1 and injecting 1 μL of the oil diluted in dichloromethane (2%). The temperature of the flame ionization detector was 280°C, and the carrier gas flow (H_2) was 2.5 mL/min (measured at 40°C). The fatty acid methyl esters were identified by a comparison of their retention times with standard Nu Chek (Elysian, MN) numbers 62, 79, and 87 and quantified by an internal normalization. The iodine and saponification values were calculated from the fatty acid profile.

2.3. Physicochemical Aspects. The free fatty acid content of the oils was determined by titration according to the American Oil Chemists' Society official method number Ca 5a 40 (AOCS) (2009) [21], and the results were expressed as oleic acid. The peroxide content (milliequivalents of peroxide/1000 g of sample) was determined according to the AOCS method number Cd 8 53 (2009). The refractive index was measured in a Bausch and Lomb Abbé refractometer at 40°C and the density in a PAAR DMA AP-46 digital densitometer at 20°C.

2.4. DPPH Assay. DPPH (2,2-diphenyl-1-picrylhydrazyl) radical scavenging was evaluated according to a previously reported procedure [22] with some modifications [23]. The DPPH solution was freshly prepared daily, stored in a flask, covered, and kept in the dark at 4°C. Briefly, one milliliter of 0.1 mM DPPH in absolute methanol was added to one milliliter of each sample dilution, with five concentration levels ranging from 0 to 200 μL dissolved in dimethyl sulfoxide (DMSO). The solutions were mixed, covered, and allowed to react in the dark at room temperature for 30 min at 25°C, and the absorbance was measured at 517 nm in a spectrophotometer (Shimadzu UV-160A spectrophotometer). The control was prepared by mixing the DPPH-methanol solution with the sample solvent or butylated hydroxytoluene (BHT, positive control). The blank was prepared with ethanol plus the extract solution. The DPPH radical scavenging activity of the sample was calculated according to the following equation: $\%\text{inhibition} = (\text{control} - \text{sample})/(\text{control} - \text{blank}) \times 100\%$. The EC_{50} values were calculated by an interpolation from the linear regression analysis.

2.5. Total Phenolic Content. The total phenolic content was estimated by the Folin-Ciocalteu method as previously described [23], using pyrocatechol as the standard and five concentrations levels (2, 5.5, 11, 22, and 33 μg/mL) for the calibration curve. DMSO was used as the solvent. The assay was carried out in a 96-well microplate. The reaction mixture contained 35 μL of Folin-Ciocalteu reagent and 35 μL of oil or different concentration of the standard solution or just solvent (blank). After 5 min of incubation, 35 μL of sodium carbonate solution at 20 mg/mL was added and the mixture was placed in the dark for 2 h at room temperature. The absorbances were read at 760 nm in a microplate reader (Quant, BioTek Instruments Inc.). The results were expressed as pyrocatechol equivalent (g per mL of oil). After a linear regression analysis, the coefficient of determination for the standard curve was found to be 0.9982.

2.6. Mutagenicity Assay (Ames Test). The mutagenicity reverse mutation test was carried out to investigate the potential of the *C. guianensis* oils to induce genetic mutation in the *Salmonella enterica* serovar Typhimurium *(S. typhimurium)* TA97, TA98, TA100, TA102, and TA1535 strains. The test was carried out according to the preincubation method, both in the absence and presence of a metabolic activation system (4% S9 mix, Aroclor-preinduced, from Moltox Inc., USA). The negative control was 10% DMSO while known mutagens were used as the positive control substances. The positive controls without the S9 mix were as follows: 4-nitroquinoline 1-oxide (4-NQO) (5 μg per plate) for TA97 and TA98; sodium azide (SA) (10 mg per plate) for TA100; mitomycin C (MMC) (1 μg per plate) for TA102; and methyl methanesulfonate (MMS) (200 μg per plate) for TA104. The positive controls with the S9 mix were 2-amineanthracene (2-AA) (10.0 μg per plate) for TA97, TA98, and TA1535 and benzo(α)pyrene (B[α]P) (50.0 μg per plate) for TA100 and TA102. A dose-finding test was carried out with and without the metabolic activation system (S9 mix) for each tester strain. A total of eight concentrations diluted in DMSO were tested from 0 to 100 μL/mL [24].

For the assays without metabolic activation, 0.5 mL of 0.1 mol/L sodium-phosphate buffer (pH 7.4) was added, and for the assays in the presence of metabolic activation, 0.5 mL of the S9 mix was mixed with 0.1 mL culture medium (2×10^9 cells/mL) plus 0.1 mL of each compound solution (0.02 to 100 μL/plate). The mixtures were incubated in a shaker at 37°C (preincubation). After 30 min preincubation protected from the light, the mixture was added to and mixed with 2 mL top agar containing 0.05 mmol/L L-histidine and D-biotin for the *S. typhimurium* strains. Each of these was then spread on a minimum glucose agar plate. After the top agar had solidified, the plates were incubated at 37°C for 60–72 h. Each tester strain was assayed in triplicate, and the number of revertant colonies was counted for each tester strain and treatment group [25]. The results were judged to be positive when the average number of revertant colonies in each treated group increased with increase in the compound concentration, reaching at least twice the number in the negative control group [24].

In order to determine the cytotoxic effects, after 30 min preincubation, the assay mixtures were diluted ($1:10^5$) in 0.9% NaCl (*w*/*v*) and a suitable aliquot of the final dilution (100 μL) of this suspension was plated on a nutrient agar (0.8% bacto nutrient broth (Difco), 0.5% NaCl, and 1.5% agar). The plates were then incubated at 37°C for 24 h, and the colonies were counted. All the experiments were done in triplicate and repeated at least twice. Statistical differences between the groups were analyzed by a one-way ANOVA ($P < 0.05$) and Tukey's post hoc test [24].

2.7. Eukaryotic Cell Cultures. Chinese Hamster Ovary (CHO-K1) and mouse macrophages (RAW264.7) cells obtained from the American Type Culture Collection (Manassas, VA) were cultured in Eagle's medium (MEM, GIBCO®, USA) containing 10% fetal bovine serum (FBS) plus 100 μg/mL streptomycin and 100 μg/mL penicillin at 37°C in a 5% CO_2 atmosphere. Logarithmic phase cells were used in all the experiments [26].

2.8. Eukaryotic Cell Viability (WST-1). Fresh RAW264.7 and CHO-K1 cells were seeded at a density of 1×10^4 cells/well. The water-soluble tetrazolium salt assay (WST-1, Roche) (4-[3-(4-iodophenyl)-2-(4-nitrophenyl)-2H-5-tetrazolio]-1,3-benzene disulfonate) (Roche Co., South San Francisco, CA) was used to determine the number of viable cells after 3 and 24 h of exposure to the oils (1–3) (10 to 100 μL/mL, diluted in DMSO). This salt is reduced by mitochondrial dehydrogenases in living cells, yielding a yellow product that is soluble in the cell culture medium. Briefly, after treatment, the culture medium was replaced by 90 μL fresh culture medium and 10 μL WST-1 reagent and incubated at 37°C with 5% CO_2 for 3 h. The absorbance was then measured at 440 nm according to the kit protocol [27]. The intensity of the yellow color in the negative control (DMSO 1%) wells was designated as 100% viability, and all further comparisons were based on this reference level to determine the lethal concentration (LC_{50}) for 50% of cultured cells. Statistical differences between the groups were analyzed by one-way ANOVA ($P < 0.01$) and Tukey's post hoc test.

2.9. Micronucleus Assay in the Cell Cultures (MN). Fresh RAW264.7 and CHO-K1 cells were seeded at a density of 1×10^5 cells/mL in 24-well plates (1 mL/per well). The oils (1–3) were then added to the medium to final concentrations from 10 to 100 μL/mL diluted in DMSO, and the incubation continued for 3 h or 24 h. DMSO (1%) was used as the negative control, and N-methyl-N′-nitro-N-nitrosoguanidine (MMNG, 500 μM) for RAW264.7 and MMC (5 μM) for CHO-K1 were the positive controls. After exposure to the compounds, the cells were incubated for a further 24 h under growth conditions before quantification of the micronuclei and cytotoxicity. The cytogenetic studies were carried out in triplicate as described previously [28]. In order to determine the mitotic index and the number of cells with micronuclei, the medium was replaced by a cold methanol-glacial acetic acid (3 : 1) fixative for 30 min, and the cells were

Table 1: Fatty acid composition (g/100 g) of *Carapa guianensis* oils.

Fatty acid	*Carapa guianensis* oils (mean ± SD)		
	Oil 1	Oil 2	Oil 3
C14:0 (myristic)	0.05 ± 0.000	0.04 ± 0.001	0.05 ± 0.000
C16:0 (palmitic)	27.71 ± 0.016	27.50 ± 0,039	28.33 ± 0.123
C16:1 (palmitoleic)	0.90 ± 0.001	0.89 ± 0.001	0.94 ± 0.005
C17:0 (margaric)	0.12 ± 0.001	0.12 ± 0.001	0.13 ± 0.001
C18:0 (stearic)	9.34 ± 0.007	9.52 ± 0.002	9.09 ± 0.025
C18:1 (oleic)	49.90 ± 0.012	49.71 ± 0.025	49.56 ± 0.074
C18:2 (linoleic)	9.58 ± 0.010	9.82 ± 0.011	9.62 ± 0.013
C18:3 (linonelic)	1.43 ± 0.002	1.43 ± 0.003	1.38 ± 0.011
C20:0 (arachidic)	0.26 ± 0.002	0.27 ± 0.001	0.23 ± 0.001
C20:1 (gondoic)	0.13 ± 0.003	0.13 ± 0.003	0.13 ± 0.004
C22:0 (behenic)	0.36 ± 0.001	0.35 ± 0.003	0.35 ± 0.004
C24:0 (lignoceric)	0.22 ± 0.004	0.22 ± 0.002	0.21 ± 0.002
Iodine value (g I_2/100 g)	196.6	196.6	196.6
Saponification value (mg KOH/g)	59.5	59.7	59.3

SD: standard deviation. No significant differences: $P > 0.05$ ANOVA and Tukey's between the oils.

then rinsed with distilled water for 2 min and air-dried. The fixed cells were stained with 4,6-diamidino-2-phenylindole (DAPI) (0.2 pg/mL) dissolved in McIlvaine buffer (0.1 M citric acid plus 0.2 M Na_2HPO_4, pH 7.0) for 60 min, washed with McIlvaine buffer for 5 min, briefly rinsed with distilled water, and mounted in glycerol. To determine the mitotic index and the number of cells with micronuclei, 1000 cells per well (3000 cells per concentration) were analyzed under a fluorescence microscope. Cells that glowed brightly and had homogenous nuclei were considered as having normal phenotypic morphology. Apoptotic nuclei were identified by the condensed chromatin at the periphery of the nuclear membrane or by fragmented nuclear body morphology. Necrotic cells presented chromatin forms with irregularly shaped aggregates, a pyknotic nucleus (shrunken and darkly stained) and cell membrane disruption, with cellular debris spilling into the extracellular milieu. The percentage of viable cells was evaluated discounting apoptotic and necrotic cells. Statistical differences between the groups were analyzed by one-way ANOVA ($P < 0.01$) and Tukey's post hoc test.

3. Results

3.1. Extractions and Oil Yields. The seed moisture was around 30%. The oil yields (dry weight basis) for pressing the dried seeds without autoclaving (oil 1) and with autoclaving (oil 2) were 14.85% and 20.62%, respectively. The Soxhlet extraction yield (oil 3) was 61.50%.

3.2. Fatty Acid Composition. Table 1 presents the fatty acid compositions of the *C. guianensis* seed oils. There were no significant differences ($P > 0.05$) between the oils evaluated. The main fatty acids were oleic acid (C18:1), palmitic acid (C16:0), linoleic acid (C18:2), and stearic acid (C18:0). The monounsaturated fatty acids comprised about 50% of the total, while the saturated and polyunsaturated fatty acid contents were around 38 and 11%, respectively. The iodine and saponification values were calculated and presented in Table 1.

3.3. Physicochemical Property Profiles. Table 2 shows some physicochemical aspects of the oils. No differences were observed between the three oils in the following aspects: acidity, peroxides, refraction, density, and phenolic compound. On the other hand, oil 1 showed a higher scavenging activity against the DPPH radical when compared to oils 2 and 3.

3.4. Salmonella/Microsome. The results of the *Salmonella*/microsome assay (Table 3) showed that only oil 2 had mutagenic activity in the presence of exogenous metabolism, because the highest MI was 2.2, although it is possible to observe a gradual increase of the MI values with no statistical significance, mainly for oils 2 and 3 after metabolic activation. All of them induced decreased survival for most conditions, suggesting cytotoxicity with respect to different strains of *S. typhimurium*. Bacterial cytotoxicity was more evident for TA1535 with oil 1 (as from 0.1 μL/plate) in the absence of S9, followed by oil 2 (as from 6.75 and 12.5 μL/plate) in the absence and presence of S9, respectively, and oil 3 (as from 12.5 μL/plate) in the absence and presence of S9.

3.5. WST-1 Assay. The cytotoxic effects in the cell lines presented different profiles. After 3 h of exposure, oil 1 was the least toxic for the CHO-K1 and RAW264.7 cells ($P < 0.01$), followed by oil 3 and oil 2 (Table 4). After 24 h of exposure, the same behavior was observed for the CHO-K1 cells, but for RAW264.7, oil 3 had the highest LC_{50} (62.91 ± 7.35), followed by oil 1 (48.10 ± 3.11) and oil 2 (46.67 ± 8.32). Finally, when comparing the two cell

Table 2: Physicochemical aspects of *Carapa guianensis* oils.

	Oil 1	Oil 2	Oil 3
Acidity (% oleic acid)	0.30[a]	0.28[a]	0.24[a]
Peroxides (meq/kg)	0.97[a]	0[a]	0[a]
Refraction (nD 40°C)	1.4595[a]	1.4603[a]	1.4593[a]
Density (g/cm^3)	0.9174[a]	0.9183[a]	0.9169[a]
EC_{50} scavenging of $DPPH^+$ (μL/mL)	89.07 ± 3.67[a]	>200[b]	>200[b]
Phenolic content (mg/g of catechol)	10.34 ± 0.04[a]	9.50 ± 0.02[a]	9.00 ± 0.03[a]

Values followed by different letters on the same line differ statistically amongst themselves according to ANOVA and the Tukey's test ($P < 0.05$). CE50: half-maximal effective concentration; DPPH: 2,2-diphenyl-1-picrylhydrazyl. Values of two independent assays.

lines, it can be seen that the cytotoxic effects were higher in the presence of CHO-Kl.

3.6. Micronucleus Assay. Figure 1 shows the results for the MN assay using CHO-K1 cells. Oil 1 did not reduce the mitotic index and was not able to induce MN formation in ovary cells (Figure 1(a)). Oil 2 induced ovarian MN increasing on 2.1 times more at 50 μL/mL and 2.7 times more at 100 μL/mL exposures in relation to the negative control. Oil 2 also significantly reduced the mitotic index at 100 μL/mL (Figure 1(b)). Oil 3 reduced the mitotic index as from 50 μL/mL and increased MN formation at 100 μL/mL (2.4-fold) (Figure 1(c)). The three oils induced a significant ($P < 0.01$) reduction in the survival rates.

Using RAW264.7 macrophages (Figure 2), oil 1 did not cause DNA damage or delay in the cell cycle (Figure 2(a)). Oil 2 (Figure 2(b)) induced significant MN induction at 50 μL/mL (2.1-fold) and 100 μL/mL (2.2-fold), and oil 3 (Figure 2(c)) also induced significant MN increasing at exposures of 50 μL/mL (2.2-fold) and 100 μL/mL (2.5-fold). None of the oils induced cytostatic effects on macrophages. Both oils 2 and 3 presented significant ($P < 0.01$) cytotoxic response at 100 μL/mL.

4. Discussion

The use of natural products in traditional Brazilian phytomedicine is widely accepted and prescribed, mainly in the poorest areas, such as the Amazon and Northeastern regions. Thus, the pharmaceutical potential of Brazilian herbs must be considered in drug discovery studies [29]. Contrary to allopathy, the traditional usage of medicinal plants is apparently considered to be safe and hence the toxicity of traditional herbal medicines has not been totally evaluated in most cases, although medicinal plants can be extremely harmful to human health. Studies have revealed that some plants frequently used in folk medicine are potentially genotoxic [30–32]. It is thus truly relevant to screen the genotoxicity during the preclinical evaluation of herbal extracts or substances, in order to verify their mutagenic potential for both safety and economic concerns, since plants are widely used in folk medicine and can be a resource for the development of new drugs [33].

The drying process was required in the oil extraction processes by both solvent extraction (Soxhlet) and screw pressing. The expeller pressing yields were similar to the results reported by Souza et al. [14]. Autoclaving before drying improved the oil yield from ~15% to 20% while the Soxhlet extraction yielded 61.5%, suggesting that the extraction process using petroleum ether at 30–60°C with no further heat treatment is the more efficient in terms of yield than the pressing, although the raw material is difficult to handle due to its rubbery texture. Under the conditions used, the Soxhlet extraction allowed for the extraction of all the oil besides other petroleum ether-soluble compounds. The screw press or hydraulic press usually used for low moisture content seeds and nuts recovers around 50 to 90% of the oil, depending on the pretreatment carried out, the capacity and design characteristics of the equipment, the temperature, and the seed moisture content, but remarkable variations were observed regarding the composition of the raw material.

The extraction methods using heating processes to improve the extraction yield have been used before in traditional use of *C. guianensis* oils for medicinal use in the Amazon area [13]. In the present work, autoclaving improved the extraction performance indicating that the thermal treatment is required to denature the cellular structure for oil removal. However, lower temperatures used in the Soxhlet extraction compared to extraction process by autoclaving increase the extraction yield.

It has been reported that *C. guianensis* seed oils contain the myristic, palmitic, oleic, linoleic, stearic, and arachidic fatty acids, tetraterpenoids [34], and flavane [35]. Here, we determine the main fatty acids found in the andiroba oil such as oleic (50%), palmitic (28%), stearic (9%), and linoleic (10%). The linolenic (C18:3) and palmitoleic (C16:1) acids were detected up to 1.4 and 0.9%, respectively. Some minor fatty acids such as C14:0, C17:0, C20:1, C20:1, C22:0, and C24:0 were detected at values below 0.4%. The acidity or free fatty acid content and peroxide value of the andiroba oil were very low and statically similar results ($P > 0.05$), as shown in Table 2, which is unusual for this oil since oil acidity of 30% has been observed using the traditional process, which allows for enzyme action and fermentation.

The seeds were collected and frozen before drying followed by the oil extraction process, hence avoiding

Table 3: Mean values ± SD (MI) of revertant *His*$^+$ colonies of *Salmonella enterica* serovar Typhimurium strains used in *Salmonella*/microssome assay after coincubation with *Carapa guianensis* oils.

		μL/plate	TA97	TA98	TA100	TA102	TA1535
Oil 1	−S9	0	67 ± 1 (1.0)	41 ± 9 (1.0)	118 ± 28 (1.0)	428 ± 16 (1.0)	14 ± 5 (1.0)
	−S9	0.02	92 ± 8 (1.4)	41 ± 12 (1.0)	168 ± 18 (1.4)	429 ± 9 (1.0)	16 ± 2 (1.1)
	−S9	0.1	89 ± 13 (1.3)	36 ± 7 (0.9)	180 ± 13 (1.5)	443 ± 39 (1.0)	Cytotoxic
	−S9	0.2	73 ± 10 (1.1)	45 ± 1 (1.1)	190 ± 19 (1.6)	462 ± 12 (1.1)	—
	−S9	1	82 ± 9 (1.2)	41 ± 4 (1.0)	172 ± 28 (1.5)	Cytotoxic	—
	−S9	2	Cytotoxic	40 ± 6 (1.0)	148 ± 18 (1.3)	—	—
	−S9	3.38	—	Cytotoxic	Cytotoxic	—	—
	+S9	0	180 ± 35 (1.0)	49 ± 7 (1.0)	169 ± 1 (1.0)	534 ± 73 (1.0)	30 ± 4 (1.0)
	+S9	0.02	185 ± 28 (1.0)	54 ± 6 (1.1)	171 ± 15 (1.0)	554 ± 34 (1.0)	31 ± 11 (1.0)
	+S9	0.1	187 ± 27 (1.0)	61 ± 20 (1.2)	179 ± 10 (1.1)	615 ± 41 (1.2)	33 ± 4 (1.1)
	+S9	0.2	166 ± 21 (0.9)	48 ± 3 (1.0)	181 ± 45 (1.1)	639 ± 39 (1.2)	36 ± 2 (1.2)
	+S9	1	150 ± 18 (0.8)	47 ± 4 (1.0)	172 ± 21 (1.0)	710 ± 70 (1.3)	36 ± 6 (1.2)
	+S9	2	139 ± 35 (0.8)	56 ± 6 (1.1)	183 ± 7 (1.1)	798 ± 10 (1.5)	44 ± 8 (1.5)
	+S9	3.38	Cytotoxic	Cytotoxic	Cytotoxic	Cytotoxic	Cytotoxic
Oil 2	−S9	0	93 ± 1 (1.0)	37 ± 3 (1.0)	146 ± 32 (1.0)	358 ± 2 (1.0)	12 ± 4 (1.0)
	−S9	2	93 ± 2 (1.0)	37 ± 6 (1.0)	148 ± 11 (1.0)	311 ± 4 (0.9)	13 ± 2 (1.1)
	−S9	3.38	93 ± 10 (1.0)	38 ± 4 (1.0)	152 ± 19 (1.0)	268 ± 33 (0.8)	13 ± 3 (1.1)
	−S9	6.75	104 ± 10 (1.1)	40 ± 6 (1.1)	164 ± 16 (1.1)	289 ± 55 (0.8)	Cytotoxic
	−S9	12.5	104 ± 15 (1.1)	33 ± 5 (0.9)	171 ± 21 (1.2)	283 ± 105 (0.8)	—
	−S9	25	99 ± 6 (1.0)	47 ± 4 (1.3)	176 ± 14 (1.2)	291 ± 44 (0.8)	—
	−S9	50	96 ± 7 (1.0)	41 ± 3 (1.1)	179 ± 17 (1.2)	280 ± 50 (0.8)	—
	−S9	100	93 ± 10 (1.0)	31 ± 7 (0.8)	Cytotoxic	388 ± 50 (1.1)	—
	+S9	0	135 ± 8 (1.0)	23 ± 3 (1.0)	173 ± 20 (1.0)	354 ± 38 (1.0)	14 ± 3 (1.0)
	+S9	2	139 ± 7 (1.0)	27 ± 5 (1.2)	189 ± 18 (1.1)	365 ± 37 (1.0)	15 ± 3 (1.1)
	+S9	3.38	133 ± 11 (1.0)	28 ± 1 (1.2)	188 ± 13 (1.1)	386 ± 42 (1.1)	16 ± 4 (1.1)
	+S9	6.75	186 ± 15 (1.4)	29 ± 5 (1.3)	228 ± 16 (1.3)	403 ± 19 (1.1)	21 ± 7 (1.5)
	+S9	12.5	191 ± 12 (1.4)	30 ± 5 (1.3)	260 ± 12 (1.5)	396 ± 31 (1.1)	Cytotoxic
	+S9	25	194 ± 13 (1.4)	39 ± 1 (1.7)	306 ± 10 (1.8)	372 ± 40 (1.0)	—
	+S9	50	208 ± 16 (1.5)	42 ± 4 (1.8)	333 ± 15 (1.9)	399 ± 18 (1.0)	—
	+S9	100	215 ± 8 (1.6)	Cytotoxic	383 ± 20 (2.2)*	454 ± 32 (1.3)	—
Oil 3	−S9	0	73 ± 3 (1.0)	31 ± 9 (1.0)	132 ± 11 (1.0)	263 ± 9 (1.0)	11 ± 4 (1.0)
	−S9	2	73 ± 3 (1.0)	31 ± 3 (1.0)	132 ± 10 (1.0)	260 ± 7 (1.0)	12 ± 4 (1.1)
	−S9	3.38	77 ± 16 (1.1)	29 ± 11 (1.0)	131 ± 18 (1.0)	268 ± 31 (1.0)	12 ± 1 (1.1)
	−S9	6.75	76 ± 9 (1.0)	33 ± 4 (1.1)	138 ± 17 (1.0)	289 ± 6 (1.1)	13 ± 1 (1.2)
	−S9	12.5	75 ± 4 (1.0)	35 ± 2 (1.1)	129 ± 29 (1.0)	259 ± 22 (1.0)	Cytotoxic
	−S9	25	91 ± 6 (1.2)	31 ± 3 (1.0)	119 ± 12 (0.9)	259 ± 22 (1.0)	—
	−S9	50	93 ± 5 (1.3)	31 ± 4 (1.0)	130 ± 27 (1.0)	365 ± 26 (1.4)	—
	−S9	100	94 ± 13 (1.3)	30 ± 5 (1.0)	108 ± 6 (0.8)	388 ± 18 (1.5)	—
	+S9	0	145 ± 9 (1.0)	29 ± 4 (1.0)	193 ± 15 (1.0)	267 ± 22 (1.0)	11 ± 2 (1.0)
	+S9	2	143 ± 7 (1.0)	31 ± 5 (1.1)	199 ± 13 (1.0)	280 ± 18 (1.0)	15 ± 1 (1.4)
	+S9	3.38	151 ± 11 (1.0)	32 ± 2 (1.1)	208 ± 9 (1.1)	299 ± 25 (1.1)	17 ± 4 (1.5)
	+S9	6.75	Cytotoxic	35 ± 3 (1.2)	Cytotoxic	318 ± 16 (1.2)	19 ± 6 (1.7)
	+S9	12.5	—	40 ± 6 (1.4)	—	344 ± 22 (1.3)	Cytotoxic
	+S9	25	—	44 ± 8 (1.5)	—	372 ± 21 (1.4)	—
	+S9	50	—	49 ± 3 (1.7)	—	Cytotoxic	—
	+S9	100	—	Cytotoxic	—	—	—

SD: standard deviation; −S9: absence of metabolic activation; +S9: presence of metabolic activation; MI: mutagenicity index; *Difference of negative control, one-way ANOVA followed by Tukey's post hoc test ($P < 0.05$). Each sample was assayed until a cytotoxic response (survival < 70%); positive controls without S9: 4-NQO (1.0 μg/pl.) for TA97, 286 ± 17 revertants, TA98 120 ± 10 revertants, and TA1535 746 ± 58 revertants; AS (1.0 μg/pl.) for TA100, 607 ± 56 revertants; MMC (0.5 μg/pl.) for TA102; with S9: 2AA (1.0 μg/pl.) for TA97, 587 ± 11 revertants for TA98, 305 ± 1 revertants and for TA100, 1436 ± 40 revertants; B[a]P (50 μg/pl.) for TA102, 1448 ± 79 revertants and for TA1535 111 ± 10 revertants.

Table 4: Cytotoxicity (LC_{50}) of *Carapa guianensis* oils after 3 h and 24 h of treatment in RAW264.7 and CHO-K1 cells.

	LC_{50} (μL/mL)			
	CHO-K1		RAW264.7	
	3 h	24 h	3 h	24 h
Oil 1	73.81 ± 2.32	40.48 ± 5.13	93.45 ± 6.82	48.10 ± 3.11
Oil 2	45.24 ± 7.67^{a}	26.19 ± 6.67^{a}	80.13 ± 6.14	46.67 ± 8.32^{a}
Oil 3	66.67 ± 3.18^{b}	28.57 ± 3.33^{a}	87.36 ± 9.41	$62.91 \pm 7.35^{a,b}$

LC_{50}: lethal concentration. $^{a}P > 0.01$ versus oil 1 and $^{b}P > 0.01$ versus oil 2; $n = 3$; one-way ANOVA followed by Tukey's post hoc test.

enzyme activity related to triacylglycerol hydrolysis and the oxidative process. Nevertheless, the cell wall degrading enzymes may release compounds besides fatty acids which show biological activity. The possible differences in the biological activity of andiroba oil due to the extraction process have not been clearly established [12, 13]. In addition, there were no statistical differences between the three oils regarding the refraction and density suggesting that the differentiated extraction processes did not alter such physicochemical aspects.

In spite of the fact that oil 1 presented a higher phenolic content, no statistical differences were observed between the three oils in the phenolic compound determination (Table 2), suggesting that the extractable phenolic compounds are not associated with free radical scavengers, since oil 1 showed greater scavenging activity against the DPPH radical. Thus, it appears that the absence of high temperature for extraction associated with the shortest processing time prevented possible degradation of active components in the extract, which led to the greatest scavenging activities. Thermal treatment, as frying or boiling, can modify the composition of other vegetable oils, as crude palm oil, soybean oil, canola oil, flaxseed oil, and sunflower oil, increasing the oxidization status and enhancing the deleterious effects on human and animal health after consumption [36–40]. Milhomem-Paixão et al. [41] evaluated several andiroba oil samples and showed IC_{50} values for DPPH scavenging activity similar to those presented here. Probably the extraction that we performed without heat contains higher amount of antioxidant compounds such as phenolic compounds extracted with water present in the material (Table 2) or volatile compounds in the seeds. Therefore, the biological properties of the oils do not appear to be associated with the presence of phenolic compounds.

In addition to fatty acids, limonoids, triterpenes, steroids, coumarins, flavonoids, and diglycerides have been isolated from several parts of *C. guianensis* [42]. *C. guianensis* seed oils are rich source in limonoids, highly oxygenated tetranortriterpenoid compounds, that are reported to present several biological activities, such as antifungal, bactericidal, antifeedant, antimalarial, antiviral, anti-inflammatory, and growth-regulator on insects [43, 44], besides several medicinal effects in animals and humans [2]. Ambrozin et al. [42] identified seven limonoids in oil sample of *C. guianensis*: 17β-hydroxyazadiradione, gedunin, 6α-acetoxygedunin, 7-deacetoxy-7-oxogedunin, 1,2-dihydro-3β-hydroxy-7-deacetoxy-7-oxogedunin, methyl angolensate, and xyloccensin K, by various chromatographic techniques. These bioactive compounds are responsible for the therapeutic effects of the oil [2]. In agreement with the literature, the present study demonstrated the presence of monounsaturated, polyunsaturated, and saturated fatty acids.

In the present study, the *Salmonella*/microsome and micronucleus tests were used to screen the *C. guianensis* seed oils for genotoxicity. As shown here, except for oil 2, in the presence of metabolic activation for TA100, no mutagenic activity by frameshift was shown (TA97 and TA98 strains) and base pair substitution mutations (TA100, TA102, and TA1535 strains) were detected for all three oils, considering that the criterion for mutagenicity is indicated for MI higher than or equal to 2, although it is possible to observe a gradual increase of the MI values with no statistical significance, mainly for oils 2 and 3 after metabolic activation. On the other hand, all oils induced cytotoxic effects. These effects may be related to the chemical composition of the oils. So, cytotoxic effects observed in the present study may be related to the bactericidal activity and can be attributed to the limonoids [2].

The WST-1 assay is based on the capacity of the cellular mitochondrial dehydrogenase enzyme in living cells to reduce the water-soluble tetrazolium salt into the yellow-colored formazan dye, which is insoluble in water. The amount of formazan produced is directly proportional to the cell number in a range of cell lines. Thus, this assay relies on the mitochondrial activity of the cells and represents a parameter for their metabolic activity [45]. The WST-1 assay showed that the cell viabilities of CHO-Kl and RAW264.7 were affected by oils 1, 2, and 3 after 3 and 24 h exposure, inducing cell death. It is worthwhile noting that after 3 h of exposure, the cytotoxicity was higher for CHO-Kl (Table 4). Considering the induction of increased cell death in the two cell lines, the MN assay was carried out after only 3 h treatment. Except for oil 1, andiroba oils induce clastogenic and aneugenic effects in Chinese hamster ovaries (Figure 1) and macrophages (Figure 2). These findings indicate that the highest extraction temperature associated with the longest processing time leads to an increase in compounds which induce DNA damage. Oils 2 and 3 also induced a decrease in the mitotic index, but only for CHO-Kl (Figure 1), suggesting cell cycle arrest. Some studies have shown that gedunin, a tetranortriterpenoid present in *C. guianensis* oil, inhibits the proliferation of cancer cells, mainly by the inhibition of cell cycle arrest in different tumor cell lines, including ovarian cancer, via the induction of apoptosis by the cleavage of cochaperone p23 [46]. In addition, corroborating the results obtained with respect to cytotoxicity for CHO-Kl, the three oils induced a reduction in the survival rates. According to Llana-Ruiz-Cabello et al. [47], considering the commercial interest in vegetable oils and their components, the sources of exposure are substantially enhanced. Thus, data concerning the genotoxicity of these substances are needed in order to better understanding these safety profiles.

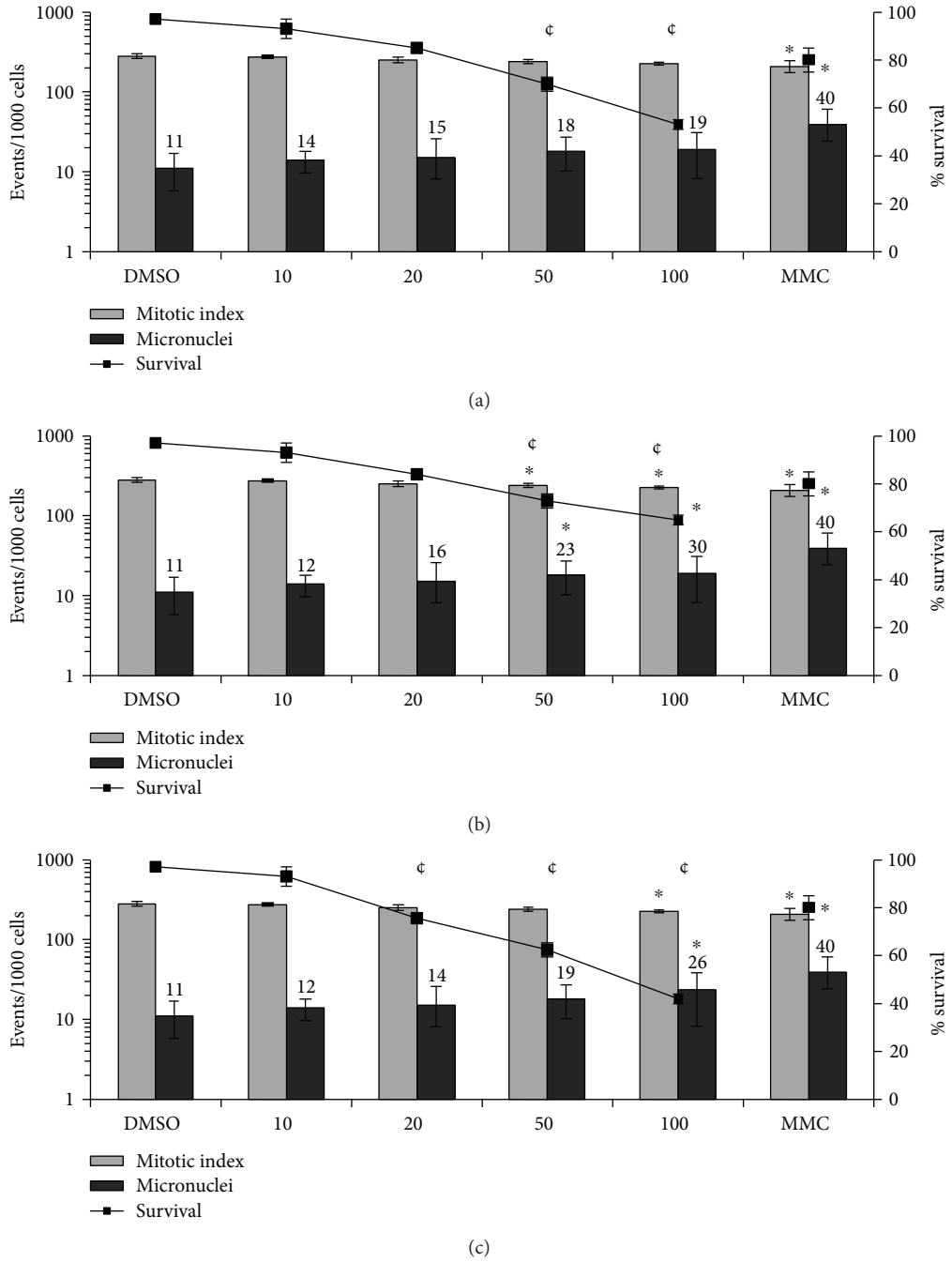

Figure 1: Micronucleus formation, mitotic indexes, and survival rate of CHO-K1 cells after 3 h of exposure. CHO-K1 cells were exposed to (a) oil 1, (b) oil 2, and (c) oil 3. 3000 cells were scored per treatment for each experiment. $n = 3$; $^*P < 0.001$on micronucleus formation or cell division and ¢ = cytotoxic ($P < 0.01$) one-way ANOVA followed by Tukey's post hoc test.

5. Conclusion

Overall, we conclude that, related to fatty acid composition and physicochemical property, there were no significant differences between the three oils. In this way, differentiated extraction processes did not alter such composition or property. Significant levels of cytotoxicity in bacterial and eukaryotic models were induced by the three oils, suggesting that these effects may be related to its chemical composition. Oil 1 obtained from *C. guianensis* seeds, which was extracted without the use of high temperatures, showed to be the safest for use and the most promising product as compared to the other oils, since it was not mutagenic or genotoxic and showed a higher scavenging activity against the DPPH radical, unlike that observed for oils 2 and 3. The data discussed in this paper contributed to the knowledge that processing the *C. guianensis* seeds at high temperatures increases the risk of adverse genotoxic effects and decreases the scavenging activities of crabwood seed oil.

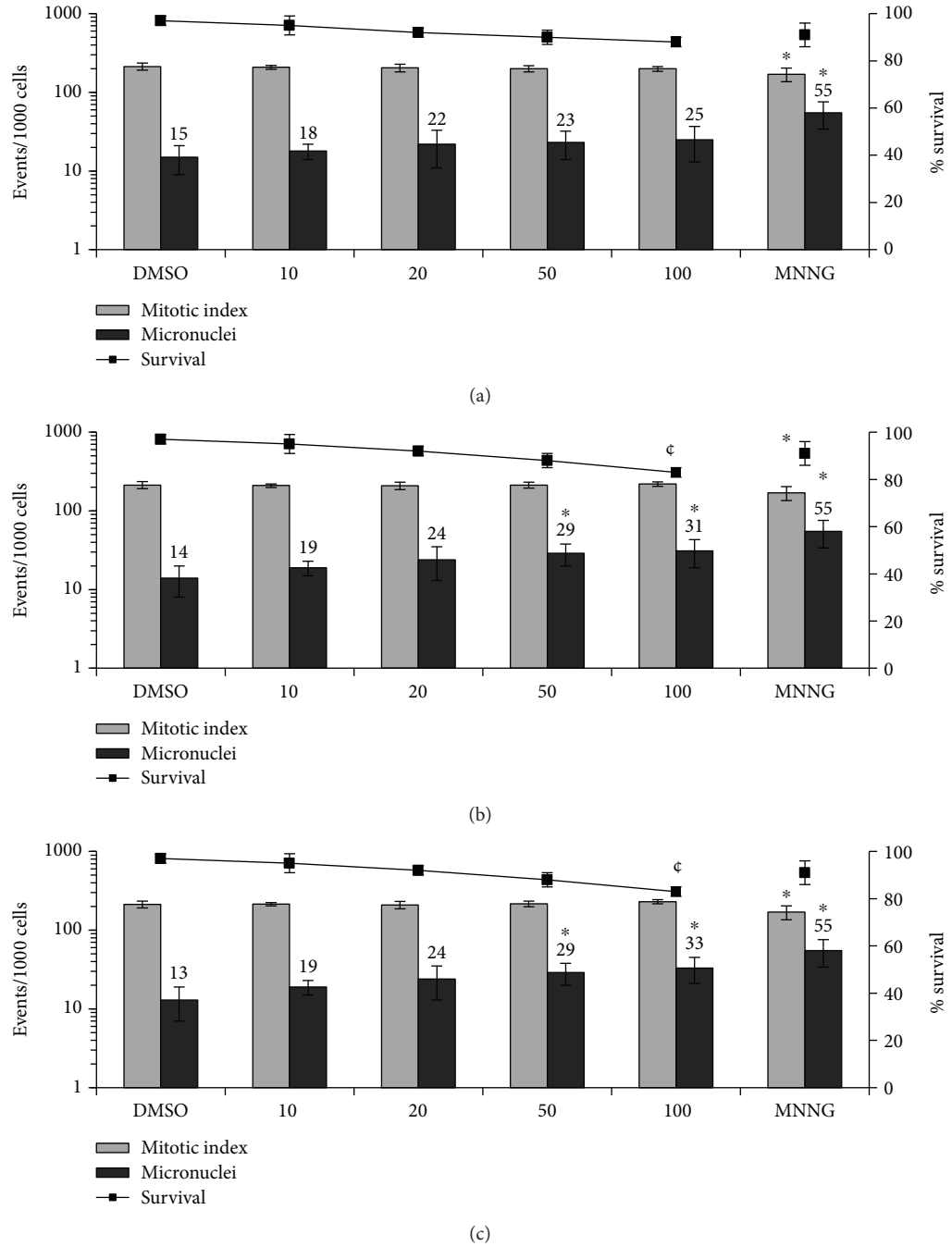

Figure 2: Micronucleus formation, mitotic indexes, and survival rate of RAW264.7 cells after 3 h of exposure. RAW264.7 cells were exposed to (a) oil 1, (b) oil 2, and (c) oil 3. 3000 cells were scored per treatment for each experiment. $n = 3$; $^*P < 0.001$ on micronucleus formation or cell division and ¢ = cytotoxic ($P < 0.01$) one-way ANOVA followed by Tukey's post hoc test.

Conflicts of Interest

The authors declare no conflicts of interest in the execution and interpretation of the information present in this study.

Authors' Contributions

Carlos F. Araujo-Lima and Andreia S. Fernandes contributed equally to the present study.

Acknowledgments

The authors are grateful to FAPERJ, CAPES, and CNPq for the fellowships granted and for other financial support and are also indebted to the Universidade do Estado do Rio de Janeiro (UERJ), Universidade Federal do Estado do Rio de Janeiro (UNIRIO), Empresa Brasileira de Pesquisa Agropecuária (EMBRAPA), and Instituto de Pesquisas Jardim Botânico do Rio de Janeiro.

References

[1] J. H. Costa-Silva, C. R. Lima, E. J. R. Silva et al., "Acute and subacute toxicity of the *Carapa guianensis* Aublet (Meliaceae) seed oil," *Journal of Ethnopharmacology*, vol. 116, no. 3, pp. 495–500, 2008.

[2] M. Henriques and C. Penido, "The therapeutic properties of *Carapa guianensis*," *Current Pharmaceutical Design*, vol. 20, no. 6, pp. 850–856, 2014.

[3] C. Penido, K. A. Costa, R. J. Pennaforte et al., "Anti-allergic effects of natural tetranortriterpenoids isolated from *Carapa guianensis* Aublet on allergen-induced vascular permeability and hyperalgesia," *Inflammation Research*, vol. 54, no. 7, pp. 295–303, 2005.

[4] C. Penido, F. P. Conte, M. S. S. Chagas, C. A. B. Rodrigues, J. F. G. Pereira, and M. G. M. O. Henriques, "Antiinflammatory effects of natural tetranortriterpenoids isolated from *Carapa guianensis* Aublet on zymosan-induced arthritis in mice," *Inflammation Research*, vol. 55, no. 11, pp. 457–464, 2006.

[5] C. M. Cazal, K. Choosang, V. G. P. Severino et al., "Evaluation of effect of triterpenes and limonoids on cell growth, cell cycle and apoptosis in human tumor cell line," *Anti-Cancer Agents in Medicinal Chemistry*, vol. 10, no. 10, pp. 769–776, 2010.

[6] F. N. de Barros, M. P. O. Farias, J. P. C. Tavares, L. C. Alves, and M. A. d. G. Faustino, "*In vitro* efficacy of oil from the seed of *Carapa guianensis* (andiroba) in the control of *Felicola subrostratus*," *Revista Brasileira de Farmacognosia*, vol. 22, no. 5, pp. 1130–1133, 2012.

[7] C. E. S. Silva, O. J. dos Santos, J. M. Ribas-Filho et al., "Effect of *Carapa guianensis* Aublet (andiroba) and *Orbignya phalerata* (babassu) in colonic healing in rats," *Revista do Colégio Brasileiro de Cirurgiões*, vol. 42, no. 6, pp. 399–406, 2015.

[8] H. A. Miot, R. F. Batistella, K. d. A. Batista et al., "Comparative study of the topical effectiveness of the andiroba oil (*Carapa guianensis*) and DEET 50% as repellent for *Aedes* sp," *Revista do Instituto de Medicina Tropical de São Paulo*, vol. 46, no. 5, pp. 253–256, 2004.

[9] F. A. C. de Mendonça, K. F. S. da Silva, K. K. dos Santos, K. A. L. Ribeiro Júnior, and A. E. G. Sant'Ana, "Activities of some Brazilian plants against larvae of the mosquito *Aedes aegypti*," *Fitoterapia*, vol. 76, no. 7-8, pp. 629–636, 2005.

[10] M. P. O. Farias, D. P. Sousa, A. C. Arruda et al., "Potencial acaricida do óleo de andiroba *Carapa guianensis* Aubl. sobre fêmeas adultas ingurgitadas de *Anocentor nitens* Neumann, 1897 e *Rhipicephalus sanguineus* Latreille, 1806," *Arquivo Brasileiro de Medicina Veterinária e Zootecnia*, vol. 61, no. 4, pp. 877–882, 2009.

[11] C. O. Carvalho, A. C. S. Chagas, F. Cotinguiba et al., "The anthelmintic effect of plant extracts on *Haemonchus contortus* and *Strongyloides venezuelensis*," *Veterinary Parasitology*, vol. 183, no. 3-4, pp. 260–268, 2012.

[12] P. Shanley and M. Londres, "Andiroba *Carapa guianensis* Aubl," in *Fruit Trees and Useful Plants in Amazonian Life. Trees and Vines*, P. Shanley, Ed., Food and Agriculture Organization of the United Nations (FAO), 2011, http://www.fao.org/docrep/015/i2360e/i2360e03.pdf.

[13] M. Nardi, A. C. Lira-Guedes, H. F. Albuquerque Cunha, M. C. Guedes, K. Mustin, and S. C. P. Gomes, "Artisanal extraction and traditional knowledge associated with medicinal use of crabwood oil (*Carapa guianensis* Aublet.) in a Peri-Urban Várzea environment in the Amazon estuary," *Evidence-based Complementary and Alternative Medicine*, vol. 2016, Article ID 5828021, 12 pages, 2016.

[14] C. R. Souza, R. M. B. Lima, C. P. Azevedo, and L. M. B. Ross, *Andiroba (Carapa guianensis Aubl)*, Embrapa Amazônia Ocidental, Manaus, Brazil, 2006, (Embrapa Amazônia Ocidental. Documentos, 48).

[15] V. P. da Silva, R. R. Oliveira, and M. R. Figueiredo, "Isolation of limonoids from seeds of *Carapa guianensis* Aublet (Meliaceae) by high-speed countercurrent chromatography," *Phytochemical Analysis*, vol. 20, no. 1, pp. 77–81, 2009.

[16] F. D. Gunstone, "Vegetable Oils," in *Bailey's Industrial Oils and Fats*, F. Shahidi, Ed., pp. 213–267, John Wiley & Sons Ltd., Chichester, UK, 6th edition, 2005.

[17] H. R. Bizzo and R. Antoniassi, "Fixed oils and antimicrobial effects," in *Recent Progress in Medicinal Plants Vol. 33 Fixed Oils and Fats*, J. N. Govil, Ed., pp. 273–285, Studium Press, England and Wales, 2012.

[18] "Guidance document on revisions to OECD genetic toxicology test guidelines," OECD, Paris, France, Genetic toxicology Guidance Document, August 2015.

[19] K. Mortelmans and E. Zeiger, "The Ames *Salmonella*/microsome mutagenicity assay," *Mutation Research/Fundamental and Molecular Mechanisms of Mutagenesis*, vol. 455, no. 1-2, pp. 29–60, 2000.

[20] L. Hartman and R. C. Lago, "Rapid preparation of fatty acid methyl esters from lipids," *Laboratory Practice*, vol. 22, no. 6, pp. 475–6 passim, 1973.

[21] AOCS, "Official methods and recommended practices of the AOCS," 2009, http://agris.fao.org/agris-search/search.do?recordID=US201300136250.

[22] X. Liu and T. Osawa, "*cis* Astaxanthin and especially 9-*cis* astaxanthin exhibits a higher antioxidant activity *in vitro* compared to the all-*trans* isomer," *Biochemical and Biophysical Research Communications*, vol. 357, no. 1, pp. 187–193, 2007.

[23] A. S. Fernandes, J. L. Mazzei, C. G. Oliveira et al., "Protection against UV-induced toxicity and lack of mutagenicity of Antarctic *Sanionia uncinata*," *Toxicology*, vol. 376, pp. 126–136, 2017.

[24] C. F. Araujo-Lima, R. J. M. Nunes, R. M. Carpes, C. A. F. Aiub, and I. Felzenszwalb, "Pharmacokinetic and toxicological evaluation of a zinc gluconate-based chemical sterilant using *in vitro* and *in silico* approaches," *BioMed Research International*, vol. 2017, Article ID 5746768, 8 pages, 2017.

[25] N. Boechat, A. S. Carvalho, K. Salomão et al., "Studies of genotoxicity and mutagenicity of nitroimidazoles: demystifying this critical relationship with the nitro group," *Memórias do Instituto Oswaldo Cruz*, vol. 110, no. 4, pp. 492–499, 2015.

[26] F. S. Cardoso, C. F. Araujo-Lima, C. A. F. Aiub, and I. Felzenszwalb, "Exposure to sorbitol during lactation causes metabolic alterations and genotoxic effects in rat offspring," *Toxicology Letters*, vol. 260, pp. 36–45, 2016.

[27] E. R. A. Ferraz, C. R. Rainho, A. S. Fernandes, and I. Felzenszwalb, "Differential toxicity of an organic $PM_{2.5}$ extract to human lung cells cultured in three dimensions (3D) and monolayers," *Journal of Toxicology and Environmental Health, Part A*, vol. 79, no. 5, pp. 221–231, 2016.

[28] I. Felzenszwalb, M. R. da Costa Marques, J. L. Mazzei, and C. A. F. Aiub, "Toxicological evaluation of *Euterpe edulis*: a potential superfruit to be considered," *Food and Chemical Toxicology*, vol. 58, pp. 536–544, 2013.

[29] R. C. Dutra, M. M. Campos, A. R. S. Santos, and J. B. Calixto, "Medicinal plants in Brazil: pharmacological studies, drug discovery, challenges and perspectives," *Pharmacological Research*, vol. 112, pp. 4–29, 2016.

[30] R. Ananthi, N. Chandra, S. T. Santhiya, and A. Ramesh, "Genotoxic and antigenotoxic effects of *Hemidesmus indicus* R. Br. root extract in cultured lymphocytes," *Journal of Ethnopharmacology*, vol. 127, no. 2, pp. 558–560, 2010.

[31] P. R. Melo-Reis, L. S. Bezerra, M. A. Vale, R. F. Canhête, and L. Chen-Chen, "Assessment of the mutagenic and antimutagenic activity of *Synadenium umbellatum* Pax latex by micronucleus test in mice," *Brazilian Journal of Biology*, vol. 71, no. 1, pp. 169–174, 2011.

[32] G. G. Regner, J. Gianesini, R. G. von Borowski et al., "Toxicological evaluation of *Pterocaulon polystachyum* extract: a medicinal plant with antifungal activity," *Environmental Toxicology and Pharmacology*, vol. 31, no. 1, pp. 242–249, 2011.

[33] G. Sponchiado, M. L. Adam, C. D. Silva et al., "Quantitative genotoxicity assays for analysis of medicinal plants: a systematic review," *Journal of Ethnopharmacology*, vol. 178, pp. 289–296, 2016.

[34] J. H. Costa-Silva, M. M. A. Lyra, C. R. Lima et al., "A toxicological evaluation of the effect of *Carapa guianensis* Aublet on pregnancy in Wistar rats," *Journal of Ethnopharmacology*, vol. 112, no. 1, pp. 122–126, 2007.

[35] Q. Shuhua, W. Dagang, M. Yunbao, and L. Xiaodong, "A novel flavane from *Carapa guianensis*," *Acta Botanica Sinica*, vol. 45, no. 9, pp. 1129–1133, 2003.

[36] A. Ammouche, F. Rouaki, A. Bitam, and M. M. Bellal, "Effect of ingestion of thermally oxidized sunflower oil on the fatty acid composition and antioxidant enzymes of rat liver and brain in development," *Annals of Nutrition & Metabolism*, vol. 46, no. 6, pp. 268–275, 2002.

[37] N. Totani, S. Tateishi, T. Mori, and E. G. Hammond, "Oxidation of frying oils during intermittent usage," *Journal of Oleo Science*, vol. 61, no. 11, pp. 601–607, 2012.

[38] I. Felzenszwalb, J. L. da Costa Mazzei, S. Feitosa, C. A. Fortes Aiub, and D. T. de Almeida, "Toxicological assessment of crude palm oil (*Elaeis guineensis* Jacq.) used in deep frying of akara (cowpea paste finger food)," *Grasas y Aceites*, vol. 65, no. 2, article e020, 2014.

[39] B. Qi, Q. Zhang, X. Sui, Z. Wang, Y. Li, and L. Jiang, "Differential scanning calorimetry study—assessing the influence of composition of vegetable oils on oxidation," *Food Chemistry*, vol. 194, pp. 601–607, 2016.

[40] C. E. Richardson, M. Hennebelle, Y. Otoki et al., "Lipidomic analysis of oxidized fatty acids in plant and algae oils," *Journal of Agricultural and Food Chemistry*, vol. 65, no. 9, pp. 1941–1951, 2017.

[41] S. S. R. Milhomem-Paixão, M. L. Fascineli, M. M. Roll et al., "The lipidome, genotoxicity, hematotoxicity and antioxidant properties of andiroba oil from the Brazilian Amazon," *Genetics and Molecular Biology*, vol. 39, no. 2, pp. 248–256, 2016.

[42] A. R. P. Ambrozin, A. C. Leite, F. C. Bueno et al., "Limonoids from andiroba oil and *Cedrela fissilis* and their insecticidal activity," *Journal of the Brazilian Chemical Society*, vol. 17, no. 3, 2006.

[43] B. S. Nayak, J. Kanhai, D. M. Milne et al., "Investigation of the wound healing activity of *Carapa guianensis* L. (Meliaceae) bark extract in rats using excision, incision, and dead space wound models," *Journal of Medicinal Food*, vol. 13, no. 5, pp. 1141–1146, 2010.

[44] R. N. C. Miranda Júnior, M. F. Dolabela, M. N. da Silva, M. M. Póvoa, and J. G. S. Maia, "Antiplasmodial activity of the andiroba (*Carapa guianensis* Aubl., Meliaceae) oil and its limonoid-rich fraction," *Journal of Ethnopharmacology*, vol. 142, no. 3, pp. 679–683, 2012.

[45] P. Ngamwongsatit, P. P. Banada, W. Panbangred, and A. K. Bhunia, "WST-1-based cell cytotoxicity assay as a substitute for MTT-based assay for rapid detection of toxigenic *Bacillus* species using CHO cell line," *Journal of Microbiological Methods*, vol. 73, no. 3, pp. 211–215, 2008.

[46] C. A. Patwardhan, A. Fauq, L. B. Peterson, C. Miller, B. S. J. Blagg, and A. Chadli, "Gedunin inactivates the co-chaperone p23 protein causing cancer cell death by apoptosis," *Journal of Biological Chemistry*, vol. 288, no. 10, pp. 7313–7325, 2013.

[47] M. Llana-Ruiz-Cabello, S. Pichardo, S. Maisanaba et al., "*In vitro* toxicological evaluation of essential oils and their main compounds used in active food packaging: a review," *Food and Chemical Toxicology*, vol. 81, pp. 9–27, 2015.

Hindawi
Oxidative Medicine and Cellular Longevity
Volume 2018, Article ID 8487248, 11 pages
https://doi.org/10.1155/2018/8487248

Research Article

Evaluation of the Protective Effect of Olive Leaf Extract on Cisplatin-Induced Testicular Damage in Rats

Rafa S. Almeer[1] **and Ahmed E. Abdel Moneim**[2]

[1]*Department of Zoology, College of Science, King Saud University, Riyadh, Saudi Arabia*
[2]*Department of Zoology and Entomology, Faculty of Science, Helwan University, Cairo, Egypt*

Correspondence should be addressed to Rafa S. Almeer; rafaalmeer16@gmail.com

Received 8 December 2017; Revised 13 March 2018; Accepted 2 April 2018; Published 26 April 2018

Academic Editor: Jaideep Banerjee

In the present investigation, the effect of olive leaf extract (OLE) on testicular damage induced in rats by an intraperitoneal injection of cisplatin (*cis*-diamminedichloroplatinum (CDDP)) at a dose of 5 mg/kg was tested. Rats were randomly divided into 4 groups: control, CDDP, OLE, and OLE + CDDP. After 5 days of CDDP treatment, body and testicular weights, histopathological alteration, and serum male sex hormone levels were determined. In addition to the biochemical and immunohistochemical changes in the testes, CDDP caused the disorganization of germinal epithelium and apoptosis by inducing Bax and inhibiting Bcl-2 protein expression. Testicular weights, catalase, serum testosterone, testicular enzymatic (including glutathione peroxidase, glutathione reductase, and superoxide dismutase) along with nonenzymatic (glutathione) antioxidants, and levels of luteinizing and follicle-stimulating hormones were significantly reduced in addition to a significant increase in testicular malondialdehyde and nitrite/nitrate levels when compared with the control group. OLE treatment markedly attenuated both biochemical and histopathological changes. The reproductive beneficial effects of OLE were mediated, at least partly, by inducing the nuclear factor erythroid 2-related factor 2 (Nrf2)/heme oxygenase 1 (HO-1) pathway.

1. Introduction

Cisplatin, *cis*-diamminedichloroplatinum (CDDP), with the molecular formula *cis*-$[Pt(NH_3)_2Cl_2]$, is widely used as a standard antineoplastic drug for treating various cancers, including bladder, lung, neck, head, and testicular cancers [1, 2]. CDDP is a DNA-alkylating molecule that exerts its antitumor activity by inducing DNA crosslinks and DNA double-strand breaks; both these actions suppress DNA transcription and replication, leading to programmed cell death/apoptosis [3]. Furthermore, CDDP induces oxidative stress by producing reactive oxygen species (ROS) that promote cellular damage and necrosis through the lipid peroxidation of tissues, DNA lesions, and protein denaturation [4]. Although CDDP is a highly effective chemotherapeutic agent, its use is mainly limited by 2 factors: resistance development to CDDP and severe toxicity to normal tissues, especially nephrotoxicity, neurotoxicity, and testicular damage [5].

The mechanism underlying CDDP-induced testicular damage includes physiological and pathohistological disturbances resulting from oxidative stress and DNA damage [4]. Hence, several antioxidants have been examined against CDDP-induced testicular damage. For example, arjunolic acid, a natural triterpenoid saponin isolated from the bark of *Terminalia arjuna* tree, significantly protected against CDDP-induced oxidative stress and inflammation in testicular tissues of rats [2]. Resveratrol administration also ameliorated CDDP-induced epididymal oxidative stress along with testicular damage, inhibited steroidogenesis and spermatogenesis, and restored normal testicular structure [3].

Olive (*Olea europaea*, Oleaceae) plant is a phytoestrogen-containing longevous tree that is socioeconomically and culturally valuable to inhabitants of the Mediterranean region. The leaves of this plant contain many flavonoid and polyphenolic compounds that possess antioxidant, anti-inflammatory, anticancer, antidiabetic, gastroprotective, and wound healing properties [6, 7]. Recently, Al-Quraishy

et al. [7] reported that oleuropein is the most abundant molecule, representing 86.9% of total identified compounds in olive leaf extract (OLE) and exerts good antioxidant and anti-inflammatory activities. In this study, we examined the potential impact of OLE on CDDP-induced testicular impairment in rats. Additionally, we explored the involvement of the nuclear factor erythroid 2-related factor 2 (Nrf2)/heme oxygenase 1 (HO-1) pathway in the protective effects of OLE.

2. Materials and Methods

2.1. Preparation of OLE. Dried olive leaves were collected from a local market (El-Yamani Corner, Riyadh, Kingdom of Saudi Arabia). The leaves were identified and confirmed by a specialized taxonomist (Department of Botany, College of Science, King Saud University, Saudi Arabia). They were cleaned and homogenized into a fine powder (50 g), which was then extracted with 500 mL of 70% methanol at 4°C with stirring every 4 h for 48 h. After filtration, the methanol was evaporated to semidryness in a vacuum evaporator, and the extract was lyophilized. The obtained OLE was dissolved in distilled water at a final concentration of 300 mg/mL and stored at −20°C in the dark until use in this study.

2.2. Experimental Protocol. Adult healthy Wistar male rats were individually housed in polypropylene cages, acclimated for 5 days before initiating the experiments, in a temperature-controlled room (22 ± 2°C) under the normal light/dark cycle of the day with unrestricted access to water and standard rodent diet. All experiments were conducted according to the guidelines of the National Program for Science and Technology of Faculty of Science, King Saud University. The study protocol was approved (IRB number: K.S.U-2017-750/PI) by the Ethical Committee of King Saud University (Riyadh, Kingdom of Saudi Arabia).

The rats ($n = 7$/group) were randomized to receive saline, CDDP, OLE, or OLE + CDDP. Cisplatin was acquired from Sigma-Aldrich (St. Louis, MO, USA). CDDP was intraperitoneally administered at 5 mg/kg on day 1, and OLE was orally administered at 300 mg/kg daily for 5 consecutive days. This dose of CDDP was selected based on published reports [1, 5]. The dosing regimen for OLE was selected based on a report by Al-Quraishy et al. [7] showing that this is a safe dosing regimen.

The rats were then sacrificed by the intravenous administration of sodium pentobarbital (300 mg, Sigma-Aldrich) 24 h after the last OLE administration. Blood was collected, and the testes were removed and washed in ice-cold 0.01 M phosphate buffer (pH 7.4). After drying well with a filter paper, the left testis was weighed and homogenized to give a 10% (*w*/*v*) homogenate. Protein concentration of the samples was determined according to the method of Lowry et al. [8].

2.3. Changes in the Testis Index of Rats. The relative weight of the testis was calculated according to the weight of the left testis as follows: (weight of left testis/body weight) × 100.

2.4. Estimation of Serum Sex Hormones. After the collection of blood samples, the samples were centrifuged (5000 rpm for 10 min at 4°C) to separate the serum, and fresh serum was used immediately for the analysis of sex hormones. Serum testosterone and luteinizing hormone (LH) and follicle-stimulating hormone (FSH) of the rats were quantitatively measured by ELISA using specific kits (MyBioSource, CA, USA). The experiment was performed as per the manufacturer's instructions.

2.5. Oxidative Stress Markers. Malondialdehyde (MDA), the main end product formed due to lipid peroxidation in the tissues, serves as a marker for lipid peroxidation. To determine MDA level in the testes, the homogenate was reacted with thiobarbituric acid using the method of Ohkawa et al. [9]. Nitrite level in the homogenate was measured by the method of Green et al. [10]. Testicular reduced glutathione (GSH) was determined using Ellman's reagent as described previously [11].

2.6. Antioxidant Status. Testicular antioxidant enzyme activities were determined as markers for the assessment of oxidant/antioxidant balance in the testis. Superoxide dismutase (SOD) activity was measured by the nitroblue tetrazolium reduction assay [12]. Catalase (CAT) activity was also assayed by reacting the testis homogenate with H_2O_2. The consumption of H_2O_2 was quantified spectrophotometrically at 340 nm for 120 s at 30 s intervals [13]. Both SOD and CAT activities are presented as units/mg protein. Glutathione reductase (GSH-R) was determined by the method of Dringen and Gutterer [14], where 1 mL of a mixture containing 0.05 M phosphate buffer (pH 7.0), 1 mM EDTA, 10 mM oxidized glutathione (GSSG), and 0.1 mM NADPH was used. GSH-R activity was determined by change in NADPH concentration with time after adding the testis homogenate. Finally, glutathione peroxidase (GSH-Px) activity was assayed as described by Paglia and Valentine [15]. In this method, GSSG produced from GSH due to GSH-Px in the presence of NADPH and GSH-R was measured. GSH-Px activity was computed from the change in NADPH concentration with time using $\varepsilon = 6270\ M^{-1}{\cdot}cm^{-1}$.

2.7. Inflammation Markers. The extent of inflammation in testis samples was estimated by measuring IL-1β and TNF-α levels using commercial kits according to the manufacturer's instructions (Merck Millipore, Australia).

2.8. Quantitative Real-Time PCR. RNA in the testis samples was isolated utilizing the TRIzol reagent (Invitrogen, CA, USA), and 1 μg of the isolated RNA was used as a template together with random primers to synthesize cDNA utilizing Thermo Scientific Maxima First Strand cDNA Synthesis Kit for RT-qPCR. Each cDNA sample was run in triplicate for real-time PCR analysis. *GAPDH* (accession number: NM_017008.4; sense: 5′-GCATCTTCTTGTGCAGTGCC-3′; antisense: 5′-GATGGTGATGGGTTTCCCGT-3′) served as a housekeeping gene. Real-time PCR reactions were performed utilizing the Power SYBR Green Applied Biosystems 7500 System (Life Technologies, CA, USA) at 94°C for 4 min, followed

by 42 cycles at 94°C for 1 min, at 60°C for 1 min, and then held for the final phase at 72°C for 10 min. Gene expression analysis employed the $2^{-\Delta\Delta Ct}$ method according to Pfaffl [16]. The PCR primers for the following genes were synthesized by Invitrogen: *SOD2* (superoxide dismutase 2, mitochondrial; accession number: NM_001270850.1; sense: 5′-AGCTGCACCACAGCAAGCAC-3′; antisense: 5′-TCCACCACCCTTAGGGCTCA-3′), *CAT* (accession number: NM_012520.2; sense: 5′-TCCGGGATCTTTTTAACGCCATTG-3′; antisense: 5′-TCGAGCACGGTAGGGACAGTTCAC-3′), *GPx1* (accession number: NM_030826.4; sense: 5′-CAGTCCACCGTGTATGCCTT-3′; antisense: 5′-GTAAAGAGCGGGTGAGCCTT-3′), *Nrf2* (accession number: NM_031789.2; sense: 5′-GGTTGCCCACATTCCCAAAC-3′; antisense: 5′-GGCTGGGAATATCCAGGGC-3′), *HO-1* (accession number: NM_012580.2; sense: 5′-GCGAAACAAGCAGAACCCA-3′; antisense: 5′-GCTCAGGATGAGTACCTCCC-3′), *Bcl-2* (accession number: NM_016993.1; sense: 5′-CTGGTGGACAACATCGCTCTG-3′; antisense: 5′-GGTCTGCTGACCTCACTTGTG-3′), and *Bax* (accession number: NM_017059.2; sense: 5′-GGCGAATTGGCGATGAACTG-3′; antisense: 5′-ATGGTTCTGATCAGCTCGGG-3′).

2.9. Histological Examination. Testis tissues were immersed in neutral buffered formalin (4%), dehydrated in 70% ethanol, and embedded in paraffin. The tissue blocks were sectioned at 4-5 μm and stained with hematoxylin-eosin. The sections were visualized under a Nikon optical microscope (Eclipse E200-LED, Tokyo, Japan). Only seminiferous tubules with their epithelium cycle between stages 9 and 13 characterized by a single generation of spermatids and 2 generations of primary spermatocytes were observed.

2.10. Immunohistochemistry. The paraffin-embedded sections were mounted on charged slides, deparaffinized, and washed with phosphate-buffered saline. The antigen sites were unmasked by heating, and the endogenous peroxidase was inactivated by 3% H_2O_2. The sections were blocked with 10% (*w*/*v*) normal goat serum for 1 h and then incubated with polyclonal rabbit anti-proliferating cell nuclear antigen (PCNA), Bcl-2, and Bax antibodies (Santa Cruz Biotechnology, Santa Cruz, CA, USA) overnight at 4°C. Afterward, all samples were incubated with biotinylated secondary antibodies (1 : 1000) for 30 min at 37°C. The specific protein immunoreactivity was visualized by the chromogen 3,3′-diaminobenzidine tetrachloride method under 400x magnification (Nikon Eclipse E200-LED, Tokyo, Japan) with an Olympus camera.

2.11. Statistical Analysis. Results are expressed as the mean ± standard deviation. Statistical analyses were performed using one-way ANOVA with the SPSS (version 20.0) followed by Tukey's post hoc test. A p value of less than 0.05 was considered as a criterion for a statistically significant difference.

3. Results

3.1. Body and Testis Weights. Upon CDDP injection, no death was observed in the rats. However, the body and testicular weights were significantly ($p < 0.05$) lower than the control weights (Figure 1). However, relative testis weight that was obtained at the end of the experiment was lower (nonsignificant) than control. The rats treated with OLE + CDDP showed significantly ($p < 0.05$) higher body weights than CDDP-treated rats.

3.2. Serum Concentrations of Sex Hormones. Serum testosterone, LH, and FSH concentrations were significantly ($p < 0.05$) lower in the CDDP-treated rats than in the control rats (Figure 2). Serum sex hormone concentrations in the OLE + CDDP treatment group increased significantly ($p < 0.05$) by the end of the experiment and returned to normal values.

3.3. Oxidative Stress Parameters. There was a significant ($p < 0.05$) elevation in testicular MDA and nitrite/nitrate levels with concomitant depletion in GSH concentration in the CDDP group compared with the control group, indicating the oxidative action of CDDP on testicular tissues. Conversely, OLE treatment with CDDP prevented changes in MDA, nitrite/nitrate, and GSH levels, demonstrating the antioxidant activity of OLE (Figure 3).

Activities of SOD, CAT, GSH-Px, and GSH-R were significantly ($p < 0.05$) lower in the CDDP-treated rats than in the control rats (Figure 4). However, these activities were only partially attenuated in rats in the OLE + CDDP group compared with those in the control group but significantly ($p < 0.05$) higher than those in CDDP-injected rats. The gene expression of antioxidant enzymes (SOD, CAT, GSH-Px, and GSH-R) was lower in the testis tissues of rats in the CDDP group than in the control group. Interestingly, OLE treatment significantly ($p < 0.05$) increased the expression of all enzymes, except CAT, compared to control. OLE treatment significantly mitigated CDDP-induced oxidative stress in the testes (Figure 4).

3.4. Nrf2 and HO-1 Overexpression Protects against CDDP-Induced Testicular Oxidative Stress. mRNA expression levels of Nrf2 and HO-1 were significantly ($p < 0.05$) lower in the CDDP-treated group than in the control group (Figure 5). HO-1 mRNA expression was significantly higher in the OLE group than in the control group. Both Nrf2 and HO-1 mRNA levels were higher in the OLE + CDDP group than in the CDDP; moreover, HO-1 mRNA level was ($p < 0.05$) upregulated compared to the control group.

3.5. Inflammation Is Involved in CDDP-Induced Testicular Damage. To elucidate whether OLE is able to reduce CDDP-induced testicular inflammation, we determined inflammatory markers in the testis homogenates. As illustrated in Figure 6, CDDP administration significantly ($p < 0.05$) elevated IL-1β and TNF-α levels in the testis compared to control. However, treatment with OLE significantly ($p < 0.05$) inhibited the production of these inflammatory markers.

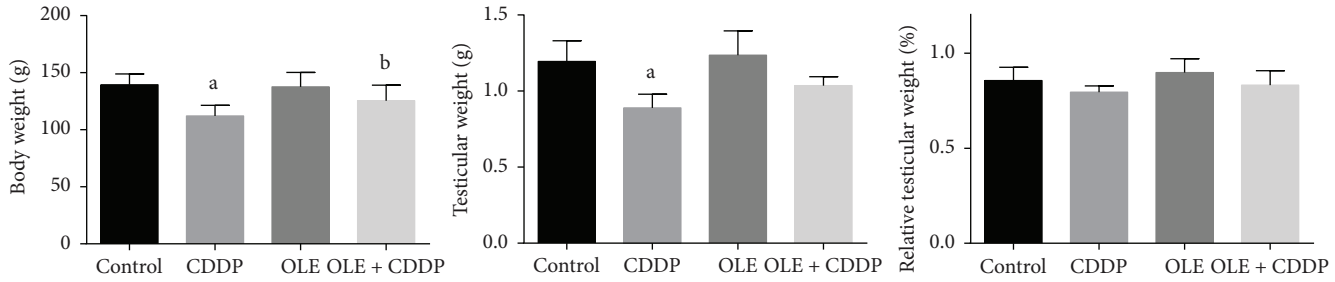

Figure 1: Potential effects of olive leaf extract (OLE) treatment on body weight, testis weight, and relative testicular weight in rats treated with cisplatin (CDDP). All data are expressed as the mean ± SEM ($n = 7$). [a]Significant change from the control group at $p < 0.05$; [b]significant change from the CDDP group at $p < 0.05$ using Tukey's post hoc test.

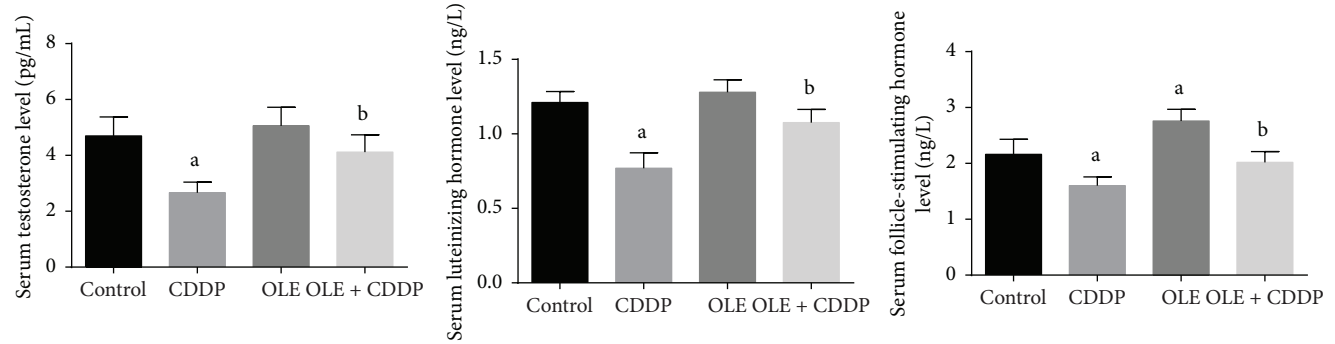

Figure 2: Effects of olive leaf extract (OLE) treatment on testosterone, luteinizing hormone, and follicle-stimulating hormone levels in the serum of rats treated with cisplatin (CDDP). All data are expressed as the mean ± SEM ($n = 7$). [a]Significant change from the control group at $p < 0.05$; [b]significant change from the CDDP group at $p < 0.05$ using Tukey's post hoc test.

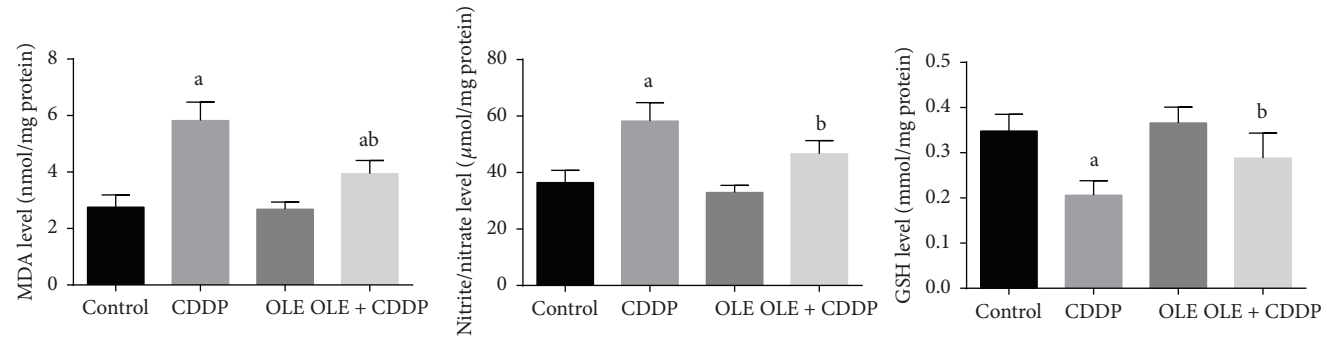

Figure 3: Effects of olive leaf extract (OLE) treatment on malondialdehyde (MDA), nitrite/nitrate, and glutathione (GSH) content in the testis of rats treated with cisplatin (CDDP). All data are expressed as the mean ± SEM ($n = 7$). [a]Significant change from the control group at $p < 0.05$; [b]significant change from the CDDP group at $p < 0.05$ using Tukey's post hoc test.

3.6. Histopathological Findings. Although CDDP injection caused testicular atrophy with a severe degeneration of the germinal epithelium in seminiferous tubules with many residual bodies and the disorganization and shedding of the germinal epithelium into the lumina (Figure 7(b)), OLE treatment ameliorated these changes in the seminiferous epithelium (Figure 7(d)). Control and OLE-treated rats appeared to have normal testicular structures with an orderly pattern of germinal epithelial and Sertoli cells (Figures 7(a) and 7(c)).

3.7. Bcl-2 Overexpression Protects against CDDP-Induced Testicular Apoptosis. In the present study, we also investigated whether the testicular protective effects of OLE are associated with its antiapoptotic activity; Bcl-2 and Bax mRNA expression levels in the testis were examined. Bcl-2 mRNA expression was significantly ($p < 0.05$) downregulated (Figure 8), whereas Bax mRNA expression was significantly ($p < 0.05$) upregulated in CDDP-treated rats. However, OLE treatment significantly downregulated Bax

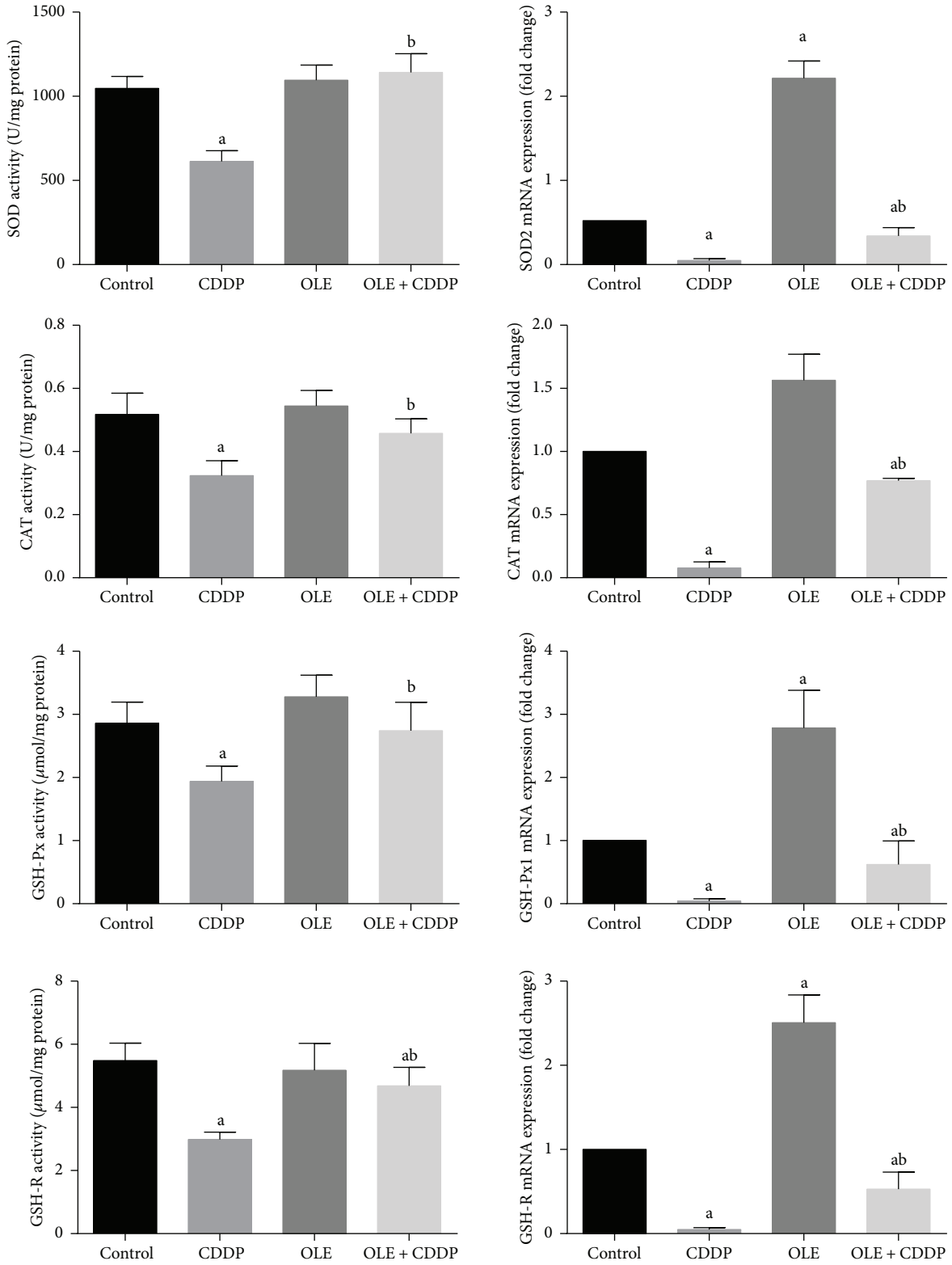

Figure 4: Effects of olive leaf extract (OLE) treatment on superoxide dismutase (SOD), catalase (CAT), glutathione peroxidase (GSH-Px), and glutathione reductase (GSH-R) activities and their corresponding mRNA expression in the testis of rats treated with cisplatin (CDDP). Data of antioxidant enzyme activities are expressed as the mean ± SEM ($n = 7$), whereas mRNA expression data are expressed as the mean ± SEM of triplicate assays, normalized to the *GAPDH* mRNA level, and shown as fold change (in log2 scale) relative to the control mRNA levels. [a]Significant change from the control group at $p < 0.05$; [b]significant change from the CDDP group at $p < 0.05$ using Tukey's post hoc test.

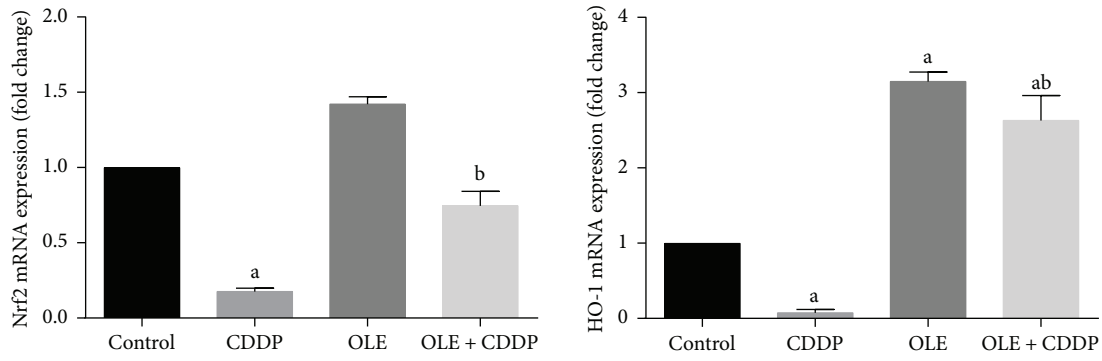

Figure 5: Effects of olive leaf extract (OLE) treatment on nuclear factor erythroid 2-related factor (Nrf2) and heme oxygenase-1 (HO-1) mRNA expression in the testis of rats treated with cisplatin (CDDP). Data of the mRNA expression are expressed as the mean ± SEM of triplicate assays, normalized to the *GAPDH* mRNA level, and shown as fold change (in log2 scale) relative to the control mRNA levels. [a]Significant change from the control group at $p < 0.05$; [b]significant change from the CDDP group at $p < 0.05$ using Tukey's post hoc test.

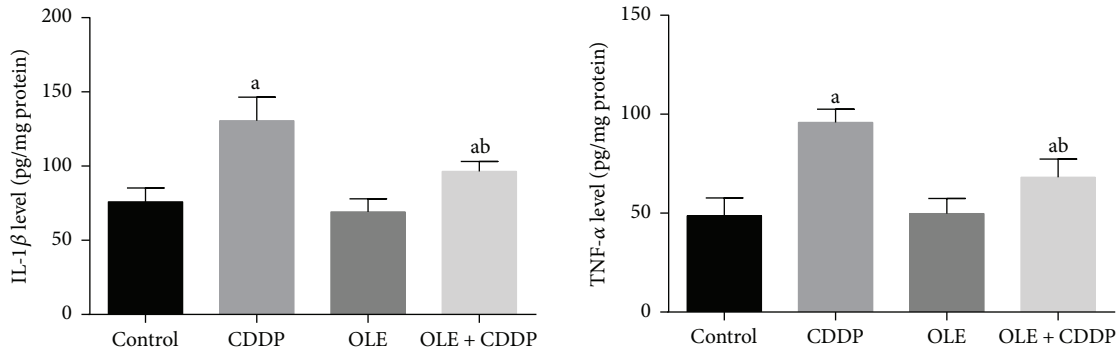

Figure 6: Effects of olive leaf extract (OLE) treatment on TNF-α and IL-1β levels in the testis of rats treated with cisplatin (CDDP). All data are expressed as the mean ± SEM ($n = 7$). [a]Significant change from the control group at $p < 0.05$; [b]significant change from the CDDP group at $p < 0.05$ using Tukey's post hoc test.

and upregulated Bcl-2 mRNA expression compared to CDDP treatment.

Consistent with RT-PCR results, immunohistochemistry showed that the number of Bcl-2-positive cells in the testicular tissues of CDDP-treated rats was markedly decreased (Figure 9(b)), whereas moderate to strong immunoreaction was observed for Bax (Figure 10(b)). The administration of OLE to rats injected with CDDP exhibited an increase in Bcl-2-positive spermatogenic cells (Figure 9(d)) with moderate immunoreaction for the proapoptotic protein, Bax (Figure 10(d)).

3.8. CDDP-Induced Downregulation in PCNA Expression. Immunohistochemical analysis revealed a lower expression of PCNA protein in the CDDP group than in the control group (Figure 11(b)). However, OLE treatment significantly increased the number of PCNA-positive cells (Figure 11(d)).

4. Discussion

Although CDDP is the most used antitumor agent in the chemotherapy of various cancers, its use is limited due to its adverse effects on the kidney, nervous system, and testis. Testicular dysfunction is the most reported consequence of CDDP toxicity because of the high proliferation rate of testicular cells. CDDP has been reported to cause sperm impairment, spermatogenic apoptosis, and abnormality in Leydig cells in experimental animals [17, 18]. CDDP administration to rats significantly decreases testis weight and disrupts male sexual hormone levels [4]. Furthermore, upon microscopic examination, notable degeneration, necrosis/apoptosis, and reduction in the circumference of seminiferous tubules and spermatogenic cell thickness have been reported after CDDP treatment. Testis weight depends on the mass of differentiated spermatogenic cells, and its structural and functional integrity requires the adequate biosynthesis of male sex hormones. Thus, a decline in testis weight in CDDP-treated rats reveals reduced spermatogenesis and steroidogenesis [17]. In the current study, CDDP administration significantly reduced male reproductive hormone levels. This may be attributed to reduced Leydig cells that produce gonadotropin, along with depressed mitochondrial side-chain cleavage and cytochrome P-450 activity [19]. CDDP also affects the function of Sertoli cells and decreases the expression of androgen-binding proteins [20]. Indeed, hormonal perturbation caused by cisplatin is mediated by its effects on the hypothalamic-pituitary-

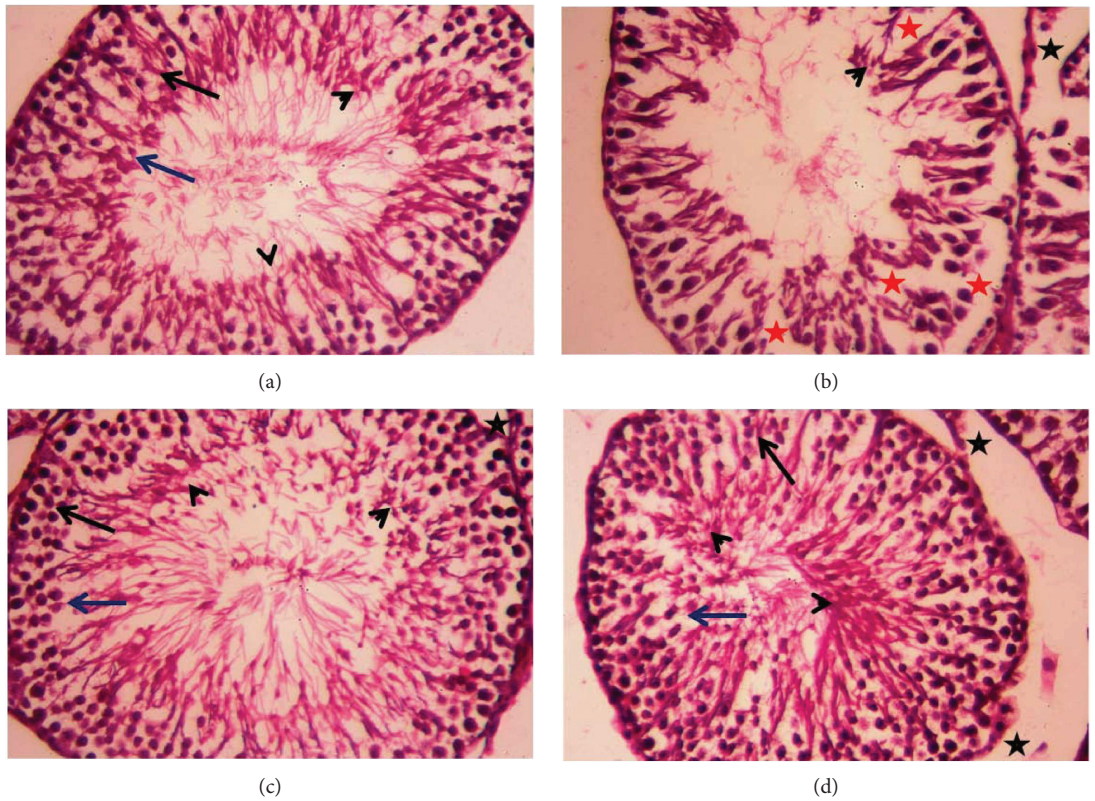

Figure 7: Light micrographs of testicular tissues of rats treated with olive leaf extract (OLE) and cisplatin (CDDP). (a) Photomicrograph of the testicular tissue of the control group showing healthy seminiferous tubules at all stages of spermatogenic cells (primary spermatocyte "black arrow" and spermatids "blue arrow") and the interstitial cells with Leydig cells (black star) filling the space between the seminiferous tubules. (b) Photomicrograph of the testicular tissue of rats treated with CDDP showing degenerative alterations (red star) in spermatogenic cells and the detachment of the spermatogenic epithelium. (c) Photomicrograph of the testicular tissue of rats treated with OLE alone showing a healthy histological structure. (d) Photomicrograph of the testicular tissue of rats treated with OLE and CDDP showing a recovery of spermatogenic epithelium in most seminiferous tubules. Sections were stained with hematoxylin and eosin (400x).

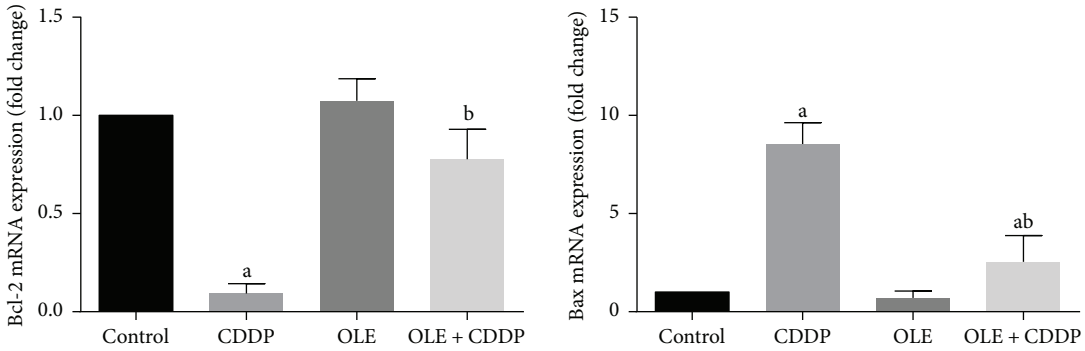

Figure 8: Effects of olive leaf extract (OLE) treatment on Bcl-2 and Bax mRNA expression in the testis of rats treated with cisplatin (CDDP). Data of the mRNA expression are expressed as the mean ± SEM of triplicate assays, normalized to the *GAPDH* mRNA level, and shown as the fold change (in log2 scale) relative to the control mRNA levels. [a]Significant change from the control group at $p < 0.05$; [b]significant change from the CDDP group at $p < 0.05$ using Tukey's post hoc test.

gonadal axis [21]. According to the obtained results, OLE treatment significantly increased testis weight and levels of male sex hormones (testosterone, LH, and FSH) compared to CDDP administration. Recent studies demonstrated that herbal extracts prevent CDDP-induced reproductive injury because of their antioxidant constituents [17, 22].

In the current study, CDDP-induced gonadal toxicity and tissue atrophy were due to increased ROS production and depleted enzymatic and nonenzymatic testicular antioxidant defense molecules. CDDP is known to disturb the oxidant/antioxidant balance in the testicular tissue [23]. In the current study, CDDP significantly elevated MDA and

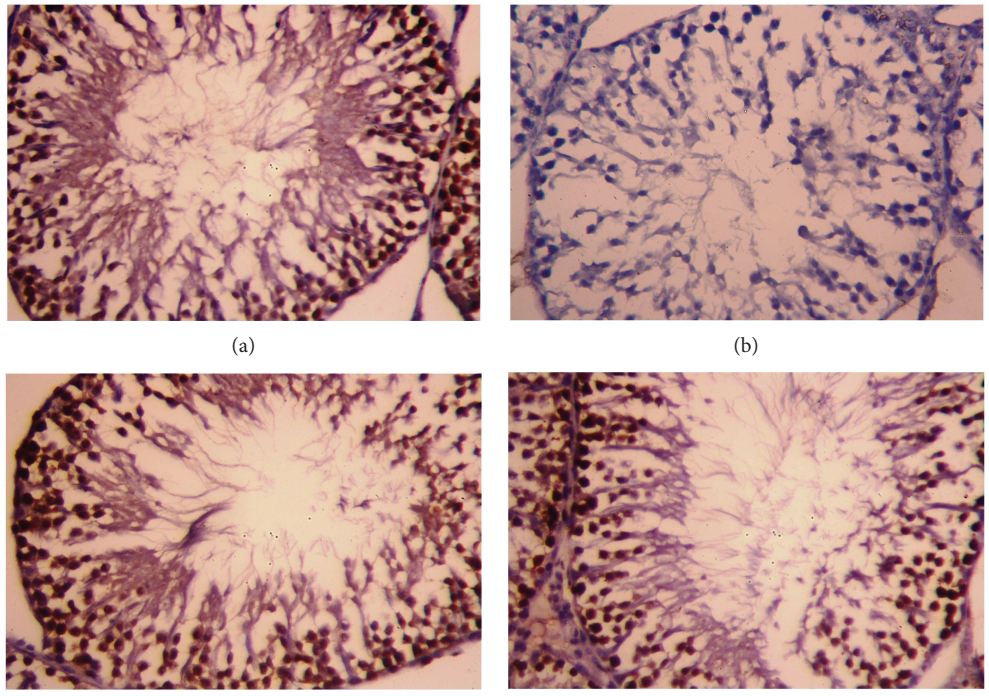

(a) (b)

(c) (d)

Figure 9: Testicular expression of Bcl-2 protein was detected using immunohistochemical staining in (a) control, (b) cisplatin (CDDP), (c) olive leaf extract (OLE), and (d) OLE + CDDP groups. In the control and OLE groups, Bcl-2-positive brown-stained cells were moderately to strongly immunostained. However, many testicular cells were weakly stained with brown color due to CDDP. In the OLE + CDDP group, the number of Bcl-2-positive cells was markedly increased. (400x).

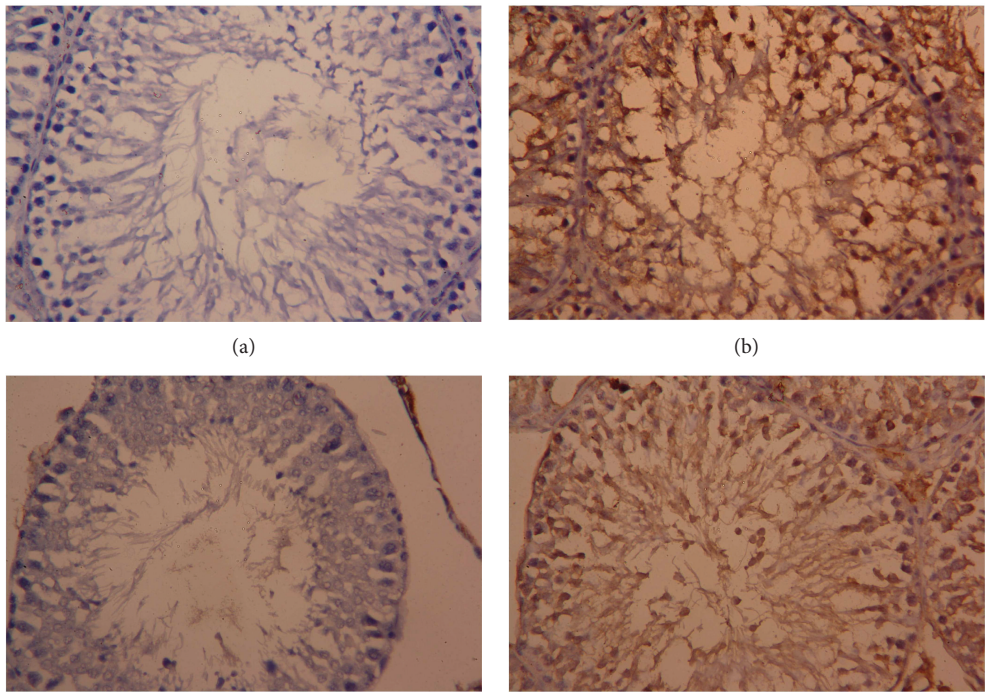

(a) (b)

(c) (d)

Figure 10: Testicular expression of Bax protein was detected using immunohistochemical staining in (a) control, (b) cisplatin (CDDP), (c) olive leaf extract (OLE), and (d) OLE + CDDP groups. In the control and OLE groups, Bax-positive brown-stained cells were sparse and weakly immunostained. However, many testicular cells exhibited apoptosis and were stained brown (Bax positive) due to CDDP. In the OLE + CDDP group, the number of Bax-positive cells was markedly increased. (400x).

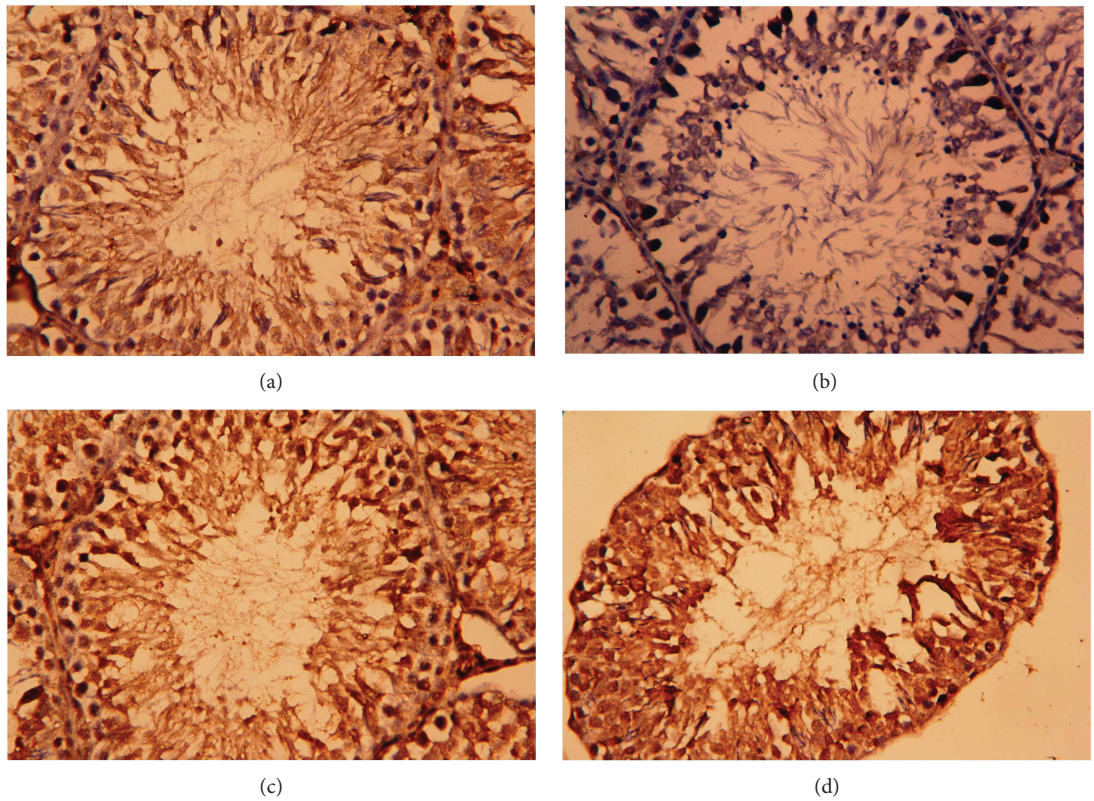

Figure 11: Testicular expression of proliferating cell nuclear antigen (PCNA) protein was detected using immunohistochemical staining in (a) control, (b) cisplatin (CDDP), (c) olive leaf extract (OLE), and (d) OLE + CDDP groups. In the control and OLE groups, PCNA-positive brown-stained cells were moderately to strongly immunostained. However, many testicular cells were weakly stained with brown color due to CDDP. In the OLE + CDDP group, the number of PCNA-positive cells was markedly increased. (400x).

nitrite/nitrate levels and depleted GSH content and activities of SOD, CAT, GSH-R, and GSH-Px in the testis, indicating that the enzymatic and nonenzymatic antioxidant molecules were inadequate for scavenging free radicals produced due to CDDP. MDA serves as a marker for oxidative stress due to the peroxidation of cellular polyunsaturated fatty acids. Both nitrate and nitrite levels have been used as indexes of nitric oxide generation and nitrosative stress [24]. GSH is the most abundant cellular sulphydryl molecule that interacts with oxidizing compounds, and a reduction in its cellular content has been considered as an indication of oxidative stress [25]. SOD presents the first preventive antioxidant enzyme that neutralizes singlet oxygen ($^1O_2$) and spontaneously dismutates superoxide radicals (O^-_2) to H_2O_2. The decomposition of H_2O_2 is successfully accomplished by CAT, thereby preventing lipid peroxidation. GSH-Px together with GSH catalyzes the reduction of H_2O_2 and lipid peroxides, whereas GSH-R promotes the NADPH-driven conversion of GSSG to GSH [26]. A depletion of these antioxidant enzymes and molecules could be associated with an overwhelming accumulation of H_2O_2 that suppresses testicular antioxidant defense systems. However, OLE treatment attenuated testicular oxidative stress and restored the antioxidant defense system in the testicular tissue, indicating that OLE prevents CDDP-induced oxidative stress and reproductive damage. The antioxidant activity of OLE has been well documented previously, and Bouaziz et al. attributed this effect to the phenolic constituents, oleuropein, luteolin, hydroxytyrosol, and orthodiphenols [27]. Servili et al. [28] mentioned that olive phenols modulate the cellular redox status by enzymes.

Nrf2 is a basic leucine zipper transcription factor that protects the cell against oxidative stress through the antioxidant response element-mediated induction of various phase 2 metabolism and antioxidant enzymes, including efflux transporters, heat shock proteins, and proteasomal degradation enzymes [29]. HO-1 is a stress-responsive enzyme that transforms heme into biliverdin and free iron along with carbon monoxide [30]. In cases of elevated oxidative stress due to exposure to a diverse array of toxic insults, HO-1 is induced as a beneficial response in cells. Moreover, the promotion of HO-1 drastically decreases CDDP-induced cytotoxicity by regulating autophagy [24]. The current investigation suggests that the beneficial effect of OLE is due to an induction of Nrf2 and HO-1, thereby maintaining the transcriptional activation status of detoxification enzymes and drug transporters and suppressing inflammation; these effects enhance the survival of germinal epithelial cells despite CDDP administration.

Inflammation is involved in CDDP-induced tissue toxicity [31]. CDDP triggers the NF-κB pathway, thereby promoting the expression of a series of inflammatory cytokines, including TNF-α and IL-1β [32]. OLE treatment prevented inflammatory cytokine production in CDDP-induced reproductive toxicity. The findings of the current investigation are

consistent with a previous study by Al-Quraishy et al. [7], in which OLE prevented gastric ulcer by reducing the production of TNF-α, IL-1β, and other proinflammatory cytokines. OLE treatment during chemotherapy can prevent TNF-α and IL-1β overexpression [33].

Germinal epithelium apoptosis has been documented as a possible mechanism for the testicular damage following CDDP treatment. In the current study, CDDP injection upregulated Bax and downregulated Bcl-2 expression in the testis. Bcl-2 is located in the outer membrane of the mitochondria, which promotes cell survival and counters the actions of the proapoptotic protein, Bax, thereby maintaining mitochondrial membrane integrity. However, Bax promotes mitochondrial permeabilization causing a discharge of both cytochrome C and ROS from the mitochondria into the cytoplasm under conditions of oxidative stress. In the cytoplasm, cytochrome C interacts with the apoptotic protease-activating factor 1 and forms an apoptosome, which finally activates caspase-3, the key regulator in the execution of apoptosis. This leads to DNA fragmentation, chromatin condensation, and biomembrane protein destruction [29, 34]. In the current study, an alternation in the mRNA levels of Bax and Bcl-2 was observed in rats injected with CDDP. The downregulation of Bcl-2 associates with a loss of survival signals, but the upregulation of Bax can be a marker of apoptosis via the intrinsic pathway. Our results were similar to the observation obtained by Cao et al. [35], which they found that CDDP-induced apoptosis in human nasopharyngeal carcinoma CNE-2 cells via upregulating Bax and downregulating Bcl-2. In the present study, OLE prevented apoptosis by upregulating Bcl-2 and downregulating Bax in the testicular tissue of CDDP-treated rats. Similarly, Al-Quraishy et al. [7] reported that the antiapoptotic activity of OLE is due to its antioxidant and anti-inflammatory properties.

5. Conclusions

In conclusion, CDDP injection in rats induces histopathological alterations and apoptosis in testicular tissues through oxidative stress induction as evidenced by elevated lipid peroxidation and nitrite/nitrate generation and depleted enzymatic and nonenzymatic antioxidants. However, OLE treatment protected against CDDP-induced testicular toxicity owing to its antioxidant, anti-inflammatory, and antiapoptotic properties. The present study also revealed that increased Nrf2 and HO-1 expression could be an effective strategy for preventing CDDP-induced testicular injury.

Conflicts of Interest

The authors declare that there is no conflict of interest regarding the publication of this paper.

Acknowledgments

This research project was supported by the Research Center of the Female Scientific and Medical Colleges, Deanship of Scientific Research, King Saud University.

References

[1] A. E. Abdel Moneim, "*Azadirachta indica* attenuates cisplatin-induced neurotoxicity in rats," *Indian Journal of Pharmacology*, vol. 46, no. 3, pp. 316–321, 2014.

[2] I. O. Sherif, A. Abdel-Aziz, and O. M. Sarhan, "Cisplatin-induced testicular toxicity in rats: the protective effect of arjunolic acid," *Journal of Biochemical and Molecular Toxicology*, vol. 28, no. 11, pp. 515–521, 2014.

[3] K. P. Reddy, P. Madhu, and P. S. Reddy, "Protective effects of resveratrol against cisplatin-induced testicular and epididymal toxicity in rats," *Food and Chemical Toxicology*, vol. 91, pp. 65–72, 2016.

[4] A. R. Fallahzadeh, Z. Rezaei, H. R. Rahimi et al., "Evaluation of the effect of pentoxifylline on cisplatin-induced testicular toxicity in rats," *Toxicology Research*, vol. 33, no. 3, pp. 255–263, 2017.

[5] A. E. Abdel Moneim, M. S. Othman, and A. M. Aref, "*Azadirachta indica* attenuates cisplatin-induced nephrotoxicity and oxidative stress," *BioMed Research International*, vol. 2014, Article ID 647131, 11 pages, 2014.

[6] M. Sarbishegi, E. Alhagh Charkhat Gorgich, and O. Khajavi, "Olive leaves extract improved sperm quality and antioxidant status in the testis of rat exposed to rotenone," *Nephro-Urology Monthly*, vol. 9, no. 3, article e47127, 2017.

[7] S. Al-Quraishy, M. S. Othman, M. A. Dkhil, and A. E. Abdel Moneim, "Olive (*Olea europaea*) leaf methanolic extract prevents HCl/ethanol-induced gastritis in rats by attenuating inflammation and augmenting antioxidant enzyme activities," *Biomedicine & Pharmacotherapy*, vol. 91, pp. 338–349, 2017.

[8] O. H. Lowry, N. J. Rosebrough, A. L. Farr, and R. J. Randall, "Protein measurement with the Folin phenol reagent," *Journal of Biological Chemistry*, vol. 193, no. 1, pp. 265–275, 1951.

[9] H. Ohkawa, N. Ohishi, and K. Yagi, "Assay for lipid peroxides in animal tissues by thiobarbituric acid reaction," *Analytical Biochemistry*, vol. 95, no. 2, pp. 351–358, 1979.

[10] L. C. Green, D. A. Wagner, J. Glogowski, P. L. Skipper, J. S. Wishnok, and S. R. Tannenbaum, "Analysis of nitrate, nitrite, and [^{15}N]nitrate in biological fluids," *Analytical Biochemistry*, vol. 126, no. 1, pp. 131–138, 1982.

[11] G. L. Ellman, "Tissue sulfhydryl groups," *Archives of Biochemistry and Biophysics*, vol. 82, no. 1, pp. 70–77, 1959.

[12] V. Peltola, M. Parvinen, and M. Ahotupa, "Superoxide dismutase activity along rat seminiferous epithelial wave: effects of ethane dimethanesulphonate and 3.0 Gy of X—irradiation," *Andrologia*, vol. 26, no. 2, pp. 79–85, 1994.

[13] B. RF Jr. and I. W. Sizer, "A spectrophotometric method for measuring the breakdown of hydrogen peroxide by catalase," *Journal of Biological Chemistry*, vol. 195, no. 1, pp. 133–140, 1952.

[14] R. Dringen and J. M. Gutterer, "[27] Glutathione reductase from bovine brain," *Methods in Enzymology*, vol. 348, pp. 281–288, 2002.

[15] D. E. Paglia and W. N. Valentine, "Studies on the quantitative and qualitative characterization of erythrocyte glutathione peroxidase," *The Journal of Laboratory and Clinical Medicine*, vol. 70, no. 1, pp. 158–169, 1967.

[16] M. W. Pfaffl, "A new mathematical model for relative quantification in real-time RT–PCR," *Nucleic Acids Research*, vol. 29, no. 9, article e45, pp. 45e–445, 2001.

[17] A. Amin, C. Abraham, A. A. Hamza et al., "A standardized extract of *Ginkgo biloba* neutralizes cisplatin-mediated reproductive toxicity in rats," *Journal of Biomedicine and Biotechnology*, vol. 2012, article 362049, 11 pages, 2012.

[18] A. Atessahin, E. Sahna, G. Turk et al., "Chemoprotective effect of melatonin against cisplatin-induced testicular toxicity in rats," *Journal of Pineal Research*, vol. 41, no. 1, pp. 21–27, 2006.

[19] M. D. Maines, P. M. Sluss, and M. Iscan, "*cis*-Platinum-mediated decrease in serum testosterone is associated with depression of luteinizing hormone receptors and cytochrome P-450scc in rat testis," *Endocrinology*, vol. 126, no. 5, pp. 2398–2406, 1990.

[20] G. A. Leblanc, P. W. Kantoff, S.-F. Ng, E. Frei III, and D. J. Waxman, "Hormonal perturbations in patients with testicular cancer treated with cisplatin," *Cancer*, vol. 69, no. 9, pp. 2306–2310, 1992.

[21] A. Aydiner, Y. Aytekin, and E. Topuz, "Effects of cisplatin on testicular tissue and the Leydig cell-pituitary axis," *Oncology*, vol. 54, no. 1, pp. 74–78, 1997.

[22] S. A. Adejuwon, O. M. Femi-Akinlosotu, and J. O. Omirinde, "Cisplatin-induced testicular dysfunction and its amelioration by *Launaea taraxacifolia* leaf extract," *Andrologia*, vol. 47, no. 5, pp. 553–559, 2015.

[23] H. Anand, M. M. Misro, S. B. Sharma, and S. Prakash, "Protective effects of *Eugenia jambolana* extract versus N-acetyl cysteine against cisplatin-induced damage in rat testis," *Andrologia*, vol. 47, no. 2, pp. 194–208, 2015.

[24] Y. I. Chirino and J. Pedraza-Chaverri, "Role of oxidative and nitrosative stress in cisplatin-induced nephrotoxicity," *Experimental and Toxicologic Pathology*, vol. 61, no. 3, pp. 223–242, 2009.

[25] A. A. Hamza, H. M. Elwy, and A. M. Badawi, "Fenugreek seed extract attenuates cisplatin-induced testicular damage in Wistar rats," *Andrologia*, vol. 48, no. 2, pp. 211–221, 2016.

[26] Y. M. Zhao, L. P. Gao, H. L. Zhang, J. X. Guo, and P. P. Guo, "Grape seed proanthocyanidin extract prevents DDP-induced testicular toxicity in rats," *Food & Function*, vol. 5, no. 3, pp. 605–611, 2014.

[27] M. Bouaziz, I. Fki, H. Jemai, M. Ayadi, and S. Sayadi, "Effect of storage on refined and husk olive oils composition: Stabilization by addition of natural antioxidants from Chemlali olive leaves," *Food Chemistry*, vol. 108, no. 1, pp. 253–262, 2008.

[28] M. Servili, B. Sordini, S. Esposto et al., "Biological activities of phenolic compounds of extra virgin olive oil," *Antioxidants*, vol. 3, no. 1, pp. 1–23, 2014.

[29] L. M. Aleksunes, M. J. Goedken, C. E. Rockwell, J. Thomale, J. E. Manautou, and C. D. Klaassen, "Transcriptional regulation of renal cytoprotective genes by Nrf2 and its potential use as a therapeutic target to mitigate cisplatin-induced nephrotoxicity," *Journal of Pharmacology and Experimental Therapeutics*, vol. 335, no. 1, pp. 2–12, 2010.

[30] U. Kilic, E. Kilic, Z. Tuzcu et al., "Melatonin suppresses cisplatin-induced nephrotoxicity via activation of Nrf-2/HO-1 pathway," *Nutrition & Metabolism*, vol. 10, no. 1, pp. 7–7, 2013.

[31] X. Zhu, X. Jiang, A. Li, Z. Zhao, and S. Li, "S-Allylmercaptocysteine attenuates cisplatin-induced nephrotoxicity through suppression of apoptosis, oxidative stress, and inflammation," *Nutrients*, vol. 9, no. 2, p. 166, 2017.

[32] A. H. Eid, N. F. Abdelkader, O. M. Abd El-Raouf, H. M. Fawzy, and E.-E.-D. S. El-Denshary, "Carvedilol alleviates testicular and spermatological damage induced by cisplatin in rats via modulation of oxidative stress and inflammation," *Archives of Pharmacal Research*, vol. 39, no. 12, pp. 1693–1702, 2016.

[33] K. M. Ahmed, "The effect of olive leaf extract in decreasing the expression of two pro-inflammatory cytokines in patients receiving chemotherapy for cancer. A randomized clinical trial," *The Saudi Dental Journal*, vol. 25, no. 4, pp. 141–147, 2013.

[34] A. A. Fouad, H. O. Qutub, A. E. A. Fouad, A. M. Audeh, and W. N. Al-Melhim, "Epigallocatechin-3-gallate counters cisplatin toxicity of rat testes," *Pharmaceutical Biology*, vol. 55, no. 1, pp. 1710–1714, 2016.

[35] L. H. Cao, H. T. Li, W. Q. Lin et al., "Morphine, a potential antagonist of cisplatin cytotoxicity, inhibits cisplatin-induced apoptosis and suppression of tumor growth in nasopharyngeal carcinoma xenografts," *Scientific Reports*, vol. 6, no. 1, article 18706, 2016.

Hindawi
Oxidative Medicine and Cellular Longevity
Volume 2018, Article ID 1346958, 15 pages
https://doi.org/10.1155/2018/1346958

Research Article

Resveratrol Inhibits ROS-Promoted Activation and Glycolysis of Pancreatic Stellate Cells via Suppression of miR-21

Bin Yan,[1] **Liang Cheng**,[1] **Zhengdong Jiang**,[1] **Ke Chen**,[1] **Cancan Zhou**,[1] **Liankang Sun**,[1] **Junyu Cao**,[1] **Weikun Qian**,[1] **Jie Li**,[1] **Tao Shan**,[2] **Jianjun Lei**,[1] **Qingyong Ma**,[1] **and Jiguang Ma**[3]

[1]*Department of Hepatobiliary Surgery, First Affiliated Hospital of Xi'an Jiaotong University, Xi'an 710061, China*
[2]*Department of General Surgery, Second Affiliated Hospital of Xi'an Jiaotong University, Xi'an 710004, China*
[3]*Department of Anesthesiology, First Affiliated Hospital of Xi'an Jiaotong University, Xi'an 710061, China*

Correspondence should be addressed to Qingyong Ma; qyma56@mail.xjtu.edu.cn and Jiguang Ma; jgma86@xjtu.edu.cn

Received 23 November 2017; Revised 28 January 2018; Accepted 15 February 2018; Published 26 April 2018

Academic Editor: Mithun Sinha

Activation of pancreatic stellate cells (PSCs) initiates pancreatic fibrosis in chronic pancreatitis and furnishes a niche that enhances the malignancy of pancreatic cancer cells (PCCs) in pancreatic ductal adenocarcinoma (PDAC). Resveratrol (RSV), a natural polyphenol, exhibits potent antioxidant and anticancer effects. However, whether and how RSV influences the biological properties of activated PSCs and the effects of these changes on tumor remain unknown. In the present study, we found that RSV impeded hydrogen peroxide-driven reactive oxygen species- (ROS-) induced activation, invasion, migration, and glycolysis of PSCs. In addition, miR-21 expression in activated PSCs was downregulated after RSV treatment, whereas the PTEN protein level increased. miR-21 silencing attenuated ROS-induced activation, invasion, migration, and glycolysis of PSCs, whereas the overexpression of miR-21 rescued the responses of PSCs treated with RSV. Moreover, RSV or N-acetyl-L-cysteine (NAC) administration or miR-21 knockdown in PSCs reduced the invasion and migration of PCCs in coculture, and the effects of RSV were partly reversed by miR-21 upregulation. Collectively, RSV inhibits PCC invasion and migration through suppression of ROS/miR-21-mediated activation and glycolysis in PSCs. Therefore, targeting miR-21-mediated glycolysis by RSV in tumor stroma may serve as a new strategy for clinical PDAC prevention or treatment.

1. Introduction

With a 7% five-year survival rate and more than 43,000 estimated deaths per year in the United States, pancreatic ductal adenocarcinoma (PDAC) is one of the most lethal cancers and causes serious public health issues and cancer burden [1]. PDAC is expected to become the second leading cancer diagnosis in the US by 2030, surpassing breast, prostate, and colorectal cancers [2]. Aggressive growth and metastasis, lack of early diagnosis, low rates of curative resection, and poor responses to radiation and chemotherapy characterize the dismal prognosis and treatment of PDAC. Modified combination regimens and novel agents are urgently needed, and the mechanisms of pharmacological therapies for PDAC remain to be further elucidated.

Current therapies focus chiefly on epithelial cancer cells, which contribute to the rapid proliferation and malignancy of the tumor. However, the tumor microenvironment, which is formed from a bulk of desmoplastic stroma comprising immune cells, inflammatory cells, endothelial cells, extracellular matrix, and, predominantly, pancreatic stellate cells (PSCs), plays an important role in tumor invasion and metastasis [3–5]. PSC activation, which is characterized by a decrease in vitamin A-containing lipid droplets and increased expression of α-SMA and collagen-I, is pivotal in the development of pancreatic fibrosis and the malignant behavior of PDAC [6, 7]. PSCs are activated by TGF-β as well as cellular reactive oxygen species (ROS), and cancer cells can secrete hydrogen peroxide (H_2O_2), which triggers oxidative stress in adjacent PSCs [8, 9]. The interaction between PSCs

(cancer-associated fibroblasts) and tumor cells is mediated by diverse secreted soluble factors such as extracellular matrix proteins, cytokines, and integrins [10], and disrupting this connection may provide novel approaches to cancer therapy.

According to the widely accepted Warburg effect, tumor cells favor a metabolic shift toward glycolysis even under aerobic conditions. Remarkably, cancer-associated fibroblasts, particularly PSCs, are commonly "corrupted" and tend to increase glycolysis and autophagy to function as factories to convert glucose to lactate and then transfer abundant metabolites to cancer cells. This two-compartment model is defined as the "reverse Warburg effect" [11, 12]. miR-21, a small single-stranded noncoding RNA classified as an oncogenic microRNA that can regulate gene expression, is aberrantly expressed in the majority of human cancers such as pancreatic cancer [13], cervical cancer [14], and breast cancer [15]. High expression of miR-21 in the tumor stroma promotes tumor progression [16–18]. Inhibition of miR-21 induces apoptosis and cell cycle arrest and enhances the chemotherapeutic sensitivity of tumors by positively modulating PTEN, PDCD4, and BCL-2 and other target genes [15, 19]. Glycolysis is also impeded by downregulation of miR-21 in bladder cancer cells [20]. However, whether aberrant miR-21 expression promotes glycolysis and the invasiveness of PSCs remains unclear.

Resveratrol (trans-3,4′,5-trihydroxystilbene, RSV), a natural polyphenol detected in grapes, berries, and peanuts, has a wide spectrum of pharmacological properties, such as antioxidant [21], anti-inflammation [22], and antitumor effects [23]. RSV inhibits tumor growth, invasion, and epithelial-mesenchymal transition [24] and enhances chemosensitivity [25]. RSV can impede tumor cell proliferation by reducing the phosphorylation of PI3K, Akt, ERK, FOXO3a (Ser253), and FOXO1 (Ser256). Furthermore, RSV induces apoptosis and cell cycle arrest in tumor cells by enhancing expression of p21, p27, Bim, and cleaved caspase-3 and by inhibiting the expression of cyclin D1 [26]. There are other typical genes and pathways regulated by RSV such as NF-κB, SIRT1-regulated pathway, and Wnt signaling pathway [27]. It is also worth noting that RSV may exert anti-inflammation and antitumor effects by targeting microRNAs [28]. Glycolysis of tumor cells is disrupted by RSV via the modulation of glucose consumption and glycolytic enzymes such as hexokinase 2 [29, 30]. However, whether and how RSV influences the invasion, migration, or glycolysis of activated PSCs and the effects of these changes on tumor biological properties remain unknown.

In this study, we demonstrated that RSV may inhibit ROS-promoted activation, invasion, and glycolysis of PSCs via suppression of miR-21. More importantly, impeded activation and lactate secretion of PSCs attenuated pancreatic cancer cell invasion and migration in coculture.

2. Materials and Methods

2.1. Reagents. Resveratrol (>99% pure), MTT (3-(4,5-dimethyl-2-thiazolyl)-2,5-diphenyl-2-H-tetrazolium bromide), and NAC (N-acetyl-L-cysteine) were purchased from Sigma-Aldrich (St. Louis, MO, USA). Analytical grade 30% H_2O_2 was obtained from Sinopharm Chemical Reagent Co., Ltd. (Shanghai, China). 2′-7′-Dichloro-dihydro-fluorescein diacetate (DCFH-DA) was obtained from Beyotime Institute of Biotechnology (Haimen, China).

2.2. Cell Lines and Cell Culture. Human PSCs were isolated from normal pancreatic tissue removed from patients undergoing liver transplantation. These tissues were obtained from the Department of Hepatobiliary Surgery at the First Affiliated Hospital of Xi'an Jiaotong University. PSCs were isolated and cultured according to methods described in previous study [31]. PSCs between passages 1 and 4 after isolation were used in our experiments. The human pancreatic cancer cell line Panc-1 was purchased from the Type Culture Collection of the Chinese Academy of Sciences (Shanghai, China) and cultured in Dulbecco's modified Eagle medium (DMEM) containing 10% FBS (HyClone, Logan, UT, USA), 100 μg/mL ampicillin, and 100 μg/mL streptomycin at 37°C with 5% CO_2 and 95% air. The study was conducted following the Declaration of Helsinki, and the protocol and consent forms were approved by the relevant ethical committee of the First Affiliated Hospital of Xi'an Jiaotong University, China.

2.3. Cell Viability Assay. PSCs were plated into 96-well plates at a density of 6000 cells/well and treated with various concentrations (0, 12.5, 25, 50, 100, and 200 μM) of RSV for 24, 48, and 72 h and different concentrations (0, 12.5, 25, 37.5, 50, 62.5, 75, 87.5, 100, 150, 200, and 300 μM) of H_2O_2 for 24 h. Cell viability was assessed by the MTT assay. Ten microliters of 5 mg/mL MTT was added to each well after removing the media and incubated at 37°C for 4 h. Then, 100 μL of DMSO was added to each well, and the optical density (OD) was measured at 490 nm on a multifunction microplate reader (POLARstar OPTIMA; BMG, Offenburg, Germany). The proliferation inhibition rate was calculated according to the following equation: proliferation inhibition rate = $(1 - \text{OD sample/OD control}) \times 100\%$.

2.4. Transfection of miRNA Inhibitor and Mimics. Loss-of-function and gain-of-function approaches were performed using the miR-21 inhibitor, negative inhibitor, miR-21 mimics, and negative mimics, which were purchased from GenePharma (Shanghai, China), and the sequences are provided in Supplementary Materials Table S1. The miRNA inhibitor and mimics were transfected into PSCs using Lipofectamine 2000 according to the manufacturer's instructions, and 8 h after transfection, the medium was replaced with fresh Dulbecco's modified Eagle medium: Nutrient Mixture F-12 (DMEM-F12) and cells were prepared for further experiments.

2.5. Western Blot Analysis. Western blot experiments have been described previously [25]. The antibodies used in this study against glucose transporter 1 (Glut1), hexokinase 2 (HK2), pyruvate kinase M2 (PKM2), and lactate dehydrogenase A (LDHA) were from Proteintech Group (Chicago, IL). The primary antibody against α-SMA was from Sigma-Aldrich. The primary antibody against PTEN was from Abcam (Cambridge, MA, UK).

2.6. Real-Time PCR. Total RNA was extracted using the Fastgen1000 RNA isolation system (Fastgen, Shanghai, China) according to the manufacturer's protocol. Total RNA was reverse-transcribed into cDNA using the PrimeScript RT reagent kit (TaKaRa, Dalian, China). A Bulge-Loop miRNA qRT-PCR primer set specific for miR-21 and U6 was obtained from RiboBio (Guangzhou, China). Real-time PCR was conducted using the CFX Manager 2.1 fluorescent quantitative PCR kit (Bio-Rad Laboratories, Hercules, CA, USA) under the following conditions: 10 min at 95°C and 40 cycles of 95°C for 2 sec, 60°C for 20 sec, and 70°C for 10 sec.

2.7. Immunofluorescence Staining. Cells were fixed in 4% formaldehyde diluted in phosphate-buffered saline (PBS) for 15 min, permeabilized with 0.3% Triton X-100, treated with blocking buffer (5% BSA in PBS), and then incubated overnight with the primary antibody at 4°C. The cells were then incubated with the Red-conjugated secondary antibody from Jackson ImmunoResearch Laboratories (West Grove, PA, USA) for 1 h at room temperature. Slides were mounted and examined using a Zeiss Instruments confocal microscope.

2.8. Measurement of Intracellular ROS. The level of intracellular ROS was measured using the ROS assay kit. In brief, after removing the media and washing the wells twice with PBS, 10 μM of DCFH-DA was added to each well. Then, the cells were incubated in the dark at 37°C for 30 min. After washing twice with PBS and trypsinization, the cells were collected and analyzed immediately by flow cytometry using a FACSCalibur (BD Biosciences, San Diego, CA, USA) instrument.

2.9. Measurement of Lactate Production. Medium from cultured cells was collected, and a lactic acid assay kit (Nanjing Jiancheng Bioengineering Institute, Nanjing, China) was used to determine lactate production. Lactate concentration was measured by an enzymatic assay, which generates a colorimetric (530 nm) product, proportional to the lactate present. All procedures were performed according to the manufacturer's instructions.

2.10. Oil Red O Staining. After washing with cold PBS, cells were fixed in 4% paraformaldehyde for 15 min at room temperature. Cells were washed again with PBS and stained using filtered Oil Red O solution (Sigma, St. Louis, MO, USA) at 60°C for 30 min. Subsequently, hematoxylin was used to stain the cell nuclei. Intracellular lipid accumulation was examined through a microscope (Nikon Instruments Inc.).

2.11. Modified Wound Healing Assay. Cell migratory ability was detected by a modified wound healing assay. To assess the migratory abilities of PSCs, PSCs (5.0×10^5 cells/2.5 mL) were seeded into 6-well plates using DME/F12. To evaluate the migratory abilities of pancreatic cancer cells (PCCs) under coculture, Panc-1 (1.0×10^6 cells/2.75 mL) and PSCs (5.0×10^5 cells/2 mL) were seeded into the basolateral and apical sides of Millicell hanging cell culture inserts (pore size 0.4 μm) in 6-well plates, respectively, using a mixed culture medium (DMEM : DME/F12 = 1 : 1). After the cells grew to 90–100% confluency, a sterile pipette tip was used to produce a wound line between the cells in the plate. Cellular debris was removed by washing with PBS, and the cells were then allowed to migrate for 24 h. Images were captured at time 0 and 24 h post wounding under a Nikon Diaphot TMD inverted microscope. The relative distance traveled by the leading edge from 0 to 24 h was assessed using the Photoshop software ($n = 3$).

2.12. Modified Transwell Matrigel Invasion Assay. Modified Transwell Matrigel invasion assays were performed in Transwell chambers. The 8.0 μm pore inserts were coated with 25 μL of Matrigel. To assess the invasive abilities of PSCs, PSC suspensions (5×10^4) were added to the upper chambers in DME/F12 containing 1% FBS. Simultaneously, 500 μL of DME/F12 containing 10% FBS was placed in the lower chambers. To evaluate the invasive abilities of PCCs under coculture, Panc-1 suspensions (5×10^4) were added to the upper chambers in DMEM/DME/F12 (1 : 1) containing 1% FBS. Simultaneously, 500 μL of DMEM/DME/F12 (1 : 1) containing 10% FBS was placed in the lower chambers with different groups of PSCs (5×10^4). The cells were allowed to migrate for 48 h at 37°C. The noninvading cells were removed from the upper surface by scraping with a wet cotton swab. After rinsing with PBS, the filter was fixed and stained with crystal violet. Invasion ability was determined by counting the stained cells on the bottom surface of each membrane in 10 random fields, and images were captured at ×200 magnification ($n = 3$).

2.13. Statistical Analysis. Each experiment was independently performed at least three times. Data are presented as means ± standard deviation. Differences were evaluated using Student's t-test, with $p < 0.05$ considered statistically significant.

3. Results

3.1. RSV Inhibits H_2O_2-Promoted PSC Activation, Migration, and Invasion. PSCs were treated with increasing doses of RSV (0, 12.5, 25, 50, 100, and 200 μM) for 24 h, 48 h, and 72 h and then subjected to MTT assays to evaluate cell viability (Figure 1(a)). RSV inhibited PSC proliferation in a dose- and time-dependent manner. Low concentrations of RSV (12.5, 25, and 50 μM) exhibited little cytotoxicity, but treatment for longer periods (48 and 72 h) and at high concentrations (100 and 200 μM) substantially decreased cell viability. Exogenous H_2O_2, a traditional cellular ROS inducer, exhibited growth-promoting action up to a concentration of approximately 50 μM (Figure 1(b)). Therefore, we chose 50 μM RSV and 50 μM H_2O_2 for subsequent experiments. Oil Red O staining showed that 50 μM H_2O_2 efficiently transferred the quiescent state of PSCs to the activated state with a considerable decline of lipid droplets (Figure S1). As shown in Figure S2, RSV at 50 μM hardly exerted function on the protein expression of α-SMA and glycolytic enzymes in quiescent PSCs, so we focused on the

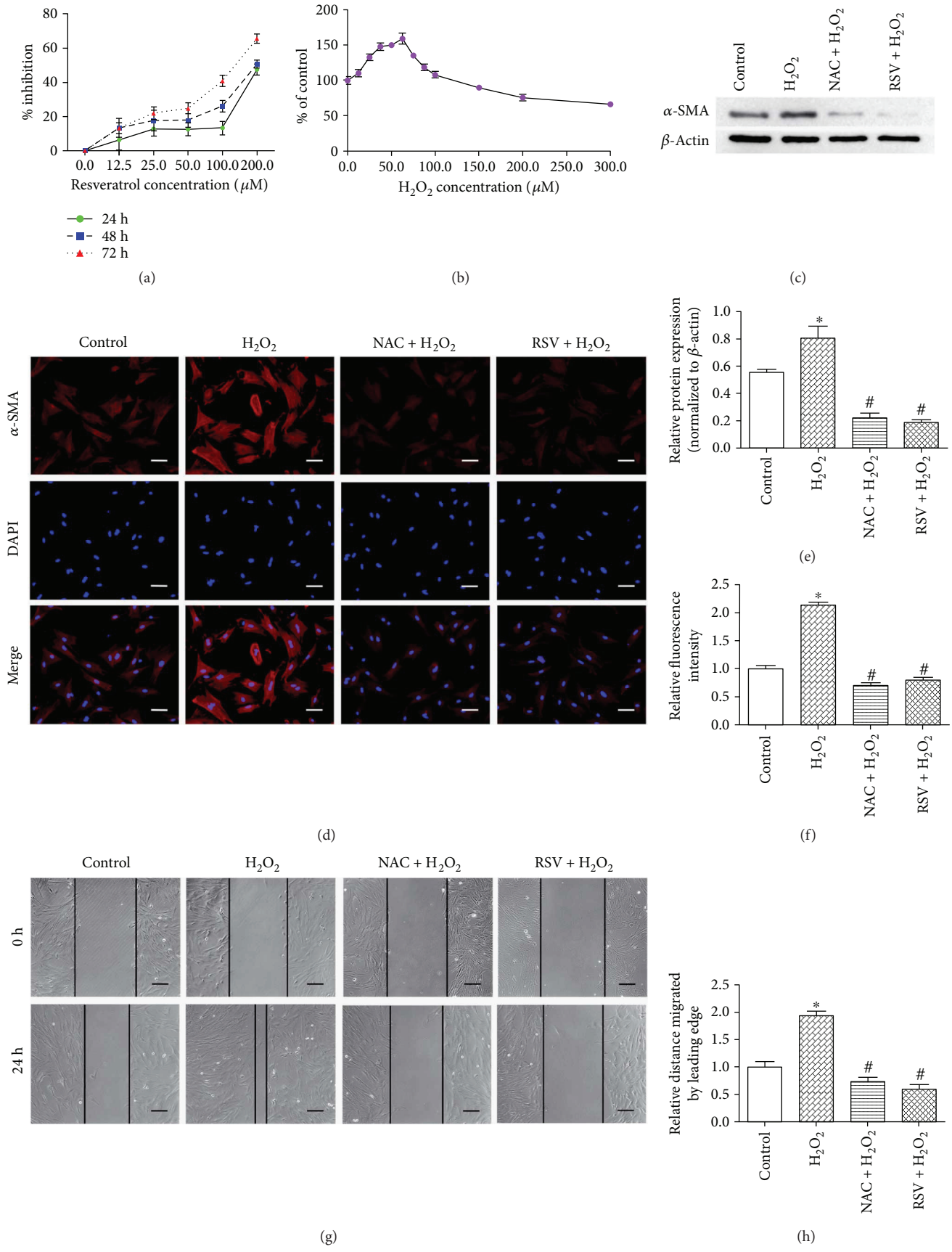

Figure 1: Continued.

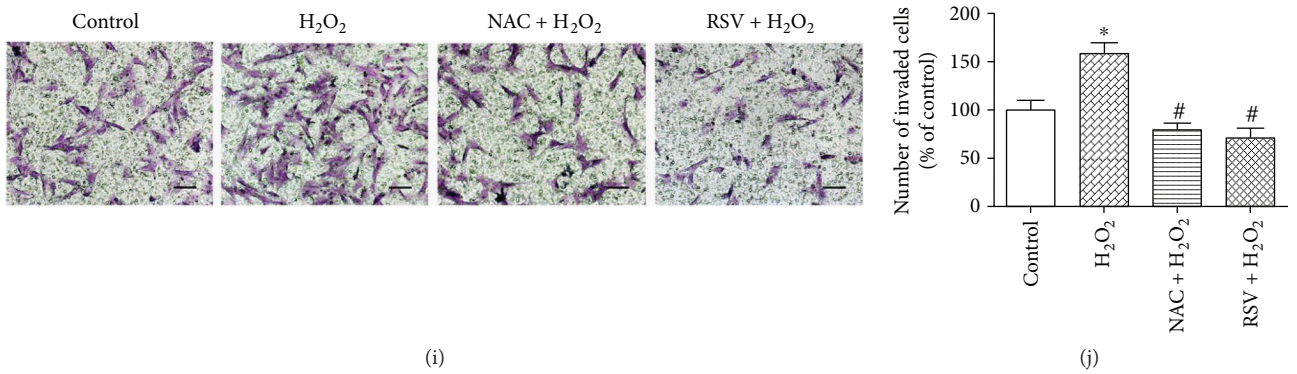

Figure 1: Resveratrol (RSV) inhibits hydrogen peroxide (H_2O_2)-promoted pancreatic stellate cell (PSC) activation, invasion, and migration. (a, b) PSCs were treated with increasing doses of RSV (0, 12.5, 25, 50, 100, and 200 μM) for 24 h, 48 h, and 72 h or H_2O_2 (0, 12.5, 25, 37.5, 50, 62.5, 75, 87.5, 100, 150, 200, and 300 μM) for 24 h and then subjected to MTT assays to evaluate cell viability. (c–f) PSCs were treated with 50 μM RSV or 10 mM N-acetyl-L-cysteine (NAC), a ROS scavenger, for 24 h prior to the 24 h incubation with 50 μM H_2O_2. Protein levels of α-SMA were analyzed using Western blot and immunofluorescence staining of α-SMA. The red signal represents α-SMA staining, and nuclear DNA staining by DAPI is shown in blue (magnification, ×200; scale bar: 50 μm). (g, h) PSCs were treated in groups as indicated, and migratory ability was determined by wound healing assays. The relative distance moved by the leading edge marked by black lines was measured 24 h after wounding with a sterile pipette tip (magnification, ×100; scale bar: 100 μm). (i, j) PSCs were treated in groups as indicated, and invasive ability was determined by Matrigel invasion assays (magnification, ×200; scale bar: 50 μm). Column: mean; bar: SD; $^*p < 0.05$ compared with the control group; $^\#p < 0.05$ compared with the H_2O_2 group.

potential functions of RSV when PSCs were activated. Next, to evaluate the effects of RSV and ROS on PSC activation, we treated PSCs with 50 μM RSV or 10 mM NAC (a ROS scavenger) for 24 h prior to the 24 h incubation with 50 μM H_2O_2. The protein expression of α-SMA was analyzed by Western blot (Figures 1(c) and 1(e)), and immunofluorescence staining of α-SMA was performed (Figures 1(d) and 1(f)). The expression of α-SMA was increased after H_2O_2 incubation, whereas NAC or RSV reversed this effect, indicating that H_2O_2-driven ROS-promoted PSC activation could be inhibited by RSV. To explore whether the migratory or invasive ability of PSCs is affected by ROS or RSV, wound healing assays and Matrigel invasion assays were performed. As shown in Figures 1(g) and 1(h), cell migratory ability was enhanced by H_2O_2 incubation, whereas NAC and RSV efficiently repressed this effect. The number of cells that invaded into the lower chamber was also increased by H_2O_2 stimulation but markedly decreased when the cells were pretreated with NAC or RSV (Figures 1(i) and 1(j)). Together, these results suggest that RSV potently inhibits H_2O_2-promoted PSC activation, invasion, and migration.

3.2. RSV Impedes H_2O_2-Driven ROS-Induced Glycolysis in PSCs. Intracellular ROS levels were detected using DCFH-DA probes. As shown in Figures 2(a) and 2(b), H_2O_2-induced ROS upregulation was downregulated by NAC and repressed by RSV. To assess whether ROS or RSV affects glycolysis in PSCs, several pivotal glycolytic enzymes were assayed. As shown in Figures 2(c) and 2(d), glucose transporter 1 (Glut1), hexokinase 2 (HK2), pyruvate kinase M2 (PKM2), and lactate dehydrogenase A (LDHA) levels were elevated under ROS treatment but decreased if cells were pretreated with NAC or RSV. Similarly, the enhancement by ROS of the production of lactate, an important metabolite transferred from PSCs to "fertilize" neighboring cancer cells [32], was hindered by pretreatment with NAC or RSV (Figure 2(e)). These results demonstrate that RSV can inhibit H_2O_2-driven ROS-induced glycolysis of PSCs.

3.3. RSV Reduces ROS-Induced miR-21 Expression and Increases PTEN Expression in PSCs. miR-21 levels are reportedly upregulated by H_2O_2 treatment in cardiac myocytes [33], and RSV inhibits miR-21 expression in several types of cancer cells [34–36]. However, whether the level of miR-21 and its target genes in PSCs are regulated by RSV or H_2O_2 is unknown. Our results showed that PSCs treated with H_2O_2 displayed higher levels of miR-21, and this enhancement was reversed by NAC or RSV (Figure 3(a)). Moreover, RSV and NAC restored PTEN expression, which was downregulated by H_2O_2 (Figures 3(b) and 3(c)).

3.4. miR-21 Downregulation Attenuates ROS-Induced Activation, Migration, Invasion, and Glycolysis of PSCs. To evaluate the role of miR-21 in the ROS-induced properties of PSCs, loss-of-function analysis using a specific antisense oligonucleotide targeting miR-21 was performed. The miR-21 inhibitor effectively repressed the expression of the microRNA (Figure 4(a)) and enhanced PTEN levels (Figure 4(b)). As shown in Figures 4(b)–4(f), miR-21 inhibited oxidative stress-promoted glycolysis, as represented by Glut1, HK2, PKM2, and LDHA expression and lactate production, and impeded PSC activation, as evidenced by the downregulated protein expression and fluorescence intensity of α-SMA. Our results further demonstrated that the enhancement of cell migratory ability by H_2O_2 incubation was reduced by miR-21 inhibitor pretreatment (Figures 4(g) and 4(h). The number of cells that invaded into the lower chamber also decreased with miR-21 pretreatment, despite H_2O_2 stimulation (Figures 4(i) and 4(j)). Taken together, these results

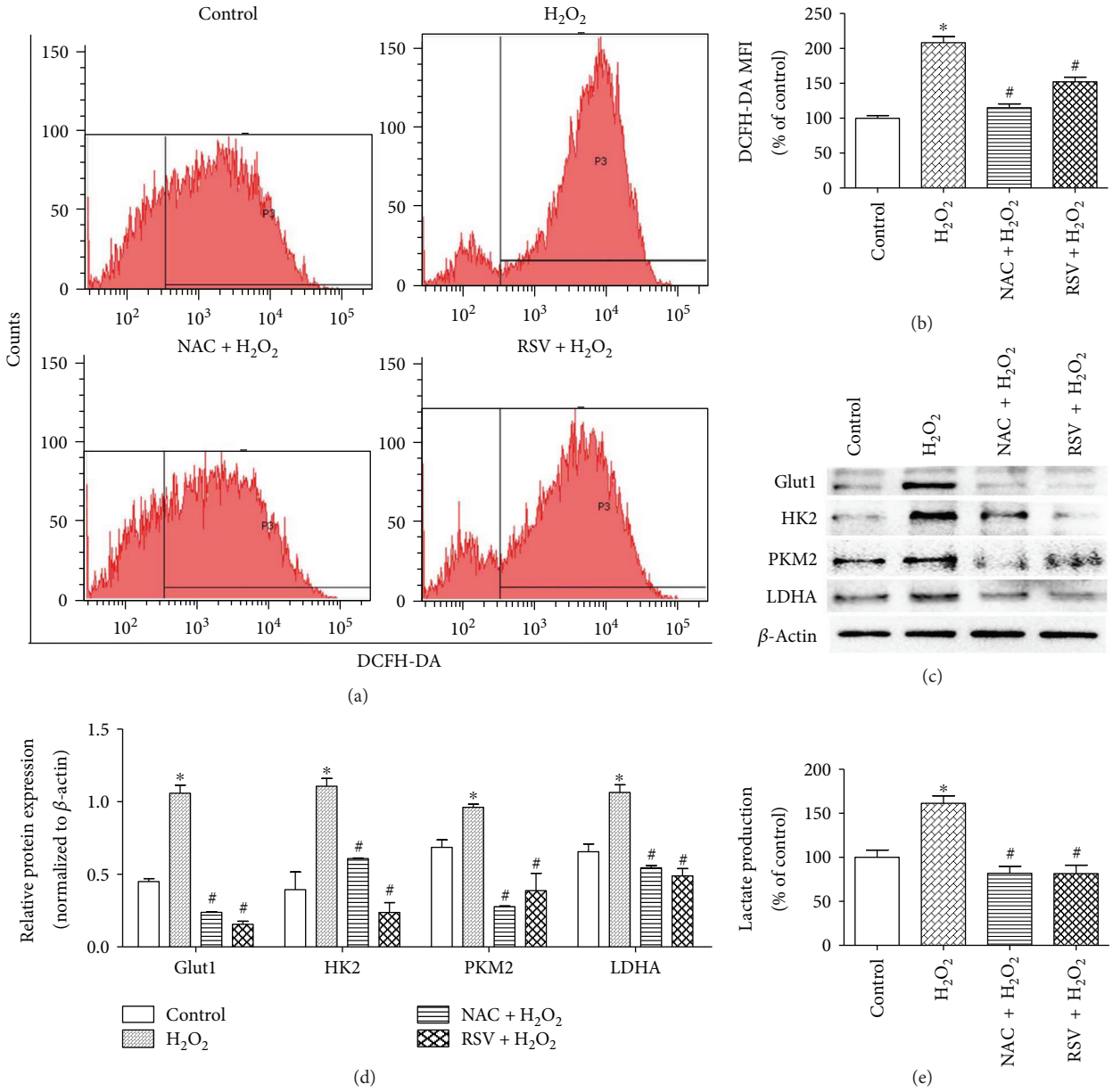

Figure 2: RSV impedes H_2O_2-driven ROS-induced glycolysis in PSCs. (a, b) PSCs were treated in groups as indicated, and ROS were detected using DCFH-DA probes. Representative flow cytometric images and the mean fluorescence intensity (MFI) of each group are shown. (c, d) PSCs from indicated groups were extracted to detect Glut1, HK2, PKM2, and LDHA levels by Western blot, (e) and the culture media (CM) were collected to measure lactate production. Lactate production was normalized by the concentration of protein in each group. Column: mean; bar: SD; $^*p < 0.05$ compared with the control group; $^\#p < 0.05$ compared with the H_2O_2 group.

suggest that miR-21 plays a vital part in the ROS-induced activation, migration, invasion, and glycolysis of PSCs.

3.5. miR-21 Is Essential for RSV-Induced Responses of PSCs. To further examine whether miR-21 mediates the RSV-induced responses of PSCs, PSCs were treated with RSV for 24 h and then transfected with miR-21 mimics or scrambled mimics (Figure 5(a)) prior to incubation with H_2O_2. As shown in Figures 5(b) and 5(d), the expression levels of the activation marker α-SMA and the glycolytic enzymes Glut1, HK2, PKM2, and LDHA were rescued by the miR-21 mimics after RSV treatment. Fluorescent images of α-SMA staining (Figures 5(e) and 5(f)) and measurement of lactate production (Figure 5(c)) further confirmed these findings. Additionally, miR-21 mimics partly reversed the suppression by RSV of the migratory abilities (Figures 5(g) and 5(h)) and invasive activities (Figures 5(i) and 5(j)) of PSCs. In conclusion, our results indicate that miR-21 plays a pivotal role in mediating the reduction of the activation, migration, invasion, and glycolysis of PSCs by RSV.

3.6. RSV Inhibits Pancreatic Cancer Cell Invasion and Migration through Suppression of ROS/miR-21 in PSCs. Many factors secreted from PSCs, such as cytokines, growth

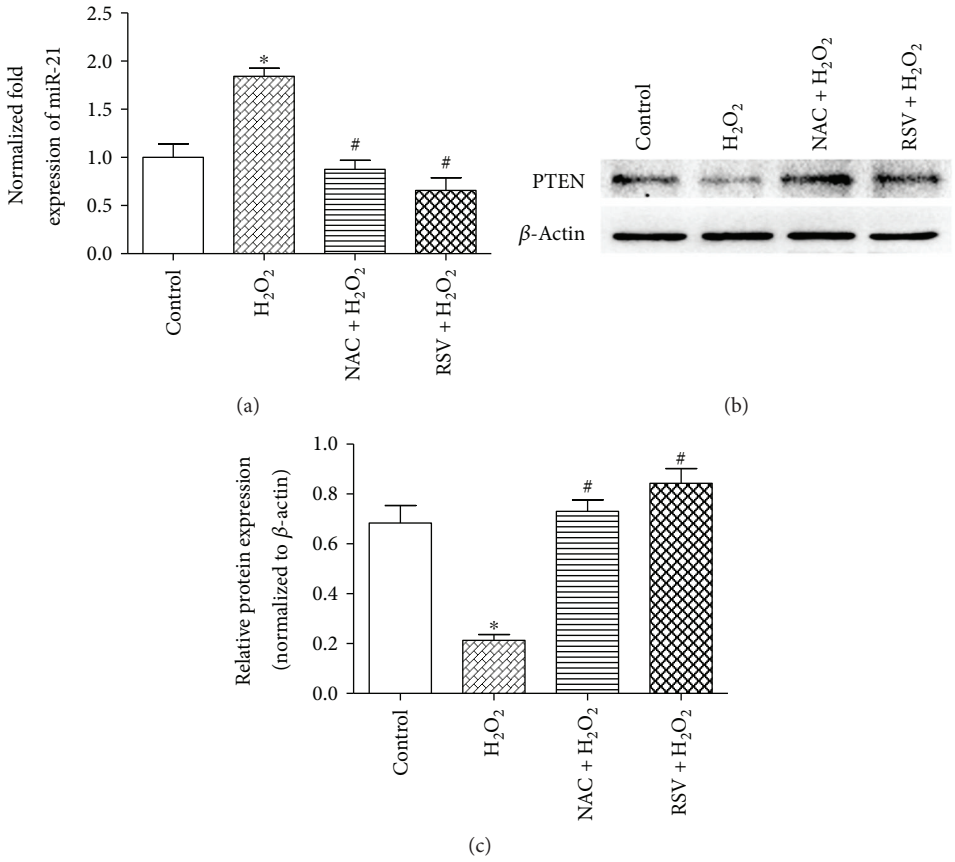

Figure 3: RSV reduces ROS-induced miR-21 expression and increases PTEN expression in PSCs. (a) PSCs were treated in groups as indicated, and qRT-PCR analysis was performed to detect miR-21 expression. (b, c) Cells were treated in groups as indicated, and the protein level of PTEN was detected by Western blot. Column: mean; bar: SD; $^{*}p < 0.05$ compared with the control group; $^{\#}p < 0.05$ compared with the H_2O_2 group.

factors, neurotrophic factors, and chemotactic factors, mediate the proinvasion and promigration abilities of PCCs [5]. Moreover, lactate secretion from PSCs is essential for accelerating tumor growth [12, 32]. Our results above demonstrated that lactate production is upregulated upon oxidative stress but reduced upon NAC treatment and that miR-21 mediates the reduction of lactate secretion by RSV. To assess whether RSV or NAC administration and miR-21 expression in PSCs modulate the invasion or migration of PCCs, we tested Panc-1 tumor cells cocultured with different groups of PSCs. Both the invasive ability (Figures 6(a) and 6(b)) and migratory activity (Figures 6(c) and 6(d)) of Panc-1 cells were enhanced when cocultured with PSCs, and these increases were mostly abrogated when PSCs were pretreated with NAC, RSV, or miR-21 inhibitor. Incubation of PSCs with miR-21 mimics partly reversed the repression of the invasive ability and migratory activity of cocultured Panc-1 cells by RSV treatment.

4. Discussion

Despite extensive study and the elucidation of the underlying mechanisms in greater detail, PDAC remains a notoriously malignant tumor characterized by the lack of an effective therapeutic strategy and poor life expectancy. Gemcitabine, the standard chemotherapeutic agent for PDAC, is indispensable but exhibits restricted effects [37], and combination chemotherapy regimens such as FOLFIRINOX, which is composed of folinic acid, 5-fluorouracil (5-FU), irinotecan, and oxaliplatin, show efficacy but also toxicity [38, 39]. Novel chemotherapeutic agents and therapeutic targets are urgently required.

RSV, a natural polyphenolic phytoalexin found in the skins of grapes and other berries and some Chinese medicines, has extensive functions in tumor therapies. RSV inhibits proliferation, induces apoptosis, represses invasion and migration, and impairs tumor-initiating stem-like properties via several signaling pathways, such as the sonic hedgehog pathway [40, 41] and the PI3K/Akt/NF-κB pathway [42]. Together with these classical regulatory pathways, RSV has been shown to regulate the expression of microRNAs (miRNAs) by which RSV may exert anti-inflammation and antitumor effects [28]. An in vivo study has explored the function of RSV on modulating the expression of miRNAs in an ischemia/reperfusion model of rat, and over 25 miRNAs were observed [43]. It was shown in breast cancer cells that miR-125b-5p, miR-200c-3p, miR-409-3p, miR-122-5p, and miR-542-3p were modulated by RSV, thereby affecting antiapoptotic and cell cycle proteins such as Bcl-2 and CDKs [44]. Using microarray approaches, 51

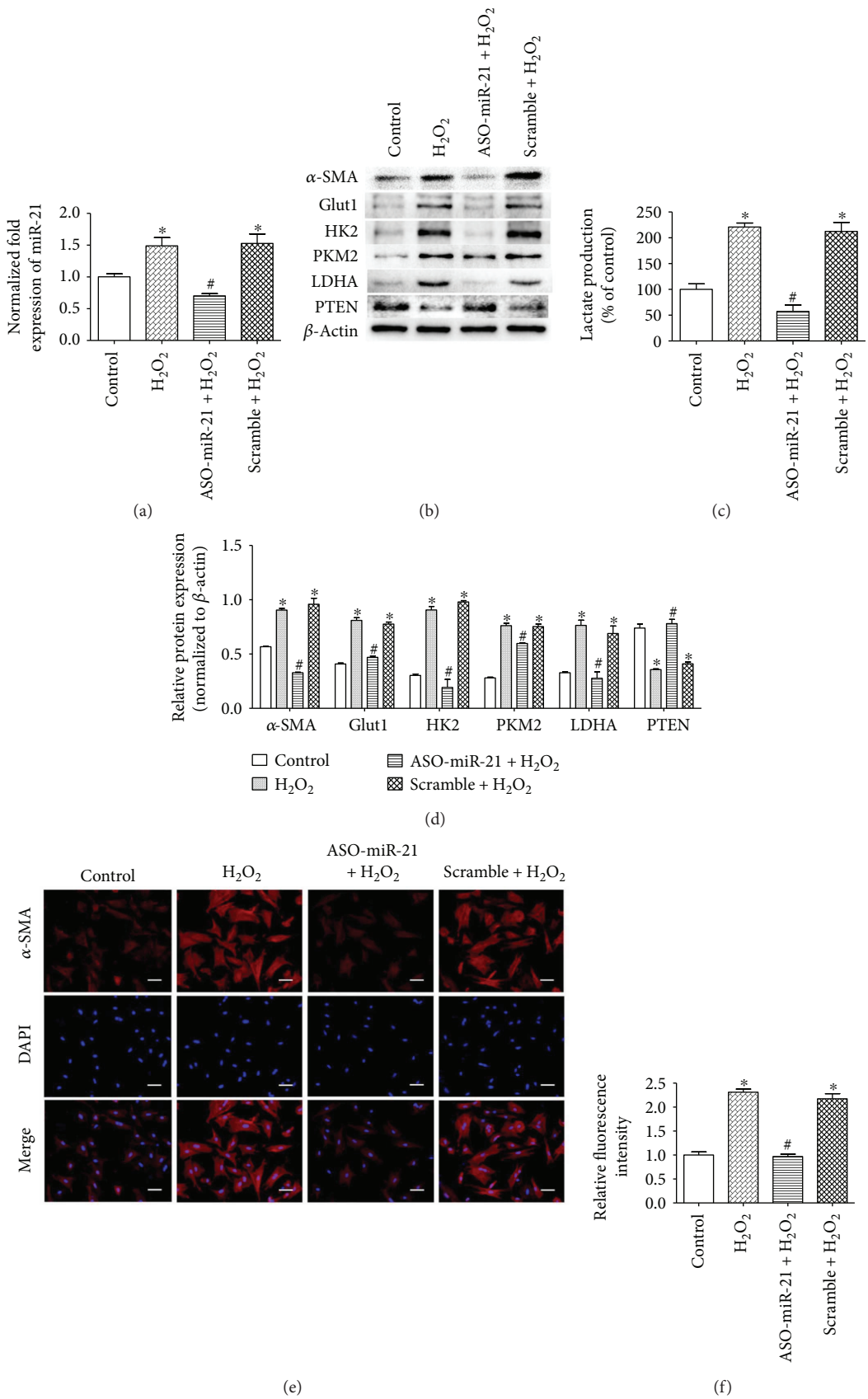

Figure 4: Continued.

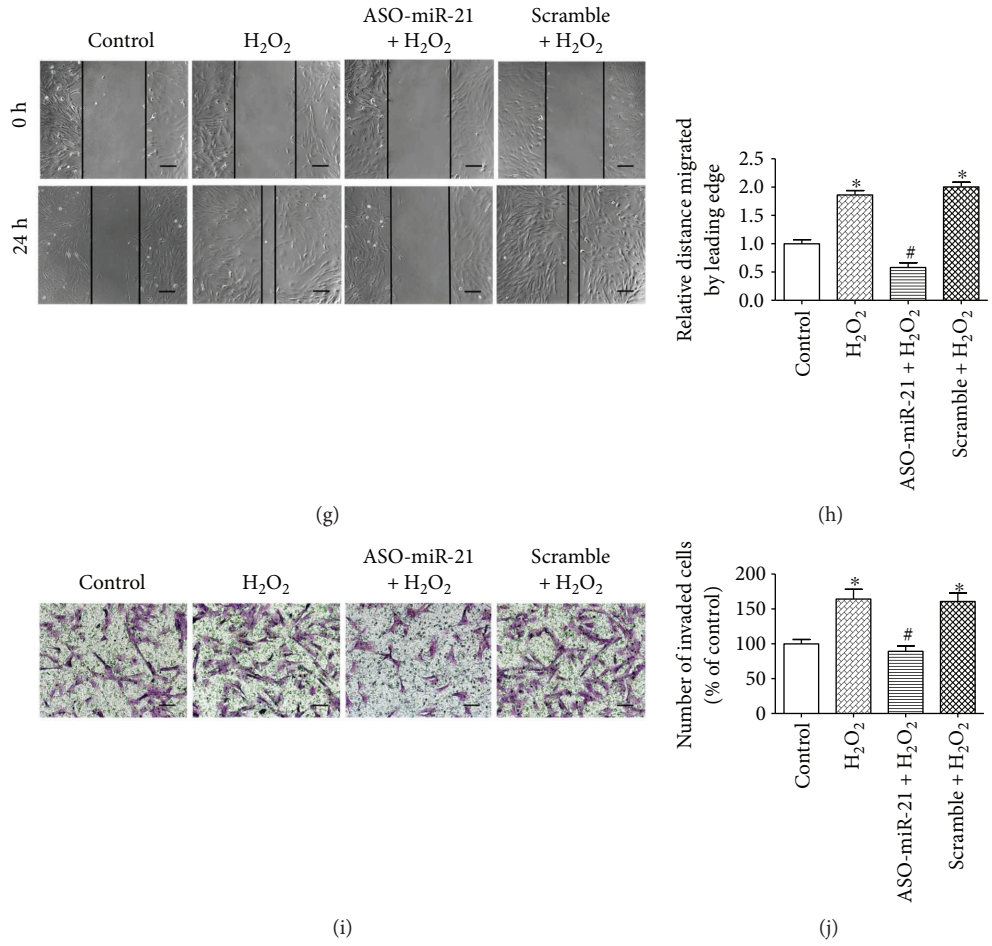

Figure 4: miR-21 downregulation attenuates the ROS-induced activation, migration, and glycolysis of PSCs. (a) PSCs were transfected with the miR-21 inhibitor (100 nM) or scrambled inhibitor (100 nM) 24 h prior to the 24 h incubation with 50 μM H_2O_2, and RT-PCR analysis was performed to detect miR-21 expression. (b–d) PSCs from indicated groups were extracted to detect α-SMA, Glut1, HK2, PKM2, LDHA, and PTEN levels by Western blot, and the CM were collected to measure lactate production. Lactate production was normalized by the concentration of protein in each group. (e, f) Immunofluorescence staining of α-SMA was performed. The red signal represents α-SMA staining, and nuclear DNA staining by DAPI is shown in blue (magnification, ×200; scale bar: 50 μm). (g, h) PSCs were treated in groups as indicated, and migratory ability was determined by wound healing assays. The relative distance moved by the leading edge marked by black lines was measured 24 h after wounding with a sterile pipette tip (magnification, ×100; scale bar: 100 μm). (i, j) PSCs were treated in groups as indicated, and invasive ability was determined by Matrigel invasion assays (magnification, ×200; scale bar: 50 μm). Column: mean; bar: SD; $^*p < 0.05$ compared with the control group; $^\#p < 0.05$ compared with the scramble + H_2O_2 group.

miRNAs were also found to be regulated by RSV in prostate cancer [45]. Combinations of single-agent treatments occasionally show synergetic effects. As food complements, RSV together with capsaicin enhances the effect of gemcitabine [23], and we previously demonstrated that RSV enhances the sensitivity of PCCs to gemcitabine [25]. However, the antitumor mechanisms of RSV warrant further study.

The desmoplastic stroma plays a critical role in tumor growth and aggression, and PSCs are at the center of this progression. When PSCs compose the cellular population of a PCC and PSC admixture at a high fraction of 0.66–0.83, a maximal effect on promoting cancer cell proliferation and invasion is observed [46]. PSCs are aberrantly activated and transformed into cancer-associated fibroblasts, which facilitate tumor malignancy. Cancer cells can secrete H_2O_2, which triggers oxidative stress in adjacent PSCs [8], and oxidative stress is essential in promoting PSC activation [47], and our data showed that H_2O_2-induced ROS promoted the expression of α-SMA in PSCs. However, Kikuta et al. [48] reported that the transformation of freshly isolated PSCs into the activated phenotype is not initiated by H_2O_2; this discrepancy may be explained by differences in culture conditions and the potential for further promotion of PSC activation by H_2O_2-induced ROS once the PSCs were preactivated in culture. All experiments were performed using human-derived PSCs in our research, and the cells were incubated with 50 μM H_2O_2 for 24 h, whereas Kikuta et al. treated freshly isolated rat PSCs with 100 μM H_2O_2 for 7 days. It was demonstrated that *trans*-resveratrol possesses potent antifibrotic activities as it suppressed TGF-beta-induced PSC activation [49]. Our results also showed that resveratrol served as a potential therapeutic agent in antifibrotic approaches by reducing ROS-induced PSC activation. In addition, RSV and NAC inhibited the migration and

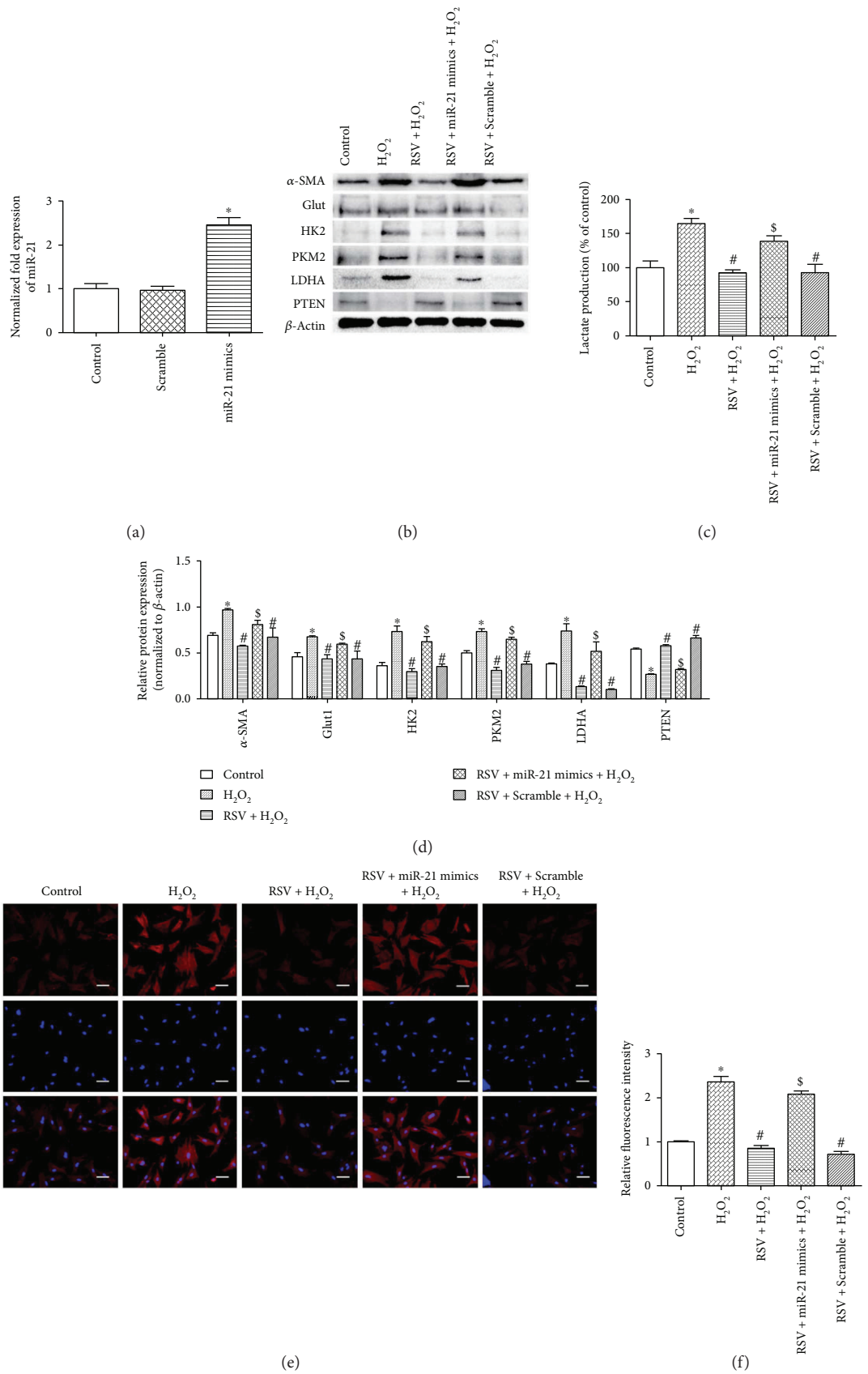

FIGURE 5: Continued.

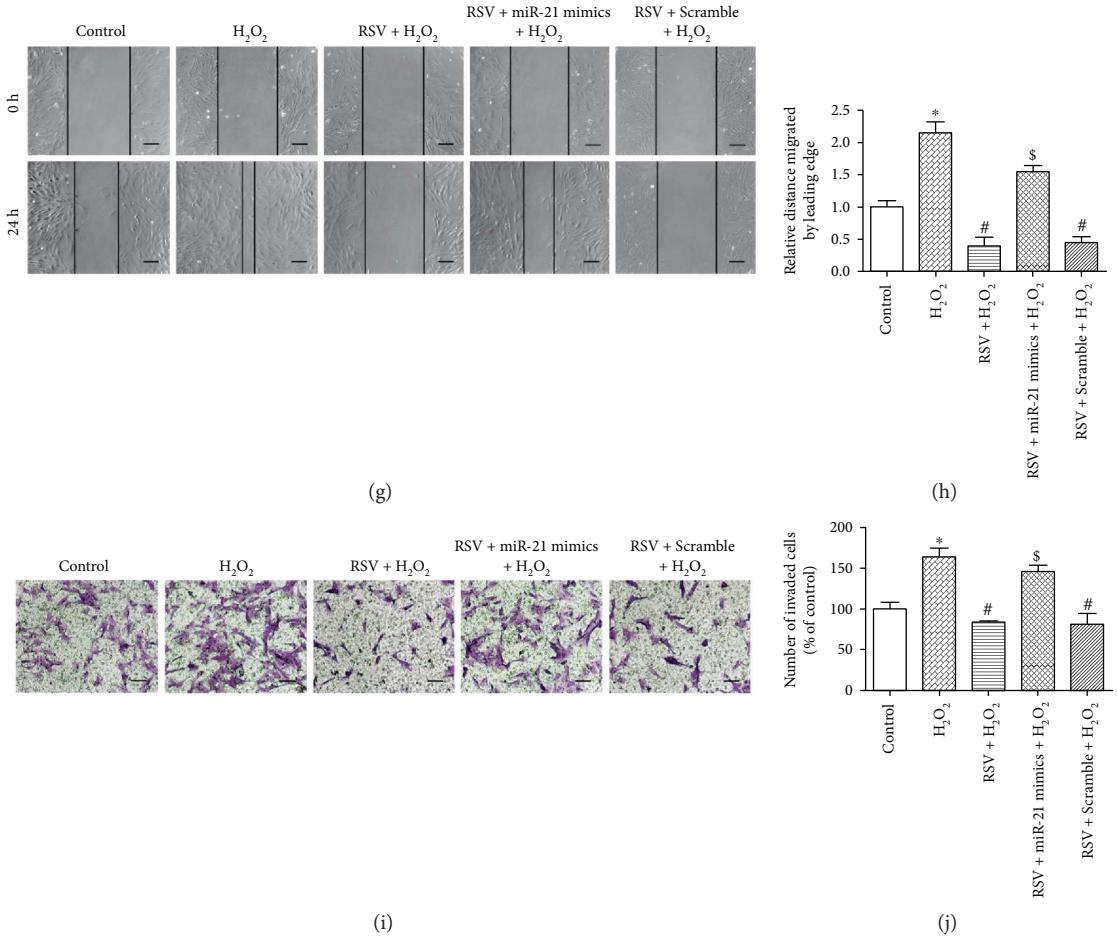

Figure 5: miR-21 is essential for RSV-mediated responses of PSCs. (a) PSCs were transfected with miR-21 mimics (20 nM) or scrambled mimics (20 nM) for 24 h, and RT-PCR analysis was performed to detect miR-21 expression. (b–d) PSCs were treated with 50 μM RSV for 24 h and then transfected with miR-21 mimics (20 nM) or scrambled mimics (20 nM) prior to the 24 h incubation with H_2O_2 at 50 μM. PSCs from indicated groups were extracted to detect α-SMA, Glut1, HK2, PKM2, LDHA, and PTEN levels by Western blot, and the CM were collected to measure lactate production. Lactate production was normalized by the concentration of protein in each group. (e, f) Immunofluorescence staining of α-SMA was performed. The red signal represents α-SMA staining, and nuclear DNA staining by DAPI is shown in blue (magnification, ×200; scale bar: 50 μm). (g, h) PSCs were treated in groups as indicated, and migratory ability was determined by wound healing assays. The relative distance moved by the leading edge marked by black lines was measured 24 h after wounding with a sterile pipette tip (magnification, ×100; scale bar: 100 μm). (i, j) PSCs were treated in groups as indicated, and invasive ability was determined by Matrigel invasion assays (magnification, ×200; scale bar: 50 μm). Column: mean; bar: SD; $^*p < 0.05$ compared with the control group; $^\#p < 0.05$ compared with the H_2O_2 group; $^\$p < 0.05$ compared with the RSV + scramble + H_2O_2 group.

invasion of PSCs, two important characteristics of activated PSCs [50].

Cancer-associated fibroblasts such as PSCs usually undergo oxidative stress, mitophagy, and autophagy and exhibit glycolytic phenotypes after "fertilization" by tumor cells. These fibroblasts then "back-nurture" adjacent cancer cells by secreting lactate, ketone, and other metabolites [11, 12, 51]. This two-compartment theory is a great addition to the traditional "Warburg effect" in tumor cells and may provide new insights on the crucial role of the microenvironment in tumor development. RSV can impede glycolysis in tumor cells [29, 30], but its effects on the glycolytic phenotypes of PSCs have not been explored. Here, we found that H_2O_2-induced ROS promoted glycolysis in PSCs, whereas RSV downregulated the expression of key glycolytic enzymes and, more importantly, decreased lactate production.

As an oncomiR or oncogenic miRNA, miR-21 is abundantly expressed in several types of cancers [13, 15, 34]. It has been reported that miR-21 and CCN2 compose a positive feedback loop during PSC activation [52] and that inhibition of miR-21 leads to decreased migration and invasion of PSCs [53]. In the present study, we found that miR-21 was necessary for ROS-promoted PSC activation, and miR-21 downregulation disrupted the ROS-promoted migration and invasion of PSCs. Previous studies have demonstrated that miR-21 is critical in maintaining the "Warburg effect" in bladder cancer cells [20] and can enhance glycolysis in nonsmall cell lung cancer cells, which might contribute to radiation resistance [54]. Accordingly, we explored the role

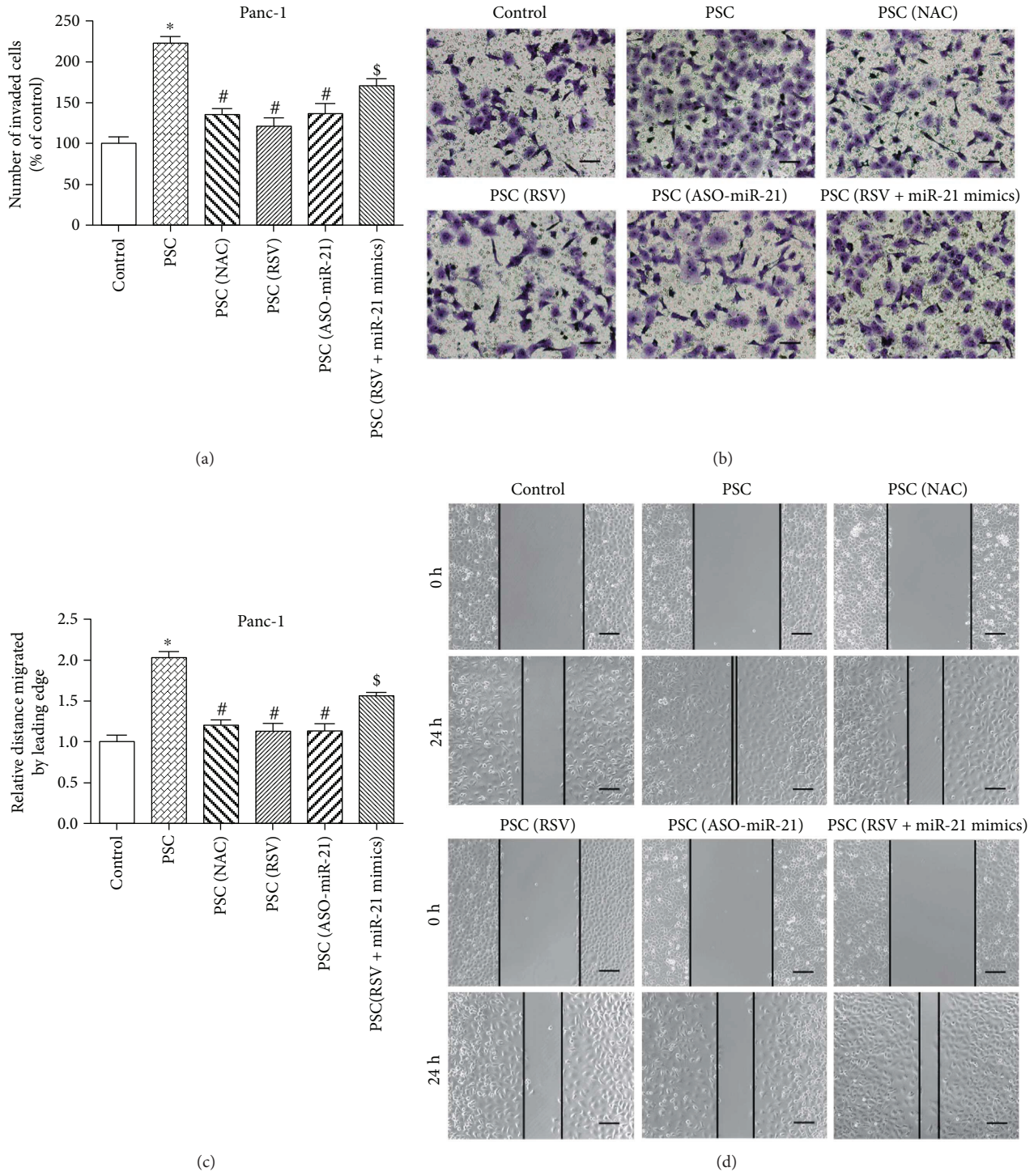

FIGURE 6: RSV inhibits pancreatic cancer cell invasion and migration through suppression of ROS/miR-21 in PSCs. (a, b) PSCs were treated in groups as indicated and then cocultured with Panc-1 cells using Transwell chambers. The invasive ability of Panc-1 cells was determined by Matrigel invasion assays (magnification, ×200; scale bar: 50 μm). (c, d) PSCs were treated in groups as indicated and then cocultured with Panc-1 cells using Millicell hanging cell culture inserts. The migratory ability of Panc-1 cells was determined by wound healing assays. The relative distance moved by the leading edge marked by black lines was measured 24 h after wounding with a sterile pipette tip (magnification, ×100; scale bar: 100 μm). Column: mean; bar: SD; $^{*}p < 0.05$ compared with the control group; $^{\#}p < 0.05$ compared with the PSC group; $^{\$}p < 0.05$ compared with the PSC (RSV) group.

of miR-21 in modulating glycolysis in PSCs and found that miR-21 was an essential component of the promotion of glycolysis in PSCs. Notably, AKT is regarded as a "Warburg kinase," and mTOR links tumor cell metabolism and oncogenic signaling [55, 56]. Accordingly, as a downstream pathway of miR-21, the PTEN/PI3K/AKT/mTOR pathway

might exhibit several functions modulating cell metabolism whose mechanisms require further elucidation. Recent studies have suggested that RSV might function by affecting miR-21 in prostate cancer cells [34] and PCCs [35]. This connection was further demonstrated in stroma, in which our results showed that miR-21 partly mediated the responses of PSCs to RSV.

Accumulating evidence indicates that the interaction between tumor and stroma is vital in tumor progression and that the underlying mechanisms are complicated. PCCs secrete stimulants such as TGF-β1, PDGF, SHH, and H_2O_2 to the microenvironment to activate the transformation of PSCs into cancer-associated myofibroblasts. In turn, activated PSCs release nutrients such as cytokines, chemokines, growth factors, and extracellular matrix proteins to further support tumor cells. It is worth noting that the lactate shuttle is an important part of the tumor-stroma interplay [32, 57]. Activated PSCs undergo metabolic reprogramming toward a Warburg phenotype, and lactate is secreted through monocarboxylate transporter 4 (MCT4) to be uploaded by monocarboxylate transporter 1 (MCT1) expressed in tumor cells for tumor growth. In the present study, we found that lactate production from PSCs was upregulated by oxidative stress but reduced by NAC treatment, and miR-21 mediated RSV-impeded lactate secretion. In line with the above findings on lactate, the enhanced invasive and migratory activities of Panc-1 cells cocultured with PSCs were mostly abrogated when PSCs were pretreated with a NAC, RSV, or miR-21 inhibitor, and RSV might function partly through modulating miR-21 in PSCs. However, direct regulation of lactate and other possible soluble factors, such as PDGF, SDF-1, and IL-6, was not assayed in the present study, which points the way for further investigation of detailed mechanisms involved in the tumor-stroma interaction.

5. Conclusions

To the best of our knowledge, this is the first study to report that miR-21 acts as a molecular switch in the "reverse Warburg effect" in PSCs and that RSV inhibits ROS-promoted PSC migration, invasion, and glycolysis, and miR-21 mediates these responses to RSV in PSCs. More importantly, RSV administration or suppression of ROS/miR-21 in PSCs ameliorates the invasive and migratory abilities of PCCs under coculture, suggesting that in addition to inhibiting the invasion and migration of PCCs directly, RSV may function by affecting PSCs or the interplay between tumor and stroma.

Conflicts of Interest

The authors declare no conflict of interest.

Authors' Contributions

Bin Yan conceived and performed the experiments, analyzed and interpreted the data, and wrote the manuscript. Liang Cheng, Zhengdong Jiang, and Ke Chen helped design the experiments and analyze the data. Cancan Zhou, Liankang Sun, Junyu Cao, Weikun Qian, Jie Li, Tao Shan, and Jianjun Lei contributed to the conception of the study and the revision of the article. Qingyong Ma and Jiguang Ma contributed to the conception of the study, the revision of the manuscript, and the final approval of the version to be published. All authors read and approved the final manuscript.

Acknowledgments

This study was supported by grants from the National Natural Science Foundation of China (nos. 81402583, 81502066, 81472248, 81672434, and 81702916).

Supplementary Materials

Table S1: the sequences of the miRNA inhibitor, mimics, and control. Figure S1: H_2O_2 transfers quiescent PSCs to the activated state determined by Oil Red O staining. Scale bar: 50 μm. Figure S2: RSV hardly affects protein expression of α-SMA and glycolytic enzymes in quiescent PSCs. (A) Quiescent PSCs were treated with 50 μM RSV for 24 h. Proteins from indicated groups were extracted to detect α-SMA, Glut1, HK2, PKM2, and LDHA levels by Western blot, and (B) the relative protein expression was normalized by β-actin in each group. *(Supplementary Materials)*

References

[1] R. L. Siegel, K. D. Miller, and A. Jemal, "Cancer statistics, 2017," *CA: A Cancer Journal for Clinicians*, vol. 67, no. 1, pp. 7–30, 2017.

[2] L. Rahib, B. D. Smith, R. Aizenberg, A. B. Rosenzweig, J. M. Fleshman, and L. M. Matrisian, "Projecting cancer incidence and deaths to 2030: the unexpected burden of thyroid, liver, and pancreas cancers in the United States," *Cancer Research*, vol. 74, no. 11, pp. 2913–2921, 2014.

[3] D. von Ahrens, T. D. Bhagat, D. Nagrath, A. Maitra, and A. Verma, "The role of stromal cancer-associated fibroblasts in pancreatic cancer," *Journal of Hematology & Oncology*, vol. 10, no. 1, p. 76, 2017.

[4] M. F. B. Nielsen, M. B. Mortensen, and S. Detlefsen, "Key players in pancreatic cancer-stroma interaction: cancer-associated fibroblasts, endothelial and inflammatory cells," *World Journal of Gastroenterology*, vol. 22, no. 9, pp. 2678–2700, 2016.

[5] J. Haqq, L. M. Howells, G. Garcea, M. S. Metcalfe, W. P. Steward, and A. R. Dennison, "Pancreatic stellate cells and pancreas cancer: current perspectives and future strategies," *European Journal of Cancer*, vol. 50, no. 15, pp. 2570–2582, 2014.

[6] A. Masamune, T. Watanabe, K. Kikuta, and T. Shimosegawa, "Roles of pancreatic stellate cells in pancreatic inflammation and fibrosis," *Clinical Gastroenterology and Hepatology*, vol. 7, Supplement 11, pp. S48–S54, 2009.

[7] D. Tang, D. Wang, Z. Yuan et al., "Persistent activation of pancreatic stellate cells creates a microenvironment favorable for the malignant behavior of pancreatic ductal adenocarcinoma," *International Journal of Cancer*, vol. 132, no. 5, pp. 993–1003, 2013.

[8] U. E. Martinez-Outschoorn, Z. Lin, C. Trimmer et al., "Cancer cells metabolically "fertilize" the tumor microenvironment with hydrogen peroxide, driving the Warburg effect: Implications for PET imaging of human tumors," *Cell Cycle*, vol. 10, no. 15, pp. 2504–2520, 2011.

[9] J. Lei, X. Huo, W. Duan et al., "α-Mangostin inhibits hypoxia-driven ROS-induced PSC activation and pancreatic cancer cell invasion," *Cancer Letters*, vol. 347, no. 1, pp. 129–138, 2014.

[10] A. Y. Wehr, E. E. Furth, V. Sangar, I. A. Blair, and K. H. Yu, "Analysis of the human pancreatic stellate cell secreted proteome," *Pancreas*, vol. 40, no. 4, pp. 557–566, 2011.

[11] S. Pavlides, D. Whitaker-Menezes, R. Castello-Cros et al., "The reverse Warburg effect: aerobic glycolysis in cancer associated fibroblasts and the tumor stroma," *Cell Cycle*, vol. 8, no. 23, pp. 3984–4001, 2009.

[12] S. Pavlides, I. Vera, R. Gandara et al., "Warburg meets autophagy: cancer-associated fibroblasts accelerate tumor growth and metastasis via oxidative stress, mitophagy, and aerobic glycolysis," *Antioxidants & Redox Signaling*, vol. 16, no. 11, pp. 1264–1284, 2012.

[13] F. Sicard, M. Gayral, H. Lulka, L. Buscail, and P. Cordelier, "Targeting miR-21 for the therapy of pancreatic cancer," *Molecular Therapy*, vol. 21, no. 5, pp. 986–994, 2013.

[14] O. Peralta-Zaragoza, J. Deas, A. Meneses-Acosta et al., "Relevance of miR-21 in regulation of tumor suppressor gene PTEN in human cervical cancer cells," *BMC Cancer*, vol. 16, no. 1, p. 215, 2016.

[15] N. S. Wickramasinghe, T. T. Manavalan, S. M. Dougherty, K. A. Riggs, Y. Li, and C. M. Klinge, "Estradiol downregulates miR-21 expression and increases miR-21 target gene expression in MCF-7 breast cancer cells," *Nucleic Acids Research*, vol. 37, no. 8, pp. 2584–2595, 2009.

[16] B. E. Kadera, L. Li, P. A. Toste et al., "MicroRNA-21 in pancreatic ductal adenocarcinoma tumor-associated fibroblasts promotes metastasis," *PLoS One*, vol. 8, no. 8, article e71978, 2013.

[17] H. Uozaki, S. Morita, A. Kumagai et al., "Stromal miR-21 is more important than miR-21 of tumour cells for the progression of gastric cancer," *Histopathology*, vol. 65, no. 6, pp. 775–783, 2014.

[18] A. K. Mitra, M. Zillhardt, Y. Hua et al., "MicroRNAs reprogram normal fibroblasts into cancer-associated fibroblasts in ovarian cancer," *Cancer Discovery*, vol. 2, no. 12, pp. 1100–1108, 2012.

[19] J. K. Park, E. J. Lee, C. Esau, and T. D. Schmittgen, "Antisense inhibition of microRNA-21 or -221 arrests cell cycle, induces apoptosis, and sensitizes the effects of gemcitabine in pancreatic adenocarcinoma," *Pancreas*, vol. 38, no. 7, pp. e190–e199, 2009.

[20] X. Yang, Y. Cheng, P. Li et al., "A lentiviral sponge for miRNA-21 diminishes aerobic glycolysis in bladder cancer T24 cells via the PTEN/PI3K/AKT/mTOR axis," *Tumour Biology*, vol. 36, no. 1, pp. 383–391, 2015.

[21] J. Jagdeo, L. Adams, H. Lev-Tov, J. Sieminska, J. Michl, and N. Brody, "Dose-dependent antioxidant function of resveratrol demonstrated via modulation of reactive oxygen species in normal human skin fibroblasts in vitro," *Journal of Drugs in Dermatology*, vol. 9, no. 12, pp. 1523–1526, 2010.

[22] M. Savi, L. Bocchi, R. Sala et al., "Parenchymal and stromal cells contribute to pro-inflammatory myocardial environment at early stages of diabetes: protective role of resveratrol," *Nutrients*, vol. 8, no. 11, p. 729, 2016.

[23] V. Vendrely, E. Peuchant, E. Buscail et al., "Resveratrol and capsaicin used together as food complements reduce tumor growth and rescue full efficiency of low dose gemcitabine in a pancreatic cancer model," *Cancer Letters*, vol. 390, pp. 91–102, 2017.

[24] F. Karimi Dermani, M. Saidijam, R. Amini, A. Mahdavinezhad, K. Heydari, and R. Najafi, "Resveratrol inhibits proliferation, invasion, and epithelial–mesenchymal transition by increasing miR-200c expression in HCT-116 colorectal cancer cells," *Journal of Cellular Biochemistry*, vol. 118, no. 6, pp. 1547–1555, 2017.

[25] Z. Jiang, X. Chen, K. Chen et al., "YAP inhibition by resveratrol via activation of AMPK enhances the sensitivity of pancreatic cancer cells to gemcitabine," *Nutrients*, vol. 8, no. 10, 2016.

[26] S. K. Roy, Q. Chen, J. Fu, S. Shankar, and R. K. Srivastava, "Resveratrol inhibits growth of orthotopic pancreatic tumors through activation of FOXO transcription factors," *PLoS One*, vol. 6, no. 9, article e25166, 2011.

[27] A. Rauf, M. Imran, H. A. R. Suleria, B. Ahmad, D. G. Peters, and M. S. Mubarak, "A comprehensive review of the health perspectives of resveratrol," *Food & Function*, vol. 8, no. 12, pp. 4284–4305, 2017.

[28] A. Kumar, A. M. Rimando, and A. S. Levenson, "Resveratrol and pterostilbene as a microRNA-mediated chemopreventive and therapeutic strategy in prostate cancer," *Annals of the New York Academy of Sciences*, vol. 1403, no. 1, pp. 15–26, 2017.

[29] W. Li, X. Ma, N. Li et al., "Resveratrol inhibits hexokinases II mediated glycolysis in non-small cell lung cancer via targeting Akt signaling pathway," *Experimental Cell Research*, vol. 349, no. 2, pp. 320–327, 2016.

[30] L. S. Gomez, P. Zancan, M. C. Marcondes et al., "Resveratrol decreases breast cancer cell viability and glucose metabolism by inhibiting 6-phosphofructo-1-kinase," *Biochimie*, vol. 95, no. 6, pp. 1336–1343, 2013.

[31] Z. Gao, X. Wang, K. Wu, Y. Zhao, and G. Hu, "Pancreatic stellate cells increase the invasion of human pancreatic cancer cells through the stromal cell-derived Factor-1/CXCR4 axis," *Pancreatology*, vol. 10, no. 2-3, pp. 186–193, 2010.

[32] D. Whitaker-Menezes, U. E. Martinez-Outschoorn, Z. Lin et al., "Evidence for a stromal-epithelial "lactate shuttle" in human tumors: MCT4 is a marker of oxidative stress in cancer-associated fibroblasts," *Cell Cycle*, vol. 10, no. 11, pp. 1772–1783, 2011.

[33] Y. Cheng, X. Liu, S. Zhang, Y. Lin, J. Yang, and C. Zhang, "MicroRNA-21 protects against the H(2)O(2)-induced injury on cardiac myocytes via its target gene PDCD4," *Journal of Molecular and Cellular Cardiology*, vol. 47, no. 1, pp. 5–14, 2009.

[34] S. Sheth, S. Jajoo, T. Kaur et al., "Resveratrol reduces prostate cancer growth and metastasis by inhibiting the Akt/MicroRNA-21 pathway," *PLoS One*, vol. 7, no. 12, article e51655, 2012.

[35] P. Liu, H. Liang, Q. Xia et al., "Resveratrol induces apoptosis of pancreatic cancers cells by inhibiting miR-21 regulation of BCL-2 expression," *Clinical & Translational Oncology*, vol. 15, no. 9, pp. 741–746, 2013.

[36] G. Wang, F. Dai, K. Yu et al., "Resveratrol inhibits glioma cell growth via targeting oncogenic microRNAs and multiple

signaling pathways," *International Journal of Oncology*, vol. 46, no. 4, pp. 1739–1747, 2015.

[37] H. Oettle, S. Post, P. Neuhaus et al., "Adjuvant chemotherapy with gemcitabine vs observation in patients undergoing curative-intent resection of pancreatic cancer: a randomized controlled trial," *JAMA*, vol. 297, no. 3, pp. 267–277, 2007.

[38] J.-c. Lee, J. W. Kim, S. Ahn et al., "Optimal dose reduction of FOLFIRINOX for preserving tumour response in advanced pancreatic cancer: using cumulative relative dose intensity," *European Journal of Cancer*, vol. 76, pp. 125–133, 2017.

[39] C. Baldini, A. Escande, O. Bouché et al., "Safety and efficacy of FOLFIRINOX in elderly patients with metastatic or locally advanced pancreatic adenocarcinoma: a retrospective analysis," *Pancreatology*, vol. 17, no. 1, pp. 146–149, 2017.

[40] W. Mo, X. Xu, L. Xu et al., "Resveratrol inhibits proliferation and induces apoptosis through the hedgehog signaling pathway in pancreatic cancer cell," *Pancreatology*, vol. 11, no. 6, pp. 601–609, 2011.

[41] W. Li, L. Cao, X. Chen, J. Lei, and Q. Ma, "Resveratrol inhibits hypoxia-driven ROS-induced invasive and migratory ability of pancreatic cancer cells via suppression of the Hedgehog signaling pathway," *Oncology Reports*, vol. 35, no. 3, pp. 1718–1726, 2016.

[42] W. Li, J. Ma, Q. Ma et al., "Resveratrol inhibits the epithelial-mesenchymal transition of pancreatic cancer cells via suppression of the PI-3K/Akt/NF-κB Pathway," *Current Medicinal Chemistry*, vol. 20, no. 33, pp. 4185–4194, 2013.

[43] P. Mukhopadhyay, S. Mukherjee, K. Ahsan, A. Bagchi, P. Pacher, and D. K. Das, "Restoration of altered microRNA expression in the ischemic heart with resveratrol," *PLoS One*, vol. 5, no. 12, article e15705, 2010.

[44] R. Venkatadri, T. Muni, A. K. V. Iyer, J. S. Yakisich, and N. Azad, "Role of apoptosis-related miRNAs in resveratrol-induced breast cancer cell death," *Cell Death & Disease*, vol. 7, no. 2, article e2104, 2016.

[45] S. Dhar, C. Hicks, and A. S. Levenson, "Resveratrol and prostate cancer: promising role for microRNAs," *Molecular Nutrition & Food Research*, vol. 55, no. 8, pp. 1219–1229, 2011.

[46] R. Kadaba, H. Birke, J. Wang et al., "Imbalance of desmoplastic stromal cell numbers drives aggressive cancer processes," *The Journal of Pathology*, vol. 230, no. 1, pp. 107–117, 2013.

[47] G. R. Ryu, E. Lee, H. J. Chun et al., "Oxidative stress plays a role in high glucose-induced activation of pancreatic stellate cells," *Biochemical and Biophysical Research Communications*, vol. 439, no. 2, pp. 258–263, 2013.

[48] K. Kikuta, A. Masamune, M. Satoh, N. Suzuki, K. Satoh, and T. Shimosegawa, "Hydrogen peroxide activates activator protein-1 and mitogen-activated protein kinases in pancreatic stellate cells," *Molecular and Cellular Biochemistry*, vol. 291, no. 1-2, pp. 11–20, 2006.

[49] S. W. Tsang, H. Zhang, Z. Lin, H. Mu, and Z. X. Bian, "Anti-fibrotic effect of trans-resveratrol on pancreatic stellate cells," *Biomedicine & Pharmacotherapy*, vol. 71, pp. 91–97, 2015.

[50] P. A. Phillips, M. J. Wu, R. K. Kumar et al., "Cell migration: a novel aspect of pancreatic stellate cell biology," *Gut*, vol. 52, no. 5, pp. 677–682, 2003.

[51] C. Capparelli, C. Guido, D. Whitaker-Menezes et al., "Autophagy and senescence in cancer-associated fibroblasts metabolically supports tumor growth and metastasis, via glycolysis and ketone production," *Cell Cycle*, vol. 11, no. 12, pp. 2285–2302, 2012.

[52] A. Charrier, R. Chen, L. Chen et al., "Connective tissue growth factor (CCN2) and microRNA-21 are components of a positive feedback loop in pancreatic stellate cells (PSC) during chronic pancreatitis and are exported in PSC-derived exosomes," *Journal of Cell Communication and Signaling*, vol. 8, no. 2, pp. 147–156, 2014.

[53] S. Ali, R. Suresh, S. Banerjee et al., "Contribution of microRNAs in understanding the pancreatic tumor microenvironment involving cancer associated stellate and fibroblast cells," *American Journal of Cancer Research*, vol. 5, no. 3, pp. 1251–1264, 2015.

[54] S. Jiang, R. Wang, H. Yan, L. Jin, X. Dou, and D. Chen, "MicroRNA-21 modulates radiation resistance through upregulation of hypoxia-inducible factor-1α-promoted glycolysis in non-small cell lung cancer cells," *Molecular Medicine Reports*, vol. 13, no. 5, pp. 4101–4107, 2016.

[55] R. B. Robey and N. Hay, "Is Akt the "Warburg kinase"?—Akt-energy metabolism interactions and oncogenesis," *Seminars in Cancer Biology*, vol. 19, no. 1, pp. 25–31, 2009.

[56] X. Zha, Q. Sun, and H. Zhang, "mTOR upregulation of glycolytic enzymes promotes tumor development," *Cell Cycle*, vol. 10, no. 7, pp. 1015-1016, 2011.

[57] T. Fiaschi, A. Marini, E. Giannoni et al., "Reciprocal metabolic reprogramming through lactate shuttle coordinately influences tumor-stroma interplay," *Cancer Research*, vol. 72, no. 19, pp. 5130–5140, 2012.

Hindawi
Oxidative Medicine and Cellular Longevity
Volume 2018, Article ID 1083596, 12 pages
https://doi.org/10.1155/2018/1083596

Research Article

The Critical Role of IL-10 in the Antineuroinflammatory and Antioxidative Effects of *Rheum tanguticum* on Activated Microglia

Jie Meng,[1] **Junjun Ni**,[1] **Zhou Wu**,[1,2] **Muzhou Jiang**,[1] **Aiqin Zhu**,[3] **Hong Qing**,[4] **and Hiroshi Nakanishi**[1]

[1]*Department of Aging Science and Pharmacology, Faculty of Dental Sciences, Kyushu University, Fukuoka 812-8582, Japan*
[2]*OBT Research Center, Faculty of Dental Sciences, Kyushu University, Fukuoka 812-8582, Japan*
[3]*Institution of Geriatric, Qinghai Provincial Hospital, Xining 810007, China*
[4]*School of Life Science, Beijing Institute of Technology, Haidian District, Beijing 100081, China*

Correspondence should be addressed to Hiroshi Nakanishi; nakan@dent.kyushu-u.ac.jp

Received 12 December 2017; Revised 28 February 2018; Accepted 18 March 2018; Published 26 April 2018

Academic Editor: Mithun Sinha

Rheum tanguticum Maxim. ex Balf. (*Rt*), a traditional Tibetan medicine, is known to exert various bioactivities, including anti-inflammatory and antioxidative activities. The present study was conducted to investigate anti-inflammatory and antioxidative effects of *Rt* on activated microglia. *Rt* (10 μg/ml) significantly inhibited the mean protein level of interleukin-1β (IL-1β) in the organotypic hippocampal slice cultures following treatment with chromogranin A (CGA, 10 nM) and pancreastatin (10 nM), endogenous microglial activators present in senile plaques. *Rt* also significantly inhibited the expression and production of inflammatory and oxidative molecules, including IL-1β, tumor necrosis factor-α, and nitric oxide, by cultured microglia after treatment with CGA. These effects of *Rt* are considered to be mediated by the secretion of interleukin-10 (IL-10) from microglia, because neutralizing antibodies against IL-10 significantly canceled these effects. To explore the causative components of *Rt* responsible for inducing the secretion of IL-10, the effects of seven components of *Rt* on the IL-10 expression in microglia were examined. Among them, aloe-emodin (10 μM) and (+)-catechin (30 μM) were able to induce the secretion of IL-10 from cultured microglia. Therefore, aloe-emodin and (+)-catechin are deemed responsible for the antineuroinflammatory and antioxidative effects of *Rt* through the secretion of IL-10 from microglia. Accordingly, *Rt* is considered potentially useful for the treatment of AD.

1. Introduction

There is increasing evidence that chronic neuroinflammation by activated microglia is closely associated with many neurological disorders, including Alzheimer's disease (AD). Furthermore, findings suggest that neuroinflammation mediated by activated microglia plays an essential role in the pathogenesis and progression of AD [1, 2]. Recently, it has been demonstrated that neuroinflammation is not a passive system activated by emerging senile plaques and neurofibrillary tangles but instead contributes as much to pathogenesis as do the plaques and tangles themselves [3]. More recently, two research groups have provided evidence that neuroinflammation is not a result of AD as much as a key driver of the disease [4, 5].

Medicinal plants can be considered an important resource for identifying anti-inflammatory agents, as they contain many kinds of natural polyphenols that exert anti-inflammatory and antioxidative activities. There is accumulating evidence indicating that medicinal plants and natural products including ginsenosides from *Panax ginseng*, curcumin from *Curucuma longaI*, and resveratrol, a natural polyphenol, have antineuroinflammatory and neuroprotective effects through inhibition of microglial activation

[6]. Furthermore, we have recently reported that green propolis, a resinous substance by honeybees as a defense against intruders, has both antineuroinflammatory and neuroprotective effects [7, 8]. *Rheum tanguticum* (*Rt*), which is endemic to the eastern part of the Qinghai-Tibet Plateau in China, is a well-known traditional medicine with purgation, antibacterial, antipyretic, and hemostatic effects. *Rt* contains twenty compounds including anthraquinones that possess anti-inflammatory effects [9]. However, little information is available about anti-inflammatory and antioxidative activities of *Rt*.

Interleukin-10 (IL-10) is known to inhibit the lipopolysaccharide- (LPS-) induced production of several inflammatory mediators, the expression of cytokine receptors, and the expression of major histocompatibility complex II in microglia [10–15]. IL-10 can also inhibit the LPS- or cytokine-induced expression of chemokines and adhesion molecules in microglia [16, 17]. Furthermore, a peripheral injection with LPS in IL-10-deficient mice causes a prominent cognitive deficit compared with wild-type mice [18]. IL-10 acts through the activation of its receptor (IL-10R). Upon binding, the receptor oligomerizes into a tetramer composed of two ligand-binding subunits (IL-10R1) and two accessory subunits (IL-10R2) that in turn activate an intracellular signaling cascade [19]. Therefore, IL-10 is considered a potent negative autocrine regulator of microglia, as microglia produce IL-10 and possess IL-10R [11, 20]. Resveratrol, a natural polyphenol first identified as a bioactive compound in 1992, is naturally present in red wine and grapes and has been to exert a neuroprotective effect through its anti-inflammatory and antioxidant effects [21]. Recently, the production and secretion of IL-10 from microglia has shown to be responsible for the anti-inflammatory and antioxidant effects of this agent [22, 23]. Moreover, it has been also reported that the protective effects of curcumin are IL-10 dependent [24].

In the present study, we thus examined the possible antineuroinflammatory and antioxidative effects of *Rt* using the organotypic hippocampal slice cultures and cultured microglia after stimulation with endogenous microglial activators localized in the senile plaques of AD patients.

2. Materials and Methods

2.1. Reagents. *Rt* was purchased from Qinghai Jinke Tibetan Medicine Pharmaceutical Co., Ltd. (Xining, China). *Rt* contained seven anthraquinones or glycosides of anthraquinones including chrysophanol, aloe-emodin, physcion, rhein, emodin, chrysophanol-8-O-β-D-glucopyranoside, and aloe-emodin-8-O-β-D-glucopyranoside. In addition, *Rt* contained two phenylbutanone glucopyranosides (lindleyin and isolindleyin), piceatannol, (+)-catechin, β-sitosterol, epicatechin-3-O-gallate, and torachrysone-8-O-β-D-glucopyranoside. The suitable concentration of methanol for cell culture was titrated in order to prevent the interference induced by the methanol solvent. Chromogranin A (CGA, synthetic human CGA286-301) and pancreastatin (PST) were purchased from Peptide Institute (Osaka, Japan). Mouse anti-IL-10 neutralizing antibody (IL-10NAb) was purchased from Abcam (Cambridge, UK). Antibodies against mouse anti-interleukin-1β (IL-1β), mouse antiphospho-IκBα, rabbit anti-IκBα, and goat antiphospho-signal transducer and activator of transcription 1 (STAT1) were purchased from Santa Cruz Biotechnology (Santa Cruz, CA, USA). Major *Rt* components including chrisophanol, physcion, β-sitosterol, emodin, aloe-emodin, (+)-catechin, and piceatannol were purchased from Abcam (UK). In preliminary experiments, minimum effective dose of either CGA or PST for mRNA expression of proinflammatory mediators in MG6 cells and primary microglia was determined to be 10 nM. Therefore, CGA and PST with the concentration of 10 nM were used in this study. On the other hand, three different concentrations (10, 30, and 100 μM) of aloe-emodin, (+)-catechin, piceatannol, chrisophanol, physcion, β-sitosterol, and emodin were used.

2.2. Cell Viability Assay. MG6 cells were seeded in 96-well plates (5×10^3 cells/well) overnight [25]. Different concentrations ranging from 5 to 500 μg/ml of *Rt* were treated for 24 h. A cell viability assay was conducted using a cell counting kit (Dojindo, Japan) according to the protocol provided by the manufacturer. The optical density was read at wavelength of 450 nm with a microplate reader. The cell viability was calculated by dividing the optical density of *Rt*-treated group by that of nontreated group. *Rt* up to 10 μg/ml had no significant toxic effect on MG6 cells, therefore 10 μg/ml *Rt* was used in further experiments.

2.3. Organotypic Hippocampal Slice Cultures. Male C57BL/6 mice (10 months of age) were sacrificed and their brains were removed. All animals were treated in accordance with the protocols approved by the animal care and use committee of Kyushu University. Sagittal sections 200 μm thick were cut using a vibratome (VT1000S; Wetzlar, Leica), and intact sections were carefully selected under a microscope and incubated in cooled dissection buffer (50% HEPES-buffered MEM, 1% penicillin-streptomycin, 10 mM Tris, pH 7.2) for 30 min at 4°C. The slices were then carefully transferred to 24-well plates containing 0.5 ml of slice culture medium (50% HEPES-buffered MEM, 25% heat-inactivated horse serum, 25% HBSS, 1 mM L-glutamine, pH; 7.4) and maintained in a cell culture incubator at 37°C, 5% CO_2. One day after preparation, the medium was changed, and *Rt* was applied at 10 μg/ml. CGA (10 nM) and PST (10 nM) were added 24 h after *Rt* treatment. The slices were collected and lysed for Western blotting at 48 h after treatment with CGA or PST. In some experiments, microglia were depleted from hippocampal slice cultures using saponin coupled to an antibody against Mac1 (Mac1-sap; Advanced Targeting Systems, San Diego, USA). Mac1-sap at 1.3 nM was applied to hippocampal slice cultures 24 h prior to stimulation with CGA or PST.

2.4. Microglia Cell Culture. The c-*myc*-immortalized mouse microglial cell line MG6 (Riken Cell Bank, Tsukuba, Japan) was maintained in DMEM supplemented with 100 μmol/L β-mercaptoethanol, 10 μg/mL of insulin, 1% penicillin-streptomycin (Invitrogen, Grand Island, NY,

USA), 4500 mg/L glucose (Invitrogen), and 10% FBS according to previously described methods. Primary cultured microglia were isolated from the mixed primary cell cultures obtained from the cerebral cortex of three-day-old C57BL/6 mice according to previously described methods [26].

2.5. Real-Time Quantitative Polymerase Chain Reaction (qRT-PCR). Total RNA was extracted using RNAiso Plus according to the manufacturer's instructions. 1 μg of total RNA was used for cDNA synthesis using the QuantiTect Reverse Transcription Kit (Qiagen, Hilden, Germany). After an initial amplification with a denaturation step at 95°C for 5 m, followed by 30–40 cycles of denaturation at 95°C for 5 s, annealing at 60°C for 10 s, and extension at 72°C for 30 s, a final extension at 72°C for 5 m was done upon completion of the cycling steps. The cDNA was amplified in duplicate using a Rotor-Gene SYBR Green RT-PCR Kit (Qiagen) with a Corbett Rotor-Gene RG-3000A Real-Time PCR System. The data were evaluated using the RG-3000A software program (version Rotor-Gene 6.1.93, Corbett, Sydney, Australia). The sequences of primer pairs were described as follows: IL-1β: 5′-CAACCAACAAGTGATATTCTCCATG-3′ and 5′-GATCCACACTCTCAGCTGCA-3′; inducible nitric oxide synthase (iNOS): 5′-GCCACCAACAATGGCAAC-3′ and 5′- CGTACCGGATGAGCTGTGAATT- 3′; TNF-α: 5′-ATGGCCTCCCTC TCAGTTC -3′ and 5′-TTGGTGGTT TGCTACGACGTG-3′; and IL-10: 5′-GACCAGCTGGA CAACATACTGC TAA-3′ and 5′-GATAAGGATTGGCA ACCCAAGTAA-3′. For data normalization, an endogenous control (actin) was assessed to control for the cDNA input, and the relative units were calculated by a comparative Ct method. All qRT-PCR experiments were repeated three times, and the results are presented as the means of the ratios ± SEM.

2.6. Western Blotting. MG6 were cultured at a density of 5×10^5 cells/mL. After treatment with *Rt* (10 μg/ml) for 24 h, microglia were treated with CGA (10 nmol/L) for various time points. The cytosolic samples were collected at various time points. Western blotting was performed with a SDS-PAGE electrophoresis system. 30 μg protein samples were resuspended in sample buffer, then electrophoresed on a 15% or 12% Tris gel, and then blotted to the PVDF membrane. After blocking, the membranes were incubated at 4°C overnight under gentle agitation with each primary antibody: mouse anti-IL-1β (1 : 1000), mouse antiphospho-IκBα (1 : 1000), rabbit anti-IκBα (1 : 1000), goat antiphospho-STAT1 (1 : 1000), and anti-β-actin (1 : 1000) antibodies overnight at 4°C. After washing, the membranes were incubated with horseradish peroxidase- (HRP-) labeled antigoat (1 : 1000; R&D Systems, Minneapolis, MN, USA), antirabbit (1 : 1000; Beckman Coulter, Tokyo, Japan), or antimouse (1 : 1000; Amersham Pharmacia Biotech, Piscataway, NJ, USA) antibodies for 2 h at 24°C and then detected using an enhanced chemiluminescence detection system (ECK kit; Amersham Pharmacia Biotech, Piscataway, NJ, USA) with an image analyzer (LAS-4000; Fuji Photo Film, Tokyo, Japan).

2.7. ELISA. The cytokines IL-1β and IL-10 were measured by enzyme-linked immunosorbent assay (ELISA) kits (R&D Systems) following the protocol provided by the manufacturer. The absorbance at 450 nm was determined using a microplate reader.

2.8. Immunostaining. The cultured microglia were fixed with 4% paraformaldehyde 48 h after CGA treatment or pretreatment with *Rt*. They were then incubated with the mouse anti-p65 overnight at 4°C. After washing with PBS, the sections were incubated with donkey antimouse Alexus 488 (1 : 500; Jackson ImmunoResearch, West Grove, PA, USA), then incubated with Hoechst (1 : 200), and mounted in Vectashield antifading medium (Vector Laboratories, Burlingame, CA, USA). Fluorescence images were taken using a confocal laser-scanning microscope (CLSM; 2si Confocal Laser Microscope, Nikon, Tokyo, Japan). The line plot profile was analyzed using Image J.

2.9. NO_2^-/NO_3^- Assay. MG6 were cultured at a density of 5×10^5 cells/mL. After treatment with *Rt* (10 μg/L) for 24 h, microglia were treated with CGA (10 nM) for 72 h, and the supernatant of the cells was collected. The amounts of NO_2^- and NO_3^- were measured by NO_2^-/NO_3^- assay kits (R&D Systems) following the protocol provided by the manufacturer. The absorbance at 540 nm was determined using a microplate reader.

2.10. Statistical Analyses. The data are represented as the mean ± standard error of the mean.

A two-tailed unpaired Student's *t*-test and a one-way analysis of variance (ANOVA) with a post hoc Tukey's test were performed for the statistical analyses by the GraphPad Prism 7 Software package (GraphPad Software Inc., San Diego, CA, USA). A value of $P < 0.05$ was considered to indicate statistical significance.

3. Results

3.1. Inhibitory Effects of Rt on the CGA- and PST-Induced Expression of IL-β in Organotypic Hippocampal Slice Cultures. The viability of MG6 cells was examined using the CCk-8 assay at 24 h after treatment with *Rt* with the concentration ranging from 5 to 500 μg/ml. *Rt* up to 10 μg/ml had no significant toxic effect on MG6 cells (Figure 1). CGA and PST with the minimum effective dose determined in preliminary experiments were used to activate microglia, as they are potent endogenous microglial activators and localize in the senile plaques of AD patients [27–29].

To elucidate the possible antineuroinflammatory effects, the effects of *Rt* (10 μg/ml) on the expression of IL-β in organotypic hippocampal slice cultures were examined by Western blotting. The mean protein level of IL-1β was significantly increased in the organotypic hippocampal slice cultures at 48 h after stimulation with CGA (10 nM). *Rt* significantly suppressed the mean protein level of IL-1β in CGA-stimulated organotypic hippocampal slice cultures (Figure 2(a)). PST (10 nM) also significantly increased the mean protein level of IL-β in the organotypic hippocampal slice cultures to a similar extent as CGA. Furthermore, *Rt*

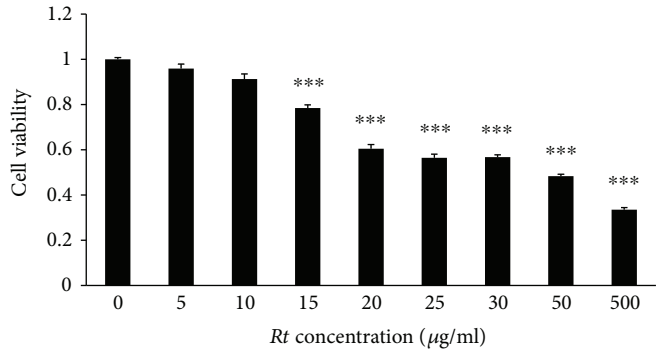

Figure 1: The cell viability of MG6 cells at 24 h after treatment with different dose of *Rt* by using a cell counting kit-8. The results represent the mean ± SEM of four independent experiments. The asterisks indicate a statistically significant difference from the value in untreated cells (***$P < 0.001$).

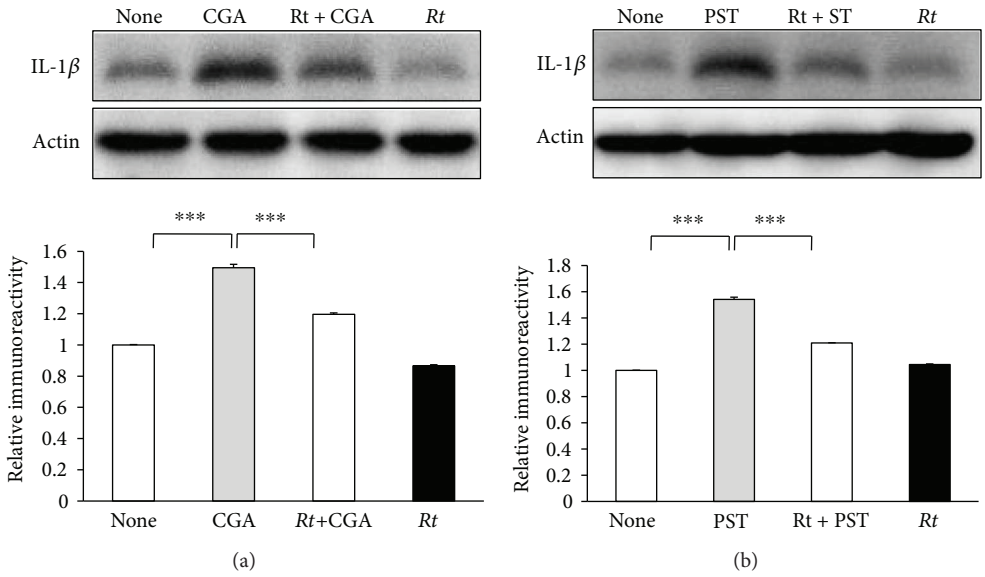

Figure 2: Inhibitory effects of *Rt* on CGA- or PST-induced IL-1β production in the hippocampal slice cultures. (a) The effect of *Rt* (10 μg/ml) on the protein level of IL-1β after stimulation with CGA using Western blotting. The results represent the mean ± SEM of three independent experiments. The asterisks indicate a statistically significant difference from the indicated value (***$P < 0.001$). (b) The effect of *Rt* (10 μg/ml) on the protein level of IL-1β after stimulation with PST. The results represent the mean ± SEM of three independent experiments. The asterisks indicate a statistically significant difference from the indicated value (***$P < 0.001$).

significantly suppressed the PST-induced IL-1β production (Figure 2(b)). Therefore, CGA286-301 may be an active component of PST, as CGA used in this study was human CGA286-301, which includes the carboxy-terminal of PST. In contrast, both CGA and PST failed to significantly increase the mean protein level of IL-1β in the Mac1-sap treated hippocampal slice cultures (Figures 3(a) and 3(b)), suggesting that microglia are responsible for the IL-1β production after treatment with CGA or PST.

3.2. Inhibitory Effects of Rt on the CGA-Induced Expression of Proinflammatory and Oxidative Mediators in Microglia. To elucidate the possible anti-inflammatory and antioxidative roles, effects of *Rt* (10 μg/ml) on the expression of proinflammatory mediators by microglia were examined at the transcriptional level using quantitative RT-PCR. *Rt* significantly suppressed the mean basal mRNA expression levels of IL-1β and iNOS, but not TNF-α, in nonstimulated MG6 cells (Figures 4(a)–4(c)). The mean mRNA expression levels of TNF-α, IL-1β, and iNOS was significantly increased in MG6 cells at 24 h after stimulation with CGA (10 nM). *Rt* significantly suppressed the mean mRNA expression levels of TNF-α, IL-1β, and iNOS in CGA-stimulated MG6 cells (Figures 5(a)–5(c)). Furthermore, the secretion of IL-1β and NO metabolites in the culture medium of MG6 cells was assessed by an ELISA and NO_2^-/NO_3^- assay, respectively. The mean levels of IL-1β and NO_2^-/NO_3^- were significantly increased in the culture medium of MG6 cells at 24 h after treatment with CGA. *Rt* also significantly decreased the mean levels of IL-1β and NO_2^-/NO_3^- in the culture medium of MG6 cells (Figures 5(d) and 5(e)).

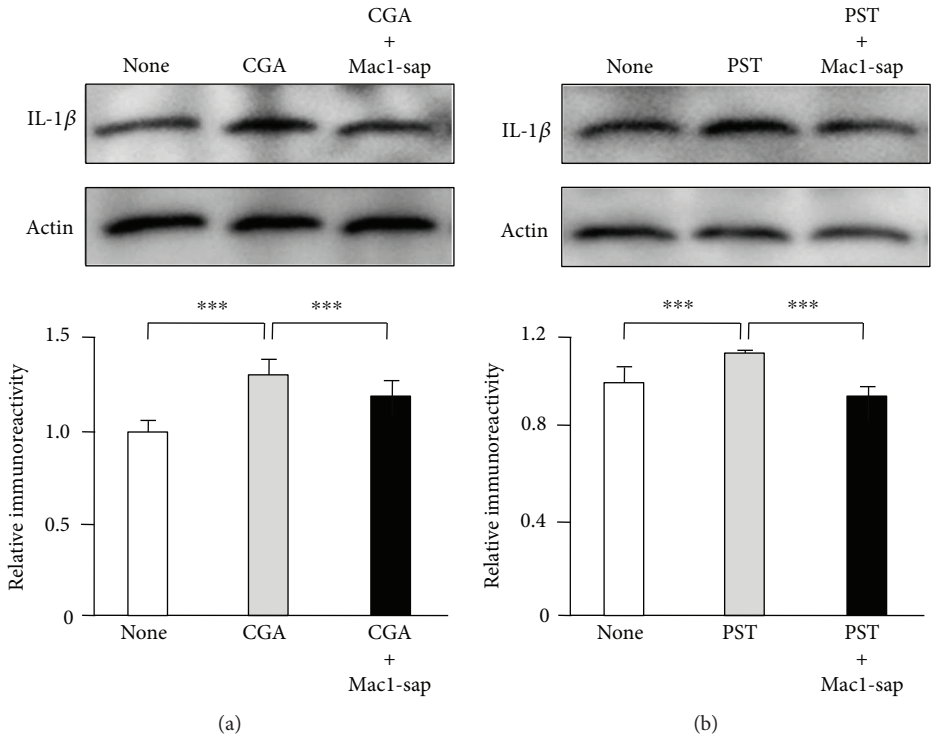

Figure 3: The failure of IL-1β production after treatment with CGA or PST in the microglia-depleted hippocampal slice cultures using Mac1-sap. (a) The effect of CGA on the protein level of IL-1β in the nontreated and Mac1-sap-treated cultures. The results represent the mean ± SEM of three independent experiments. The asterisks indicate a statistically significant difference from the indicated value ($^{***}P < 0.001$). (b) The effect of PST on the protein level of IL-1β in the nontreated and Mac1-sap-treated culture. The results represent the mean ± SEM of three independent experiments. The asterisks indicate a statistically significant difference from the indicated value ($^{***}P < 0.001$).

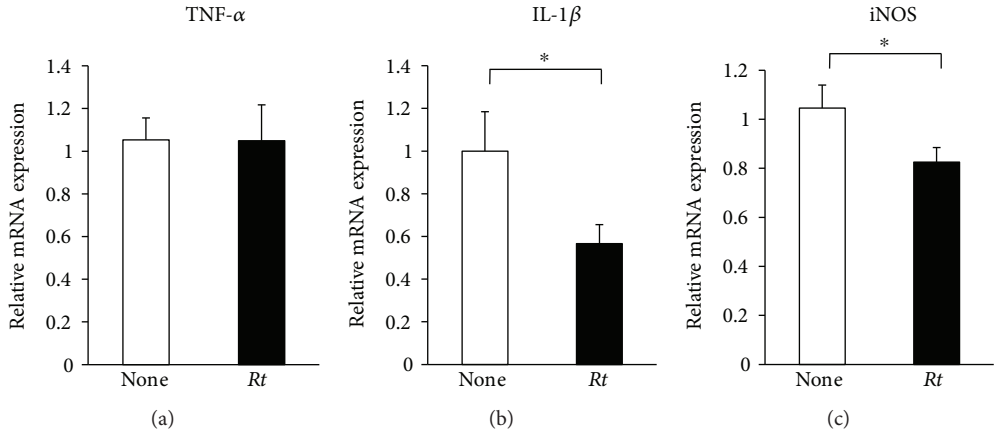

Figure 4: The inhibitory effects of *Rt* on the CGA-induced expression of proinflammatory and oxidative mediators in microglia. The effect of *Rt* (10 μg/ml) on the basal mRNA expression of TNF-α (a), IL-1β (b), and iNOS (c) in the nonstimulated MG6 cells. Each column and bar represents the mean ± SEM ($n = 4$ each). The asterisks indicate a statistically significant difference from the indicated value ($^{*}P < 0.05$).

RT-PCR and ELISA were also performed to determine whether or not *Rt* was able to regulate the production of the anti-inflammatory cytokine IL-10. CGA (10 nM) alone failed to increase the mean mRNA level of IL-10, whereas the combination of CGA and *Rt* significantly increased the mean mRNA level of IL-10 (Figure 5(f)), suggesting that *Rt* was able to upregulate the expression of IL-10. As expected, the mean mRNA expression of IL-10 in MG6 cells was significantly increased at 12 h and peaked at 24 h after treatment with *Rt* alone at 5 μg/ml (Figure 6(a)). *Rt* was able to significantly increase the mean mRNA expression level of IL-10 in MG6 cells at 24 h after treatment at >5 μg/ml (Figure 6(b)) without affecting the expression of IL-1β (data not shown). In contrast, the mean level of IL-10 in the culture medium of MG6 cells significantly increased at 24 h and peaked at 48 h after treatment of *Rt* at 5 μg/ml (Figure 6(c)). The mean level of IL-10 secretion was significantly increased at 48 h after treatment with *Rt* at >5 μg/ml in the culture medium

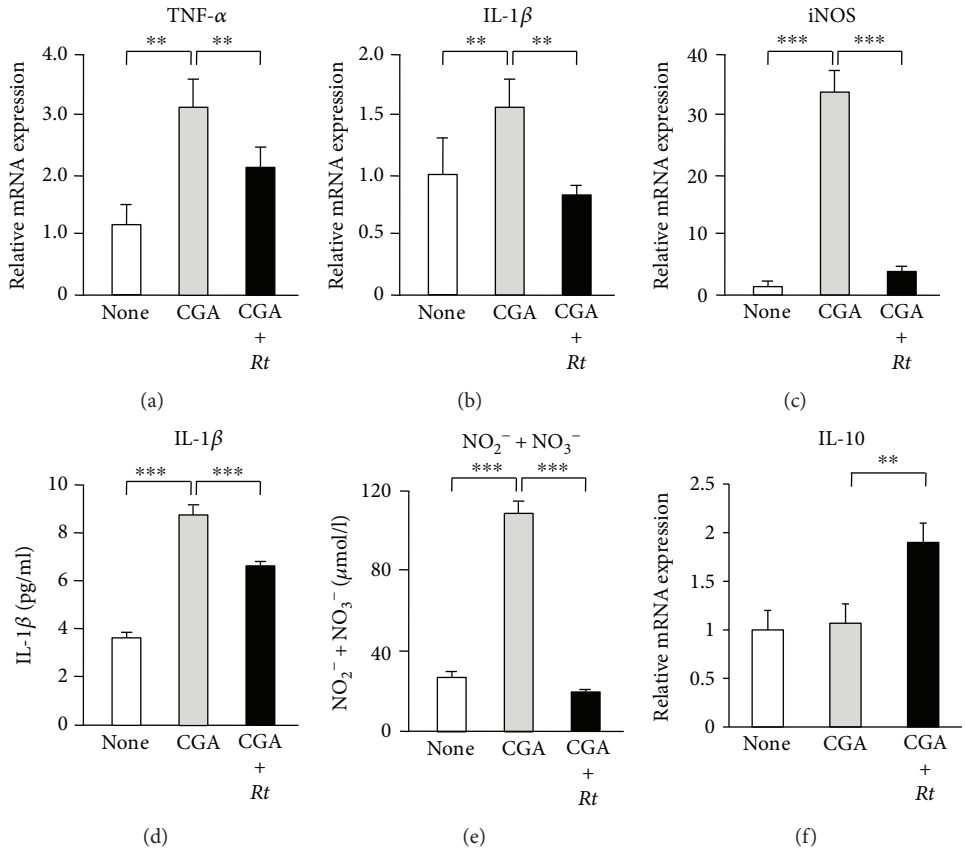

Figure 5: The inhibitory effects of *Rt* on the CGA-induced expression of proinflammatory and oxidative mediators in microglia. (a–c) The effect of *Rt* (10 μg/ml) on the mRNA expression of TNF-α (a), IL-1β (b), and iNOS (c) in the MG6 cells after stimulation with CGA. Each column and bar represents the mean ± SEM ($n = 4$ each). The asterisks indicate a statistically significant difference from the indicated value ($^{**}P < 0.01$, $^{***}P < 0.001$). (d) The secretion of IL-1β in the MG6 cells 96 h after stimulation with CGA with or without pretreatment with *Rt*. The results represent the mean ± SEM of three independent experiments. The asterisks indicate a statistically significant difference from the indicated value ($^{***}P < 0.001$). (e) The examination of NO metabolites in the culture medium of MG6 cells 72 h after stimulation with CGA with or without pretreatment with *Rt* by NO_2^-/NO_3^- assay. The results represent the mean ± SEM of three independent experiments. The asterisks indicate a statistically significant difference from the indicated value. ($^{***}P < 0.001$). (f) The effect of *Rt* (10 μg/ml) on the mRNA expression of IL-10 in the MG6 cells after stimulation with CGA. The results represent the mean ± SEM of four independent experiments. The asterisks indicate a statistically significant difference from the indicated value ($^{**}P < 0.01$).

of both MG6 cells and primary cultured murine microglia (Figure 6(d)). Of note, the mean level of IL-10 in the culture medium of primary cultured microglia (200 pg/mL) was more than tenfold greater than that of MG6 cells (14 pg/mL) after treatment with *Rt* (10 μg/mL).

3.3. Possible Role of IL-10 in the Anti-Inflammatory Effects of Rt on CGA-Stimulated Microglia. To investigate the involvement of IL-10 in the anti-inflammatory effects of *Rt* (10 μg/ml) on inflammatory responses of microglia, we evaluated the effects of IL-10NAb on the *Rt*-mediated inhibition of the TNF-α and IL-1β expression in CGA-stimulated MG6 cells. IL-10NAb inhibited the mean mRNA expression of TNF-α and IL-1β in CGA-stimulated MG6 cells in the presence of *Rt* (Figures 7(a) and 7(b)). There was no significant difference between the mean percentage recovery from *Rt*-induced inhibition of TNF-α and IL-1β mRNA expression after treatment with IL-10NAb (66.7% for TNF-α and IL-1β for 63.6%). These observations strongly suggest that IL-10 plays a critical role in the anti-inflammatory property of *Rt* in microglia.

3.4. Effects of Rt on the Nuclear Factor (NF)-κB and STAT1 Activation Pathways in CGA-Stimulated Microglia. The effects of *Rt* on the nuclear translocation of p65 induced by treatment with CGA were examined. *Rt* (10 μg/ml) significantly inhibited the CGA-induced nuclear translocation of p65 in MG6 cells (Figure 8(a)). When IL-10 was neutralized, the CGA-induced nuclear translocation of p65 in MG6 cells returned to levels in the absence of *Rt* (Figure 8(a)). These observations clearly show that *Rt* can inhibit CGA-induced activation of the NF-κB pathway in MG6 cells through production of IL-10.

The activation of NF-κB and STAT1 pathways were further examined after treatment with CGA (10 nM) in MG6 cells by immunoblotting, as these two signaling pathways are required for the production of TNF-α, IL-1β, and NO. The mean levels of phospho-IκBα and phospho-

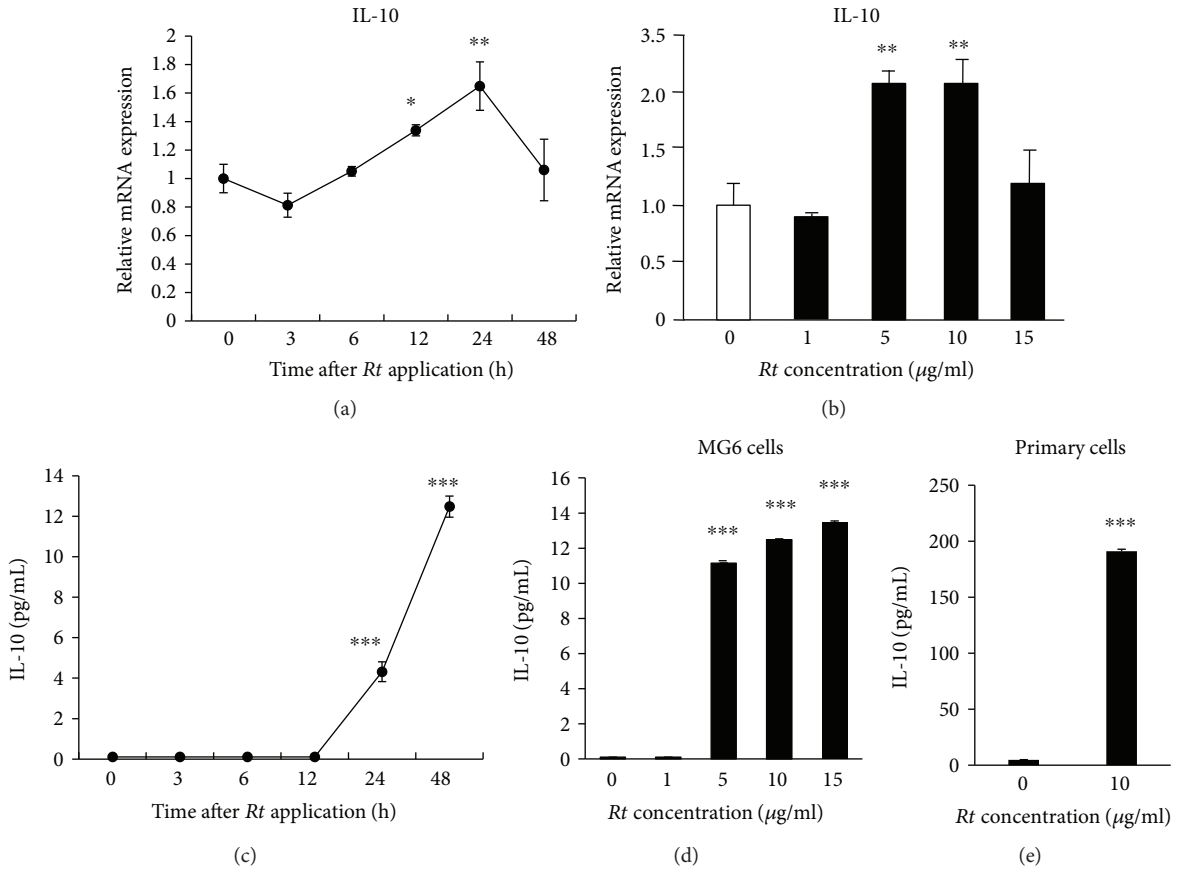

Figure 6: The capable regulation of IL-10 by *Rt* in MG6 cells and primary cultured microglia. (a) The mRNA changes of IL-10 at different time points after treatment with *Rt* (10 μg/ml). The results represent the mean ± SEM of three independent experiments. The asterisks indicate a statistically significant difference from the value at the start of experiments (0 h) ($^{*}P < 0.05$, $^{**}P < 0.01$). (b) The mRNA changes of IL-10 24 h after treatment with different doses of *Rt*. The results represent the mean ± SEM of three independent experiments. The asterisks indicate a statistically significant difference from the value in untreated cells ($^{**}P < 0.01$). (c) The secretion of IL-10 in the cultured medium of MG6 cells at different time points after treatment with *Rt* (10 μg/ml). The results represent the mean ± SEM of three independent experiments. The asterisks indicate a statistically significant difference from the value at the start of experiments (0 h) ($^{***}P < 0.001$). (d) The secretion of IL-10 in the cultured medium of MG6 cells 24 h after treatment with different doses of *Rt*. The results represent the mean ± SEM of three independent experiments. The asterisks indicate a statistically significant difference from the value in untreated cells ($^{***}P < 0.001$). (e) The secretion of IL-10 in the cultured medium of primary cultured microglia 24 h after treatment with *Rt* (10 μg/ml). The results represent the mean ± SEM of three independent experiments. The asterisks indicate a statistically significant difference from the value in untreated cells ($^{***}P < 0.001$).

STAT1 were significantly increased in MG6 cells after treatment with CGA at 10 min and 3 h, respectively (Figures 8(b) and 9(a)). *Rt* at 10 μg/ml significantly decreased the mean levels of phospho-IκBα (Figure 8(c)) and phospho-STAT1 (Figure 9(b)) in CGA-stimulated MG6 cells. Furthermore, the neutralization of IL-10 using IL-10NAb significantly inhibited the mean levels of phospho-IκBα (Figure 8(c)) and phospho-STAT1 (Figure 9(b)) in CGA-stimulated MG6 cells in the presence of *Rt*. These observations suggest that IL-10 plays a critical role in the *Rt*-induced anti-inflammatory antioxidative effects through the suppression of NF-κB and STAT1 activation pathways.

3.5. Possible Components of Rt Responsible for the Production of IL-10 by Microglia. Finally, to explore the components of *Rt* responsible for the production of IL-10 in microglia, RT-PCR was performed to examine the effects of major components of *Rt* including on the mRNA expression in MG6 cells. Effects of three different concentrations (10, 30, and 100 μM) of major *Rt* components including chrisophanol, physcion, β-sitosterol, emodin, aloe-emodin, (+)-catechin, and piceatannol were examined at 24 h on the mRNA expression of IL-10 in MG6 cells. Among the major components of *Rt*, three components, namely, aloe-emodin, (+)-catechin, and piceatannol, were found to significantly increase the mRNA expression of IL-10 in MG6 cells at 24 h after treatment (Figure 10(a)). The minimum effective doses of aloe-emodin, (+)-catechin, and piceatannol were determined to be 10, 30, and 100 μM, respectively. In contrast, chrisophanol, physcion, β-sitosterol, or emodin at concentrations up to 100 μM had no effect on the mRNA expression of IL-10 in MG6 cells.

Then, effects of aloe-emodin, (+)-catechin, and piceatannol with the most effective doses on the secretion of IL-10

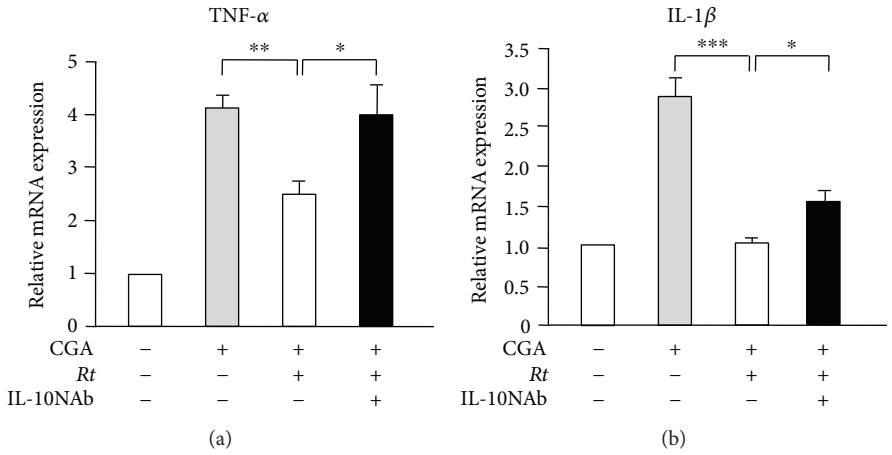

Figure 7: Possible role of IL-10 in the anti-inflammatory effects of *Rt* on CGA-stimulated microglia. (a, b) The mRNA changes of TNF-α (a) and IL-1β (b) of CGA stimulated MG6 cells in the presence or absence of *Rt* (10 μg/ml) and IL-10 neutralizing antibody (IL-10NAb). The results represent the mean ± SEM of three independent experiments. The asterisks indicate a statistically significant difference from the indicated value ($^{*}P < 0.05$, $^{**}P < 0.01$, $^{***}P < 0.001$).

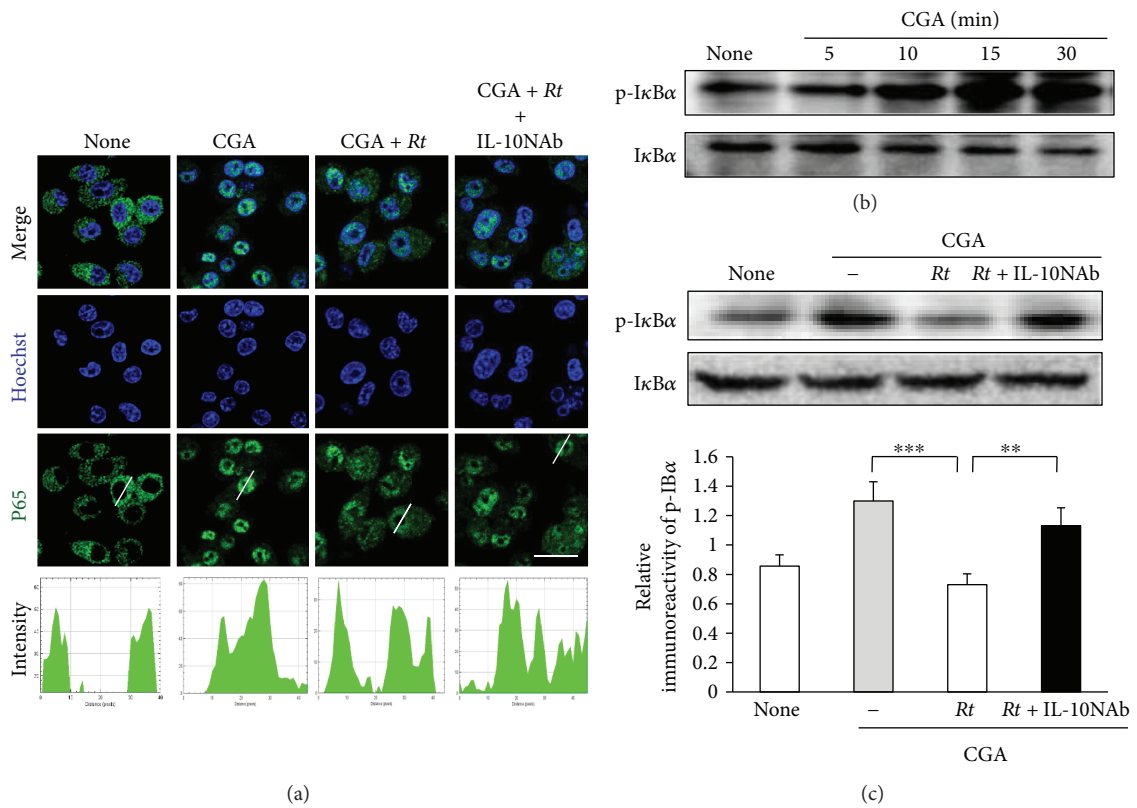

Figure 8: Effects of *Rt* on the NF-κB activation pathways in CGA-stimulated microglia. (a) Immunofluorescence CLMS images indicating the nuclear translocation of p65 (green) in MG6 cells with Hoechst-stained nuclei (blue) at 24 h after stimulation with CGA (10 nM) in the presence or absence of *Rt* (10 μg/ml) and IL-10NAb. Scale bar, 15 μm. The typical cells were analyzed by line plot profile to show the cytosol and nuclear location of p65. (b) The protein expression of phospho-IκBα at different time points after stimulation with CGA. (c) The protein expression of phospho-IκBα in MG6 cells 30 min after CGA stimulation in the presence or absence of *Rt* (10 μg/ml) and IL-10NAb and the quantitative analyses of the immunoblotting for phospho-IκBα. The results represent the mean ± SEM of four independent experiments. The asterisks indicate a statistically significant difference from the indicated value ($^{**}P < 0.01$, $^{***}P < 0.001$).

from MG6 cells and primary cultured microglia were examined at three different experimental time points (24, 48, and 72 h). Figure 10(b) showed the mean amounts of IL-10 secreted in the culture medium of MG6 cells and primary cultured microglia after treatment of aloe-emodin and (+)-catechin with the minimum effective doses at the most effective experimental time points. On the other hand, piceatannol (100 μM) failed to secrete IL-10 even at 72 h after

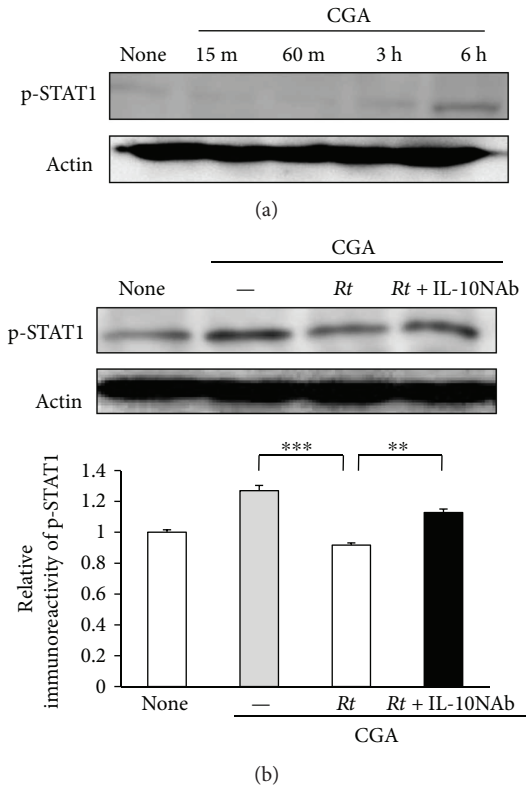

Figure 9: Effects of *Rt* on the STAT1 activation pathways in CGA-stimulated microglia. (a) The protein expression of phospho-STAT1 at different time points after stimulation with CGA. (b) The protein expression of phospho-STAT1 in MG6 cells 6 h after CGA stimulation in the presence or absence of *Rt* (10 μg/ml) and IL-10NAb and the quantitative analyses of the immunoblotting for phospho-STAT1. The results represent the mean ± SEM of four independent experiments. The asterisks indicate a statistically significant difference from the indicated value ($^{**}P < 0.01$, $^{***}P < 0.001$).

treatment. Of note, the mean level of IL-10 in the culture medium of primary cultured microglia was approximately tenfold greater than that of MG6 cells.

4. Discussion

In the present study, we demonstrated the antineuroinflammatory effects of *Rt* in CGA-stimulated organotypic hippocampal slice cultures, MG6 cells, and primary cultured microglia. *Rt* with the concentration of 10 μg/mL significantly suppressed the CGA-induced production of IL-1β in the organotypic hippocampal cultures. *Rt* at >5 μg/mL also significantly suppressed the CGA-induced expression of TNF-α, IL-1β, and NO, major molecules produced by neurotoxic microglia. Furthermore, we demonstrated that *Rt* alone was able to upregulate IL-10 at both the mRNA and protein levels, without the upregulation of proinflammatory and oxidative molecules. When IL-10 was neutralized, the mean expression levels of TNF-α and IL-1β returned to the levels observed in the absence of *Rt*. These observations indicate that *Rt* may act as a neuroprotective agent during neuroinflammation through inducing the production and secretion of IL-10, a potent negative autocrine regulator of microglia. More recently, IL-10 has been reported to alter macrophage function by promoting the clearance of damaged mitochondria and modulating cellular metabolism to inhibit inflammation [30]. Therefore, *Rt* may increase the capacity of microglia to produce IL-10 through enhanced clearance of damaged mitochondria. In this regard, *Rt* may act as a polarizing agent in microglia, favoring the shifting towards M2-like phenotype, more efficient as IL-10 producer.

The activation of the NF-κB and STAT1 signaling pathways is considered to play a critical role in the polarization of microglia in the neurotoxic phenotype, as NF-κB and STAT1 are transcription factors required for the production of TNF-α, IL-1β, and NO. The *Rt*-induced inhibition of the NF-κB and STAT1 signaling pathways activated in CGA-stimulated microglia was inhibited by neutralizing antibody against IL-10. These observations suggest that the *Rt*-induced production of IL-10 is responsible for the anti-inflammatory and antioxidative effects of *Rt* in activated microglia through the inhibition of the NF-κB and STAT1 signaling pathways. Of further note, the mean level of IL-10 in the culture medium of primary cultured microglia (200 pg/mL) was approximately seventeenfold greater than that of MG6 cells (10–14 pg/mL). MG6 cells are a mouse microglial cell line immortalized by a replication-deficient retroviral vector containing the human c-myc gene. Therefore, the c-MYC expression in microglia may result in an increased production of proinflammatory mediators and decreased production of IL-10.

We next examined the effects of seven components of *Rt*, including aloe-emodin, (+)-catechin, natannol, chrisophanol, physcion, β-sitosterol, and emodin, on the increased mRNA expression of IL-10 in microglia. Among them, aloe-emodin and (+)-catechin were able to induce the secretion of IL-10 from microglia. On the other hand, there was a discrepancy between mRNA expression and secretion of IL-10 following treatment with piceatannol. After mRNA expression, the secretion of IL-10 could be affected by many steps including translation, posttranslational modification and secretion. The present study does not allow us to exclude any of these steps.

(+)-Catechin is a naturally occurring polyphenolic compound that has been shown to have anti-inflammatory, antioxidant, and free radical-scavenging properties in vitro. (+)-Catechin has been shown to decrease the production of the proinflammatory cytokines, including IL-1β and TNF-α, and to enhance the production of the anti-inflammatory cytokine IL-10. (+)-Catechin suppresses the production of proinflammatory mediators by mouse microglia BV-2 cells and mitigation of NF-κB through intracellular signaling cascades, including Akt, extracellular-signal-regulated kinase, p38 mitogen-activated protein kinase, and AMP-activated protein kinase [31]. In contrast, aloe-emodin is a major anthraquinone in aloe plants that contains a polyphenolic structure. Aloe-emodin has been also shown to suppress the LPS-induced production of NO and prostaglandin E_2 in mouse macrophage RAW 264.7 cells [32]. Therefore,

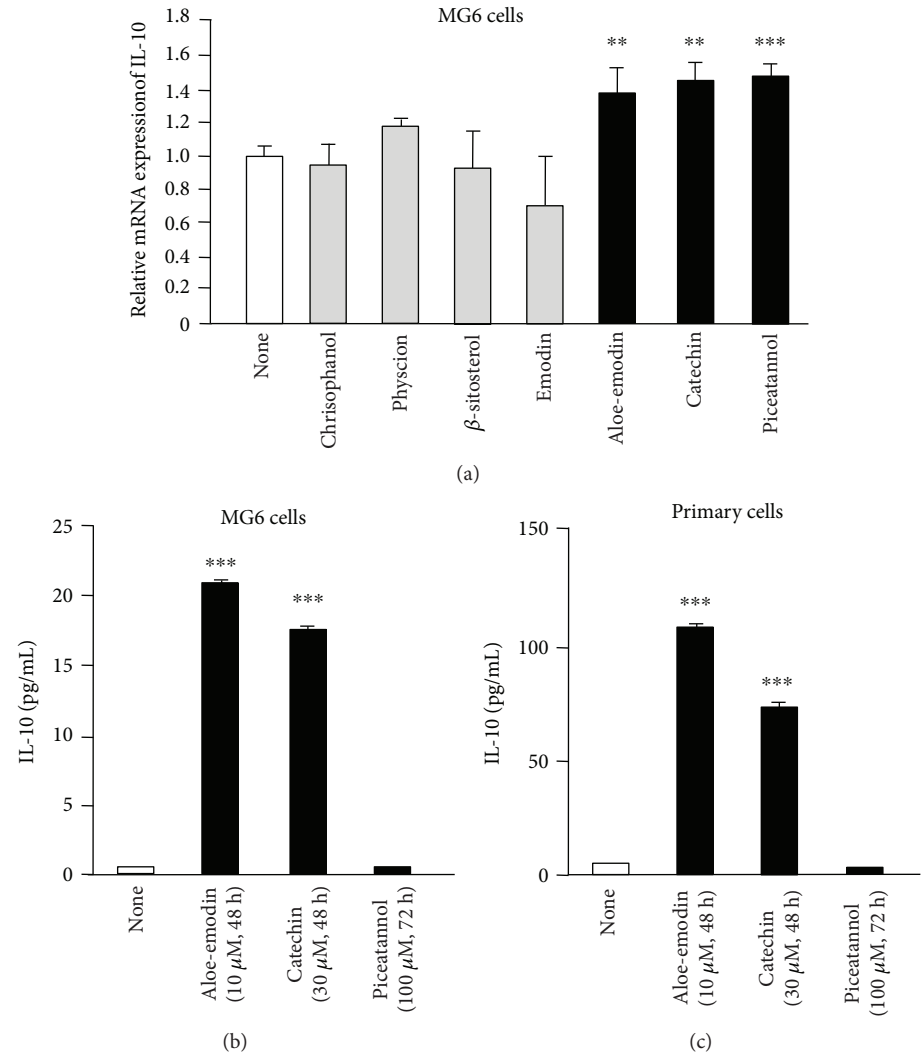

Figure 10: Possible components of *Rt* responsible for the production of IL-10 in microglia. (a) The change in the mRNA of IL-10 in MG6 cells 24 h after treatment with components of *Rt*, *including* chrisophanol, physcion, β-sitosterol, emodin, aloe-emodin, (+)-catechin, and piceatannol. The results show the relative mRNA expression of IL-10 after treatment with aloe-emodin (10 μM), (+)-catechin (30 μM), and piceatannol (100 μM) with the minimum effective doses, which were determined after treatment with three different doses (10, 30, and 100 μM) for 24 h. On the other hand, chrisophanol, physcion, β-sitosterol, and emodin with the concentration of 100 μM were applied for 24 h. The results represent the mean ± SEM of three independent experiments. The asterisks indicate a statistically significant difference from the indicated value ($^{**}P < 0.01$, $^{***}P < 0.001$). (b) The secretion of IL-10 in the medium of MG6 cells and primary cultured microglia after treatment with aloe-emodin, (+)-catechin, and piceatannol. The results show the mean IL-10 secreted in the culture medium after treatment with aloe-emodin (10 μM for 48 h) and (+)-catechin (30 μM for 48 h) with the minimum effective doses for the most effective experimental time points. The most effective experimental time points were determined after examination of three different experimental time points (24, 48 and 72 h). On the other hand, piceatannol with 100 μM was applied for 72 h. The results represent the mean ± SEM of three independent experiments. The asterisks indicate a statistically significant difference from the value in untreated cells ($^{***}P < 0.001$).

the present study suggests that the anti-inflammatory and antioxidant activities of (+)-catechin and aloe-emodin are due their abilities to induce the production and secretion of IL-10.

It has been also reported that the gene delivery of IL-10-adeno-associated virus significantly reduces neuroinflammation, enhances neurogenesis, and improves the spatial cognitive dysfunction in a transgenic AD mouse model [33]. Furthermore, it has been suggested that the IL-10 gene polymorphisms process, which favours the development of AD, reinforces the link between inflammation and cognitive decline in elderly people [34]. IL-10 has been shown to reduce IL-1β production by preventing the excessive generation of reactive oxygen species from complex II in damaged mitochondria and limiting the inflammasome activation in macrophages [30], which are characteristics of aged microglia associated with cognitive dysfunction [35, 36]. These findings support the notion that IL-10 may ameliorate neuroinflammation, cognitive dysfunction, and neurodegeneration associated with AD. Therefore, *Rt* may be useful for

the pharmacological intervention against excessive inflammatory and oxidative responses associated with AD by inducing the production of IL-10 by microglia, because some of active components of *Rt* including (+)-catechin can cross the blood-brain barrier [37].

5. Conclusions

Rt downregulates the production of proinflammatory and oxidative mediators, including IL-1β, TNF-α, and NO, by cultured activated microglia through the production of IL-10. Two components of *Rt*, aloe-emodin and (+)-catechin, are deemed responsible for the antineuroinflammatory and antioxidative effects of *Rt* through the secretion of IL-10 from microglia. Therefore, *Rt* may be useful for the pharmacological intervention against excessive inflammatory and oxidative responses associated with AD by inducing the production of IL-10 by microglia.

Disclosure

Hiroshi Nakanishi present address is Department of Pharmacology, Faculty of Pharmaceutical Sciences, Yasuda Women's University, Hiroshima 731-0153, Japan.

Conflicts of Interest

The authors declare no competing interests.

Authors' Contributions

Jie Meng performed the most of experiments, analyzed the data, and wrote the manuscript. Junjun Ni performed the experiments and analyzed the data. Zhou Wu analyzed the data and wrote the manuscript. Muzhou Jiang performed the experiments. Aiqin Zhu and Hong Qing provided materials and supervised some of the experiments. Hiroshi Nakanishi designed and supervised the experiments and wrote the manuscript.

Acknowledgments

This work was supported by Grants-in-Aid for Scientific Research (no. 17K17093 to Junjun Ni, nos. 16K11478 and 16H0848 to Zhou Wu, and no. 15H05015 to Hiroshi Nakanishi), MEXT, Japan.

References

[1] P. L. McGeer, E. McGeer, J. Rogers, and J. Sibley, "Anti-inflammatory drugs and Alzheimer disease," *The Lancet*, vol. 335, no. 8696, p. 1037, 1990.

[2] P. L. McGeer and E. G. McGeer, "The amyloid cascade-inflammatory hypothesis of Alzheimer disease: implications for therapy," *Acta Neuropathologica*, vol. 126, no. 4, pp. 479–497, 2013.

[3] B. Zhang, C. Gaiteri, L.-G. Bodea et al., "Integrated systems approach identifies genetic nodes and networks in late-onset Alzheimer's disease," *Cell*, vol. 153, no. 3, pp. 707–720, 2013.

[4] A. Olmos-Alonso, S. T. T. Schetters, S. Sri et al., "Pharmacological targeting of CSF1R inhibits microglial proliferation and prevents the progression of Alzheimer's-like pathology," *Brain*, vol. 139, no. 3, pp. 891–907, 2016.

[5] E. E. Spangenberg, R. J. Lee, A. R. Najafi et al., "Eliminating microglia in Alzheimer's mice prevents neuronal loss without modulating amyloid-β pathology," *Brain*, vol. 139, no. 4, pp. 1265–1281, 2016.

[6] D. K. Choi, S. Koppula, and K. Suk, "Inhibitors of microglial neurotoxicity: focus on natural products," *Molecules*, vol. 16, no. 2, pp. 1021–1043, 2011.

[7] Z. Wu, A. Zhu, F. Takayama et al., "Brazilian green propolis suppresses the hypoxia-induced neuroinflammatory responses by inhibiting NF-κB activation in microglia," *Oxidative Medicine and Cellular Longevity*, vol. 2013, Article ID 906726, 10 pages, 2013.

[8] J. Ni, Z. Wu, J. Meng et al., "The neuroprotective effects of Brazilian green propolis on neurodegenerative damage in human neuronal SH-SY5Y cells," *Oxidative Medicine and Cellular Longevity*, vol. 2017, Article ID 7984327, 13 pages, 2017.

[9] X. Peigen, H. Liyi, and W. Liwei, "Ethnopharmacologic study of Chinese rhubarb," *Journal of Ethnopharmacology*, vol. 10, no. 3, pp. 275–293, 1984.

[10] K. Frei, H. Lins, C. Schwerdel, and A. Fontana, "Antigen presentation in the central nervous system. The inhibitory effect of IL-10 on MHC class II expression and production of cytokines depends on the inducing signals and the type of cell analyzed," *The Journal of Immunology*, vol. 152, no. 6, pp. 2720–2728, 1994.

[11] T. Mizuno, M. Sawada, T. Marunouchi, and A. Suzumura, "Production of interleukin-10 by mouse glial cells in culture," *Biochemical and Biophysical Research Communications*, vol. 205, no. 3, pp. 1907–1915, 1994.

[12] P. A. Lodge and S. Sriram, "Regulation of microglial activation by TGF-β, IL-10, and CSF-1," *Journal of Leukocyte Biology*, vol. 60, no. 4, pp. 502–508, 1996.

[13] L. Minghetti, E. Polazzi, A. Nicolini, and G. Levi, "Opposite regulation of prostaglandin E_2 synthesis by transforming growth factor-β1 and interleukin 10 in activated microglial cultures," *Journal of Neuroimmunology*, vol. 82, no. 1, pp. 31–39, 1998.

[14] G. M. O'Keefe, V. T. Nguyen, and E. N. Benveniste, "Class II transactivator and class II MHC gene expression in microglia: modulation by the cytokines TGF-β, IL-4, IL-13 and IL-10," *European Journal of Immunology*, vol. 29, no. 4, pp. 1275–1285, 1999.

[15] M. Sawada, A. Suzumura, H. Hosoya, T. Marunouchi, and T. Nagatsu, "Interleukin-10 inhibits both production of cytokines and expression of cytokine receptors in microglia," *Journal of Neurochemistry*, vol. 72, no. 4, pp. 1466–1471, 1999.

[16] P. Shrikant, E. Weber, T. Jilling, and E. N. Benveniste, "Intercellular adhesion molecule-1 gene expression by glial cells. Differential mechanisms of inhibition by IL-10 and IL-6," *The Journal of Immunology*, vol. 155, no. 3, pp. 1489–1501, 1995.

[17] S. Hu, C. C. Chao, L. C. Ehrlich et al., "Inhibition of microglial cell RANTES production by IL-10 and TGF-β," *Journal of Leukocyte Biology*, vol. 65, no. 6, pp. 815–821, 1999.

[18] A. F. Richwine, N. L. Sparkman, R. N. Dilger, J. B. Buchanan, and R. W. Johnson, "Cognitive deficits in interleukin-10-

deficient mice after peripheral injection of lipopolysaccharide," *Brain, Behavior, and Immunity*, vol. 23, no. 6, pp. 794–802, 2009.

[19] K. W. Moore, R. de Waal Malefyt, R. L. Coffman, and A. O'Garra, "Interleukin-10 and the interleukin-10 receptor," *Annual Review of Immunology*, vol. 19, no. 1, pp. 683–765, 2001.

[20] A. Ledeboer, J. J. P. Brevé, A. Wierinckx et al., "Expression and regulation of interleukin-10 and interleukin-10 receptor in rat astroglial and microglial cells," *European Journal of Neuroscience*, vol. 16, no. 7, pp. 1175–1185, 2002.

[21] F. Zhang, J. Liu, and J.-S. Shi, "Anti-inflammatory activities of resveratrol in the brain: role of resveratrol in microglial activation," *European Journal of Pharmacology*, vol. 636, no. 1–3, pp. 1–7, 2010.

[22] J. Song, S. Cheon, W. Jung, W. Lee, and J. Lee, "Resveratrol induces the expression of interleukin-10 and brain-derived neurotrophic factor in BV2 microglia under hypoxia," *International Journal of Molecular Sciences*, vol. 15, no. 9, pp. 15512–15529, 2014.

[23] A. Cianciulli, T. Dragone, R. Calvello et al., "IL-10 plays a pivotal role in anti-inflammatory effects of resveratrol in activated microglia cells," *International Immunopharmacology*, vol. 24, no. 2, pp. 369–376, 2015.

[24] C. B. Larmonier, J. K. Uno, K.-M. Lee et al., "Limited effects of dietary curcumin on Th-1 driven colitis in IL-10 deficient mice suggest an IL-10-dependent mechanism of protection," *American Journal of Physiology-Gastrointestinal and Liver Physiology*, vol. 295, no. 5, pp. G1079–G1091, 2008.

[25] T. Takenouchi, K. Ogihara, M. Sato, and H. Kitani, "Inhibitory effects of U73122 and U73343 on Ca^{2+} influx and pore formation induced by the activation of P2X7 nucleotide receptors in mouse microglial cell line," *Biochimica et Biophysica Acta (BBA) - General Subjects*, vol. 1726, no. 2, pp. 177–186, 2005.

[26] D. F. Sastradipura, H. Nakanishi, T. Tsukuba et al., "Identification of cellular compartments involved in processing of cathepsin E in primary cultures of rat microglia," *Journal of Neurochemistry*, vol. 70, no. 5, pp. 2045–2056, 1998.

[27] O. Yasuhara, I. Akiguchi, S. Nakamura et al., "Pancreastatin-like immunoreactivity in globular dystrophic neurites of senile plaques in brains of patients with Alzheimer's disease," *Neuroscience Letters*, vol. 208, no. 3, pp. 167–170, 1996.

[28] C.-M. Rangon, S. Haïk, B. A. Faucheux et al., "Different chromogranin immunoreactivity between prion and a-beta amyloid plaque," *NeuroReport*, vol. 14, no. 5, pp. 755–758, 2003.

[29] Z. Wu, L. Sun, S. Hashioka et al., "Differential pathways for interleukin-1β production activated by chromogranin A and amyloid β in microglia," *Neurobiology of Aging*, vol. 34, no. 12, pp. 2715–2725, 2013.

[30] W. K. E. Ip, N. Hoshi, D. S. Shouval, S. Snapper, and R. Medzhitov, "Anti-inflammatory effect of IL-10 mediated by metabolic reprogramming of macrophages," *Science*, vol. 356, no. 6337, pp. 513–519, 2017.

[31] S. S. Syed Hussein, M. N. A. Kamarudin, and H. Abdul Kadir, "(+)-Catechin attenuates NF-κB activation through regulation of Akt, MAPK, and AMPK signaling pathways in LPS-induced BV-2 microglial cells," *The American Journal of Chinese Medicine*, vol. 43, no. 5, pp. 927–952, 2015.

[32] M.-Y. Park, H.-J. Kwon, and M.-K. Sung, "Evaluation of aloin and aloe-emodin as anti-inflammatory agents in aloe by using murine macrophages," *Bioscience, Biotechnology, and Biochemistry*, vol. 73, no. 4, pp. 828–832, 2009.

[33] T. Kiyota, K. L. Ingraham, R. J. Swan, M. T. Jacobsen, S. J. Andrews, and T. Ikezu, "AAV serotype 2/1-mediated gene delivery of anti-inflammatory interleukin-10 enhances neurogenesis and cognitive function in APP+PS1 mice," *Gene Therapy*, vol. 19, no. 7, pp. 724–733, 2012.

[34] C. A. Magalhães, M. d. G. Carvalho, L. P. d. Sousa, P. Caramelli, and K. B. Gomes, "Alzheimer's disease and cytokine IL-10 gene polymorphisms: is there an association?," *Arquivos de Neuro-Psiquiatria*, vol. 75, no. 9, pp. 649–656, 2017.

[35] H. Nakanishi and Z. Wu, "Microglia-aging: roles of microglial lysosome- and mitochondria-derived reactive oxygen species in brain aging," *Behavioural Brain Research*, vol. 201, no. 1, pp. 1–7, 2009.

[36] H. Nakanishi, Y. Hayashi, and Z. Wu, "The role of microglial mtDNA damage in age-dependent prolonged LPS-induced sickness behavior," *Neuron Glia Biology*, vol. 7, no. 1, pp. 17–23, 2011.

[37] L. Wu, Q. L. Zhang, X. Y. Zhang et al., "Pharmacokinetics and blood–brain barrier penetration of (+)-catechin and (−)-epicatechin in rats by microdialysis sampling coupled to high-performance liquid chromatography with chemiluminescence detection," *Journal of Agricultural and Food Chemistry*, vol. 60, no. 37, pp. 9377–9383, 2012.

Hindawi
Oxidative Medicine and Cellular Longevity
Volume 2018, Article ID 4039753, 15 pages
https://doi.org/10.1155/2018/4039753

Research Article

Antifibrogenic Influence of *Mentha piperita* L. Essential Oil against CCl_4-Induced Liver Fibrosis in Rats

Hanan A. Ogaly,[1] **Nadia A. Eltablawy**,[2] **and Reham M. Abd-Elsalam**[3]

[1]*Department of Chemistry, College of Sciences, King Khalid University, Abha, Saudi Arabia*
[2]*Biochemistry Division, National Organization for Drug Control and Research (NODCAR), Giza, Egypt*
[3]*Department of Pathology, Faculty of Veterinary Medicine, Cairo University, Giza, Egypt*

Correspondence should be addressed to Hanan A. Ogaly; ohanan@kku.edu.sa

Received 11 October 2017; Revised 10 January 2018; Accepted 18 January 2018; Published 19 April 2018

Academic Editor: Sudipta Saha

Essential oils of some aromatic plants provide an effective nonmedicinal option to control liver fibrosis. *Mentha piperita* L. essential oil (MPEO) have been reported to possess protective effects against hepatotoxicity. However, its effect against liver fibrosis remains unknown. The present study investigated the antifibrogenic potential of MPEO and its underlying mechanisms. Forty male rats divided into 4 groups were used: group 1 served as normal control, group 2 (liver fibrosis) received CCl_4 (2.5 mL/kg, IP, twice weekly) for 8 weeks, group 3 concurrently received CCl_4 plus MPEO (50 mg/kg, IP, daily, from the 3rd week), and group 4 received MPEO only. MPOE significantly improved the liver injury markers, lipid peroxidation (LPO), antioxidant capacity, CYP2E1 gene expressionand liver histology. Furthermore, MPOE ameliorated liver fibrosis as evidenced by the reduced expression of desmin, α-smooth muscle actin (α-SMA), transforming growth factor-β1 (TGF-β1), and SMAD3 proteins. In addition, MPOE counteracted the p53 upregulation induced by CCl_4 at both mRNA and protein levels. In conclusion, MPOE could effectively attenuate hepatic fibrosis mainly through improving the redox status, suppressing p53 and subsequently modulating TGF-β1 and SMAD3 protein expression. These data promote the use of MPOE as a promising approach in antifibrotic therapy.

1. Introduction

Liver fibrosis and cirrhosis are the ultimate consequences of chronic hepatic injury induced by various etiological agents [1]. The mechanism of liver fibrosis has been extensively studied. However, effective antifibrotic therapies are lacking [2]. The pathogenesis of hepatic fibrosis is generally based on the activation of HSCs and excessive extracellular matrix (ECM) production [2]. Oxidative stress plays a central role in triggering these inflammatory and fibrotic responses [3]. Among the various signaling pathways involved in pathogenesis of liver fibrosis, TGF-β1/SMAD is considered the most significant signaling pathway [4]. Therefore, inhibiting TGF-β1 was found to be efficient in attenuating liver fibrosis [5, 6]. The tumor suppressor p53 is another important cell signal primarily stimulated in response to oxidative damage and oncogene activation [7]. Accumulating evidences suggested the involvement of p53 in the pathophysiology of various nontumoral fibrotic liver diseases in both human and animals [8, 9]. These data suggest that p53 regulation could serve as an important therapeutic target for fibrotic liver diseases.

Medicinal plants and their derivatives contain a wide variety of bioactive phytochemicals with a diverse pharmacological spectrum [10, 11]. Essential oils constituents including terpenes, terpenoids, phenylpropenes, and other degradation products have been reported to exhibit strong antioxidant and anti-inflammatory activities [12]. The effectiveness of some essential oils to alleviate the hepatotoxicity [13] and hepatic fibrosis [14] has been proven. *Mentha piperita* L. (peppermint) is one of the most popular and widely used herbs. Pharmacological investigations have

demonstrated that *M. piperita* possesses analgesic, antifungal [15], antibacterial [16], antiparasitic, and immunomodulatory activities [17]. Moreover, the hepatoprotective effects of *M. piperita* leaves extract [18], oil [19, 20], or its active components menthol and menthone [21] have been reported. However, to the best of our knowledge, the effect against hepatic fibrosis has not been reported. Therefore, the present study aimed to investigate the effects of *Mentha piperita* L. essential oil (MPEO) against hepatic fibrosis and to elucidate the potential underlying molecular mechanisms.

2. Material and Methods

2.1. MPOE Preparation and Characterization. *Mentha piperita* L. leaves were purchased from Harraz Drug stores (Cairo, Egypt). A voucher specimen of the studied plant material was deposited at Biochemistry Department, National Organization for Drug Control and Research (NODCAR), Egypt. Essential oil was extracted and characterized for its chemical composition using gas-liquid chromatography coupled to mass spectrometry (GC-MS) as described by Ogaly et al. [14].

2.2. Experimental Design. Adult male rats (150–170 g) were obtained from the breeding unit of the Research Institute of Ophthalmology (Giza, Egypt). Rats were housed under constant temperature and 12 h light/dark cycle with free access to water and standard chow diet. All animal procedures were performed according to the protocol approved by the Institutional Animal Care and Use Committee (IACUC), Cairo University (CU-II-F-1-18).

Forty rats were randomly divided into four groups. Group 1 (control) was given corn oil (2 mL/kg, IP). Group 2 (fibrosis model) was given CCl_4 1 : 4 mixture with corn oil (2.5 mL/kg, IP) twice weekly for eight weeks. Rats in group 3 received CCl_4 for two weeks to establish liver injury and fibrosis and then treated with MPOE (50 mg/kg, IP), daily from the 3rd to 8th week. Group 4 received MPOE (50 mg/kg, IP) from the 3rd to 8th week. The selected dose for MPOE (50 mg/kg) was previously reported to be hepatoprotective for rats [20].

2.3. Samples Collection. At the end of experiment, animals were anesthetized with ethyl ether. Blood samples (3-4 mL) were collected by retro-orbital puncture, and serum was separated by centrifugation (4000 rpm/10 min). Afterward, all animals were sacrificed by cervical dislocation under ethyl ether anesthesia for humane reasons; the whole liver was immediately removed, rinsed in cold normal saline, and kept at −20°C until further analyses. Liver homogenates (10%) were prepared in 0.1 M ice-cold phosphate buffered saline (pH 7.4) followed by centrifugation at 14,000 ×g, 15 min at 4°C. The separated supernatants were kept at −20°C. For histopathological examination, parts of liver were fixed in 10% neutral buffered formalin and underwent routine processing for paraffin embedding.

2.4. Biochemical Analyses. Serum samples were used to measure liver injury markers alanine aminotransferase (ALT) and aspartate aminotransferase (AST) according to the method of Reitman and Frankel [22]. Liver homogenates were used for measurement of nitric oxide (NO) [23], malondialdehyde (MDA) as a thiobarbituric acid reactive substance (TBARS) [24], superoxide dismutase (SOD) activity [25], catalase (CAT) activity [26], reduced glutathione (GSH) level [27], and total antioxidant capacity (TAC) using commercial kits (Biodiagnostic, Cairo, Egypt). Total protein content was measured according to the method of Bradford [28].

2.5. Histopathological Analyses. Seven liver samples were harvested from each experimental group and fixed in 10% neutral buffered formalin and then processed to obtain 4 μm paraffin-embedded sections. The sections were stained with hematoxylin and eosin (H&E) and Masson's trichrome (MT). MT staining was performed to assess collagen fibers distribution and to determine liver fibrosis %. A numerical scoring system [29] was performed to assess the grade of fibrosis, as follows: 0, no fibrosis (normal); 1, fibrous expansion of some portal areas; 2, fibrous expansion of most portal areas; 3, fibrous expansion of most portal areas with occasional portal-to-portal bridging; 4, fibrous expansion of portal areas with marked bridging (portal to portal as well as portal to central); 5, marked bridging (portal to central as well as central to central) with occasional nodules formation; and 6, cirrhosis.

2.6. Immunohistochemical Analyses. The immunohistochemical (IHC) analyses were done according to the methods of Ogaly et al. [14]. Briefly, tissue sections were deparaffinized and rehydrated. The antigen retrieval was performed by pretreating the tissue sections for 20 min with citrate buffer pH 6 at microwave oven. Sections were incubated with rabbit polyclonal antibody to α-SMA diluted 1 : 200 (ab5694; Abcam, Cambridge, UK), rabbit polyclonal antidesmin antibody diluted 1 : 200 (ab15200; Abcam, Cambridge, UK), rabbit polyclonal anti-TGF-β1 antibody with concentration of 20 μg/mL (ab92486; Abcam, Cambridge, UK), rabbit polyclonal anti-SMAD3 antibody diluted 1 : 100 (ab28379; Abcam, Cambridge, UK), and rabbit polyclonal anti-Tp53 antibody diluted 1 : 100 (ab131442; Abcam, Cambridge, UK) for two hours in a humidified chamber. The tissue sections were incubated with goat antirabbit IgG H&L (HRP) (ab205718; Abcam, Cambridge, UK). Finally, the slides were incubated for 10 min with 3,3′-diaminobenzidine tetrahydrochloride (DAB; Sigma) as chromagen, counterstained with hematoxylin, and mounted with DPX. The image analyses of the stained sections were performed by Leica Qwin 500 Image Analyzer (Leica, Cambridge, England). In each group, seven sections were examined. The percentage of the immunopositive area (%) was calculated as mean of 10 fields/section.

2.7. Gene Expression Analyses. Total RNA isolated from liver tissues using RNeasy Mini Kit (Qiagen) was reverse transcribed and subjected to quantitative real-time RT-PCR as previously described [14]. mRNA expression levels of Tp53 and CYP2E1 genes were assessed using GAPDH gene as the reference gene. Briefly, cDNA was added to a Quantifast SYBR Green qPCR Master Mix (Qiagen) containing 30 pg/mL of each primer (Table 1). The thermal program

Table 1: Primers sequences.

Gene		Primer sequence	Ref.
GAPDH	Forward	5′-ACCACAGTCCATGCCATCAC-3′	[81]
	Reverse	5′-TCCACCACCCTGTTGCTGTA-3′	
TP53	Forward	5′-TCCCTAAGTATCCTCAGTGA-3′	[82]
	Reverse	5′-GTAATCGAAGCGTTTGTTGA-3′	
CYP2E1	Forward	5′-TCCAGGTTTGCACCAGACTCT-3′	[14]
	Reverse	5′-TCCACCACCCTGTTGCTGTA-3′	

Table 2: Chemical composition of MPEO by GC/MS.

Retention time	Compound	Relative %
4.8	Limonene	0.78
5.1	1,8-Cineol	1.35
6.8	*p*-Menthone	18.30
7.6	Beta pinene	1.10
8.2	*iso*-Menthone	5.31
8.4	Menthol	46.70
8.9	Pulegone	6.30
8.92	D-Camphor	3.30
9.1	L-Carvone	15.20
12.8	*trans*-Caryophyllene	0.95
	Total	99.35

included 40 cycles of denaturation at 95°C for 15 s, annealing at 60°C for 15 s, and extension at 72°C for 45 s. The first denaturation was extended to 1 min. Calculation of gene expression was done following Livak and Schmittgen [30].

2.8. Statistical Analysis. SPSS version 16.0 statistical package was used to analyze the data. All data were expressed as mean ± standard error (SE). One-way analysis of variance (ANOVA) was used to assess the differences between groups. Difference was considered statistically significant at $p < 0.05$ by Duncan's multiple comparisons.

3. Results

3.1. Chemical Composition of MPEO. Hydrodistilled MPEO was subjected to qualitative and quantitative analyses using gas chromatography coupled with mass spectrophotometry (GC-MS). Ten chemical constituents could be identified by elution on HP-5872 column (Table 2). The major constituents of MPEO, in order of their percentage (Figure 1), were menthol (46.7%), *p*-menthone (18.3%), L-carvone (15.2%), pulegone (6.3%), *iso*-menthone (5.3%), and D-camphor (3.3%). Small amounts of 1,8-cineol, beta pinene, *trans*-caryophyllene, and limonene were also identified.

3.2. MPEO Improves Liver Functions in CCl_4-Induced Liver Fibrosis. As shown in Table 3, CCl_4-intoxicated rats (group 2) showed a severe increase in liver marker enzymes, ALT and AST, to about 62- and 23-folds, respectively, compared to the control group. MPOE coadministration (group 3) exerted a significant reduction of ALT and AST levels to 76.8% and 60.4%, respectively, as compared to the CCl_4 group. There were no significant differences in liver enzymes between groups 1 and 4 (Table 3).

3.3. MPEO Attenuates Oxidative Stress in CCl_4-Induced Liver Fibrosis. CCl_4 caused a marked disruption of oxidant/antioxidant balance in liver as indicated by the statistically significant elevation in MDA and NO levels to 236% and 407% in group 2 as compared to the control group (Table 3). Besides, there was a marked reduction in SOD and CAT antioxidant enzymes activities with a dramatic depletion in hepatic GSH content to 24.4%, 43.2%, and 23.4% of the control levels, respectively (Table 4). In the same line, TAC of the liver of CCl_4-intoxicated group showed a significant reduction to 39.7% (Table 4). Administration of MPOE concurrently with CCl_4 for 6 weeks (group 3) showed a significant reduction of MDA and NO levels compared to those of group 2 (Table 3). MPOE partially restored SOD and CAT activities and GSH level (Table 4). Improvement of CCl_4-induced oxidative stress by MPOE was confirmed by the significant elevation of TAC, reaching 74% of the normal control level (Table 4). There were no significant differences in all measured oxidative stress markers or antioxidant parameters between groups 1 and 4 (Tables 3 and 4).

3.4. MPEO Ameliorates Fibrotic Alterations in CCl_4-Induced Liver Fibrosis. The histopathological examination of the normal and MPOE groups revealed normal histological hepatic architecture (Figures 2(a) and 2(d)). The fibrosis control group (group 2) showed marked fatty degeneration of the hepatocytes, hepatocellular necrosis with mononuclear inflammatory cell aggregation, and collagen fibers bridging (Figure 2(b)). Group 3, receiving CCl_4 + MPOE, showed marked attenuation of the previously described histopathological lesions compared to the fibrotic control group (Figure 2(c)). With MT staining, the liver of the control and MPEO groups showed normal distribution of collagen fibers (Figures 3(a) and 3(d)). The fibrotic control group showed severe bridging fibrosis with marked collagen deposition in the liver extending from portal to portal, portal to central, and central to central and formation of pseudolobules (Figure 3(b)). In group 3 (CCl_4 + MPEO), the collagen deposition was markedly reduced, and the collagenous septa became thinner than those of the fibrotic control group (Figure 3(c)). The histopathological grading of liver fibrosis and the morphometric analysis of liver fibrosis % in different groups are shown in Table 5 and Figure 3(e), respectively, group 1 and 4 showed no significant difference in the liver fibrosis grading or fibrosis % (Figure 3(e) and Table 5). Group 3 (CCl_4 + MPEO) showed significant reduction of the grading of liver fibrosis and fibrosis % compared to the fibrosis control group 2 as shown in Figure 3(e) and Table 5.

3.5. MPEO Regulates Profibrogenic Protein Expression in CCl_4-Induced Fibrosis. α-SMA and desmin immunoreactivity

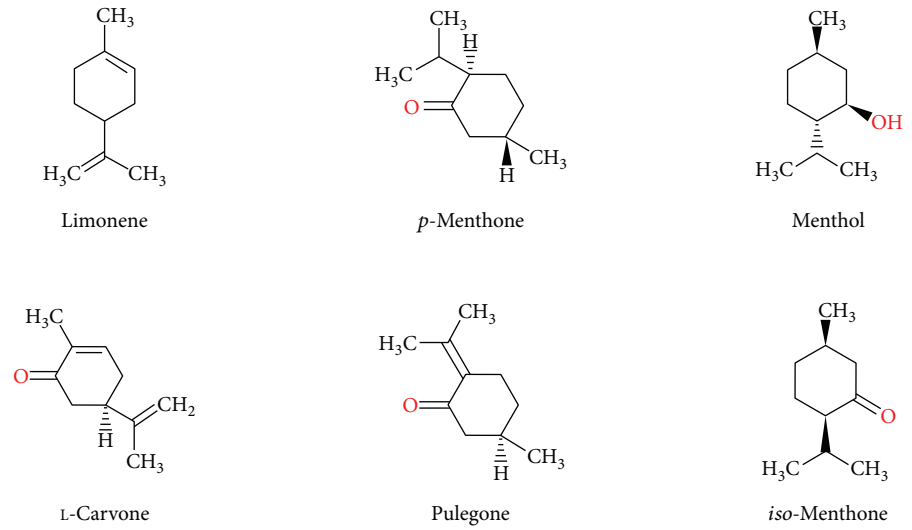

Figure 1: Antioxidant volatile constituents found in *Mentha piperita* essential oil.

Table 3: Effects of MPEO on liver enzymes, NO content, and lipid peroxidation byproduct (MDA) in CCl_4-induced liver fibrosis.

Experimental groups	ALT (U/L)	AST (U/L)	MDA (μM/g tissue)	NO (mmol/L)
Group 1	18.4 ± 0.84	46 ± 1.52	60.8 ± 2.47	3.98 ± 0.32
Group 2	1147.2 ± 42.25	1088 ± 65.73	143.8 ± 3.97	16.21 ± 0.89
Group 3	882 ± 83.19	657 ± 31.74	89.14 ± 3.16	7.11 ± 0.72
Group 4	34 ± 1.12	69 ± 1.47	71.32 ± 2.36	5.42 ± 0.68

Group 1: normal control; group 2: liver fibrosis control; group 3: MPEO-treated; group 4: MPEO control. Values are expressed as mean ± SE. Different superscripts mean significant differences between groups in the same column at $p < 0.05$. ALT: alanine transaminase; AST: aspartate transaminase; NO: nitric oxide; MDA: malondialdehyde.

Table 4: Effects of MPEO on the hepatic antioxidant profile in CCl_4-induced liver fibrosis.

Experimental groups	GSH (μM/g liver)	SOD (U/mg protein)	CAT (U/mg protein)	TAC (μmol/g liver)
Group 1	12.48 ± 0.32^a	82.95 ± 2.56^a	2.15 ± 0.07^a	5.24 ± 0.25^a
Group 2	2.93 ± 0.14^b	20.29 ± 1.13^b	0.93 ± 0.06^b	2.08 ± 0.16^b
Group 3	4.8 ± 0.19^c	47.6 ± 1.22^c	1.37 ± 0.05^c	3.88 ± 0.12^c
Group 4	11.6 ± 0.31^a	72.45 ± 2.10^a	1.94 ± 0.04^a	4.30 ± 0.22^a

Group 1: normal control; group 2: liver fibrosis control; group 3: MPEO-treated; group 4: MPEO control. Values are expressed as mean ± SE. Different superscripts mean significant differences between groups in the same column at $p < 0.05$. GSH: reduced glutathione; SOD: superoxide dismutase; CAT: catalase; TAC: total antioxidant capacity.

appeared to be cytoplasmic and stained brown in colour. α-SMA expression was seen in smooth muscle cells of the blood vessels in the normal control and the MPOE control (Figures 4(a) and 4(d)). In the liver fibrosis control group, α-SMA staining located in the myofibroblast cells along collagenous septa bridging portal areas and central areas and desmin immunostaining was observed in perisinusoidal cells and interstitial myofibroblasts. α-SMA and desmin protein expression were significantly elevated in liver fibrosis control group than in the normal control (Figures 4 and 5). Group 3 (MPOE-treated) showed a significant reduction of α-SMA and desmin protein expression compared to the liver fibrosis control group (Figures 4 and 5). TGF-β1 was a cytoplasmic immunostaining, and it was observed in periductal cells in the portal tract of the normal control and MPOE control groups (Figures 6(a) and 6(d)). SMAD3 expression was nuclear and cytoplasmic immunostaining. The fibrotic control group showed TGF-β1 immunoreactivity in the periductal cells in the portal tract, in perisinusoidal cells, around the blood vessels, in sinusoidal lining cells, in inflammatory cells, and in the network around the necrotic hepatocytes; and a small amount was observed in necrotic hepatocytes. TGF-β1 and SMAD3 protein expression were significantly increased in the liver fibrosis control group than in the normal control (Figures 6 and 7). Group 3 (MPOE-treated) showed a sustained reduction of TGF-β1 and SMAD3 protein expression compared to the liver fibrosis control group (Figures 6 and 7, resp.). No significant difference was recorded between the normal control and MPOE control groups.

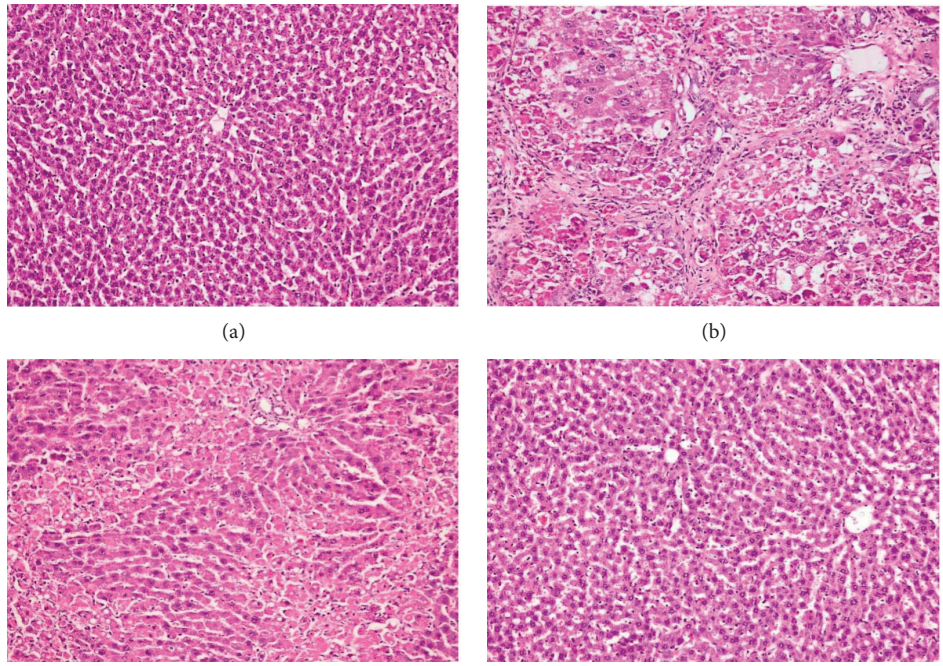

Figure 2: Histopathological examination of the liver tissues (H&E, ×200). (a) Group 1 (normal control) showing normal histological picture of the liver. (b) Group 2 (fibrosis control) showing fatty degeneration of the hepatocytes, hepatocellular necrosis, and mononuclear inflammatory cells aggregation along the collagenous septa. (c) Group 3 (MPEO-treated) showing moderate hepatocellular necrosis, marked reduction of collagenous septa formation and mononuclear inflammatory cells aggregation. (d) Group 4 (MPEO control) showing normal hepatic cellular architecture.

3.6. MPEO Downregulates p53 Expression in CCl_4-Induced Fibrosis. Tp53 gene expression level showed a significant elevation in the liver fibrosis control (group 2). Tp53 mRNA level reached to about 16-folds of the control level. This CCl_4-induced overexpression of Tp53 was markedly suppressed in MPOE-treated rats to about 2-fold as compared to that in the control (Figure 8(a)). At the protein level, p53 immunoreactivity was significantly increased in the liver fibrosis control. Group 3 treated with CCl_4 + MPOE showed significantly decreased p53 immunoreactivity (Figure 9(c)). Figure 9(e) summarizes the IHC analysis of p53 protein expression in the different groups. Nonsignificant differences in p53 mRNA and protein levels were detected between groups 1 and 4 (Figures 8(a) and 9), respectively.

3.7. MPEO Restored CYP2E1 Expression in CCl_4-Induced Liver Fibrosis. Quantitative RT-PCR analysis showed a significant decrease in CYP2E1 mRNA in the liver fibrosis control group to 27% of that of the control group. MPOE-treated rats in group 3 showed marked increase in mRNA level to +2.32-folds of the normal level (Figure 8(b)).

4. Discussion

Fibrogenesis is a multicellular wound healing process that occurs as a frequent consequence of many chronic liver injuries [1]. Regardless of its etiology, hepatic fibrosis is generally characterized by oxidative tissue damage, inflammatory cells infiltration, HSCs activation, and excessive collagen deposition [31, 32]. Accumulating clinical and experimental evidences have shown that the halting of the fibrogenic process may allow the reversal of liver fibrosis. Indeed, resolution of liver fibrosis or even cirrhosis may occur upon eradication of the causative insult [33, 34]. Oxidative stress has been proposed as a conjoint pathological mechanism in the initiation and progression of fibrosis [3]. Thereby, inhibition of ROS-mediated fibrogenesis might yield great potential therapeutic benefits. In this context, attention is progressively shifting towards herbal products and their antioxidant constituents [3, 11]. *M. piperita* has been known for its great multipharmaceutical benefits [35, 36]. The active phytocompounds of MPEO contribute to many of its profound therapeutic actions. Although the hepatoprotective effect of MPOE was previously demonstrated [18, 19], its antifibrogenic influence against hepatic fibrosis has not been investigated yet. The present study aimed to evaluate the potential of MPOE to ameliorate CCl_4-induced hepatic fibrosis in rats and to elucidate some aspects of its underlying molecular mechanisms.

MPEO was reported to have a wide range of components, including menthol, menthone, menthofuran, and methyl acetate, and other pharmacologically active compounds such as flavonoids, tannins, and caffeic acid [37]. In the current study, the chemical profile of MPEO, as presented in Table 2, is characterized by the dominant presence of the oxygenated monoterpenes menthol (46.7%) and menthone (18.3%). A high percentage of carvone (15%) was observed compared to that of the composition previously reported by Sun et al. [38].

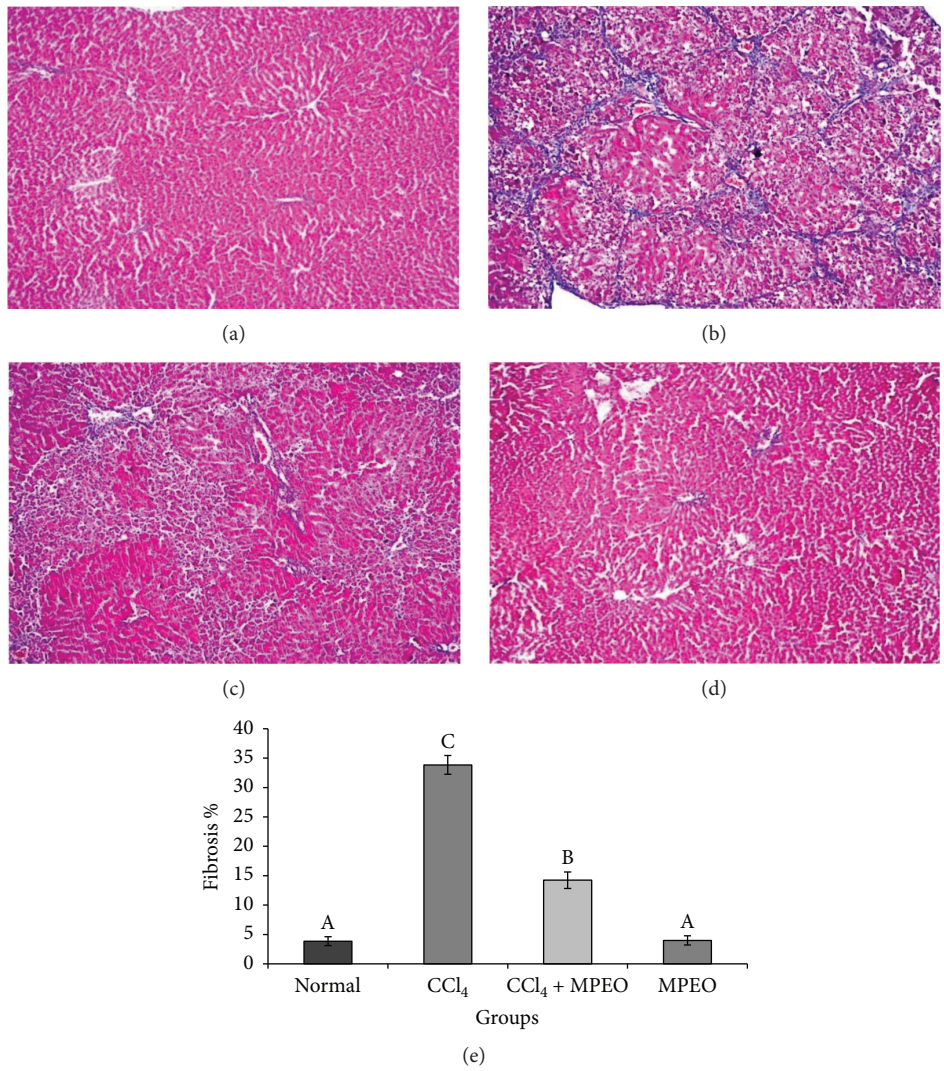

Figure 3: Photomicrograph of liver stained with MT stain (×100). (a and d) The normal control (group 1) and MPEO control (group 4) showing normal distribution of collagen fibers in the portal areas. (b) Group 2 (fibrosis control) showing marked fibrous bridging with excessive collagen fibers deposition. (c) Group 3 (MPEO-treated) showing marked attenuation of collagen fibers distribution and deposition. (e) Bar chart represents the hepatic fibrosis expressed as fibrosis %. Mean values with different superscripts are significantly different ($p < 0.05$).

Table 5: Effect of MPEO on the pathological grading of CCl_4-induced fibrotic liver in rats.

Group	n	Pathological grading of hepatic fibrosis							p value
		0	I	II	III	IV	V	VI	
Group 1	7	7	0	0	0	0	0	0	—
Group 2	7	0	0	0	2	4	1	0	0.00[a]
Group 3	7	0	3	3	1	0	0	0	0.011[b]
Group 4	7	7	0	0	0	0	0	0	—

Group 1: normal control; group 2: liver fibrosis control; group 3: MPEO-treated; group 4: MPEO control. Data are presented as the mean of ten fields. n: number of rats. [a]Significant difference from the control group at $p < 0.01$. [b]Significant difference from model group at $p < 0.05$.

Different chemotypes of *M. piperita* were reported in other countries in which the major constituent in MPEO is linalool as in *M. piperita* collected from Brazil [39] or limonene as in *M. piperita* collected from India [40]. This diversity in the chemical composition may be attributed to geographical and soil condition, biosynthetic factors, and collection time [38]. However, the composition of MPEO presented in the current study still maintains a certain level of chemosimilarity with some previously reported MPEO compositions [38]. Mentha species are known for their ability to exhibit strong antioxidant and radical scavenging activities owing to the presence of valuable secondary metabolites in the essential oil and phenolic substances [41]. Previous studies showed that the radical scavenging activity of essential oil of *M. piperita* species is attributed to the presence of menthone and menthol, with the presence of the hydroxyl radical ($^{\bullet}OH$). The vast

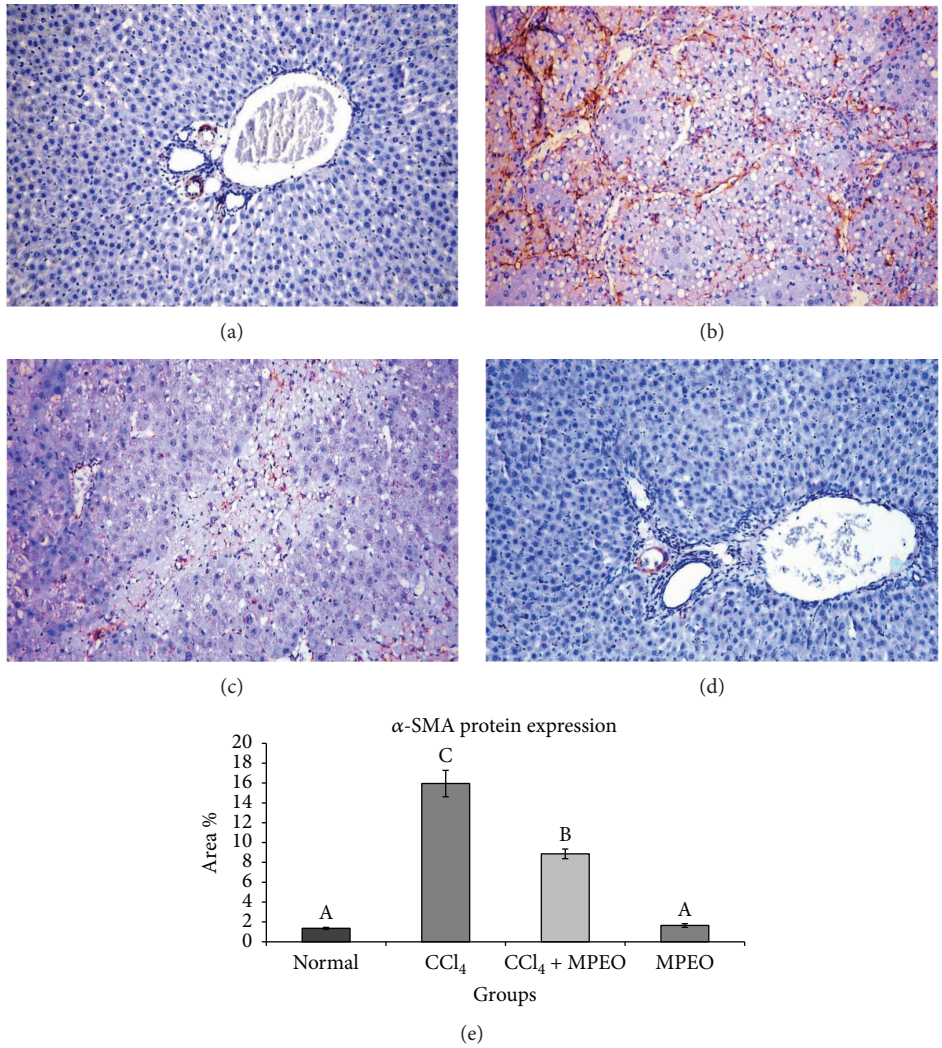

Figure 4: Representative α-SMA immunohistochemistry in liver tissues of the different experimental groups (×200). (a and d) The normal control (group 1) and MPEO control (group 4) showing α-SMA staining in the smooth muscle cells of the hepatic vessels. (b) Liver fibrosis control (group 2) showing strong immunostaining reaction in myofibroblast cells. (c) MPEO-treated (group 3) showing marked reduction in immunopositive reactive areas. (e) Bar chart represents the α-SMA immunohistochemistry expressed as area %. Mean values with different superscripts are significantly different ($p < 0.05$).

majority of these antioxidants (Figure 1) have the ability to trap the free radicals and interrupt the chain reaction due to the presence of at least one aromatic ring in their structures [42].

CCl_4-induced fibrosis has been extensively used as an *in vivo* model for the study of liver damage [14, 43, 44]. CCl_4 toxicity represents a multifactorial process involving its detoxification by CYP450 into the highly reactive CCl_4-derived free radicals, covalent binding to macromolecules, stimulation of inflammatory cytokines, oxidative damage with subsequent necrosis of hepatocytes, and activation of HSCs [44].

Fibrogenesis is mediated by a complex interplay of signaling pathways. Of particular note, TGF-β1/SMAD is one of the core mechanisms of fibrogenesis [45]. Recently, much information has emerged concerning the central role of TGF-β1 as the principal driver of excessive scarring and tissue fibrosis. TGF-β1, in HSCs, acts by stimulating collagen I expression and inhibiting ECM degradation [4, 46]. Excessive TGF-β1 release by necrotic hepatocytes is considered as one of the first signals to adjacent quiescent HSCs to be activated by transdifferentiation into myofibroblasts-like cells [47]. Upon activation, TGF-β1 binds to its cell-surface receptor complexes and initiates an intracellular signaling cascade resulting in phosphorylation of SMAD2 and SMAD3. Subsequently, the activated SMAD2 and SMAD3 form stable oligomer complexes with SMAD4. These complexes actively shuttle into the nucleus to regulate the transcription of target genes [48, 49]. It has been demonstrated that SMAD3 is a key element in TGF-β1–induced fibrosis [50]. A number of fibrogenic genes (e.g., collagens) and markers (e.g., α-SMA) are SMAD3-dependent as SMAD3 directly binds to the DNA regulatory sequences of these target genes [51, 52]. Moreover, SMAD3 inhibits matrix metalloprotease 1 activity in fibroblasts and activates tissue inhibitor of metalloproteases and thus inhibits

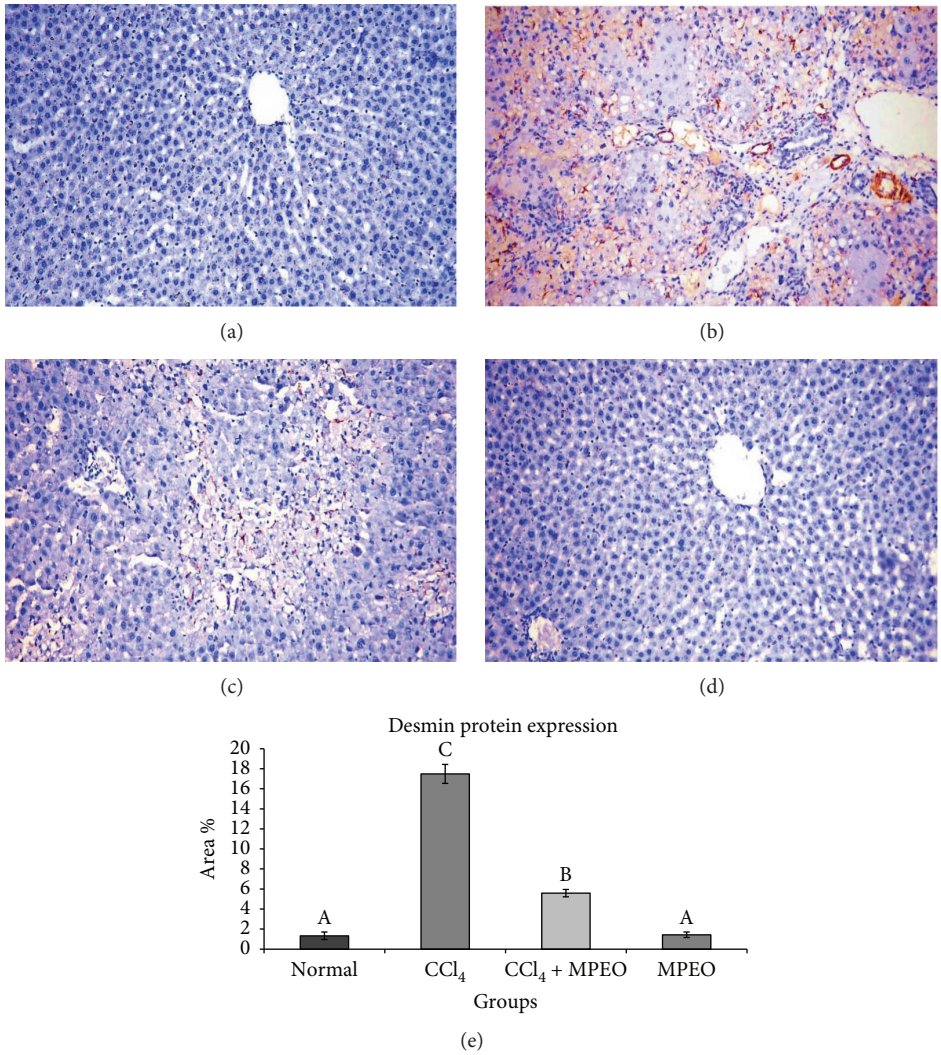

Figure 5: Representative desmin immunohistochemistry in liver tissues of the different experimental groups (×200). (a and d) The normal control (group 1) and MPEO control (group 4) showing very weak immunopositive reaction. (b) Liver fibrosis control (group 2) showing strong immunostaining reaction in perisinusoidal cells. (c) MPEO-treated (group 3) showing weak immunostaining of perisinusoidal cells. (e) Bar chart represents desmin immunohistochemistry expressed as area %. Mean values with different superscripts are significantly different ($p < 0.05$).

ECM degradation [53]. Considering this major role of TGF-β1 signaling in the pathobiology of liver fibrosis, TGF-β1 or its downstream mediators may provide important targets for the new therapeutic strategies of liver fibrosis [5].

In the present study, eight weeks of CCl_4 administration was sufficient to induce severe hepatotoxic changes detected by the considerably elevated activities of serum ALT and AST markers (Table 3). Increased release of these cytosolic enzymes in the serum reflects hepatocyte damage and leakage and provides important diagnostic biomarkers for hepatic diseases [54]. Moreover, high AST and ALT levels are associated with an increased risk of fibrosis progression [55]. MPEO administration reversed the elevated levels of ALT and AST compared to those of the CCl_4 group. These findings are consistent with those of previous studies [18, 19].

LPO is thought to be the initiation step of CCl_4 hepatotoxicity [56]. Lipid hydroperoxides are unstable and so degrade rapidly into a variety of secondary metabolites such as MDA, 4-hydroxynonenal (4-HNE), and other conjugated dienes [57]. MDA serves as a main biomarker to assess the level of lipoperoxidative tissue damage [58]. In accordance with previous studies [59, 60], a significant increase in liver MDA content was observed in the CCl_4 group, suggesting an enhanced LPO (Table 3).

Furthermore, CCl_4-intoxicated rats showed a significant increase in the liver NO (Table 3). This elevated NO indicates the stimulation of inflammatory cells and release of inflammatory cytokines [61]. NO participates in the induction of fibrosis through its reaction with superoxide anions forming highly reactive peroxynitrite radicals, which induce HSCs activation and accelerate the progression of liver fibrosis [56]. The obtained results

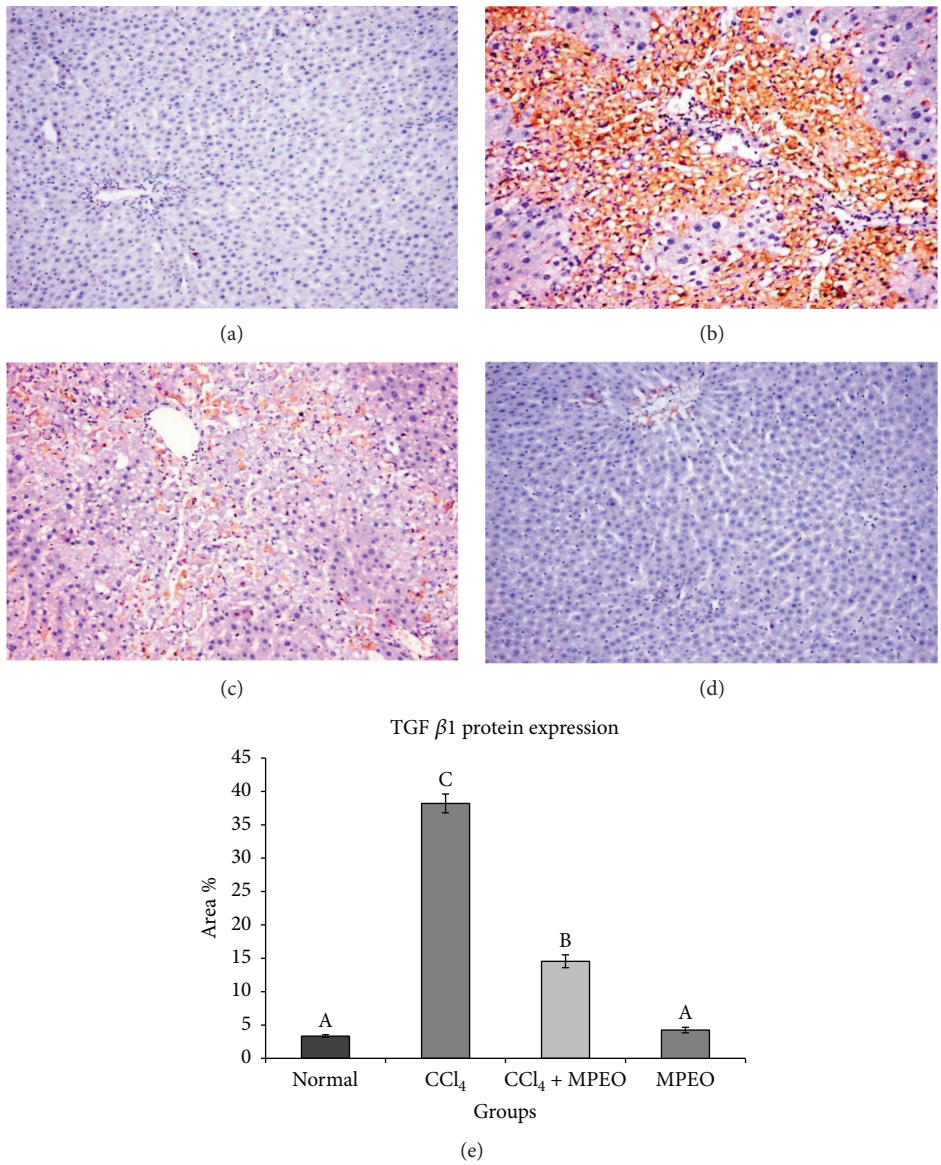

Figure 6: Representive TGF-β1 immunohistochemistry in liver tissue of the different experimental groups (×200). (a and d) The normal control (group 1) and MPEO control (group 4) showing weak immunopositive reaction in portal areas. (b) Liver fibrosis control (group 2) showing intense immunostaining in periductal cells in the portal tract, in perisinusoidal cells, around the blood vessels, and in sinusoidal lining cells. (c) MPEO-treated (group 3) showing mild reaction in some perisinusoidal cells. (e) Bar chart represents the TGF-β1 immunohistochemistry in liver expressed as area %. Mean values with different superscripts are significantly different ($p < 0.05$).

closely agreed with those mentioned by Sagor et al. [62] and Abdel Salam et al. [63], who suggested the correlation between the hepatic NO content and the degree of liver fibrosis.

On the other hand, a significant decline in the liver antioxidant capacity was detected in the CCl_4 group evidenced by the decreased SOD and CAT activities and the depletion in GSH content (Table 4). This disturbance in the prooxidants/antioxidants balance was further verified by the low TAC (Table 4).

Histopathological analysis of liver sections provided an initial evidence of CCl_4-induced liver hepatocellular damage and fibrosis (Figure 2 and Table 5). Degenerative changes including fatty degeneration, congestion, and cytoplasmic vacuolization were observed in the liver fibrosis control group (Figure 2(b)). These findings were in agreement with those obtained by Ogaly et al. [14] and Yacout et al. [64]. Additionally, MT staining revealed clear fibrotic bridging in the liver sections of group 2 (Figure 3(b)).

Immunohistochemical analysis of desmin, a hallmark of both quiescent and activated HSCs, revealed a significant elevation in desmin-immunopositive cells in the livers of CCl_4-injured group 2 (Figure 5(b)). In accordance with Fujii et al. [65], this finding implicates increased numbers of HSCs in the livers of CCl_4-treated animals, as expression of desmin together with the stellate-shaped morphology is the main characteristic feature of HSCs [66].

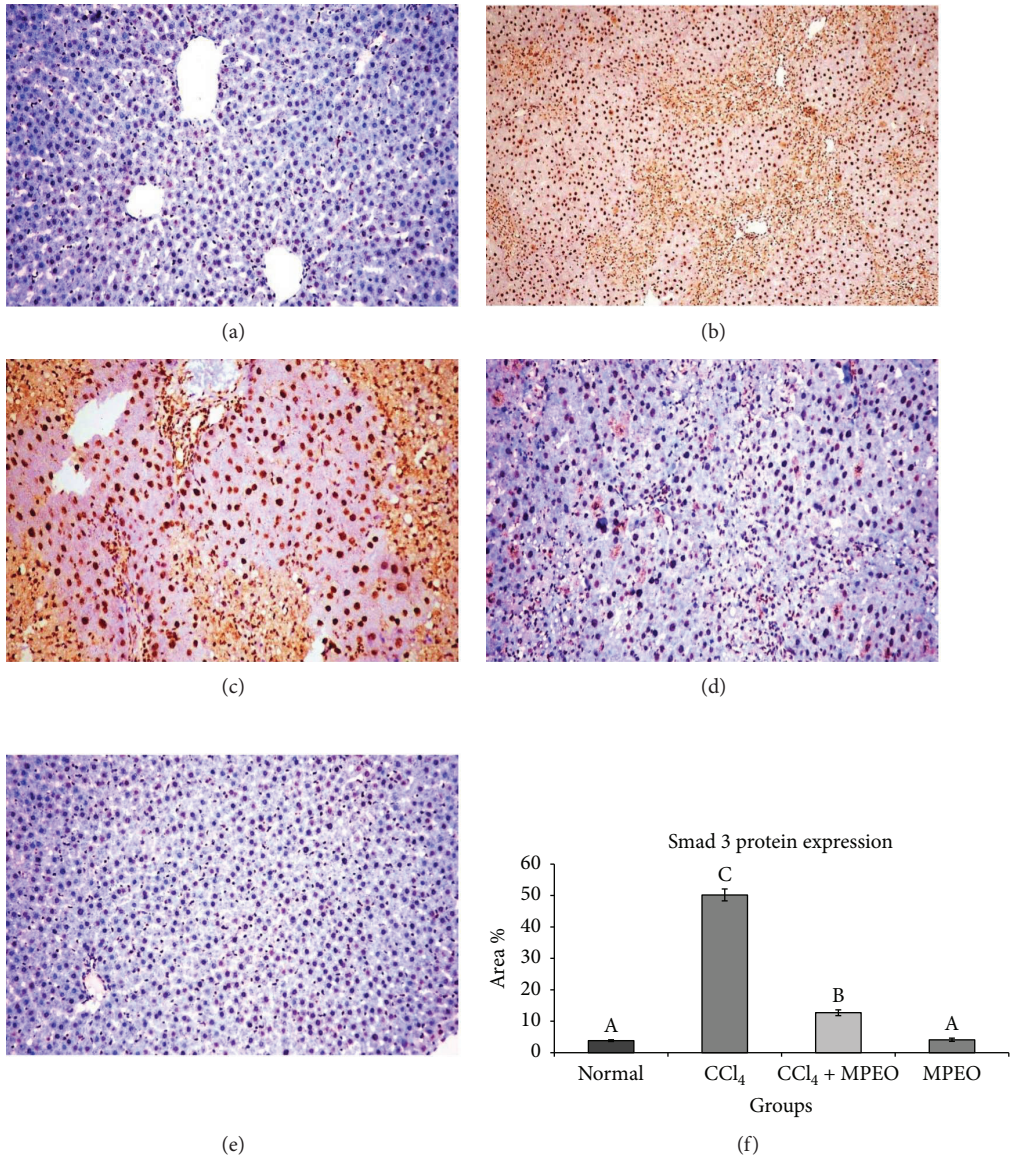

Figure 7: Representive SMAD3 immunohistochemistry in liver tissues of the different experimental groups. (a and e) The normal control and MPEO control (×200). (b) Liver fibrosis control (group 2) showing intense immunostaining reaction (×100). (c) Liver fibrosis control (group 2) showing strong cytoplasmic and nuclear staining (×200). (d) MPEO-treated (group 3) showing marked reduction of immunostaining reaction (×200). (f) Bar chart represents SMAD3 immunohistochemistry expressed as area %. Mean values with different superscripts are significantly different ($p < 0.05$).

Another important evidence for the activation of HSCs and progression of fibrosis was the significantly increased number of α-SMA-immunopositive cells in the CCl_4 fibrosis group (Figure 4(b)), as compared to the control group (Figure 4(a)). α-SMA is a reliable hallmark for HSCs activation into the myofibroblastic phenotype and considered as an important myogenic marker that plays a significant role in collagen I deposition by activated HSCs [67]. These obtained findings, in accordance with Rockey et al. [68], indicate that CCl_4 stimulated HSCs activation and transdifferentiation. Moreover, it was found that SMAD3 increases α-SMA production and stimulates its organization into stress fibers [69].

In the current study, the livers of group 2 showed an augmented expression of TGF-β1 and SMAD3 proteins as detected by the increased immunoreactivity compared to those of the control group (Figures 6 and 7). Similar findings were previously reported in rats [44].

MPOE at the investigated dose (50 mg/kg) significantly improved the liver indices, antioxidant profile, and histological picture of liver tissue. MPOE significantly reduced serum ALT and AST, indicating a preserved liver integrity and improved function (Table 3). MPOE treatment markedly increased the liver antioxidant capacity by restraining the LPO byproduct (MDA) and simultaneously enhancing the activities of SOD, catalase, and regeneration of GSH

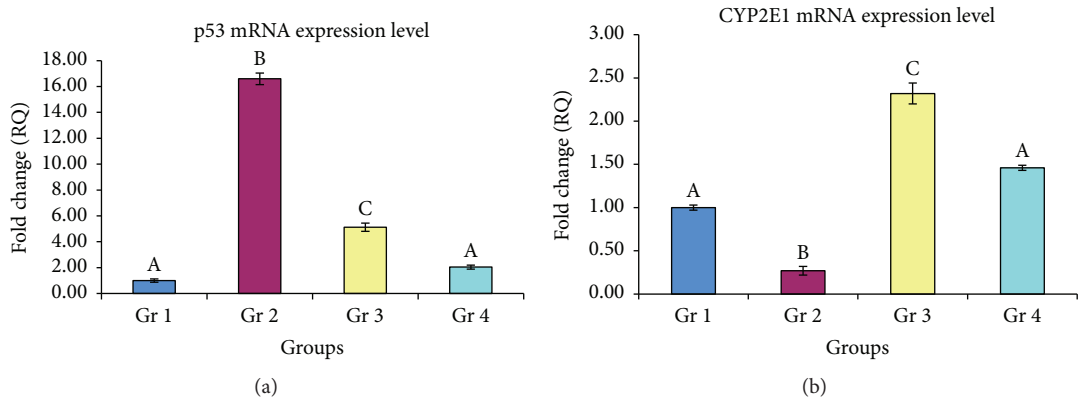

Figure 8: Quantitative real-time PCR of Tp53 and CYP2E1 mRNA in liver tissues of the different experimental groups. Values are expressed as means ± SD. GAPDH was used as an invariant housekeeping control gene for calculating the fold changes (RQ) in mRNA levels. Mean values having different letters are significantly different ($p < 0.05$).

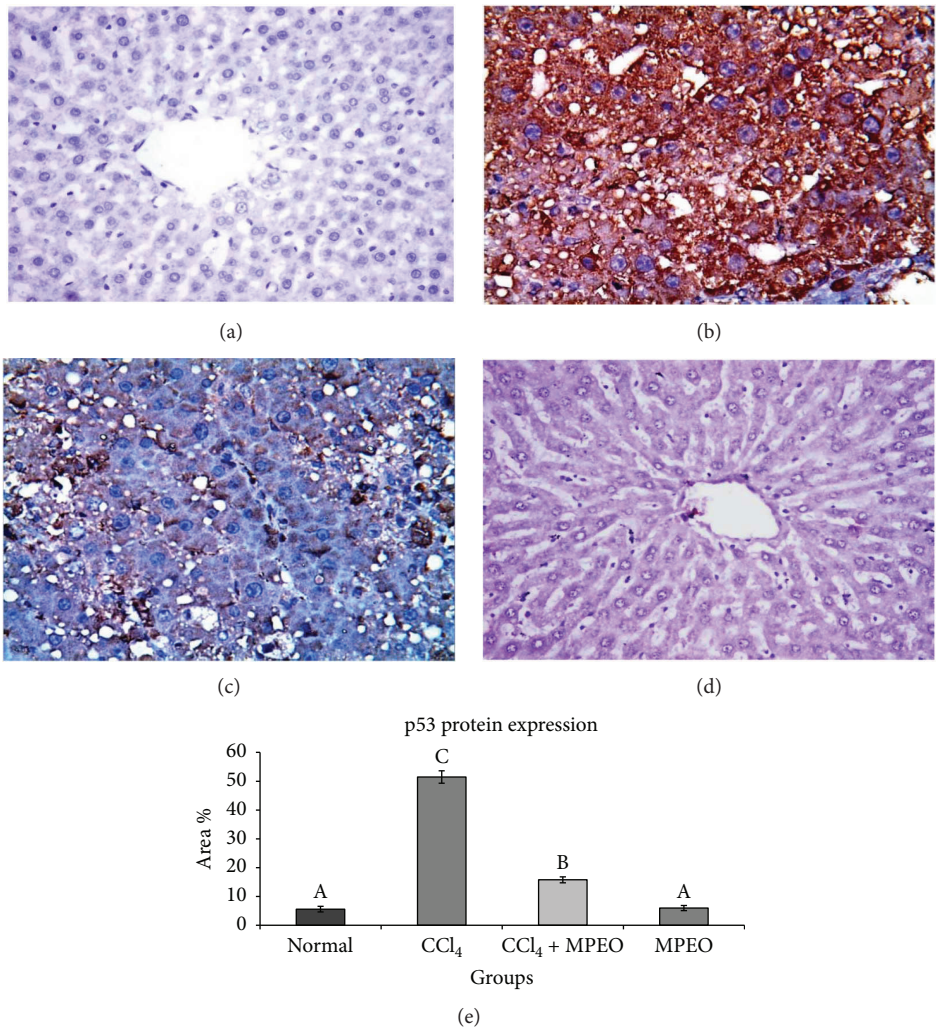

Figure 9: Representive p53 immunohistochemistry in liver tissues of the different experimental groups (×400). (a and d) The normal control and MPEO control very weak immunopositive reaction. (b) Liver fibrosis control (group 2) showing intense immunostaining in most of the hepatic cells. (c) MPEO-treated (group 3) showing immunopositive reaction in some hepatic cells. (e) Bar chart represents the p53 immunohistochemistry in liver tissues expressed as area %. Mean values with different superscripts are significantly different ($p < 0.05$).

(Table 4). Our data come in line with previous studies that reported the hepatoprotective effect of *M. piperita* [18] or its oil [19]. It was suggested that several active components of Mentha have antioxidant and antiperoxidant activities that provoke the capacity of endogenous antioxidant systems and protect against toxic hepatic damages [18, 19, 70].

Coadministration of MPOE with CCl_4 significantly improved the liver histopathology (Figure 2) and reduced the fibrotic changes (Figure 3, Table 5). Furthermore, the MPOE-treated group showed a marked reduction in both α-SMA- and desmin-immunopositive cells (Figures 4(c) and 5(c)). These data reflect the efficacy of MPOE to reduce the hepatocellular toxic effects of CCl_4 and to suppress HSCs activation and proliferation as well.

In the same context, MPOE-treated group 3 showed marked reductions in TGF-β1 and SMAD3 proteins expression (Figures 6(c) and 7(c)) compared to the CCl_4 fibrosis group (Figures 6(b) and 7(b)). According to Kanzler et al. [47] and Chen et al. [71], the observed suppression in TGF-β1 protein expression and the subsequent downregulation of SMAD3 in the livers of group 3 could explain the observed reduction of α-SMA-positive cells (Figure 4(c)), collagen deposition (Figure 3(c)), and fibrosis % (Figure 3(e)) and the reduced fibrosis scores (Table 5) in this group in comparison with the liver fibrosis control group. These findings support the antifibrogenic potential of MPOE against CCl_4-induced liver fibrosis.

p53 is a tumor-suppressor protein that regulates the transcription of a plethora of target proteins involved in the cell cycle, differentiation, and apoptosis [72]. In normal redox state, p53 expression and degradation are tightly regulated by a variety of proteins to maintain a low level of p53 [73]. Different stress signals including ROS, hypoxia, and oncogene activation induce p53 that becomes transcriptionally active, leading to cell cycle arrest, DNA repair, and apoptosis [8, 9]. It was reported that hepatocyte p53 activation resulted in spontaneous liver fibrosis and induced hepatocyte apoptosis, in addition to upregulation of connective tissue growth factor (CTGF) [74]. *In vitro* study showed that p53 induces CTGF in hepatocytes that occur via regulation of microRNA [75].

Recent studies highlighted the possible involvement of p53 in fibrogenesis as a profibrotic mediator [8, 9, 74]. p53 has been implicated as an inducer of several profibrotic effectors such as TGF-β1, CTGF, α-SMA, and fibronectin [76]. During the fibrogenic process, a crosstalk between p53 and TGF-β1 has been suggested to stimulate transcription of the fibrogenic target genes [77, 78]. Under oxidative stress, excessive ROS induces various transcription factors such as p53, activator protein-1 (AP-1), and NF-κB by altering the DNA binding sites or by oxidizing the cysteine residues of such proteins resulting in conformational change of their tertiary structure with subsequent protein degradation activation or inhibition. Activated p53 plays a crucial role in inducing apoptosis to prevent the propagation of DNA damage [72].

Few reports on the role of p53 and TGF-β1 and their interplay in the mechanism of fibrogenesis have arisen [75–78]. This encouraged our team to study the possible role of p53 and TGF-β1 in MPEO antifibrogenic mechanism. In the current investigation, Tp53 mRNA level showed a significant increase in response to CCl_4 fibrosis (Figure 8(a)). Consequently, a considerable level of p53 protein was detected in the livers of the fibrosis group (Figure 9). These findings agreed with those of previous studies that reported that p53 expression increases following the onset of liver injury [8, 9]. In the MPOE-treated group, both Tp53 mRNA (Figure 8(a)) and p53 protein expression (Figure 9(c)) were significantly suppressed. This p53 downregulation might have contributed to the reduced hepatic fibrosis in this group.

Pharmacological p53 inhibitors have been proposed as a therapeutic application to alleviate tissue fibrosis [8].

Analysis of CYP2E1 gene expression aimed to evaluate for the detoxifying capacity of the liver. CCl_4 intoxication resulted in a significant suppression in CYP2E1 mRNA (Figure 8(b)). This specific CYP2E1 downregulation in CCl_4 hepatic fibrosis was previously reported [18] and may have contributed to a direct attack of CYP2E1 transcript by the reactive CCl_4 metabolites leading to its degradation. Besides, the inflammatory response associated with fibrosis could exert a suppressive effect on CYP2E1 expression [79]. Interestingly, MPOE treatment counteracted this CYP2E1 downregulation (Figure 8). This preservation of CYP2E1 expression could be one of the MPOE hepatoprotective and antifibrogenic actions [80]. These findings are consistent with those of previous studies [62] that reported the ability of peppermint to modulate both phase I and phase II liver drug-metabolizing enzymes. Besides, eugenol, an active component of MPOE (Table 2), has been previously shown to induce detoxification enzymes [18].

5. Conclusion

MPEO significantly ameliorates the severity of CCl_4-induced liver fibrosis through improving the oxidative status and restoring hepatic CYP2E1 expression. These MPEO actions could be mediated by inhibiting TGF-β1/SMAD signaling proteins and downregulation of p53 at both gene and protein levels. These data suggest that MPEO might be an effective antifibrogenic agent in the prevention of liver fibrosis progression. MPEO could help in developing a promising approach against oxidation-caused liver fibrosis.

Conflicts of Interest

The authors declare no conflict of interest.

Acknowledgments

The authors extend their appreciation to the Deanship of Scientific Research at King Khalid University for funding this work through General Research Project under grant number (G.R.P-267-38).

References

[1] S. L. Friedman, "Mechanisms of hepatic fibrogenesis," *Gastroenterology*, vol. 134, no. 6, pp. 1655–1669, 2008.

[2] X. Zhang, X. Han, L. Yin et al., "Potent effects of dioscin against liver fibrosis," *Scientific Reports*, vol. 5, no. 1, article 9713, 2015.

[3] S. Li, H.-Y. Tan, N. Wang et al., "The role of oxidative stress and antioxidants in liver diseases," *International Journal of Molecular Sciences*, vol. 16, no. 11, pp. 26087–26124, 2015.

[4] N. C. Henderson and D. Sheppard, "Integrin-mediated regulation of TGFβ in fibrosis," *Biochimica et Biophysica Acta (BBA) - Molecular Basis of Disease*, vol. 1832, no. 7, pp. 891–896, 2013.

[5] J. Rosenbloom, F. A. Mendoza, and S. A. Jimenez, "Strategies for anti-fibrotic therapies," *Biochimica et Biophysica Acta (BBA) - Molecular Basis of Disease*, vol. 1832, no. 7, pp. 1088–1103, 2013.

[6] F. Verrecchia and A. Mauviel, "Transforming growth factor-β and fibrosis," *World Journal of Gastroenterology*, vol. 13, no. 22, pp. 3056–3062, 2007.

[7] K. H. Vousden and X. Lu, "Live or let die: the cell's response to p53," *Nature Reviews Cancer*, vol. 2, no. 8, pp. 594–604, 2002.

[8] T. Kodama, T. Takehara, H. Hikita et al., "Increases in p53 expression induce CTGF synthesis by mouse and human hepatocytes and result in liver fibrosis in mice," *The Journal of Clinical Investigation*, vol. 121, no. 8, pp. 3343–3356, 2011.

[9] A. M. Attallah, G. E. Shiha, H. Ismail, S. E. Mansy, R. El-Sherbiny, and I. El-Dosoky, "Expression of p53 protein in liver and sera of patients with liver fibrosis, liver cirrhosis or hepatocellular carcinoma associated with chronic HCV infection," *Clinical Biochemistry*, vol. 42, no. 6, pp. 455–461, 2009.

[10] J. P. Simon and S. Evan Prince, "Natural remedies for non-steroidal anti-inflammatory drug-induced toxicity," *Journal of Applied Toxicology*, vol. 37, no. 1, pp. 71–83, 2017.

[11] F. Cheung, Y. Feng, N. Wang, M. F. Yuen, Y. Tong, and V. T. Wong, "Effectiveness of Chinese herbal medicine in treating liver fibrosis: a systematic review and meta-analysis of randomized controlled trials," *Chinese Medicine*, vol. 7, no. 1, p. 5, 2012.

[12] T. A. Misharina, M. B. Terenina, and N. I. Krikunova, "Antioxidant properties of essential oils," *Prikladnaia Biokhimiia i Mikrobiologiia*, vol. 45, no. 6, pp. 710–716, 2009.

[13] S. A. Sheweita, L. S. El-Hosseiny, and M. A. Nashashibi, "Protective effects of essential oils as natural antioxidants against hepatotoxicity induced by cyclophosphamide in mice," *PLoS One*, vol. 11, no. 11, article e0165667, 2016.

[14] H. A. Ogaly, N. A. Eltablawy, A. M. El-Behairy, H. El-Hindi, and R. M. Abd-Elsalam, "Hepatocyte growth factor mediates the antifibrogenic action of *Ocimum bacilicum* essential oil against CCl_4-induced liver fibrosis in rats," *Molecules*, vol. 20, no. 8, pp. 13518–13535, 2015.

[15] M. J. Saharkhiz, M. Motamedi, K. Zomorodian, K. Pakshir, R. Miri, and K. Hemyari, "Chemical composition, antifungal and antibiofilm activities of the essential oil of *Mentha piperita* L," *ISRN Pharmaceutics*, vol. 2012, Article ID 718645, 6 pages, 2012.

[16] M. B. Goudjil, S. Ladjel, S. E. Bencheikh, S. Zighmi, and D. Hamada, "Chemical composition, antibacterial and antioxidant activities of the essential oil extracted from the *Mentha piperita* of Southern Algeria," *Research Journal of Phytochemistry*, vol. 9, no. 2, pp. 79–87, 2015.

[17] N. N. Dejani, L. C. Souza, S. R. P. Oliveira et al., "Immunological and parasitological parameters in *Schistosoma mansoni*-infected mice treated with crude extract from the leaves of *Mentha* × *piperita* L," *Immunobiology*, vol. 219, no. 8, pp. 627–632, 2014.

[18] A. Sharma, M. K. Sharma, and M. Kumar, "Protective effect of *Mentha piperita* against arsenic-induced toxicity in liver of Swiss albino mice," *Basic & Clinical Pharmacology & Toxicology*, vol. 100, no. 4, pp. 249–257, 2007.

[19] A. F. Khalil, H. O. Elkatry, and H. F. El Mehairy, "Protective effect of peppermint and parsley leaves oils against hepatotoxicity on experimental rats," *Annals of Agricultural Sciences*, vol. 60, no. 2, pp. 353–359, 2015.

[20] A. Marjani, R. Rahmati, A. R. Mansourian, and G. Veghary, "Effect of peppermint oil on serum lipid peroxidation and hepatic enzymes after immobility stress in mice," *The Open Biochemistry Journal*, vol. 6, no. 1, pp. 51–55, 2012.

[21] M. G. Zaia, T. di Orlando Cagnazzo, K. A. Feitosa et al., "Anti-inflammatory properties of menthol and menthone in *Schistosoma mansoni* infection," *Frontiers in Pharmacology*, vol. 7, p. 170, 2016.

[22] S. Reitman and S. Frankel, "A colorimetric method for the determination of serum glutamic oxalacetic and glutamic pyruvic transaminases," *American Journal of Clinical Pathology*, vol. 28, no. 1, pp. 56–63, 1957.

[23] K. M. Miranda, M. G. Espey, and D. A. Wink, "A rapid, simple spectrophotometric method for simultaneous detection of nitrate and nitrite," *Nitric Oxide*, vol. 5, no. 1, pp. 62–71, 2001.

[24] Z. A. Placer, L. L. Cushman, and B. C. Johnson, "Estimation of product of lipid peroxidation (malonyl dialdehyde) in biochemical systems," *Analytical Biochemistry*, vol. 16, no. 2, pp. 359–364, 1966.

[25] A. Nandi and I. B. Chatterjee, "Assay of superoxide dismutase activity in animal tissues," *Journal of Biosciences*, vol. 13, no. 3, pp. 305–315, 1988.

[26] A. K. Sinha, "Colorimetric assay of catalase," *Analytical Biochemistry*, vol. 47, no. 2, pp. 389–394, 1972.

[27] E. Beutler, O. Duron, and B. M. Kelly, "Improved method for the determination of blood glutathione," *The Journal of Laboratory and Clinical Medicine*, vol. 61, pp. 882–888, 1963.

[28] M. M. Bradford, "A rapid and sensitive method for the quantitation of microgram quantities of protein utilizing the principle of protein-dye binding," *Analytical Biochemistry*, vol. 72, no. 1-2, pp. 248–254, 1976.

[29] K. Ishak, A. Baptista, L. Bianchi et al., "Histological grading and staging of chronic hepatitis," *Journal of Hepatology*, vol. 22, no. 6, pp. 696–699, 1995.

[30] K. J. Livak and T. D. Schmittgen, "Analysis of relative gene expression data using real-time quantitative PCR and the $2^{-\Delta\Delta C}$T method," *Methods*, vol. 25, no. 4, pp. 402–408, 2001.

[31] S. L. Devi and C. V. Anuradha, "Oxidative and nitrosative stress in experimental rat liver fibrosis: protective effect of taurine," *Environmental Toxicology and Pharmacology*, vol. 29, no. 2, pp. 104–110, 2010.

[32] S. Li, M. Hong, H. Y. Tan, N. Wang, and Y. Feng, "Insights into the role and interdependence of oxidative stress and inflammation in liver diseases," *Oxidative Medicine and Cellular Longevity*, vol. 2016, Article ID 4234061, 21 pages, 2016.

[33] C. Trautwein, S. L. Friedman, D. Schuppan, and M. Pinzani, "Hepatic fibrosis: concept to treatment," *Journal of Hepatology*, vol. 62, no. 1, Supplement 1, pp. S15–S24, 2015.

[34] P. Ramachandran, J. P. Iredale, and J. A. Fallowfield, "Resolution of liver fibrosis: basic mechanisms and clinical relevance," *Seminars in Liver Disease*, vol. 35, no. 2, pp. 119–131, 2015.

[35] S. M. Sharafi, I. Rasooli, P. Owlia, M. Taghizadeh, and S. D. A. Astaneh, "Protective effects of bioactive phytochemicals from *Mentha piperita* with multiple health potentials," *Pharmacognosy Magazine*, vol. 6, no. 23, pp. 147–153, 2010.

[36] D. L. McKay and J. B. Blumberg, "A review of the bioactivity and potential health benefits of peppermint tea (*Mentha piperita* L.)," *Phytotherapy Research*, vol. 20, no. 8, pp. 619–633, 2006.

[37] R. Singh, M. A. M. Shushni, and A. Belkheir, "Antibacterial and antioxidant activities of *Mentha piperita* L," *Arabian Journal of Chemistry*, vol. 8, pp. 322–328, 2011.

[38] Z. Sun, H. Wang, J. Wang, L. Zhou, and P. Yang, "Chemical composition and antiinflammatory, cytotoxic and antioxidant activities of essential oil from leaves of *Mentha piperita* grown in China," *PLoS One*, vol. 9, no. 12, article e114767, 2014.

[39] R. da Silva Ramos, A. B. L. Rodrigues, A. L. F. Farias et al., "Chemical composition and *in vitro* antioxidant, cytotoxic, antimicrobial, and larvicidal activities of the essential oil of *Mentha piperita* L. (Lamiaceae)," *The Scientific World Journal*, vol. 2017, Article ID 4927214, 8 pages, 2017.

[40] A. K. Tyagi and A. Malik, "Antimicrobial potential and chemical composition of *Mentha piperita* oil in liquid and vapour phase against food spoiling microorganisms," *Food Control*, vol. 22, no. 11, pp. 1707–1714, 2011.

[41] N. Ahmad, H. Fazal, I. Ahmad, and B. H. Abbasi, "Free radical scavenging (DPPH) potential in nine *Mentha* species," *Toxicology and Industrial Health*, vol. 28, no. 1, pp. 83–89, 2012.

[42] M. S. Brewer, "Natural antioxidants: sources, compounds, mechanisms of action, and potential applications," *Comprehensive Reviews in Food Science and Food Safety*, vol. 10, no. 4, pp. 221–247, 2011.

[43] L. Niu, X. Cui, Y. Qi et al., "Involvement of TGF-β1/Smad3 signaling in carbon tetrachloride-induced acute liver injury in mice," *PLoS One*, vol. 11, no. 5, article e0156090, 2016.

[44] A. M. Abdel-Moneim, M. A. Al-Kahtani, M. A. El-Kersh, and M. A. Al-Omair, "Free radical-scavenging, anti-inflammatory/anti-fibrotic and hepatoprotective actions of taurine and silymarin against CCl_4 induced rat liver damage," *PLoS One*, vol. 10, no. 12, article e0144509, 2015.

[45] W. R. Bi, C. Q. Yang, and Q. Shi, "Transforming growth factor-β1 induced epithelial-mesenchymal transition in hepatic fibrosis," *Hepato-Gastroenterology*, vol. 59, no. 118, pp. 1960–1963, 2012.

[46] Y. Inagaki and I. Okazaki, "Emerging insights into transforming growth factor β Smad signal in hepatic fibrogenesis," *Gut*, vol. 56, no. 2, pp. 284–292, 2007.

[47] S. Kanzler, A. W. Lohse, A. Keil et al., "TGF-β1 in liver fibrosis: an inducible transgenic mouse model to study liver fibrogenesis," *American Journal of Physiology-Gastrointestinal and Liver Physiology*, vol. 276, no. 4, Part 1, pp. G1059–G1068, 1999.

[48] X.-M. Meng, A. C. K. Chung, and H. Y. Lan, "Role of the TGF-β/BMP-7/Smad pathways in renal diseases," *Clinical Science*, vol. 124, no. 4, pp. 243–254, 2013.

[49] F. Xie, Z. Zhang, H. van Dam, L. Zhang, and F. Zhou, "Regulation of TGF-β superfamily signaling by SMAD mono-ubiquitination," *Cell*, vol. 3, no. 4, pp. 981–993, 2014.

[50] Q. Y. Yao, B. L. Xu, J. Y. Wang, H. C. Liu, S. C. Zhang, and C. T. Tu, "Inhibition by curcumin of multiple sites of the transforming growth factor-beta1 signalling pathway ameliorates the progression of liver fibrosis induced by carbon tetrachloride in rats," *BMC Complementary & Alternative Medicine*, vol. 12, no. 1, p. 156, 2012.

[51] G. Latella, A. Vetuschi, R. Sferra et al., "Targeted disruption of Smad3 confers resistance to the development of dimethylnitrosamine-induced hepatic fibrosis in mice," *Liver International*, vol. 29, no. 7, pp. 997–1009, 2009.

[52] A. Masszi and A. Kapus, "Smaddening complexity: the role of Smad3 in epithelial-myofibroblast transition," *Cells, Tissues, Organs*, vol. 193, no. 1-2, pp. 41–52, 2011.

[53] M. Sato, Y. Muragaki, S. Saika, A. B. Roberts, and A. Ooshima, "Targeted disruption of TGF-β1/Smad3 signaling protects against renal tubulointerstitial fibrosis induced by unilateral ureteral obstruction," *The Journal of Clinical Investigation*, vol. 112, no. 10, pp. 1486–1494, 2003.

[54] M. Martinot-Peignoux, N. Boyer, D. Cazals-Hatem et al., "Prospective study on anti-hepatitis C virus-positive patients with persistently normal serum alanine transaminase with or without detectable serum hepatitis C virus RNA," *Hepatology*, vol. 34, no. 5, pp. 1000–1005, 2001.

[55] M. Vuda, R. D'Souza, S. Upadhya et al., "Hepatoprotective and antioxidant activity of aqueous extract of *Hybanthus enneaspermus* against CCl_4-induced liver injury in rats," *Experimental and Toxicologic Pathology*, vol. 64, no. 7-8, pp. 855–859, 2012.

[56] T. M. Leung, M. L. Fung, E. C. Liong, T. Y. Lau, A. A. Nanji, and G. L. Tipoe, "Role of nitric oxide in the regulation of fibrogenic factors in experimental liver fibrosis in mice," *Histology and Histopathology*, vol. 26, no. 2, pp. 201–211, 2011.

[57] S. Sundaresan and P. Subramanian, "*S*-Allylcysteine inhibits circulatory lipid peroxidation and promotes antioxidants in N-nitrosodiethylamine-induced carcinogenesis," *Polish Journal of Pharmacology*, vol. 55, no. 1, pp. 37–42, 2003.

[58] M. R. Khan and D. Ahmed, "Protective effects of *Digera muricata* (L.) Mart. on testis against oxidative stress of carbon tetrachloride in rat," *Food and Chemical Toxicology*, vol. 47, no. 6, pp. 1393–1399, 2009.

[59] H. Ghaffari, M. Venkataramana, S. C. Nayaka et al., "Hepatoprotective action of *Orthosiphon diffusus* (Benth.) methanol active fraction through antioxidant mechanisms: an *in vivo* and *in vitro* evaluation," *Journal of Ethnopharmacology*, vol. 149, no. 3, pp. 737–744, 2013.

[60] H. Sadeghi, S. Hosseinzadeh, M. Akbartabar Touri, M. Ghavamzadeh, and M. Jafari Barmak, "Hepatoprotective effect of *Rosa canina* fruit extract against carbon tetrachloride induced hepatotoxicity in rat," *Avicenna Journal of Phytomedicine*, vol. 6, no. 2, pp. 181–188, 2016.

[61] S. Iwai, R. Karim, M. Kitano et al., "Role of oxidative DNA damage caused by carbon tetrachloride-induced liver injury—enhancement of MeIQ-induced glutathione *S*-transferase placental form-positive foci in rats," *Cancer Letters*, vol. 179, no. 1, pp. 15–24, 2002.

[62] A. T. Sagor, M. R. H. Chowdhury, N. Tabassum, H. Hossain, M. M. Rahman, and M. A. Alam, "Supplementation of fresh ucche (*Momordica charantia* L. var. *muricata* Willd) prevented oxidative stress, fibrosis and hepatic damage in CCl_4

treated rats," *BMC Complementary & Alternative Medicine*, vol. 15, no. 1, p. 115, 2015.

[63] O. M. Abdel Salam, A. A. Sleem, and N. Shafee, "Effect of trazodone and nefazodone on hepatic injury induced by carbon tetrachloride," *Drug Discoveries & Therapeutics*, vol. 4, no. 4, pp. 285–297, 2010.

[64] G. A. Yacout, N. M. Elguindy, and E. F. El Azab, "Hepatoprotective effect of basil (*Ocimum basilicum* L.) on CCl_4-induced liver fibrosis in rats," *African Journal of Biotechnology*, vol. 11, no. 90, pp. 15702–15711, 2012.

[65] T. Fujii, B. C. Fuchs, S. Yamada et al., "Mouse model of carbon tetrachloride induced liver fibrosis: histopathological changes and expression of CD133 and epidermal growth factor," *BMC Gastroenterology*, vol. 10, no. 1, p. 79, 2010.

[66] C. Kordes, I. Sawitza, A. Müller-Marbach et al., "$CD133^+$ hepatic stellate cells are progenitor cells," *Biochemical and Biophysical Research Communications*, vol. 352, no. 2, pp. 410–417, 2007.

[67] S. Lotersztajn, B. Julien, F. Teixeira-Clerc, P. Grenard, and A. Mallat, "Hepatic fibrosis: molecular mechanisms and drug targets," *Annual Review of Pharmacology and Toxicology*, vol. 45, no. 1, pp. 605–628, 2005.

[68] D. C. Rockey, N. Weymouth, and Z. Shi, "Smooth muscle α actin (*Acta2*) and myofibroblast function during hepatic wound healing," *PLoS One*, vol. 8, no. 10, article e77166, 2013.

[69] F. Xu, C. Liu, D. Zhou, and L. Zhang, "TGF-β/SMAD pathway and its regulation in hepatic fibrosis," *Journal of Histochemistry & Cytochemistry*, vol. 64, no. 3, pp. 157–167, 2016.

[70] P. Kumaravelu, S. Subramaniyam, D. P. Dakshinamoorthy, and N. S. Devaraj, "The antioxidant effect of eugenol on CCl_4-induced erythrocyte damage in rats," *The Journal of Nutritional Biochemistry*, vol. 7, no. 1, pp. 23–28, 1996.

[71] H. B. Chen, J. G. Rud, K. Lin, and L. Xu, "Nuclear targeting of transforming growth factor-β-activated Smad complexes," *The Journal of Biological Chemistry*, vol. 280, no. 22, pp. 21329–21336, 2005.

[72] K. H. Vousden and C. Prives, "Blinded by the light: the growing complexity of p53," *Cell*, vol. 137, no. 3, pp. 413–431, 2009.

[73] J. P. Kruse and W. Gu, "Modes of p53 regulation," *Cell*, vol. 137, no. 4, pp. 609–622, 2009.

[74] X.-F. Tian, F.-J. Ji, H.-L. Zang, and H. Cao, "Activation of the miR-34a/SIRT1/p53 signaling pathway contributes to the progress of liver fibrosis *via* inducing apoptosis in hepatocytes but not in HSCs," *PLoS One*, vol. 11, no. 7, article e0158657, 2016.

[75] D. Pollutri, L. Gramantieri, L. Bolondi, and F. Fornari, "TP53/microRNA interplay in hepatocellular carcinoma," *International Journal of Molecular Sciences*, vol. 17, no. 12, article 2029, 2016.

[76] R. Samarakoon, A. D. Dobberfuhl, C. Cooley et al., "Induction of renal fibrotic genes by TGF-β1 requires EGFR activation, p53 and reactive oxygen species," *Cellular Signalling*, vol. 25, no. 11, pp. 2198–2209, 2013.

[77] J. M. Overstreet, R. Samarakoon, K. K. Meldrum, and P. J. Higgins, "Redox control of p53 in the transcriptional regulation of TGF-β1 target genes through SMAD cooperativity," *Cellular Signalling*, vol. 26, no. 7, pp. 1427–1436, 2014.

[78] M. Cordenonsi, S. Dupont, S. Maretto, A. Insinga, C. Imbriano, and S. Piccolo, "Links between tumor suppressors: p53 is required for TGF-β gene responses by cooperating with Smads," *Cell*, vol. 113, no. 3, pp. 301–314, 2003.

[79] D. S. Riddick, C. Lee, A. Bhathena et al., "Transcriptional suppression of cytochrome P_{450} genes by endogenous and exogenous chemicals," *Drug Metabolism and Disposition*, vol. 32, no. 4, pp. 367–375, 2004.

[80] G. Xie, C. C. Wong, K. W. Cheng, L. Huang, P. P. Constantinides, and B. Rigas, "Regioselective oxidation of phospho-NSAIDs by human cytochrome P450 and flavin monooxygenase isoforms: implications for their pharmacokinetic properties and safety," *British Journal of Pharmacology*, vol. 167, no. 1, pp. 222–232, 2012.

[81] R. E. Mostafa, A. A. S. Salama, R. F. Abdel-Rahman, and H. A. Ogaly, "Hepato-and neuro-protective influences of biopropolis on thioacetamide-induced acute hepatic encephalopathy in rats," *Canadian Journal of Physiology and Pharmacology*, vol. 95, no. 5, pp. 539–547, 2016.

[82] N. A. Eltablawy and H. A. Ogaly, "Responsiveness of p53 expression and genetic mutation to CCl_4-induced DNA damage in rat's liver," *International Journal of Genomics and Proteomics*, vol. 5, no. 1, pp. 99–105, 2014.

Hindawi
Oxidative Medicine and Cellular Longevity
Volume 2018, Article ID 1821359, 10 pages
https://doi.org/10.1155/2018/1821359

Research Article

Recovery of Cardiac Remodeling and Dysmetabolism by Pancreatic Islet Injury Improvement in Diabetic Rats after Yacon Leaf Extract Treatment

Klinsmann Carolo dos Santos[1], **Sarah Santiloni Cury**[2], **Ana Paula Costa Rodrigues Ferraz**[1], **José Eduardo Corrente**[1], **Bianca Mariani Gonçalves**[3], **Luiz Henrique de Araújo Machado**[3], **Robson Francisco Carvalho**[2], **Ana Cláudia de Melo Stevanato Nakamune**[4], **Alexandre Todorovic Fabro**[5], **Paula Paccielli Freire**[2], **and Camila Renata Corrêa**[1]

[1]*Medical School, São Paulo State University (UNESP), Botucatu, SP, Brazil*
[2]*Institute of Biosciences, São Paulo State University (UNESP), Botucatu, SP, Brazil*
[3]*School of Veterinary Medicine and Animal Science, São Paulo State University (UNESP), Botucatu, SP, Brazil*
[4]*School of Dentistry, São Paulo State University (UNESP), Araçatuba, SP, Brazil*
[5]*Medical School, University of São Paulo (USP), Ribeirão Preto, SP, Brazil*

Correspondence should be addressed to Klinsmann Carolo dos Santos; klinsmanncarolo@gmail.com

Received 14 December 2017; Accepted 12 March 2018; Published 10 April 2018

Academic Editor: Jaideep Banerjee

Yacon (*Smallanthus sonchifolius*) is a native Andean plant rich in phenolic compounds, and its effects on dysmetabolism and cardiomyopathy in diabetic rats was evaluated. The rats (10/group) were allocated as follows: C, controls; C + Y, controls treated with Yacon leaf extract (YLE); DM, diabetic controls; and DM + Y, diabetic rats treated with YLE. Type 1 diabetes (T1DM) was induced by the administration of streptozotocin (STZ; 40 mg^{-1}/kg body weight, single dose, i.p.), and treated groups received 100 mg/kg body weight YLE daily via gavage for 30 d. The YLE group shows an improvement in dysmetabolism and cardiomyopathy in the diabetic condition (DM versus DM + Y) promoting a significant reduction of glycemia by 63.39%, an increase in insulin concentration by 49.30%, and a decrease in serum triacylglycerol and fatty acid contents by 0.39- and 0.43-fold, respectively, by ameliorating the pancreatic islet injury, as well as increasing the activity of the antioxidant enzymes (catalase, superoxide dismutase, and glutathione peroxidase) and decreasing the fibrosis and cellular disorganization in cardiac tissue. The apparent benefits of YLE seem to be mediated by ameliorating dysmetabolism and oxidative stress in pancreatic and cardiac tissues.

1. Introduction

Type 1 diabetes mellitus (T1DM) is a chronic state of insulin deficiency which results from the destruction of β-cells by the immune system, leading to a structural disorganization of the pancreatic islets. The Epidemiology of Diabetes Interventions and Complications study showed that intensive blood glucose control reduces the risk of several diseases, especially those related to the cardiac tissue [1].

Several studies have demonstrated that the development of cardiovascular disease is frequently observed in diabetic patients and in experimental models, and it is one of the major causes that elevates the incidence of morbidity [2–5]. Basically, in diabetic heart, there is a dramatic shift of the glucose utilization and almost complete reliance on fatty acid oxidation for energy production, resulting in the loss of metabolic flexibility as well as morphological changes in the cardiomyocytes [3, 6]. In summary, the dysmetabolism in diabetic heart leads to several biochemical and molecular

pathway alterations [7]. Deregulated metabolism may be linked to increased production of reactive oxygen species (ROS) that leads to oxidative damage of DNA, proteins, and lipids as well as the activation of stress-sensitive pathways and development of cardiac oxidative stress in diabetes [8, 9].

The use of medicinal plants and herbs, for the treatment of many chronic diseases such as diabetes and its complications, has been recognized by a number of scientists and physicians based on their therapeutic properties [6]. Additionally, based on recommendations of the World Health Organization [10], antidiabetic agents derived from plants are an important alternative, as cotherapy, for the treatment of this condition. Over the past years, great attention has been given to the use of natural products, based on their pharmacological properties, as a form of complementary therapy.

Yacon (*Smallanthus sonchifolius*) is a perennial plant originally cultivated in the Andean highlands of South America, and its tubers are commonly used as food [11]. A number of studies have demonstrated the presence of large amounts of phenolic compounds in extracts from Yacon leaves and tubers [12, 13]. So, since diabetic cardiomyopathy is tightly related to oxidative stress—originally from persistent hyperglycemia and the metabolic shift in the cardiac tissue [14, 15], the treatment with Yacon leaves can be useful in diminishing oxidative damage and decreasing or preventing the progression of diabetic cardiomyopathy. Based on these information, the aim of the present study was to investigate the protective effect of Yacon leaf treatment on STZ-induced dysmetabolism and cardiomyopathy based on its antioxidant properties.

2. Material and Methods

2.1. Plant Material and Extract Preparation. The *S. sonchifolius* specimen was cultivated at the Department of Plant Science and Crop Protection, Federal University of Paraná, Curitiba, Paraná, Brazil. Briefly, the leaves from *S. sonchifolius* were dried for seven days at 50°C, powdered (3 μm), and subjected to percolation at room temperature using a mixture of ethanol : H_2O (7 : 3, *v*/*v*) with a flux of 2.0 mL/min/kg. The solvents were evaporated to dryness under low pressure (45°C) using a rotary evaporator in a vacuum system to afford the crude Yacon leaf extract (YLE). More information about the plant material, production of leaf extract, and phytochemical characterization can be found in a previous study of our group [13].

2.2. Experimental Design. Forty male Wistar rats, 60 d of age, were maintained in an environmentally controlled room (22 ± 3°C; 12-hour light/dark cycle and relative humidity of 60 ± 5%) and were fed with a standard rat pellet diet (Purina Ltd., Campinas, SP, Brazil) and water ad libitum. The experimental protocol was approved by the Ethics Committee on the Use of Animals (CEUA) at the Botucatu Medical School, São Paulo State University (UNESP) under number 1082-2014 (approved in April 24, 2014). The animals were randomly assigned to one of four groups ($n = 10$): control group (C); control group receiving YLE (C + Y); diabetic rats (DM); and diabetic rats receiving YLE (DM + Y). Diabetes mellitus was induced by the i.p. administration of streptozotocin for one time (STZ; 40 mg/kg body weight). Blood glucose was measured at 48 h and at 7 days after the STZ administration. The animals with blood glucose greater than 250 mg/dL were considered diabetic. The animals received YLE (100 mg/kg body weight/day constituted in 1 mL of 0.9% saline) for gavage for 30 days after the 7th day of the established diabetic condition. The dose of the treatment was selected based on a previous study conducted by our team [13], where 3 different doses were tested (Y25, Y50, and Y100) and the highest dose presented a better glycemic control (Figure 1). Control animals were given the same volume of saline. The animals were fasted overnight and killed by decapitation after anesthesia with ketamine (50 mg/kg body weight) and xylazine (0.5 mg/kg body weight) by intraperitoneal injection, and all efforts were made to minimize suffering. Blood was collected in tubes and then centrifuged at 3500 ×g. The serum and heart tissues were collected and stored at −80°C until analysis.

2.3. Biochemical and Hormonal Measurement. Serum glucose and triacylglycerol levels were measured using an automatic enzymatic analyzer system (biochemical analyzer BS-200, Mindray, China) and a commercial kit (Bioclin®, Belo Horizonte, Minas Gerais, Brazil), nonesterified fatty acid (NEFA) levels were determined by colorimetric kits (Wako NEFA-C, Wako Pure Chemical Industries, Tokyo, Japan), and insulin levels (EMD Millipore Corporation, Billerica, MA, USA) were measured by an immunoassay using a microplate reader (Spectra Max 190; Molecular Devices, Sunnyvale, CA, USA).

2.4. Redox State Markers

2.4.1. Preparation of the Cardiac Tissue for Analysis. 100 mg of the tissue was homogenized in 1.0 mL of a phosphate-buffered saline (PBS) pH 7.4 cold solution using a T 25 digital ULTRA-TURRAX® basic disperser (IKA® Werke Staufen, Germany) and centrifuged at 800*g* at 4°C for 10 min. The supernatant was used for measuring malondialdehyde and antioxidant enzyme activity levels, conducting histopathological analysis, immunohistochemistry, and fractal dimension analysis, and evaluating heart histology.

(1) Malondialdehyde (MDA). Briefly, we added 700 μL of 1% orthophosphoric acid and 200 μL of thiobarbituric acid (42 mM) to 100 μL of the supernatant and then boiled it for 60 min in a water bath; the sample was cooled on ice immediately after that. 200 μL was transferred to a 2 mL tube containing 200 μL of sodium hydroxide-methanol (1 : 12 *v*/*v*). The sample was vortex mixed for 10 s and centrifuged for 3 min at 1.000 ×g. The supernatant (200 μL) was transferred to a 300 μL glass vial and 50 μL was injected into the column. The HPLC was a Shimadzu LC-10AD system (Kyoto, Japan) equipped with a C18 Luna column (5 μm, 150 × 4.60 mm, Phenomenex Inc., Torrance, CA, USA), a Shimadzu RF-535 fluorescence detector (excitation: 525 nm, emission: 551 nm), and 0.5 mL/min flow of phosphate buffer (KH_2PO_4

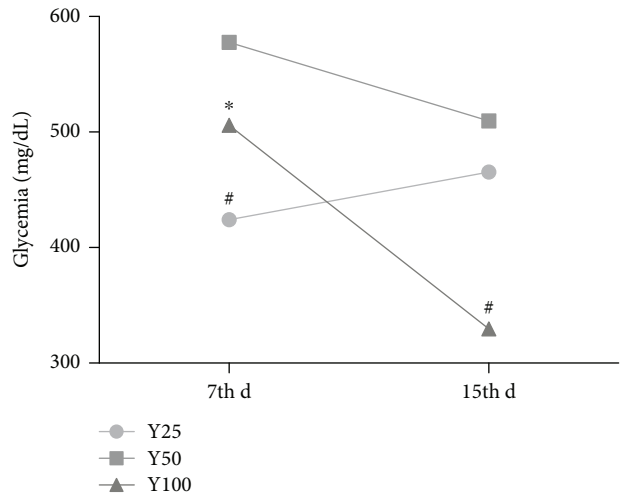

Figure 1: Dose-response profile of Yacon leaves. The animals were randomly assigned to one of three groups: Y25, Y50, and Y100 (25, 50, and 100 mg/kg body weight/day of Yacon extract constituted in 1 mL of 0.9% saline, resp.). Diabetes mellitus was induced by one i.p. administration of streptozotocin (STZ; 40 mg/body weight), and the animals received HEYL for gavage for 15 days after the establishment of the diabetic condition and glycemia was measured at day 7 (7th d) and day 15 (15th d). C: controls; C + Y: controls treated with Yacon leaf extract; DM: diabetic controls; and DM + Y: diabetic rats treated with Yacon. The data are represented as the median. Statistical analysis was performed using the generalized linear model and one-way analysis of variance test. Significant values are represented by $P < 0.05$. *Versus Y25; #versus Y50.

1 mM, pH 6.8) [16]. MDA was quantified by area determination of the peaks in the chromatograms relative to a standard curve of known concentrations.

(2) Antioxidant Enzymes. Superoxide dismutase activity was measured based on the inhibition of a superoxide radical reaction with pyrogallol, and the absorbance values were measured at 420 nm [17]. Catalase activity was evaluated by following the decrease in the levels of hydrogen peroxide. The absorbance values were measured at 240 nm [18]. The activity is expressed as pmol of H_2O_2 reduced/min/mg protein. Glutathione peroxidase activity was measured by following β-nicotinamide adenine dinucleotide phosphate (NADPH) oxidation at 340 nm as described by Flohé and Günzler [19]; the results were expressed as μmol of hydroperoxide reduced/min/mg protein. The values for the enzyme activities were corrected by protein content. Protein was quantified based on Lowry et al.'s method [20], using bovine serum albumin as the standard.

(3) Pancreatic Histology and Pathologic Scoring. For histopathological analysis, pancreatic tissue was fixed overnight in 10% formaldehyde, embedded in paraffin, and maintained in 70% ethanol until sliced. After being sliced in a microtome (4 μm), cross sections were stained with hematoxylin and eosin (H&E). Pathology analyses were performed in pancreatic islets by scoring the tissue injury using a method described earlier with some modifications [21]. The total surface of the slide was scored for two different variables determining the severity of islet damage, such as the size and architecture of islets. The size criteria used were defined as follows: severe, less than 20% of the total field occupation; moderate, less than 50% of the total field occupation; slight, less than 70% of the total field occupation; and normal size islets, occupying around 70–80% of the field. For the architecture criteria, the following items were used: severe, islets presenting a nonsymmetric shape and totally disorganized nuclei; moderate, flat islets and clustered nuclei in the islet periphery; slight, semioval islets with 50% of the nuclei distributed more peripherally; and normal architecture islets, islets more rounded or oval and nuclei distributed symmetrically throughout the islet.

(4) Immunohistochemistry. The immunohistochemistry procedure was carried out following the manufacturer's protocol, starting with antigen retrieval for paraffin-sectioned slides using the standard laboratory protocol. The pancreas slides were incubated in the EnVision™ FLEX peroxidase-blocking reagent for 5 minutes to block endogenous enzyme activity. Subsequently, the EnVision FLEX anti-insulin primary antibody (1 : 2000) was incubated for 20 minutes, and after washing to remove primary antibodies, the slides were incubated with EnVision FLEX/horseradish peroxidase (HRP) for 20 minutes, followed by two washes, and the procedure continued by incubating the slides with diaminobenzidene (DAB) chromogen for 10 minutes. Finally, the slides were stained with hematoxylin and dried for xylene preparation. Insulin was quantified through ImageJ® image processing program.

(5) Heart Histology. Hearts were harvested for histological evaluation of potential fibrosis and tissue disorganization. The hearts were fixed in 10% formaldehyde overnight, embedded in paraffin, and maintained in 70% ethanol until sliced. The hearts were sliced, with cross sections about 4 μm thick, using a microtome. The staining with H&E and Picro Sirius Red (PSR) was performed according to standard histological processing. PSR stained sections were used to quantify the collagen area using the ImageJ image processing program, following software instructions. The fractal dimension was accessed using H&E stained sections. Three random sections from each animal were photographed through a 20x objective lens, using a light microscope (Leica, Germany).

(6) Fractal Dimension Analysis. To quantify the heart nucleus disorganization, H&E stained sections were analyzed using the fractal dimension methodology based on Pacagnelli et al.'s description [22]. Using the ImageJ software, the images of the slides with the heart tissue were binarized, and the fractal dimension was estimated by using a tool that quantifies pixel distribution in the binarized images; this tool, "Fractal box-count," is capable of generating a fractal dimension value (D), which ranges from 0 to 2. A value close to 2 represents more pixel disorganization.

2.5. Statistical Analysis. For normally distributed data, the analyses were performed using two-way ANOVA followed

Table 1: Serum biochemical and hormonal outcomes.

Outcomes	Groups			
	C	C + Y	DM	DM + Y
Initial glycemia (mg/dL)	128 ± 14.75	119.6 ± 14.76	416.11 ± 15.55*	395.33 ± 19.05#
Final glycemia (mg/dL)	94 ± 17.90	88.66 ± 18.87	299.75 ± 20.02*	109.71 ± 19.46†
Insulin (pmol/L)	32.25 ± 2.45	30.87 ± 2.60	20.24 ± 3.30*	30.22 ± 3.01†
TG (mg/dL)	54.74 ± 3.26	71.53 ± 3.64*	89.77 ± 3.89*	64.42 ± 4.21†
NEFA (mEq/L)	0.34 ± 0.03	0.38 ± 0.03	0.43 ± 0.03	0.30 ± 0.03†

The data are represented as the mean ± SEM. Statistical analysis was performed using the generalized linear model and two-way analysis of variance test complemented with a nonparametric test. Significant values are represented by $P < 0.05$. *Versus C; #versus C + Y; †versus DM; C: controls; C + Y: controls treated with Yacon leaf extract; DM: diabetic controls; DM + Y: diabetic rats treated with Yacon; TG: triacylglycerol; NEFA: nonesterified fatty acid.

by the nonparametric test. For scoring islet damage, the linear model for a binomial distribution with a logistic link was used, followed by the multiple Wald comparison test for islet size and architecture. Statistical tests were performed using SAS for Windows, v. 9.3. Statistical significance was considered when $P < 0.05$.

3. Results

3.1. Yacon Treatment Improves Dysmetabolism in Diabetic Condition. After 30 d of treatment with 100 mg/kg body weight/d—based on a dose-response pilot study (Figure 1), YLE promoted a significant reduction of glycemia at 63.39% in the DM + Y group when compared to the untreated group, whereas it increased the insulin concentration by 49.30% in the treated group (Table 1). Additionally, Yacon treatment decreased the serum TG and NEFA contents (DM versus DM + Y) by 0.39- and 0.43-fold, respectively (Table 1). On the other hand, treatment with Yacon increased the TG content in the control group when compared to the untreated control group.

3.2. Yacon Treatment Ameliorates Oxidative Stress Markers in Heart Tissue. To investigate the effect of Yacon treatment in redox status response in the heart of diabetic animals, markers of antioxidant defense and oxidative stress were measured. The antioxidant defense enzymes catalase, glutathione peroxidase, and superoxide dismutase levels were significantly decreased in the DM group compared with the control group, and increased in diabetic animals treated with Yacon compared to untreated diabetic animals (Figures 2(a)–2(c)). In an opposite manner, the oxidative stress marker (malondialdehyde) level was increased in the DM group compared to the control group and decreased in diabetic animals treated with Yacon when compared with the DM group. We also verified an increase in this marker in the control group treated with Yacon when compared to the untreated control group (Figure 2(d)).

3.3. Yacon Treatment Reduces Pancreas Severe Phenotype and Increases Insulin Production. To analyze the effect of the treatment on the Langerhans islet size and architecture, we used a linear model for binomial distribution with a logistic link followed by the multiple comparison Wald test. For the analysis of the islet number, the results showed that the DM group presented fewer islets with a normal size compared to the control group, and the treatment with Yacon (DM + Y) increased the number of islets with a normal size (Figure 3(b)). For the slight, moderate, and severe alterations, the DM group showed an increase in islets with these characteristics, whereas the treatment seems to prevent these alterations in the diabetic group (Figure 3(b)). Moreover, the architecture analysis showed a reduction in the number of islets with a normal architecture. Notably, we verified a higher number of islets with an altered architecture (moderate and severe) in DM when compared to DM + Y, suggesting that the treatment with Yacon could alleviate the islet architecture deterioration in the diabetic condition. No moderate or severe changes were observed in the control group (Figure 3(b)). The description of the results for the islet staging criteria are exposed in Table S1 and Figure S1 (Supplementary Materials).

3.4. Yacon Decreases Fibrosis and Nuclear Disorganization in the Heart of Diabetic Rats. To verify the effect of the treatment in diabetic heart fibrosis, we analyzed histological sections stained with PSR, which is responsible for collagen staining. Animals belonging to the untreated diabetic group present an increased collagen area in the extracellular matrix compared to that of the control group. Furthermore, the diabetic rats treated with Yacon showed a decrease in fibrosis accumulation compared to the rats of the DM group (Figures 4(a) and 4(c)). Moreover, we analyzed heart tissue organization by assessing the fractal dimension of nucleus localization using histological sections stained with H&E. Fractal analysis showed that the nucleus disorganization in diabetics is worse than that in the control. Additionally, the treatment with Yacon was able to reverse the nuclear disorganization in diabetics (Figures 4(b) and 4(d)). These data indicate the beneficial effect of Yacon in reducing heart extracellular matrix fibrosis in the diabetic condition and the potential to ameliorate heart tissue disorganization.

4. Discussion

It is known that the hyperglycemia that occurs in diabetes is a major cause of diabetic complications. Since the STZ model of diabetes induction causes the destruction of

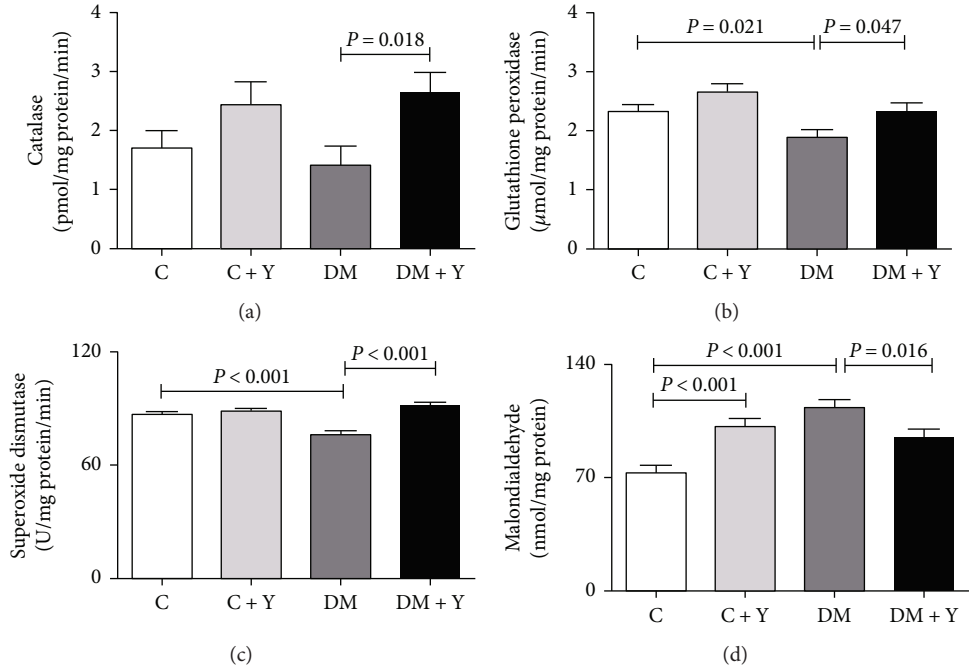

Figure 2: Redox state markers. (a) Catalase; (b) glutathione peroxidase; (c) superoxide dismutase activities; and (d) malondialdehyde concentration in the cardiac tissue. The data are represented as the mean ± SEM. Significance were represented by P values. C: controls; C + Y: controls treated with Yacon leaf extract; DM: diabetic controls; DM + Y: diabetic rats treated with Yacon.

pancreatic β-cells, simulating the physiopathological process of the disease, it generates a deficiency in insulin biosynthesis and secretion and, consequently, an increase in serum glycemia content since it becomes unavailable to insulin-sensitive tissue. In the present study, diabetic animals underwent a hyperglycemic condition after 7 d of STZ administration (Table 1). This condition can be better visualized based on the histological analyses where the DM group presented a deterioration of the architecture and size of the islets (Figures 3(a) and 3(b)) and a decrease in insulin production (Figures 3(c) and 3(d)). Additionally, under these conditions, the breakdown of the structural protein and lipolysis is increased, promoting weight loss and an increase of circulating lipids (e.g., triacylglycerol and fatty acid) [3]. Concomitantly, the serum levels of NEFA were enhanced in the DM group (Table 1); this represents an increase in the availability of NEFA to the heart for energy generation since the cardiac tissue (insulin dependent) does not utilize glucose adequately as an energy source under a diabetic condition [23]. An increase in myocardial fatty acid uptake and oxidation has been described in humans with both type 1 and type 2 diabetes, as well as in many animal models [24]. Elevated circulating glucose [25] and free fatty acid [26, 27] have been shown to possess an important role in the complications of both type 1 and type 2 diabetes. On the other hand, the treated diabetic group presented a decrease in serum glucose and circulating lipids. This can be attributed to an improvement of the glycemic control, suggesting a greater peripheral utilization of glucose and the maintenance of the adipose and muscle tissues. These biochemical and hormonal improvements are potentially linked to the preservation and/or regeneration of the remaining pancreatic islets that were partially destroyed by STZ and, consequently, the potentiation of the insulin secretion from the protected/regenerated β-cells [28, 29]. In agreement with our data, some authors demonstrated that the hydroethanolic extract of Yacon leaves significantly reduced glucose levels in diabetic rats and in genetically type 2 diabetic mice [11, 30, 31]; in parallel, Honoré et al. [32] and Habib et al. [33], respectively, demonstrated that immunofluorescent staining of the pancreatic tissues in a diabetic animal presented a decrease of insulin density whereas diabetic rats treated with a Yacon leaf decoction or Yacon root flour showed strong insulin immunostaining.

In summary, there is extensive evidence that the hyperglycemia established in the diabetic condition is associated with the generation of reactive oxygen species (ROS) and a weakening of the antioxidant defense, resulting in enhanced oxidative stress [13, 34]. Indeed, the activity of several antioxidant enzymes is decreased in the diabetic heart in both rats and humans [13, 35, 36]. Here, we have demonstrated that the activity of the antioxidant enzymes catalase, superoxide dismutase, and glutathione peroxidase is decreased in the diabetic group and MDA concentration is elevated in cardiac tissue (Figures 2(a)–2(d)), indicating an oxidative stress process. These enzymes are regarded as the first line of the antioxidant defense system and work together to diminish ROS generation during oxidative stress [37]. The deleterious effects of oxidative stress in the diabetic heart are well established, including cell death and cardiac fibrosis [38–40]. Cardiac fibrosis is a major feature of diabetic cardiomyopathy [41]. Diabetic cardiomyopathy is defined as a ventricular

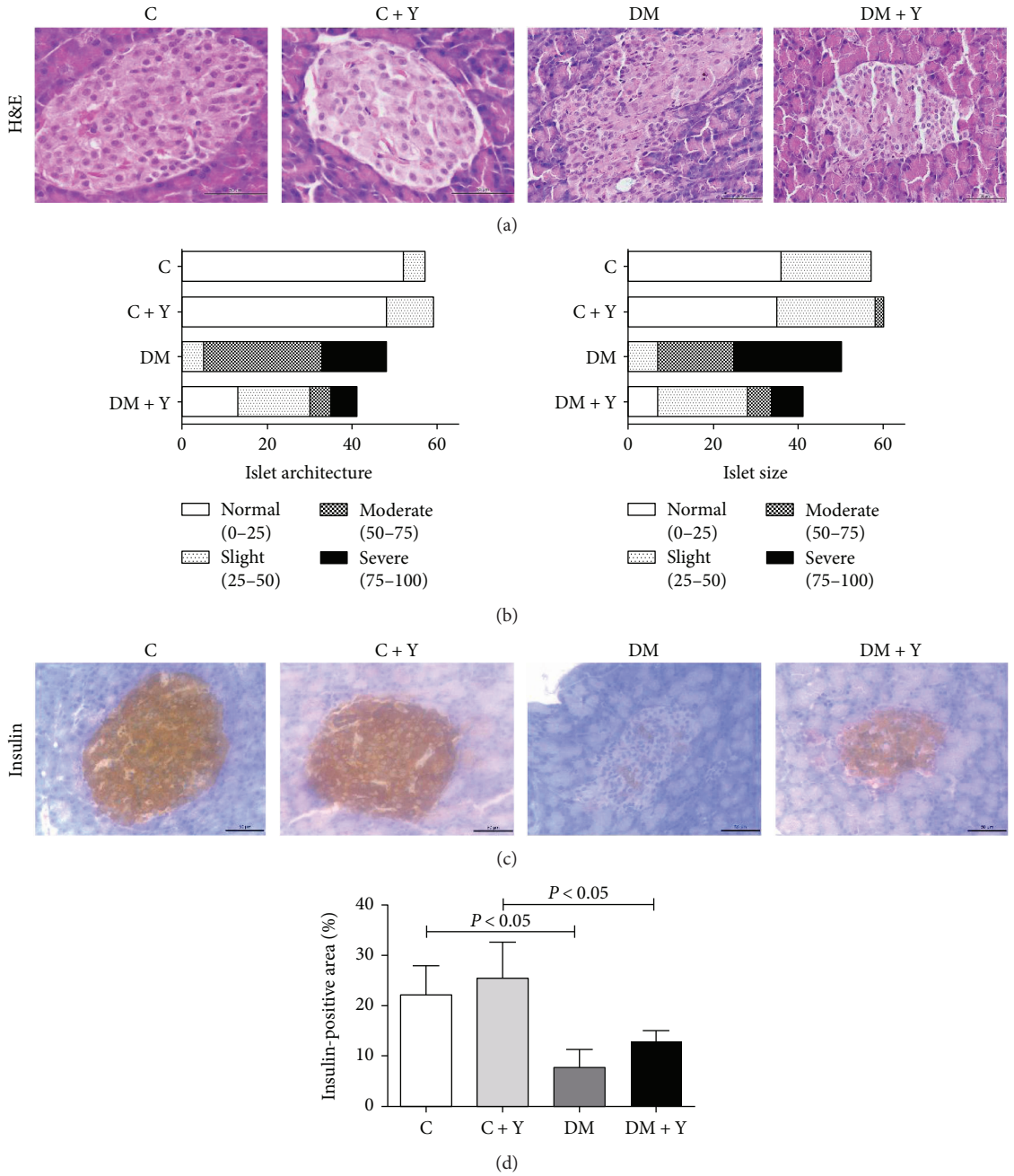

Figure 3: Pancreatic histology, pathologic scoring, and immunohistochemistry analysis. (a) Pancreas histological sections stained with hematoxylin and eosin. (b) Pancreas scoring among groups using architecture and islet size as parameters. (c) Histological analysis of the pancreas by immunohistochemistry for insulin. (d) Quantitative analysis of the positive area for insulin in the pancreatic islets quantified using the imaging software ImageJ. Original magnification, ×20. Scale bars, 50 μm. The data represent the mean ± standard deviation. Statistical analysis was performed using the generalized linear model and two-way analysis of variance test complemented with a nonparametric test for the insulin-positive area or the generalized linear model (binomial) followed by the Wald test for scoring analysis. Significance were represented by P values. C: controls; C + Y: controls treated with Yacon leaf extract; DM: diabetic controls; DM + Y: diabetic rats treated with Yacon; H&E: hematoxylin and eosin.

dysfunction that occurs in diabetic patients not related to another cause (e.g., hypertension or coronary artery disease) [4, 42]. Somaratne et al. [43] reported that 56% of diabetic patients had diabetic cardiomyopathy. Although the etiology of the diabetic cardiomyopathy is not yet completely understood, the pathophysiology of this condition is believed to be multifactorial. Existing evidence suggests that persistent hyperglycemia-induced oxidative stress is an important contributor to it [14, 15]. In this condition, an excessive production of the extracellular matrix protein leads to an increased myocardial hardness and consequent cardiac dysfunction and, consequently, resulting in cardiac failure [44].

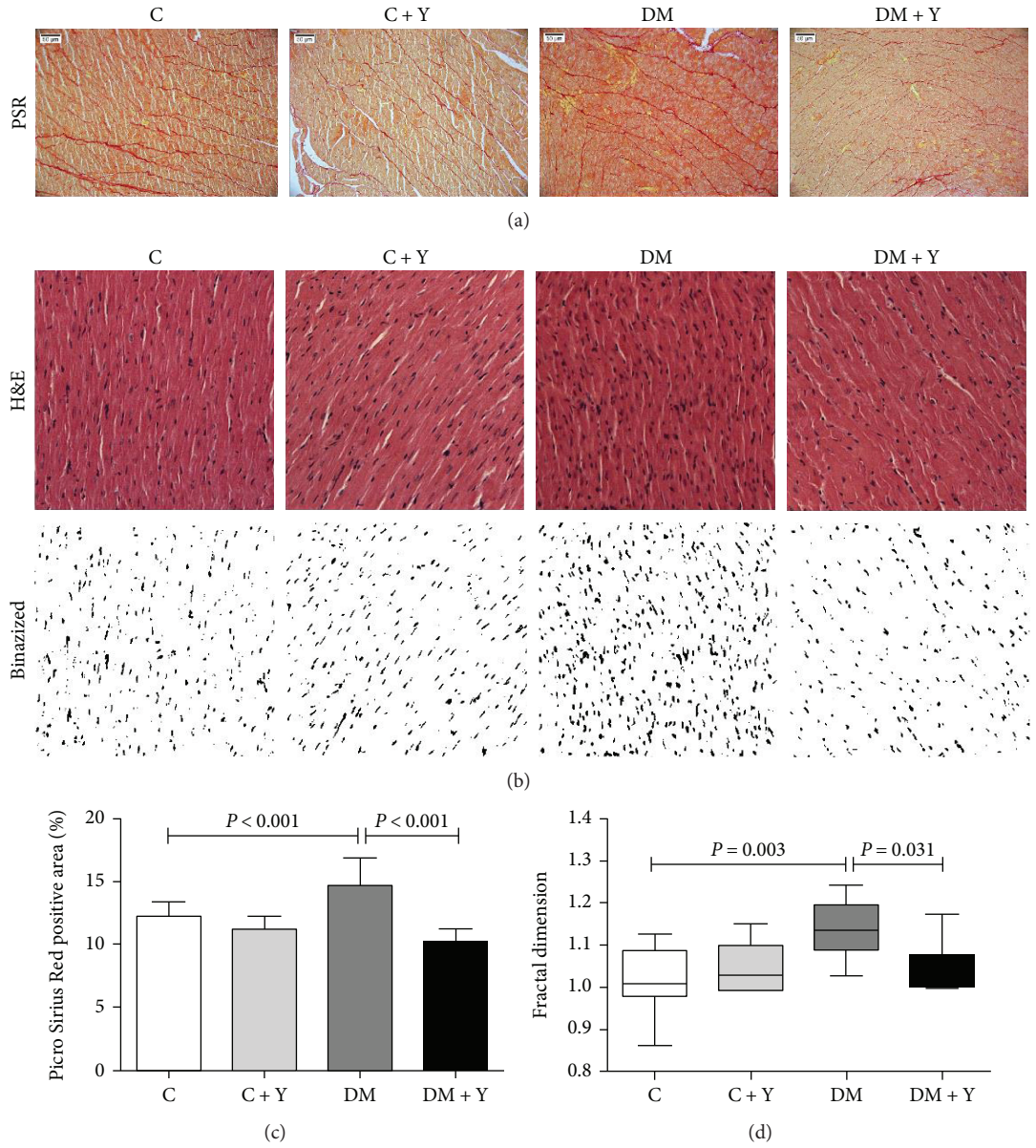

Figure 4: Extracellular matrix collagen area and nuclear disorganization in the cardiac tissue. (a) Heart histological sections of control, diabetic, and treated animals stained with Picro Sirius Red to access extracellular matrix fibrosis. (b) Histological sections of the heart stained with hematoxylin and eosin and the corresponding images after binarization of each group. Original magnification, ×20. Scale bars, 50 μm. (c) Quantitative analysis of the collagen area in the PSR-stained sections. (d) Fractal dimension quantified by imaging software ImageJ. The data represent the mean ± standard deviation, and for fractal analysis data are expressed as a box plot graphic showing the first and third quartiles and the median, minimum, and maximum. Statistical analysis was performed using the two-way analysis of variance test complemented with a nonparametric test. Significance were represented by P values. C: controls; C + Y: controls treated with Yacon leaf extract; DM: diabetic controls; and DM + Y: diabetic rats treated with Yacon; PSR: Picro Sirius Red; H&E: hematoxylin and eosin.

Concomitantly, our data indicate that the diabetic condition leads to an increase of collagen deposit and nuclear disorganization in cardiac tissue (Figures 4(a)–4(d)). Diabetic patients have a 2- to 5-fold increased risk of developing heart failure, one of the greatest contributors to morbidity and mortality [45]. Here we have also showed an increase of oxidative stress in the heart of the untreated DM group, whereas the Yacon treatment promoted a decrease of the oxidative stress marker and an increase of the antioxidant enzyme activity. We have previously demonstrated the antioxidant activity of Yacon leaves in the soleus muscle, potentially due to the presence of several antioxidant compounds in the extract [13]. Additionally, phytochemical studies of Yacon leaves showed the presence of high-polarity antioxidant compounds such as caffeic, chlorogenic, and three dicaffeoylquinic acids [46]. It is known that compounds such as phenolic acids, polyphenols, and flavonoids can scavenge free radicals such as peroxide, hydroperoxide, or lipid peroxyl and thus inhibit the oxidative mechanisms that lead to diabetes complications. So, since oxidative

stress is related to the cardiac remodeling and fibrosis through several mechanisms [38, 39, 47], this could be the mechanism by which DM + Y presented an improvement of the cardiac alterations mentioned above. Given the fundamental role of oxidative stress in the pathogenesis of diabetes and diabetic cardiomyopathy, there is growing interest in the use of antioxidants as a complementary therapeutic approach to prevent/treat these conditions. Numerous studies demonstrated that ameliorating oxidative stress through antioxidant treatment might be an effective strategy for reducing diabetic cardiomyopathy [48, 49].

The important findings of this study are the cardio- and pancreatic protective effects of Yacon treatment in experimental STZ-induced diabetic cardiomyopathy and pancreatic islet dysfunction in terms of the preservation of the Langerhans islet architecture and insulin production as well as an inhibition of collagen content accumulation and enhancement of antioxidant enzyme activities in cardiac tissue. Summarizing, our results demonstrated that STZ administration successfully induced diabetes and diabetic cardiomyopathy as indicated by the fractal analysis, indicating cellular disorganization, as well as an increase in collagen deposition in heart tissue and a decrease of insulin production and preservation of the architecture of the pancreatic β-cells. Interestingly, these cardiac and pancreatic abnormalities were improved by the administration of the Yacon extract. Furthermore, exploring the potential therapeutic effects of plants and herbal medicine could contribute to the detection of new targets and treatments. Our findings, even as a basic research model, provide information that can guide future studies aimed at elucidating new therapeutic alternatives for diabetic complications.

Conflicts of Interest

The authors declare that there are no conflicts of interest regarding the publication of this paper.

Acknowledgments

The authors thank the São Paulo Research Foundation (FAPESP Grant no. 2018/05103-6) for financial support and the Coordination of Improvement of Higher Education Personnel (CAPES) for scholar stipend.

Supplementary Materials

Table S1: analysis of the islets by scores. Description of the results for the islet staging criteria (normal, slight, moderate, and severe) obtained after the linear model for a binomial distribution with a logistic link followed by the multiple Wald comparison test for islet size and architecture. C: controls; C + Y: controls treated with Yacon leaf extract; DM: diabetic controls; and DM + Y: diabetic rats treated with Yacon; ND: no difference; NT: not tested. The linear model for a binomial distribution followed by the multiple Wald comparison test analyzed statistical significance. Figure S1: analysis of the islets by scores. Description of the results for the islet staging criteria (normal, slight, moderate, and severe) obtained after the linear model for a binomial distribution with a logistic link followed by the multiple Wald comparison test for islet size and architecture. Blue lines represent statistical significance while red lines mean no difference (ND) or not tested (NT) among the groups. *(Supplementary Materials)*

References

[1] M. Copenhaver and R. P. Hoffman, "Type 1 diabetes: where are we in 2017?," *Translational Pedriatrics*, vol. 6, no. 4, pp. 359–364, 2017.

[2] T. Miki, S. Yuda, H. Kouzu, and T. Miura, "Diabetic cardiomyopathy: pathophysiology and clinical features," *Heart Failure Reviews*, vol. 18, no. 2, pp. 149–166, 2013.

[3] M. Bayeva, K. T. Sawicki, and H. Ardehali, "Taking diabetes to heart—deregulation of myocardial lipid metabolism in diabetic cardiomyopathy," *Journal of the American Heart Association*, vol. 2, no. 6, article e000433, 2013.

[4] I. Falcão-Pires and A. F. Leite-moreira, "Diabetic cardiomyopathy: understanding the molecular and cellular basis to progress in diagnosis and treatment," *Heart Failure Reviews*, vol. 17, no. 3, pp. 325–344, 2012.

[5] L. A. Suzuki, M. Poot, R. G. Gerrity, and K. E. Bornfeldt, "Diabetes accelerates smooth muscle accumulation in lesions of atherosclerosis: lack of direct growth-promoting effects of high glucose levels," *Diabetes*, vol. 50, no. 4, pp. 851–860, 2001.

[6] J. Tian, Y. Zhao, Y. Liu, Y. Liu, K. Chen, and S. Lyu, "Roles and mechanisms of herbal medicine for diabetic cardiomyopathy: current status and perspective," *Oxidative Medicine and Cellular Longevity*, vol. 2017, Article ID 8214541, 15 pages, 2017.

[7] U. Varma, P. Koutsifeli, V. L. Benson, K. M. Mellor, and L. M. D. Delbridge, "Molecular mechanisms of cardiac pathology in diabetes—experimental insights," *Biochimica et Biophysica Acta (BBA) - Molecular Basis of Disease*, 2017.

[8] H. Tsutsui, S. Kinugawa, S. Matsushima, and T. Yokota, "Oxidative stress in cardiac and skeletal muscle dysfunction associated with diabetes mellitus," *Journal of Clinical Biochemistry and Nutrition*, vol. 48, no. 1, pp. 68–71, 2011.

[9] T. V. Fiorentino, A. Prioletta, P. Zuo, and F. Folli, "Hyperglycemia-induced oxidative stress and its role in diabetes mellitus related cardiovascular diseases," *Current Pharmaceutical Design*, vol. 19, no. 32, pp. 5695–5703, 2013.

[10] World Health Organization (WHO), *Traditional Medicine Strategy 2005:1–6*, http://www.wpro.who.int/health_technology/book_who_traditional_medicine_strategy_2002_2005.pdf.

[11] S. Baroni, F. Suzuki-Kemmelmeier, S. M. Caparroz-Assef, R. K. N. Cuman, and C. A. Bersani-Amado, "Effect of crude extracts of leaves of *Smallanthus sonchifolius* (yacon) on glycemia in diabetic rats," *Revista Brasileira de Ciências Farmacêuticas*, vol. 44, no. 3, pp. 521–530, 2008.

[12] B. Simonovska, I. Vovk, S. Andrenšek, K. Valentová, and J. Ulrichová, "Investigation of phenolic acids in yacon (*Smallanthus sonchifolius*) leaves and tubers," *Journal of Chromatography A*, vol. 1016, no. 1, pp. 89–98, 2003.

[13] K. C. Dos Santos, B. G. Bueno, L. F. Pereira et al., "Yacon (*Smallanthus sonchifolius*) leaf extract attenuates hyperglycemia and skeletal muscle oxidative stress and inflammation in diabetic rats," *Evidence-Based Complement and Alternative Medicine*, vol. 2017, article 6418048, 9 pages, 2017.

[14] S. Boudina and E. D. Abel, "Diabetic cardiomyopathy, causes and effects," *Reviews in Endocrine and Metabolic Disorders*, vol. 11, no. 1, pp. 31–39, 2010.

[15] J. S. Dobrin, D. Lebeche, and G. L. L. Place, "Diabetic cardiomyopathy: signaling defects and therapeutic approaches," *Expert Review of Cardiovascular Therapy*, vol. 8, no. 3, pp. 373–391, 2010.

[16] D. T. Pierine, M. E. L. Navarro, I. O. Minatel et al., "Lycopene supplementation reduces TNF-α via RAGE in the kidney of obese rats," *Nutrition & Diabetes*, vol. 4, no. 11, article e142, 2014.

[17] S. L. Marklund, "Product of extracellular-superoxide dismutase catalysis," *FEBS Letters*, vol. 184, no. 2, pp. 237–239, 1985.

[18] H. Aebi, "[13] Catalase *in vitro*," *Methods in Enzymology*, vol. 105, pp. 121–126, 1984.

[19] L. Flohé and W. A. Günzler, "[12] Assays of glutathione peroxidase," *Methods in Enzymology*, vol. 105, pp. 114–120, 1984.

[20] O. H. Lowry, N. J. Rosebrough, A. L. Farr, and R. J. Randall, "Protein measurement with the Folin phenol reagent," *The Journal of Biological Chemistry*, vol. 193, no. 1, pp. 265–275, 1951.

[21] R. Jain, D. M. Tartar, R. K. Gregg et al., "Innocuous IFNγ induced by adjuvant-free antigen restores normoglycemia in NOD mice through inhibition of IL-17 production," *Journal of Experimental Medicine*, vol. 205, no. 1, pp. 207–218, 2008.

[22] F. L. Pacagnelli, A. K. D. A. Sabela, T. B. Mariano et al., "Fractal dimension in quantifying experimental-pulmonary-hypertension-induced cardiac dysfunction in rats," *Arquivos Brasileiros de Cardiologia*, vol. 107, no. 1, pp. 33–39, 2016.

[23] C. M. Galhardi, Y. S. Diniz, L. A. Faine et al., "Toxicity of copper intake: lipid profile, oxidative stress and susceptibility to renal dysfunction," *Food and Chemical Toxicology*, vol. 42, no. 12, pp. 2053–2060, 2004.

[24] E. D. Abel, S. E. Litwin, and G. Sweeney, "Cardiac remodeling in obesity," *Physiological Reviews*, vol. 88, no. 2, pp. 389–419, 2008.

[25] D. M. Nathan and for the DCCT/EDIC Research Group, "The diabetes control and complications trial/epidemiology of diabetes interventions and complications study at 30 years: overview," *Diabetes Care*, vol. 37, no. 1, pp. 9–16, 2014.

[26] H. C. Chiu, A. Kovacs, D. A. Ford et al., "A novel mouse model of lipotoxic cardiomyopathy," *The Journal of Clinical Investigation*, vol. 107, no. 7, pp. 813–822, 2001.

[27] H. Yagyu, G. Chen, M. Yokoyama et al., "Lipoprotein lipase (LpL) on the surface of cardiomyocytes increases lipid uptake and produces a cardiomyopathy," *The Journal of Clinical Investigation*, vol. 111, no. 3, pp. 419–426, 2003.

[28] M. J. Aybar, A. N. Sánchez Riera, A. Grau, and S. S. Sánchez, "Hypoglycemic effect of the water extract of *Smallantus sonchifolius* (yacon) leaves in normal and diabetic rats," *Journal of Ethnopharmacology*, vol. 74, no. 2, pp. 125–132, 2001.

[29] K. Valentová, A. Lebeda, I. Dolezalová et al., "The biological and chemical variability of yacon," *Journal of Agricultural and Food Chemistry*, vol. 54, no. 4, pp. 1347–1352, 2006.

[30] T. M. Miura, Y. Itoh, T. Kaneko et al., "Corosolic acid induces GLUT4 translocation in genetically type 2 diabetic mice," *Biological and Pharmaceutical Bulletin*, vol. 27, no. 7, pp. 1103–1105, 2004.

[31] T. M. Miura, "Antidiabetic activity of *Fuscoporia oblique* and *Samallanthus sonchifolius* in genetically type 2 diabetic mice," *Journal of Traditional Medicine*, vol. 24, no. 2, pp. 47–50, 2007.

[32] S. M. Honoré, W. M. Cabrera, S. B. Genta, and S. S. Sánchez, "Protective effect of yacon leaves decoction against early nephropathy in experimental diabetic rats," *Food and Chemical Toxicology*, vol. 50, no. 5, pp. 1704–1715, 2012.

[33] N. C. Habib, S. M. Honoré, S. B. Genta, and S. S. Sánchez, "Hypolipidemic effect of *Smallanthus sonchifolius* (yacon) roots on diabetic rats: biochemical approach," *Chemico-Biological Interactions*, vol. 194, no. 1, pp. 31–39, 2011.

[34] P. T. Yeh, H. W. Huang, C. M. Yang, W. S. Yang, and C. H. Yang, "Astaxanthin inhibits expression of retinal oxidative stress and inflammatory mediators in streptozotocin-induced diabetic rats," *PloS One*, vol. 11, no. 1, article e0146438, 2016.

[35] J. S. Johansen, A. K. Harris, D. J. Rychly, and A. Ergul, "Oxidative stress and the use of antioxidants in diabetes: linking basic science to clinical practice," *Cardiovascular Diabetology*, vol. 4, no. 1, p. 5, 2005.

[36] K. C. dos Santos, C. P. Braga, P. O. Barbanera, F. Seiva, A. F. Junior, and A. Ange, "Cardiac energy metabolism and oxidative stress biomarkers in diabetic rat treated with resveratrol," *PLoS One*, vol. 9, no. 7, article e102775, 2014.

[37] J. M. Matés, C. Pérez-Gómez, and I. Núñez de Castro, "Antioxidant enzymes and human diseases," *Clinical Biochemistry*, vol. 32, no. 8, pp. 595–603, 1999.

[38] A. Aneja, W. H. W. Tang, S. Bansilal, M. J. Garcia, and M. E. Farkouh, "Diabetic cardiomyopathy: insights into pathogenesis, diagnostic challenges, and therapeutic options," *The American Journal of Medicine*, vol. 121, no. 9, pp. 748–757, 2008.

[39] Z. Y. Fang, J. B. Prins, and T. H. Marwick, "Diabetic cardiomyopathy: evidence, mechanisms, and therapeutic implications," *Endocrine Reviews*, vol. 25, no. 4, pp. 543–567, 2004.

[40] D. Cai, M. Yuan, D. F. Frantz et al., "Local and systemic insulin resistance resulting from hepatic activation of IKK-β and NF-κB," *Nature Medicine*, vol. 11, no. 2, pp. 183–190, 2005.

[41] B. Li, Z. Zheng, Y. Wei et al., "Therapeutic effects of neuregulin-1 in diabetic cardiomyopathy rats," *Cardiovascular Diabetology*, vol. 10, no. 1, p. 69, 2011.

[42] S. Boudina and E. D. Abel, "Diabetic cardiomyopathy revisited," *Circulation*, vol. 115, no. 25, pp. 3213–3223, 2007.

[43] J. B. Somaratne, G. A. Whalley, K. K. Poppe et al., "Screening for left ventricular hypertrophy in patients with type 2 diabetes mellitus in the community," *Cardiovascular Diabetology*, vol. 10, no. 1, p. 29, 2011.

[44] C. Li, L. Lv, H. Li, and D. Yu, "Cardiac fibrosis and dysfunction in experimental diabetic cardiomyopathy are ameliorated by alpha-lipoic acid," *Cardiovascular Diabetology*, vol. 11, no. 1, pp. 73–10, 2012.

[45] D. S. H. Bell, "Heart failure: the frequent, forgotten, and often fatal complication of diabetes," *Diabetes Care*, vol. 26, no. 8, pp. 2433–2441, 2003.

[46] S. B. Genta, W. M. Cabrera, M. I. Mercado, A. Grau, C. A. Catalán, and S. S. Sánchez, "Hypoglycemic activity of leaf organic extracts from *Smallanthus sonchifolius*: constituents of the most active fractions," *Chemico-Biological Interactions*, vol. 185, no. 2, pp. 143–152, 2010.

[47] L. Cai, Y. Wang, G. Zhou et al., "Attenuation by metallothionein of early cardiac cell death via suppression of mitochondrial oxidative stress results in a prevention of diabetic

cardiomyopathy," *Journal of the American College of Cardiology*, vol. 48, no. 8, pp. 1688–1697, 2006.

[48] M. A. Haidara, H. Z. Yassin, M. Rateb, H. Ammar, and M. A. Zorkani, "Role of oxidative stress in development of cardiovascular complications in diabetes mellitus," *Current Vascular Pharmacology*, vol. 4, no. 3, pp. 215–227, 2006.

[49] V. Kain, S. Kumar, and S. L. Sitasawad, "Azelnidipine prevents cardiac dysfunction in streptozotocin-diabetic rats by reducing intracellular calcium accumulation, oxidative stress and apoptosis," *Cardiovascular Diabetology*, vol. 10, no. 1, p. 97, 2011.

Hindawi
Oxidative Medicine and Cellular Longevity
Volume 2018, Article ID 2627917, 11 pages
https://doi.org/10.1155/2018/2627917

Research Article

The Encapsulation of Lycopene in Nanoliposomes Enhances Its Protective Potential in Methotrexate-Induced Kidney Injury Model

Nenad Stojiljkovic,[1] **Sonja Ilic**,[1] **Vladimir Jakovljevic**,[2,3] **Nikola Stojanovic**,[4] **Slavica Stojnev**,[5] **Hristina Kocic**,[6] **Marko Stojanovic**,[4] **and Gordana Kocic**[7]

[1]*Department of Physiology, Faculty of Medicine, University of Niš, Bulevar Zorana Đinđića 81, 18000 Niš, Serbia*
[2]*Department of Physiology, Faculty of Medical Sciences, University of Kragujevac, Svetozara Markovica 69, 34000 Kragujevac, Serbia*
[3]*Department of Human Pathology, I.M. Sechenov First Moscow State Medical University, Moscow, Russia*
[4]*Faculty of Medicine, University of Niš, Bulevar Zorana Đinđića 81, 18000 Niš, Serbia*
[5]*Department of Pathology, Faculty of Medicine, University of Niš, Bulevar Zorana Đinđića 81, 18000 Niš, Serbia*
[6]*Faculty of Medicine, University of Maribor, Magdalenski trg 5, SI-2000 Maribor, Slovenia*
[7]*Department of Biochemistry, Faculty of Medicine, University of Niš, Bulevar Zorana Đinđića 81, 18000 Niš, Serbia*

Correspondence should be addressed to Vladimir Jakovljevic; drvladakgbg@yahoo.com

Received 3 November 2017; Accepted 1 January 2018; Published 13 March 2018

Academic Editor: Mithun Sinha

Methotrexate is an antimetabolic drug with a myriad of serious side effects including nephrotoxicity, which presumably occurs due to oxidative tissue damage. Here, we evaluated the potential protective effect of lycopene, a potent antioxidant carotenoid, given in two different pharmaceutical forms in methotrexate-induced kidney damage in rats. Serum biochemical (urea and creatinine) and tissue oxidative damage markers and histopathological kidney changes were evaluated after systemic administration of both lycopene dissolved in corn oil and lycopene encapsulated in nanoliposomes. Similar to previous studies, single dose of methotrexate induced severe functional and morphological alterations of kidneys with cell desquamation, tubular vacuolation, and focal necrosis, which were followed by serum urea and creatinine increase and disturbances of tissue antioxidant status. Application of both forms of lycopene concomitantly with methotrexate ameliorated changes in serum urea and creatinine and oxidative damage markers and markedly reversed structural changes of kidney tissue. Moreover, animals that received lycopene in nanoliposome-encapsulated form showed higher degree of recovery than those treated with free lycopene form. The findings of this study indicate that treatment with nanoliposome-encapsulated lycopene comparing to lycopene in standard vehicle has an advantage as it more efficiently reduces methotrexate-induced kidney dysfunction.

1. Introduction

Methotrexate (MTX) is antimetabolic drug which is often used for the treatment of several autoimmune disorders such as rheumatoid arthritis, psoriasis, and various malignant tumors including lymphoblastic leukemia, lymphoma, osteosarcoma, breast cancer, and head and neck cancer [1]. Clinical use of MTX is limited due to its side effects that include bone marrow suppression, hepatotoxicity, nephrotoxicity, pulmonary fibrosis, and gastrointestinal mucosal damage. Since MTX is primarily excreted by kidneys [2], severity of nephrotoxicity depends on both the dose and frequency of MTX administration [3]. Similar to other agents with nephrotoxic effect, MTX-induced renal impairment is clinically followed by hematuria and increased levels of serum creatinine and urea in humans. These effects can be faithfully reproduced in experimental animals after single dose of MTX [4, 5].

Lycopene, a red-colored carotenoid, found mainly in tomatoes but also in other fruits and vegetables (watermelons,

Momordica cochinchinensis, Spreng fruit, papayas, etc.), possesses a strong antioxidant activity. It protects cells against damage caused by free radicals with its reactive oxygen species (ROS) scavenging properties [6, 7]. It is proven to be more potent than similar antioxidants, like β-carotene and vitamin E [6, 8], largely due to its several conjugated double bonds. Besides the numerous beneficial properties (anti-inflammatory, anticancer, etc.), investigations revealed that lycopene has protective effect in animal models of nephrotoxicity [8, 9].

Nanoliposomes are bilayer lipid vesicles which can be encapsulated with various bioactive agents including medicaments, pharmaceuticals, nutritional supplements, antioxidants, polynucleotides, and polypeptides [10]. Nanoliposomes have the potential to increase solubility and bioavailability, *in vitro* and *in vivo* stability, improve time-controlled drug releasing, minimize concentrations required for optimum therapeutic efficacy, enable cell-specific targeting, and decrease adverse effects of drugs on healthy cells and tissues [11, 12]. In the case of lycopene, formulation with nanoliposomes could prevent its rapid interaction with highly reactive compounds, like plasma proteins or metal ions, allowing it to reach the targeted damaged tissue. Moreover, using nanoliposomes as carriers to incorporate lycopene into membranes might be an initial step in cell prevention as it is proposed that damage of cell membrane by ROS causes the onset of number of pathological events leading to oxidative injury [13].

Since, to the best of our knowledge, no study exists which shows potential of using lycopene in this new pharmaceutical formulation to treat drug-induced tissue injury, we aimed at evaluating characteristics of the nanoliposome encapsulation and efficacy of this preparation in preventing/ameliorating methotrexate-induced kidney injury. To achieve this, we first measured in vitro properties of encapsulated lycopene and then compared its efficacy with free form lycopene through the evaluation of changes in serum and tissue oxidative stress markers and quantification of kidney tissue damages induced by MTX.

2. Materials and Methods

2.1. Drugs and Chemicals. Methotrexate was obtained from EBEWE Pharma (Ges.m.b.H.NFG.KG, Austria), while ketamine (Ketamidor 10%) was purchased from Richter Pharma (AG, Wels, Austria). Lycopene was purchased from Sigma-Aldrich (St. Louis, USA) and all other used chemicals were obtained from either Sigma-Aldrich (St. Louis, USA) or Carl Roth (Karlsruhe, Germany).

2.2. Experimental Protocol In Vitro

2.2.1. Nanoliposomes Encapsulation with Lycopene. The 10% solution of phospholipid nanoparticles, in a form of nanospheres, purchased from Nattermann Phospholipids (Germany), was encapsulated by lycopene at the concentration of 4 mg/ml. Encapsulated nanoparticles were isolated by centrifugation at 6500g for 30 min at 4°C according to the method of Kocic et al. [13].

2.2.2. Efficacy of Lycopene Encapsulation. The efficacy of encapsulation was determined based on a method previously described in great detail [14]. Briefly, after mixing the lycopene-loaded liposomes and petroleum ether (3 ml), the mixture was further vortexed for 3 min followed by a centrifugation (2000 rpm, 5 min). The upper layer was separated and its absorbance was measured at 470 nm (V-1800 Shimadzu spectrophotometer). The encapsulation efficacy (%) was calculated as (amount of incorporated lycopene)/(initial amount of added lycopene) × 100.

2.2.3. Sustained Release of Encapsulated Lycopene. The mixture of lycopene nanoparticles with phosphate buffer saline was incubated at 37°C for 24 h from which the aliquots were taken in order to measure the release of lycopene from nanoliposomes. At the defined time points (0, 1, 2, 4, 8, 12, and 24 h), the aliquots were taken and diluted in petroleum ether in order to measure their absorbance at 470 nm and quantify the amount of free lycopene present. The content of lycopene was calculated using a standard curve.

2.2.4. pH Dependent Stability of Encapsulated Lycopene. The stability of free and encapsulated lycopene in different pH buffers (6.5, 7.4, 8.0, and 9.0) was studied following previously described method [15]. The mixture containing either free or encapsulated lycopene and buffer solution with different pH values (1 : 10, *v*/*v*) was incubated at 37°C, from which the aliquots were taken after 0, 20, 40, 60, 120, and 180 minutes. The residual rate of lycopene present in the mixture at designated time point was determined spectrophotometrically at 470 nm using a standard curve for lycopene. Residual rate is the residual amount of lycopene expressed in percentages in relation to the initial amount of lycopene.

2.2.5. Metal Ion Chelating Properties of Encapsulated Lycopene. The stability of formed lycopene nanoliposomes in the presence of different metal ions (K^+, Ca^{2+}, Mg^{2+}, Al^{3+}, or Cu^{2+}) was evaluated according to the method described by Chen et al. [15]. The free/encapsulated lycopene was incubated with 1 mmol/l of metal solution for 2 h at 37°C. After the incubation period, the mixture was centrifuged in order to separate the formed lycopene-metal chelate. The obtained supernatant was mixed with petroleum ether, and the absorbance of the solution was measured at 470 nm in order to determine the residual rate of lycopene, where residual rate is the residual amount of lycopene expressed in percentages in relation to the initial amount of lycopene.

2.2.6. Susceptibility of Encapsulated Lycopene to H_2O_2. After centrifugated nanoparticles were resuspended and both lycopene encapsulated and native nanoparticles as well as free lycopene were exposed to H_2O_2 for 30 min at 37°C [13]. The intensity of lipid peroxidation was determined using colorimetric method that involves thiobarbituric acid as a reagent [16].

2.3. Experimental Protocol In Vivo

2.3.1. Animals and Housing. Forty-eight male Wistar rats (200–250 g) were divided into 8 groups of 6 animals and

maintained under standard laboratory conditions at the Vivarium of the Institute of Biomedical Research, Medical Faculty, Niš, Serbia. Laboratory was kept under standard temperature (22°C) and humidity (60%), with equal duration of light/dark cycle. During the entire experiment, animals had free access to food and water. All experiments were conducted at the Institute of Biomedical Research, Medical Faculty, Niš, Serbia, and are in accordance with all ethical regulations of European Union (EU Directive of 2010; 2010/63/EU) and Republic of Serbia (332-07-00073/2017-05/1).

2.3.2. Animal Treatment. Treatment protocol included 8 groups of 6 rats treated daily by an intraperitoneal injection (i.p.), as following:

(i) Control (C) group: the animals were given corn oil (0.2 ml/day) for 10 days.

(ii) Nanoliposomes (NL) group: the animals were given empty nanoliposomes (10 ml/kg) for 10 days.

(iii) Lycopene (LYC) group: the animals were given lycopene dissolved in corn oil (6 mg/kg) for 10 days.

(iv) Encapsulated nanoliposomes (ENL) group: the animals were given encapsulated lycopene (6 mg/kg) for 10 days.

(v) Methotrexate (MTX) group: the animals were given MTX (20 mg/kg) at day 1 and corn oil (0.2 ml/day) for 10 days.

(vi) Methotrexate-nanoliposomes (MTX-NL) group: the animals were given MTX (20 mg/kg) at day 1 and empty nanoliposomes (10 ml/kg) for 10 days.

(vii) Methotrexate-lycopene (MTX-LYC) group: the animals were given MTX (20 mg/kg) at day 1 and lycopene dissolved in corn oil (6 mg/kg) for 10 days.

(viii) Methotrexate-encapsulated nanoliposomes (MTX-ENL) group: the animals were given MTX (20 mg/kg) at day 1 and encapsulated lycopene (6 mg/kg) for 10 days.

Twenty-four hours after administration of the last dose, all animals were sacrificed by ketamine overdose. For biochemical analysis, blood was taken from the aorta and the kidneys were removed postmortem for tissue biochemical (frozen and stored at −80°C) and histopathological (fixated in 10% buffered formalin) studies. Kidney tissue homogenate (10% *w*/*v*) was made in ice-cold distilled water and was centrifugated at 14000 rpm for 10 min (at 4°C) in order to obtain clear supernatant for further analysis.

2.4. Biochemical Analysis

2.4.1. Serum Biochemical Parameters Estimation. The collected blood was allowed to clot at room temperature and afterwards centrifugated in order to obtain serum. Kidney functional state was estimated using serum creatinine and urea levels that were assayed by Olympus AU680® Chemistry-Immuno Analyzer.

2.4.2. Determination of Protein Concentration. Protein concentration in kidney tissue homogenates was measured according to Lowry's method, using bovine serum as standard, as described previously [17].

2.4.3. Malondialdehyde Levels Determination. The determination of the extent of tissue lipid peroxidation was based on the amount of formed malondialdehyde (MDA) estimated by a spectrophotometric method (532 nm), Multiskan Ascent (Labsystems, Finland) using thiobarbituric acid reaction [16]. The amount of tissue MDA was expressed as nmol/mg of kidney tissue proteins.

2.4.4. Catalase Activity Determination. Tissue catalase (CAT) activity was determined using hydrogen peroxide (H_2O_2) as substrate, where after the incubation period the reaction was stopped by the addition of ammonium molybdate [18]. The absorbance of the reaction was measured at 405 nm and the results were expressed as IU/mg of proteins.

2.4.5. Advanced Oxidized Proteins Determination. The concentration of advanced oxidized proteins products (AOPP) in renal tissue homogenates was determined by a spectrophotometric method previously described in detail [17]. The method is based on the reaction of AOPP with potassium iodide (KI) in an acidic medium. The intensity of the reaction was measured immediately at 340 nm, and the concentrations of AOPP were expressed as μmol/mg of proteins.

2.4.6. Myeloperoxidase Activity Determination. Myeloperoxidase (MPO) activity was determined in kidney tissue homogenates using *o*-phenylenediamine activated with H_2O_2 as described previously [19]. Shortly after the incubation, the reaction was stopped with H_2SO_4 solution, and optical densities (OD) were determined at 540 nm using a microplate reader. The results are expressed as OD/mg of proteins.

2.4.7. Tissue Nitrite Concentration Determination. The concentration of nitrites present in tissue homogenates was measured using a Griess reagent [20]. The mixture consisting of tissue homogenate and Griess reagent was incubated at room temperature for 10 min, and the absorbance of each sample was measured at 540 nm using a microplate reader. The nitrite concentrations were calculated using a standard curve of sodium nitrite.

2.5. Histopathological Analysis. After fixation of kidney samples in buffered formaldehyde solution (10%, *w*/*v*), the tissues were routinely processed and embedded in paraffin. Embedded tissue was cut into 4-5 μm thick sections, stained with hematoxylin and eosin (H&E) and periodic acid-Schiff (PAS) as described previously [21] and analyzed using Olympus BH2 light microscope. The extent of kidney tissue damage was evaluated based on morphological changes in sections stained with H&E. The PAS staining allowed a better insight into glomerular and tubular structures appearance and the detection of PAS-positive tubular casts. Semiquantitative scoring system for tubular, interstitial, and glomerular changes was used in order to evaluate the extent of kidney

tissue damage. The evaluation criteria were as follows: none (—), mild (+), moderate (++), and severe (+++) [22].

2.6. Statistical Analysis. The results were expressed as the mean values ± standard deviation (SD). One-way analysis of variance (ANOVA) followed by Tukey's post hoc test for multiple comparisons (GraphPad Prism version 5.03, San Diego, CA, USA) was used for the determination of statistically significant differences. Probability values (p) ≤ 0.05 were considered to be statistically significant.

3. Results

3.1. Efficacy of Lycopene Encapsulation. The efficacy of encapsulation was 71.9%.

3.2. Evaluation of Encapsulated Lycopene Stability

3.2.1. Sustained Release of Encapsulated Lycopene and Susceptibility of Encapsulated Lycopene to H_2O_2. The lycopene sustained release curve showed linear growth over 8 h period and stabilization around 12 h, where only 5% of lycopene was released from the nanoliposomes after 2 h and about 50% after 12 h period (Figure 1(a)).

The determined MDA levels after incubation of free lycopene, empty nanoliposomes, and lycopene nanoliposomes with H_2O_2 showed that encapsulation of lycopene increases its antioxidant capacity (Figure 1(b)). Lycopene nanoliposomes showed enhanced antioxidant activity, where the concentrations of MDA were significantly decreased in the aliquots of encapsulated nanoliposomes compared to the free lycopene ($p < 0.01$) and empty nanoliposomes ($p < 0.001$) (Figure 1(b)).

3.2.2. pH Dependent Stability of Encapsulated Lycopene. The degradation of lycopene (both free and encapsulated) was the slowest in low pH solutions (6.4 and 7.4) where after 180 min the residual rate of encapsulated lycopene was more than 50% (Table 1). The rapid degradation of free lycopene was observed particularly in solution with pH 9, where residual rate of lycopene after 20 min was 10.4 ± 0.1% and after 180 min 4.1 ± 0.1%. The degradation of encapsulated lycopene in nanoliposomes was slow, and in the first 60 min, the residual rate of lycopene was very high, for example, 60 min after incubation in solution with pH 9 approximately 62% of lycopene remained (Table 1).

3.2.3. Metal Ion Chelating Properties of Encapsulated Lycopene. As shown in Table 2, all metals were chelated more intensively with free lycopene compared to the encapsulated one. The lycopene residual rate in mixtures of K^+, Ca^{2+}, Mg^{2+}, Al^{3+}, and Cu^{2+} ions and free/encapsulated lycopene was around 35/45, 38/51, 24/38, 24/36, and 33/48%, respectively (Table 2).

3.3. In Vivo Evaluation of Free and Encapsulated Lycopene Nephroprotective Activity

3.3.1. Serum Biochemical Parameters Estimation. Serum levels of creatinine and urea were statistically significantly increased in animals treated with MTX (Figure 2). The increase in serum levels of these two parameters, especially the levels of urea, following MTX injection, was statistically significantly decreased ($p < 0.001$ compared to MTX-treated group) with the application of lycopene and encapsulated lycopene (Figure 2). Levels of creatinine and urea were statistically significantly decreased in MTX-ENL group compared to MTX-LYC ($p < 0.001$) (Figure 2).

3.3.2. Histopathological Analysis. Kidney sections of C, NL, LYC, and ENL groups demonstrated normal morphology of rat kidney, with no pathologic findings in glomeruli, tubules, and interstitium (Figures 3(a)–3(d), Table 3). Group of animals treated with MTX showed marked histological damage of renal cortex where the epithelium of proximal tubules showed severe vacuolation and desquamation, with focal tubular necrosis and apoptotic body formation (Figure 3(e), Table 3). In the same group of animals, cast formation was observed in significant proportion of kidney tubules. Glomeruli displayed mild degeneration and edema, with narrowed Bowman's space. There was a significant congestion in glomerular and peritubular capillaries, with mild to moderate interstitial inflammatory infiltrate. In MTX-NL group, micromorphologic changes similar to the MTX group were found (Figure 3(f), Table 3). In the kidneys of animals treated with lycopene after a single dose of MTX, only moderate tubular degeneration, with less prominent vacuolation and desquamation of epithelial cells, was visible (Figure 3(g), Table 3). Tubular cell necrosis was scarce and only occasional tubular casts could be seen. Glomeruli were slightly edematous in appearance, and in interstitium, only mild congestion and with the presence of few inflammatory cells were detected (Figure 3(g), Table 3). In the MTX-ENL group, tubular damage was mildly expressed, with rare small tubular casts (Figure 3(h), Table 3). Glomerular degeneration was not present and the architecture of glomeruli and Bowman's space was well preserved. Interstitial edema and inflammation were unremarkable (Figure 3(h), Table 3).

PAS-positive epithelial surface, which could be related to microvilli, with thin and well-defined basement membranes of glomerular capillaries and renal tubules, could be seen in the kidney sections of C, NL, LYC, and ENL group of animals (Figures 4(a)–4(d)). In the MTX and MTX-NL groups, loss of brush border in the majority of proximal tubule epithelium, as well as prominent PAS-positive tubular casts, was found (Figures 4(e) and 4(f), Table 3). Several glomeruli matrix expansion was observed as well (Figures 4(e) and 4(f)). Simultaneous treatment with MTX and free lycopene showed significant attenuation of noticeable changes, with less deterioration in brush border and only occasional PAS-positive tubular casts. In the MTX-ENL group, epithelial surface structures were predominantly preserved from MTX toxic damage. Fine tubular brush border and membrane structures were found, and there were no significant changes of glomerular morphology (Figures 4(g) and 4(h), Table 3).

3.3.3. Catalase Activity Determination. Methotrexate application to rats produced a statistically significant decrease in CAT activity in kidney tissue homogenates ($p < 0.001$) (Table 4). The decrease in CAT activity following MTX

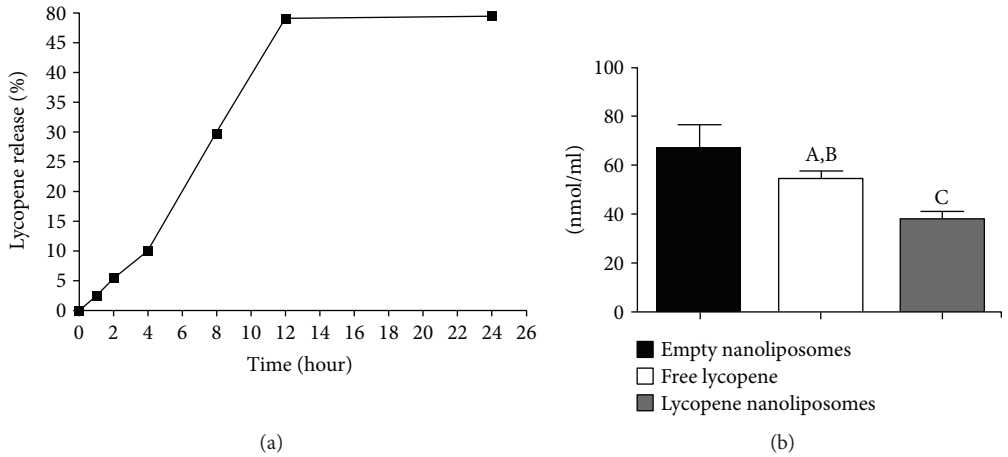

Figure 1: Encapsulated lycopene sustained release curve (a) and MDA levels (b) after exposure of free lycopene, empty nanoliposomes, and encapsulated lycopene nanoliposomes to oxidative damage by incubation with H_2O_2. Data are presented as mean value ± SD. $^{A}p < 0.05$ versus empty nanoliposomes; $^{B}p < 0.01$ versus lycopene nanoliposomes; $^{C}p < 0.001$ versus empty nanoliposomes.

Table 1: Stability of lycopene nanoliposomes in solutions with different pH values.

pH value	Samples	Residual rate (%) at different time points (minutes)					
		0	20	40	60	120	180
6.4	Free lycopene	62.2 ± 0.6	42.4 ± 1.3	36.4 ± 1.8	33.9 ± 0.9	19.9 ± 1.1	9.0 ± 0.6
	Lycopene nanoliposomes	97.4 ± 0.3	88.4 ± 1.1	75.5 ± 0.3	75.0 ± 0.5	68.4 ± 1.4	58.2 ± 0.4
7.4	Free lycopene	75.15 ± 0.03	32.3 ± 0.6	22.8 ± 0.9	22.1 ± 1.6	16.1 ± 0. 8	4.2 ± 0.3
	Lycopene nanoliposomes	100 ± 0.0	74.2 ± 1.7	60.2 ± 1.9	59.6 ± 0.4	58.6 ± 0.9	53.9 ± 0.0
8	Free lycopene	66.4 ± 0.0	32.1 ± 1.6	25.1 ± 0.9	22.0 ± 0.6	9.5 ± 0.7	3.6 ± 0.3
	Lycopene nanoliposomes	100 ± 0.00	57.6 ± 0.1	53.8 ± 0.6	52.9 ± 0.1	45.5 ± 1.48	44.4 ± 0.2
9	Free lycopene	49.6 ± 0.141	10.4 ± 0.1	10.12 ± 0.2	6.5 ± 0.2	5.65 ± 0.2	4.1 ± 0.1
	Lycopene nanoliposomes	100 ± 0.00	94.9 ± 1.4	87.2 ± 1.1	62.1 ± 0.1	23.2 ± 1.5	20.9 ± 0.177

Data are presented as mean percentage values ± SD.

Table 2: Stability of lycopene nanoliposomes against metal ions.

Metal ions	K^+	Ca^{2+}	Mg^{2+}	Al^{3+}	Cu^{2+}
Free lycopene (lycopene residual rate %)	34.75 ± 1.22	38.5 ± 1.64	24.25 ± 0.7	23.75 ± 0.66	33.25 ± 1.05
Lycopene nanoliposomes (lycopene residual rate %)	45.3 ± 2.21	51.22 ± 2.89	38.33 ± 1.69	36.24 ± 1.21	48.1 ± 2.07

Data are presented as mean value ± SD.

application was prevented by a prolonged application of both free and encapsulated lycopene (Table 4). The encapsulation of lycopene was found to statistically significantly ($p < 0.001$) enhance the activity of lycopene (Table 4).

3.3.4. Myeloperoxidase Activity Determination. Application of MTX statistically significantly increases MPO activity in kidney tissue compared to the control group of animals ($p < 0.001$) (Table 4). The activity of MPO in the kidneys of animals from MTX-LYC and MTX-ENL groups was statically significantly decreased compared to the MTX-treated animals ($p < 0.001$) (Table 4).

3.3.5. Advanced Oxidized Protein Determination. The extent of protein oxidation in kidney tissues of rats treated with MTX was statistically significantly increased compared to the control group ($p < 0.001$) (Table 4). Ten days of animal treatment, following methotrexate injection, with free or encapsulated lycopene, statistically significantly decreased AOPP formation in the kidneys ($p < 0.001$) (Table 4). The encapsulated lycopene treatment that followed MTX administration completely abolished the formation of AOPP (no statistically significant difference between this group and control group of animals).

3.3.6. Tissue Nitrite Concentration Determination. Application of a single dose of MTX to rats caused a statistically significant increase in renal tissue nitric oxide (NO) concentration, compared to control animals (Table 4). This increase was ameliorated by both free and encapsulated lycopene (Table 4), where the effect of the encapsulated lycopene was

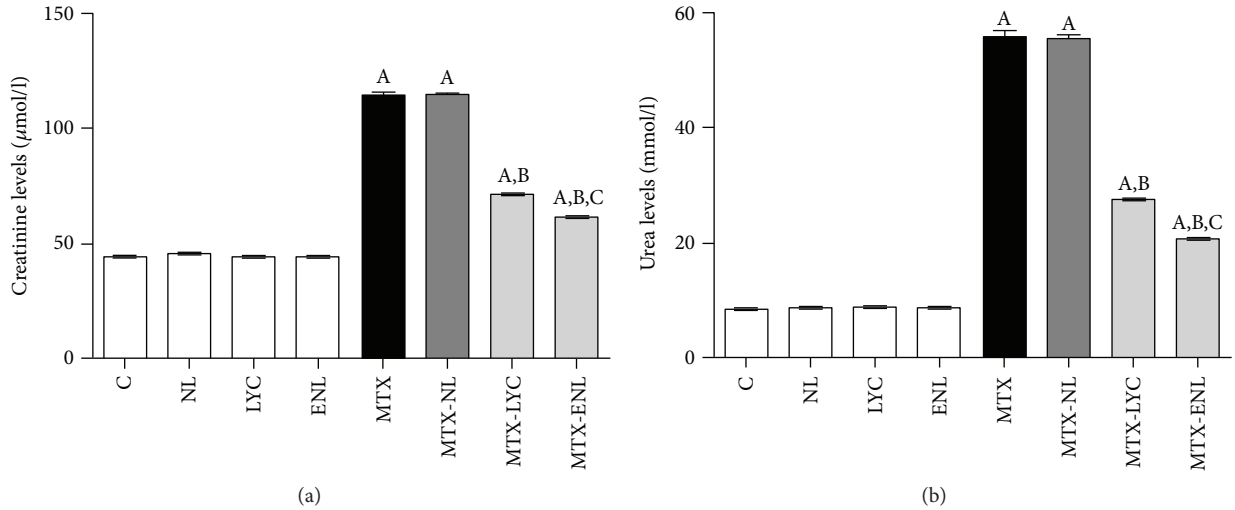

Figure 2: Statistical comparison of serum levels of creatinine (a) and urea (b) between groups of animals after different experimental treatments. Data are presented as mean ± SD, $n = 6$. $^{A}p < 0.001$ versus control group; $^{B}p < 0.001$ versus methotrexate group; $^{C}p < 0.001$ versus methotrexate-lycopene group.

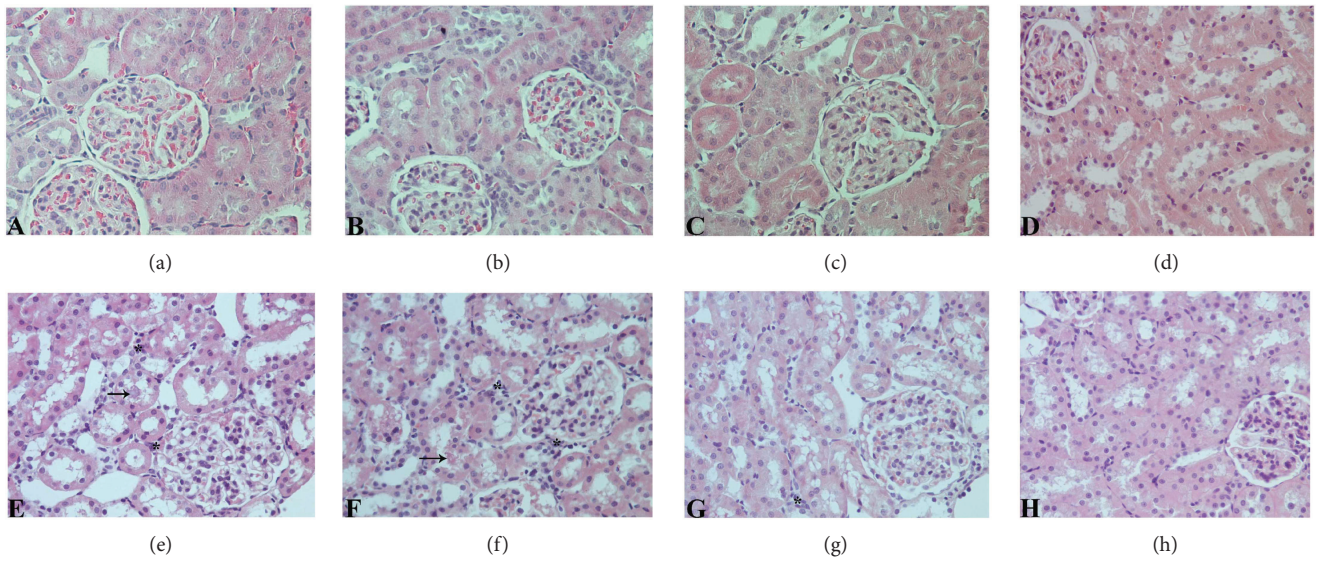

Figure 3: Histological evaluation of renal tissue sections stained with H&E (original magnification, 400x). Sections from control (c) group (a), nanoliposomes (NL) group (b), lycopene (LYC) group (c), and encapsulated nanoliposomes (ENL) group (d) showing normal kidney morphology; (e) methotrexate (MTX) and (f) methotrexate-empty nanoliposomes (MTX-NL) groups with significant damage of renal cortex structures that include glomerular degeneration and interstitial inflammatory infiltration (marked with asterisk) with tubule cell vacuolation and apoptosis and with occasional tubule cast present (marked with arrow); (g) methotrexate-lycopene (MTX-LYC) group showing significantly milder kidney structure changes and (h) methotrexate-encapsulated nanoliposomes (MTX-ENL) group showing higher degree of recovery than those treated with free lycopene form.

statistically significantly higher ($p < 0.001$) than that of the free one (Table 4).

3.3.7. Malondialdehyde Level Determination. The applied dose of MTX produced statistically significant increase in amount of MDA, compared to the control group ($p < 0.001$) (Table 4). These significant changes in MDA products were less pronounced in animals treated with MTX and lycopene and even less in MTX and encapsulated lycopene-treated ones ($p < 0.001$) (Table 4). Also, there is a statistically significant difference ($p < 0.05$) in MDA levels between groups that received lycopene and encapsulated lycopene after MTX (Table 4).

4. Discussion

Antioxidants are commonly used as protective agents in numerous pathological conditions; however, their

Table 3: Semiquantitative histopathological score analysis of renal tissue damage.

Histopathological lesion	C	NL	LYC	ENL	MTX	MTX-NL	MTX-LYC	MTX-ENL
Tubular changes								
Tubular degeneration	—	—	—	—	+++	+++	++	+
Tubular cell edema/vacuolation	—	—	—	—	+++	+++	++	+
Tubular apoptosis/necrosis	—	—	—	—	++	++	+	—
Hyaline intratubular casts	—	—	—	—	++	++	+	—
Interstitial changes								
Mononuclear cell infiltration	—	—	—	—	+++	+++	+	+
Interstitial swelling	—	—	—	—	+++	+++	++	+
Vascular congestion	—	—	—	—	+++	++	++	+
Glomerular changes								
Glomerular degeneration	—	—	—	—	++	++	+	—

Scoring was done as follows: none (—), mild (+), moderate (++), and severe (+++).

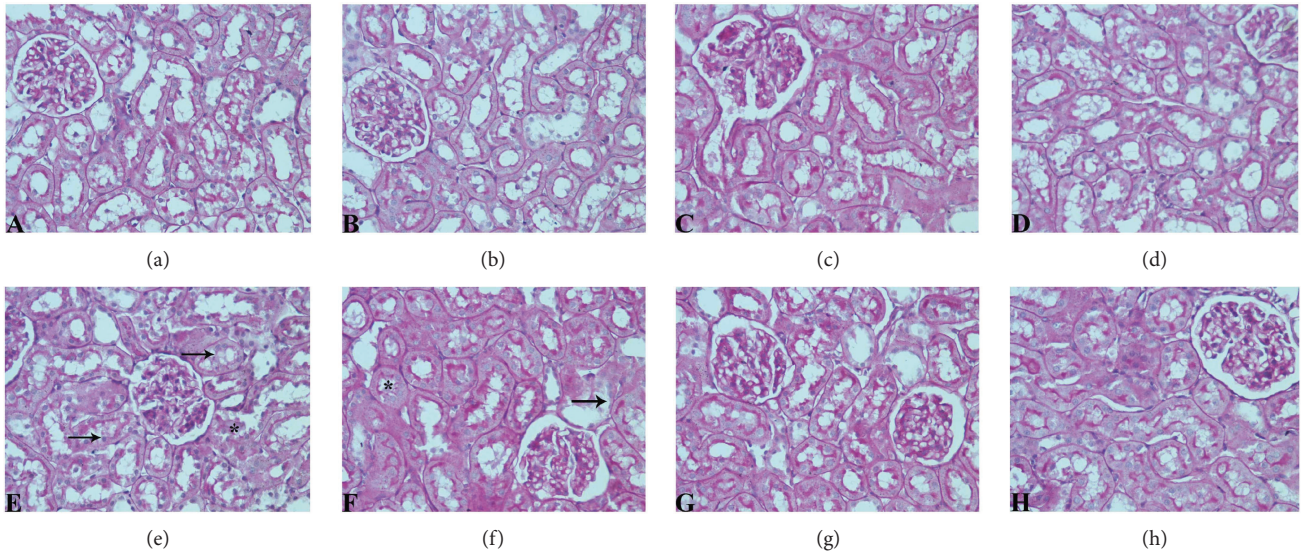

Figure 4: Light photomicrographs of PAS-stained sections of rat renal cortex showing normal histology of kidney tissue and regular morphology of microvilli-covered epithelial surface, with thin and well-defined basement membranes in control (c) group (a) nanoliposomes (NL) group (b), lycopene (LYC) group (c), and encapsulated nanoliposomes (ENL) group (d); significant destruction of brush border (marked with arrow), and presence of PAS-positive tubular casts (marked with asterisk) in (e) methotrexate (MTX) and (f) methotrexate-empty nanoliposomes (MTX-NL) group; attenuation of visible changes, with less destruction of brush in rats treated with methotrexate and lycopene (MTX-LYC group) (g) and almost complete prevention of histopathological alterations in group treated with methotrexate and encapsulated nanoliposomes (MTX-ENL group) (h). (PAS, original magnification, 400x).

application is often limited due to their low bioavailability, rapid degradation, and delivery of low concentrations to the target tissues. Encapsulation of antioxidants in nanoparticles increases their concentration in cells and antioxidant activity. The initial step, the encapsulation of lycopene, was performed in order to evaluate both its *in vitro* antioxidant activity and *in vivo* protective properties of this highly reactive carotenoid. The efficacy of lycopene encapsulation was determined to be 71.9% which is in accordance with previous investigations (from 60% to 80%) [14]. This range of efficacy of encapsulation can be explained by the strong lipophilicity of lycopene molecules, allowing them to be positioned deeply in bilayer hydrophobic core of nanoliposomes [23]. Our results showed slow release of lycopene from nanoliposomes which reflects its good stability and it can be explained by the fact that lycopene is positioned inside the nanoliposome bilayer. Good sustained release might reflect the potential interaction of free lycopene with plasma proteins and could prolong the presence of lycopene in circulation, allowing it to reach the target tissue.

Since the lycopene has the ability to quench singlet oxygen, which is related to its double bonds in molecule and the opening of the β-ionone ring, we examined and compared antioxidant activity of both free and encapsulated lycopene in *in vitro* oxidative damage model. Lycopene showed significant antioxidant activity, which is in accordance with the high reactivity of lycopene with singlet oxygen and free radicals [24]; however, in the present study, the effect of

Table 4: Kidney oxidative status in animals after different experimental treatments.

Group/parameter	CAT (IU/mg proteins)	MPO (OD/mg proteins)	AOPP (μmol/mg proteins)	MDA (nmol/mg proteins)	NO (μmol/l)
Control (corn oil treated)	120 ± 2.1	111 ± 4.6	13.5 ± 4.9	10.2 ± 0.6	26.5 ± 5.7
Lycopene	115 ± 3.2	99.5 ± 21.9	12.9 ± 4.3	11.2 ± 1.9	29.5 ± 10.0
Empty nanoliposomes	114 ± 1.3	117.5 ± 6.3	14.2 ± 0.9	11.3 ± 1.4	31.6 ± 7.8
Lycopene nanoliposomes	120 ± 3.5	119 ± 1.4	12.9 ± 1.6	9.9 ± 0.5	30.6 ± 2.8
Methotrexate	24.5 ± 7.5^{a}	189 ± 2.3^{a}	29.6 ± 6.1^{a}	27.9 ± 0.4^{a}	65.6 ± 5.8^{a}
Lycopene + methotrexate	$67.1 \pm 2.1^{a,b}$	$159 \pm 11.3^{a,d}$	$21.2 \pm 0.4^{a,d}$	$17.8 \pm 2.2^{a,b}$	$41.9 \pm 11.5^{b,e}$
Empty nanoliposomes + methotrexate	30 ± 4.3^{a}	170 ± 13.8^{a}	28.9 ± 2.6^{e}	$25.9 \pm 1.6^{a,}$	66.3 ± 3.5^{a}
Lycopene nanoliposomes + methotrexate	$83.1 \pm 3.2^{a,b,c}$	$141.5 \pm 14^{a,b}$	17.9 ± 1.8^{b}	$14.6 \pm 2.4^{a,b,f}$	$39.3 \pm 1.4^{b,c,e}$

[a]$p < 0.001$ versus control group treated with corn oil; [b]$p < 0.001$ versus methotrexate group; [c]$p < 0.001$ versus lycopene + methotrexate group; [d]$p < 0.01$ versus methotrexate group; [e]$p < 0.05$ versus control group treated with corn oil; [f]$p < 0.05$ versus lycopene + methotrexate group

encapsulated form was more pronounced than the activity of free lycopene (Figure 1(b)). Our results are similar to those of Tan et al. [14], where it was showed that lower concentrations of lycopene in nanoliposomes preserved integrity of liposomal membrane and displayed antioxidant activity in lipid peroxidation assays. One can say that the antioxidant activity of lycopene was not only related to its chemical structure, but also to its incorporation in nanoliposomes, where the encapsulated lycopene was able to significantly counteract H_2O_2-induced oxidative stress.

It was previously documented that lycopene is rather stable at low pH values, that is, optimal pH range of lycopene is 3.5–4.5 [24], and that its stability decreases with the increase in solutions pH. Having that in mind, we examined whether the encapsulation of lycopene in nanoliposomes can increase its stability in various alkaline solutions with pH varying from 6.4 to 9. The results presented in Table 1 demonstrate the stability of free and encapsulated lycopene in solutions with different pH values where lycopene stability was enhanced by its encapsulation in nanoliposomes. Free lycopene was proven to be less stable than the encapsulated one in alkaline pH, which is in accordance with previous studies [25]. This increased stability of encapsulated lycopene can possibly be explained by its position in the nanoliposomes lipid bilayer, where the polar lycopene is deep in hydrophobic core where it is protected from direct contact with the solution.

Also, we examined the stability of free and lycopene encapsulated in nanoliposomes in the presence of different metal ions (Table 2). The chelation activity of lycopene could reduce its stability and pharmacological activity; thus, by its encapsulation in nanoliposomes, the stability of lycopene against metal ions was improved. This decrease in lycopene chelation after the encapsulation could possibly be related to its higher stability in nanoliposomes and prevention of direct contact of lycopene and metal ions by nanoliposomes membrane.

In *in vivo* experiment, an increase in serum levels of creatinine and urea is direct consequence of kidney tissue injury, a known side effect of MTX application [26]. The changes in kidney tissue following MTX exposure include decrease in glomerular filtration rate, due to vasoconstriction of afferent arterioles, and direct damage of the tubule cells [27]. The increased concentration of MTX in urine, achieved by glomerular filtration and tubular secretion, leads to intratubular crystal formation, causing obstruction [27]. Also an additional mechanism of MTX nephrotoxicity, considered to be key mechanism of toxicity, involves the increase in ROS generation, especially H_2O_2, in kidney tubules [28]. Results of biochemical analysis were in accordance with histopathological findings. MTX toxicity may also result in acute renal failure due to precipitation of its metabolite 7-OH-MTX in renal tubules and MTX direct damage of tubules as well [29], which was observed as increased amount of PAS-positive tubular casts (Figure 4(e), Table 3). In the kidneys of animals treated with encapsulated lycopene after MTX, only mild degenerative changes were observed (Table 3), pointing to its strong nephroprotective potential.

Since there is relation between MTX application and oxidative stress, we examined parameters such as CAT, AOPP, MDA, NO, and MPO in kidney homogenates and investigated whether application of free lycopene and nanoliposomes encapsulated with lycopene can improve oxidative status. Catalase is one of the key enzymes that regulate amounts of H_2O_2 in cells and indirectly the extent of tissue damage originating from cell structure peroxidation. The decrease (inhibition) in CAT activity could be caused directly by MTX [30], which seems logical since it is proven that methotrexate increases H_2O_2 amounts [28]. Also, CAT activity is tightly connected with the amounts of H_2O_2 that can cause both inactivation and/or consumption of CAT in kidney tissue [28]. Thus, we can speculate that lycopene, either free or encapsulated, increases kidney CAT activity. This is in good correlation with previous publications where lycopene increased enzymatic antioxidant status (CAT, glutathione S-transferase, peroxidase, and reductase) of liver tissue in animals treated with high-fat diet that causes tissue oxidative damage [31]. Myeloperoxidase activity represents

a sensitive marker of tissue infiltration with neutrophils, due to a good correlation between its activity and histopathological finding [32]. Methotrexate is also known to induce the releases of free radicals, MPO among them, from stimulated polymorphonuclear neutrophils causing cellular oxidative damage [28, 32]. Generated products of MPO, chlorinating oxidants arriving from chlorides and H_2O_2, are able to cause cell damage by reacting with amino acids, proteins, carbohydrates, lipids, and nucleobases [32]. The application of both forms of lycopene statistically significant decreases MPO activity (Table 4), which is in accordance with previous studies where it is shown that lycopene decreases MPO activity in the damaged kidney [33, 34] and myocardial [35] and pancreatic [36] tissues.

Nitric oxide represents an important cell mediator that is involved in numerous both physiological and pathophysiological processes [37]. One of the theories explaining MTX nephrotoxicity involves NO signaling and increase of inducible nitric oxide synthase (iNOS), which is barely detectable in normal renal tissue [38]. Nitric oxide is also involved in macrophage activation, and during the inflammatory processes in the kidneys, macrophages produce large amounts of NO playing an important role in renal tissue pathology [39]. Previous studies evaluated the effects of free lycopene (10 mg/kg, orally applied) on MTX-induced kidney damage and consequential NO increase [38]. However, no statistically significant effects on NO concentrations were detected. On the other hand, in the model of unilateral ureteral obstruction-induced kidney damage, lycopene was proven to reduce tissue NO levels [33], similarly to the findings of the present study (Table 4). The difference in the obtained results may lay in the different routes of lycopene administration (i.p. and per os), and these results could possibly be explained through high reactivity of lycopene, whose activity significantly decreases when applied orally due to its interaction with numerous compounds leading to its isomerization, oxidation, and/or degradation [14]. In the present study, this was potentially avoided by the application of lycopene via i.p. route and by its encapsulation with nanoliposomes.

The formation of AOPP is believed to be one of the initial steps in cell oxidative stress that further signals the development of renal diseases [40]. Activated MPO in the tissue generates hypochlorous acid which mediates protein modifications causing tyrosine chlorination and formation of chloramines and carbonyls [32]. The accumulation of AOPP in renal cortex, especially in glomerulus, is known to decrease the Bowman's spaces and thus causing the impairments in kidney function [41]. Such pathological findings, as well as increase in AOPP concentration, were detected in animals treated with MTX (Figure 4(e) and Table 4). In addition to ROS-mediated protein damage during exposure to MTX, generated ROS damages unsaturated lipids as well [42], making MDA products a sensitive marker of lipid peroxidation. The formation of MDA could be connected with damaging activity of both peroxynitrite, from superoxide anion and nitric oxide, and hypochlorous acid [28, 32]. Since the activity of MPO and NO concentrations is statistically significantly decreased by both forms of lycopene, it is not surprising that the MDA and AOPP amounts are statistically significantly decreased in these groups as well (Table 4).

This study primarily aimed at comparing efficacy of two different pharmaceutical forms of lycopene on MTX-induced toxicity at kidney tissue level. However, it is limited in defining potential differences of their sites of action at particular kidney tissue cell targets. Previous *in vitro* studies revealed that lycopene can accumulate in epithelial cells and affect different protein synthesis depending on concentration applied [43]. The present study should warrant future work focusing on more detailed action of nanoliposome-encapsulated lycopene at the cellular level.

5. Conclusion

Lycopene is presumed to protect cells from oxidative damage by stabilization of the membrane and/or scavenging free radicals generated within the tissue [44]. In this study, we demonstrated that nanoliposome-encapsulated lycopene represents a protected form of this highly reactive carotenoid with enhanced activity. The methotrexate-induced nephrotoxicity model allowed us to investigate and compare the efficacy of the free and encapsulated lycopene in preventing reactive oxygen species-induced kidney tissue damage, which is considered to be a key mechanism of methotrexate toxicity. Our results demonstrated that encapsulated lycopene showed stronger antioxidant activity than free one. Since lycopene is widely used as a dietary supplement, encapsulation of lycopene should be taken as a potential "shelter" when considering lycopene formulation. Also, in this form, it should be recommended for simultaneous application with methotrexate therapy.

Conflicts of Interest

The authors declare that there is no conflict of interest regarding the publication of this article.

Acknowledgments

This work was funded by the project of the Faculty of Medicine, University of Niš, Serbia (Project no. INT-MFN-13).

References

[1] B. C. Widemann, F. M. Balis, B. Kempf-Bielack et al., "High-dose methotrexate-induced nephrotoxicity in patients with osteosarcoma," *Cancer*, vol. 100, no. 10, pp. 2222–2232, 2004.

[2] S. Kivity, Y. Zafrir, R. Loebstein, R. Pauzner, M. Mouallem, and H. Mayan, "Clinical characteristics and risk factors for low dose methotrexate toxicity: a cohort of 28 patients," *Autoimmunity Reviews*, vol. 13, no. 11, pp. 1109–1113, 2014.

[3] N. Jahovic, G. Sener, H. Cevik, Y. Ersoy, S. Arbak, and B. C. Yegen, "Amelioration of methotrexate-induced enteritis by melatonin in rats," *Cell Biochemistry & Function*, vol. 22, no. 3, pp. 169–178, 2004.

[4] I. Asvadi, B. Hajipour, A. Asvadi, N. A. Asl, L. Roshangar, and A. Khodadadi, "Protective effect of pentoxyfilline in renal toxicity after methotrexate administration," *European Review for*

Medical and Pharmacological Sciences, vol. 15, no. 9, pp. 1003–1009, 2011.

[5] N. Vardi, H. Parlakpinar, B. Ates, A. Cetin, and A. Otlu, "The protective effects of *Prunus armeniaca* L (apricot) against methotrexate-induced oxidative damage and apoptosis in rat kidney," *Journal of Physiology and Biochemistry*, vol. 69, no. 3, pp. 371–381, 2013.

[6] S. S. Palabiyik, P. Erkekoglu, N. D. Zeybek et al., "Protective effect of lycopene against ochratoxin A induced renal oxidative stress and apoptosis in rats," *Experimental and Toxicologic Pathology*, vol. 65, no. 6, pp. 853–861, 2013.

[7] W. Stahl and H. Sies, "Antioxidant activity of carotenoids," *Molecular Aspects of Medicine*, vol. 24, no. 6, pp. 345–351, 2003.

[8] A. Atessahin, S. Yilmaz, I. Karahan, A. O. Ceribasi, and A. Karaoglu, "Effects of lycopene against cisplatin-induced nephrotoxicity and oxidative stress in rats," *Toxicology*, vol. 212, no. 2-3, pp. 116–123, 2005.

[9] A. Dogukan, M. Tuzcu, C. A. Agca et al., "A tomato lycopene complex protects the kidney from cisplatin-induced injury via affecting oxidative stress as well as Bax, Bcl-2, and HSPs expression," *Nutrition and Cancer*, vol. 63, no. 3, pp. 427–434, 2011.

[10] S. K. Sahoo, S. Parveen, and J. J. Panda, "The present and future of nanotechnology in human health care," *Nanomedicine: Nanotechnology, Biology, and Medicine*, vol. 3, no. 1, pp. 20–31, 2007.

[11] G. A. Hughes, "Nanostructure-mediated drug delivery," *Nanomedicine: Nanotechnology, Biology, and Medicine*, vol. 1, no. 1, pp. 22–30, 2005.

[12] M. R. Mozafari, "Bioactive entrapment and targeting using nanocarrier technologies: an introduction," in *Nanocarrier Technologies: Frontiers of Nanotherapy*, M. R. Mozafari, Ed., pp. 1–16, Springer, Netherlands, 2005.

[13] G. Kocic, K. Tomovic, H. Kocic et al., "Antioxidative, membrane protective and antiapoptotic effects of melatonin, *in silico* study of physico-chemical profile and efficiency of nanoliposome delivery compared to betaine," *RSC Advances*, vol. 7, no. 3, pp. 1271–1281, 2017.

[14] C. Tan, J. Xue, S. Abbas, B. Feng, X. Zhang, and S. Xia, "Liposome as a delivery system for carotenoids: comparative antioxidant activity of carotenoids as measured by ferric reducing antioxidant power, DPPH assay and lipid peroxidation," *Journal of Agricultural and Food Chemistry*, vol. 62, no. 28, pp. 6726–6735, 2014.

[15] X. Chen, L. Q. Zou, J. Niu, W. Liu, S. F. Peng, and C. M. Liu, "The stability, sustained release and cellular antioxidant activity of curcumin nanoliposomes," *Molecules*, vol. 20, no. 8, pp. 14293–14311, 2015.

[16] J. A. Buege and S. D. Aust, "Microsomal lipid peroxidation," *Methods in Enzymology*, vol. 52, pp. 302–310, 1978.

[17] S. Ilic, N. Stojiljkovic, S. Veljkovic et al., "Morphometric study of structural kidney damages caused by cisplatin in rats. Effects of quercetin," *Acta Microscopica*, vol. 25, no. 4, pp. 128–137, 2016.

[18] L. Goth, "A simple method for determination of serum catalase activity and revision of reference range," *Clinica Chimica Acta*, vol. 196, no. 2-3, pp. 143–151, 1991.

[19] S. S. Jacob, P. Shastry, and P. R. Sudhakaran, "Influence of non-enzymatically glycated collagen on monocyte–macrophage differentiation," *Atherosclerosis*, vol. 159, no. 2, pp. 333–341, 2001.

[20] N. S. Radulovic, P. J. Randjelovic, N. M. Stojanovic, N. D. Cakic, G. A. Bogdanovic, and A. V. Zivanovic, "Aboriginal bush foods: a major phloroglucinol from Crimson Bottlebrush flowers (*Callistemon citrinus*, Myrtaceae) displays strong antinociceptive and antiinflammatory activity," *Food Research International*, vol. 77, Part 2, pp. 280–289, 2015.

[21] N. Stojiljkovic, M. Stoiljkovic, P. Randjelovic, S. Veljkovic, and D. Mihailovic, "Cytoprotective effect of vitamin C against gentamicin-induced acute kidney injury in rats," *Experimental and Toxicologic Pathology*, vol. 64, no. 1-2, pp. 69–74, 2012.

[22] P. Randjelovic, S. Veljkovic, N. Stojiljkovic et al., "Salicylic acid attenuates gentamicin-induced nephrotoxicity in rats," *The Scientific World Journal*, vol. 2012, Article ID 390613, 6 pages, 2012.

[23] M. van de Ven, M. Kattenberg, G. van Ginkel, and Y. K. Levine, "Study of the orientational ordering of carotenoids in lipid bilayers by resonance-Raman spectroscopy," *Biophysical Journal*, vol. 45, no. 6, pp. 1203–1209, 1984.

[24] T. Anguelova and J. Warthesen, "Degradation of lycopene, α-carotene, and β-carotene during lipid peroxidation," *Journal of Food Science*, vol. 65, no. 1, pp. 71–75, 2000.

[25] M. F. Salama, E. I. Seliem, K. F. Mahmoud, and A. A. Amin, "Physiochemical characterization and oxidative stability of encapsulated nano lycopene pigments extracted by CO_2 fluid extraction," *International Journal of Current Microbiology and Applied Sciences*, vol. 4, no. 3, pp. 307–320, 2015.

[26] R. Singh, R. Shah, C. Turner, O. Regueira, and T. L. Vasylyeva, "N-acetylcysteine renoprotection in methotrexate induced nephrotoxicity and its effects on B-cell lymphoma," *Indian Journal of Medical and Paediatric Oncology*, vol. 36, no. 4, pp. 243–248, 2015.

[27] M. A. Perazella, "Crystal-induced acute renal failure," *The American Journal of Medicine*, vol. 106, no. 4, pp. 459–465, 1999.

[28] W. Ahmed, A. Zaki, and T. Nabil, "Prevention of methotrexate-induced nephrotoxicity by concomitant administration of garlic aqueous extract in rat," *Turkish Journal of Medical Sciences*, vol. 45, no. 3, pp. 507–516, 2015.

[29] B. C. Widemann and P. C. Adamson, "Understanding and managing methotrexate nephrotoxicity," *The Oncologist*, vol. 11, no. 6, pp. 694–703, 2006.

[30] C. L. Coleshowers, O. O. Oguntibeju, M. Ukpong, and E. J. Truter, "Effects of methotrexate on antioxidant enzyme status in a rodent model," *Medical Technology SA*, vol. 24, no. 1, pp. 5–9, 2010.

[31] S. K. Choi and J. S. Seo, "Lycopene supplementation suppresses oxidative stress induced by a high fat diet in gerbils," *Nutrition Research and Practice*, vol. 7, no. 1, pp. 26–33, 2013.

[32] V. K. Kolli, P. Abraham, B. Isaac, and D. Selvakumar, "Neutrophil infiltration and oxidative stress may play a critical role in methotrexate-induced renal damage," *Chemotherapy*, vol. 55, no. 2, pp. 83–90, 2009.

[33] H. I. Atilgan, A. Aydin, M. Sadic et al., "The protective effect of lycopene on kidney against experimentally induced unilateral ureteral obstruction," *Acta Medica Mediterranea*, vol. 32, pp. 1631–1636, 2016.

[34] M. Sadic, H. I. Atilgan, A. Aydin et al., "Scintigraphic, histopathologic, and biochemical evaluation of lycopene effects on renal ischemia reperfusion injury in rats," *Serbian Archives of Medicine*, vol. 145, no. 3-4, pp. 153–158, 2017.

[35] U. Aman, P. Vaibhav, and R. Balaraman, "Tomato lycopene attenuates myocardial infarction induced by isoproterenol: electrocardiographic, biochemical and anti-apoptotic study," *Asian Pacific Journal of Tropical Biomedicine*, vol. 2, no. 5, pp. 345–351, 2012.

[36] E. Ozkan, C. Akyüz, E. Dulundu et al., "Protective effects of lycopene on cerulein-induced experimental acute pancreatitis in rats," *The Journal of Surgical Research*, vol. 176, no. 1, pp. 232–238, 2012.

[37] Y. C. Hou, A. Janczuk, and P. G. Wang, "Current trends in the development of nitric oxide donors," *Current Pharmaceutical Design*, vol. 5, no. 6, pp. 417–441, 1999.

[38] E. Oguz, S. Kocarslan, S. Tabur, H. Sezen, Z. Yilmaz, and N. Aksoy, "Effects of lycopene alone or combined with melatonin on methotrexate-induced nephrotoxicity in rats," *Asian Pacific Journal of Cancer Prevention*, vol. 16, no. 14, pp. 6061–6066, 2015.

[39] U. Rolle, H. Shima, and P. Puri, "Nitric oxide, enhanced by macrophage-colony stimulating factor, mediates renal damage in reflux nephropathy," *Kidney International*, vol. 62, no. 2, pp. 507–513, 2002.

[40] S. Yamagishi and T. Matsui, "Advanced glycation end products, oxidative stress and diabetic nephropathy," *Oxidative Medicine and Cellular Longevity*, vol. 3, no. 2, pp. 101–108, 2010.

[41] Y. Liu, "Advanced oxidation protein products: a causative link between oxidative stress and podocyte depletion," *Kidney International*, vol. 76, no. 11, pp. 1125–1127, 2009.

[42] E. Uz, F. Oktem, H. R. Yilmaz, E. Uzar, and F. Ozguner, "The activities of purine-catabolizing enzymes and the level of nitric oxide in rat kidneys subjected to methotrexate: protective effect of caffeic acid phenethyl ester," *Molecular and Cellular Biochemistry*, vol. 277, no. 1-2, pp. 165–170, 2005.

[43] H. L. Hantz, L. F. Young, and K. R. Martin, "Physiologically attainable concentrations of lycopene induce mitochondrial apoptosis in LNCaP human prostate cancer cells," *Experimental Biology and Medicine*, vol. 230, no. 3, pp. 171–179, 2016.

[44] G. Krishnamoorthy, K. Selvakumar, P. Venkataraman, P. Elumalai, and J. Arunakaran, "Lycopene supplementation prevents reactive oxygen species mediated apoptosis in Sertoli cells of adult albino rats exposed to polychlorinated biphenyls," *Interdisciplinary Toxicology*, vol. 6, no. 2, pp. 83–92, 2013.